2009, VOLUME 2

PROGRESS IN PHYSICS

"All scientists shall have the right to present their scientific research results, in whole or in part, at relevant scientific conferences, and to publish the same in printed scientific journals, electronic archives, and any other media." — Declaration of Academic Freedom, Article 8

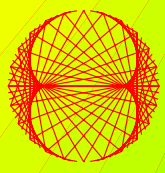

ISSN 1555-5534

The Journal on Advanced Studies in Theoretical and Experimental Physics, including Related Themes from Mathematics

PROGRESS IN PHYSICS

A quarterly issue scientific journal, registered with the Library of Congress (DC, USA). This journal is peer reviewed and included in the abstracting and indexing coverage of: Mathematical Reviews and MathSciNet (AMS, USA), DOAJ of Lund University (Sweden), Zentralblatt MATH (Germany), Scientific Commons of the University of St. Gallen (Switzerland), Open-J-Gate (India), Referativnyi Zhurnal VINITI (Russia), etc.

To order printed issues of this journal, contact the Editors. Electronic version of this journal can be downloaded free of charge:

http://www.ptep-online.com
http://www.geocities.com/ptep_online

Postal address

Chair of the Department
of Mathematics and Science,
University of New Mexico,
200 College Road,
Gallup, NM 87301, USA

ISSN: 1555-5534 (print)
ISSN: 1555-5615 (online)

Standard Address Number: 297-5092
Printed in the United States of America

APRIL 2009 **VOLUME 2**

CONTENTS

Information for Authors and Subscribers

Progress in Physics has been created for publications on advanced studies in theoretical and experimental physics, including related themes from mathematics and astronomy. All submitted papers should be professional, in good English, containing a brief review of a problem and obtained results.

All submissions should be designed in LaTeX format using *Progress in Physics* template. This template can be downloaded from *Progress in Physics* home page http://www.ptep-online.com. Abstract and the necessary information about author(s) should be included into the papers. To submit a paper, mail the file(s) to the Editor-in-Chief.

All submitted papers should be as brief as possible. We usually accept brief papers, no larger than 8–10 typeset journal pages. Short articles are preferable. Large papers can be considered in exceptional cases to the section *Special Reports* intended for such publications in the journal. Letters related to the publications in the journal or to the events among the science community can be applied to the section *Letters to Progress in Physics*.

All that has been accepted for the online issue of *Progress in Physics* is printed in the paper version of the journal. To order printed issues, contact the Editors.

This journal is non-commercial, academic edition. It is printed from private donations. (Look for the current author fee in the online version of the journal.)

The Neutrino: Evidence of a Negative-Energy Vacuum State

William C. Daywitt

National Institute for Standards and Technology (retired), Boulder, Colorado, USA

E-mail: wcdaywitt@earthlink.net

This note argues that the neutrino is a phonon packet that exists and propagates within the negative-energy Planck vacuum. Simple calculations connect the three neutrinos to their corresponding leptons and show: that the neutrino mass is a ficticious or effective mass; that the neutrino mass cannot be zero; that each of the three neutrinos has a unique mass that determines its velocity; and that flavor (neutrino-type) mixing does not involve mass mixing.

The total energy E of a relativistic particle of rest mass m is

$$E = (m^2c^4 + c^2p^2)^{1/2}, \tag{1}$$

where c is the speed of light, $p = m\gamma v$ is the relativistic momentum, $\gamma^2 = 1/(1-\beta^2)$, $\beta = v/c$, and v is the particle velocity. Rearranging (1) leads to

$$\frac{v}{c} = \left[1 - \left(\frac{mc^2}{E}\right)^2\right]^{1/2}, \tag{2}$$

which can be used to determine the particle mass by measuring its velocity and relativistic energy. For any measurement set (v, E), the same mass will emerge within the measurement accuracy. When this measurement procedure is applied to the neutrino [1, pp. 534–536], however, different masses emerge. Thus the neutrino is not an elementary particle in the usual sense of the term "elementary particle". It is not surprising, then, that the "mystery of neutrino mass" is currently the most important subject of study in neutrino physics [1, p. 180].

The present note argues that the neutrino is a massless phonon packet traveling within the negative-energy Planck vacuum (PV), the primary task being to determine the structure of that packet. Taking the decay of the neutron into a proton and an electron as an example, the heuristic calculations proceed as follows: the sudden appearance of the electron as a decay product sets up a periodic disturbance in the PV from which the packet emerges; it is then assumed that the packet is the same as a phonon packet traveling a linear lattice whose lattice points are separated by a distance equal to the electron's Compton wavelength. Treating the neutrino as a phonon packet tracks the solid state theory remarkably well, but the presentation here is sketchy because of the formal complexity of the latter theory with its "undergrowth of suffixes" as Ziman would put it [2, p. 17]. The more precise details are left to a subsequent paper.

The PV [3] is an omnipresent degenerate gas of negative-energy Planck particles (PP) characterized by the triad (e_*, m_*, r_*), where e_*, m_*, and r_* $(\lambda_*/2\pi)$ are the PP charge, mass, and Compton radius respectively. The vacuum is held together by van-der-Waals forces. The charge e_* is the bare (true) electronic charge common to all charged elementary particles and is related to the observed electronic charge e through the fine structure constant $\alpha = e^2/e_*^2$ which is a manifestation of the PV polarizability. The PP mass and Compton radius are equal to the Planck mass and length respectively. The particle-PV interaction is the source of the gravitational $(G = e_*^2/m_*^2)$ and Planck $(\hbar = e_*^2/c)$ constants, and the Compton relations $(r_* m_* c^2 = r_c mc^2 = e_*^2)$ relating the PV and its PPs to the observed elementary particles, where the charged elementary particles are characterized by the triad (e_*, m, r_c), m and r_c being the mass and Compton radius $(\lambda_c/2\pi)$ of the particle (particle spin is not yet included in the theory). A feedback mechanism in the particle-PV interaction leads to the Lorentz transformation. The zero-point random motion of the PP charges e_* about their equilibrium positions within the PV, and the PV dynamics, are the source of the quantum vacuum [4].

The mean power flux of phonons traveling a linear lattice chain in an elastic medium is [2, p. 15]

$$U = \langle \mathcal{U} \rangle = \left\langle \sum_k \hbar\omega_k v_k a_k^* a_k \right\rangle = \sum_k \hbar\omega_k v_k N_k\,, \tag{3}$$

where $0 \leqslant k \leqslant \pi/r_a$, $\hbar\omega_k$ is the phonon energy for the k-th mode, v_k is the phonon group velocity, a_k^* and a_k are the phonon creation and annihilation operators, and $N_k = \langle a_k^* a_k \rangle$ is the number of phonons per unit length in the kth mode. Restricting k to non-negative values (non-positive values would work just as well) implies that only traveling waves (rather than standing waves) are of interest in the calculations.

The dispersion relation connecting the phonon frequency ω_k and wavenumber k is [2, p. 12]

$$\omega_k = \left(\frac{4g_a}{m}\right)^{\frac{1}{2}} \left|\sin\left(\frac{\phi_{n,k}}{2}\right)\right| = \left(\frac{4g_a}{m}\right)^{\frac{1}{2}} \sin\left(\frac{kr_a}{2}\right), \tag{4}$$

where g_a is the "spring constant". The angle $\phi_{n,k} = 2n\pi + kr_a$, where $n\,(=0, 1, 2, \dots)$ are the positive branches or Brillouin zones of interest and $k_a\,(=2\pi/\lambda_a = 1/r_a)$ is the k-axis scaling factor. The absence of absolute-value bars in the

final expression follows from the fact that $0 \leqslant kr_a \leqslant \pi$. The group velocity

$$v_k = \frac{d\omega_k}{dk} = \left(\frac{r_a^2 g_a}{m}\right)^{1/2} \cos\left(\frac{kr_a}{2}\right) \tag{5}$$

is the velocity of the k-mode phonons. The phonon number N_k is then the number of k-phonons per unit r_a.

For a single phonon packet (a neutrino) traveling the chain, i.e. for a single value of n and k, (3) leads to

$$U_k = \hbar\omega_k \cdot v_k \cdot N_k = E_k \cdot v_k \tag{6}$$

where $\hbar\omega_k$ is the phonon energy of the packet and $E_k \equiv \hbar\omega_k N_k$ is the total energy carried by the packet. The index k corresponds to the type of neutrino (ν_e, ν_μ, or ν_τ) participating in the decay or capture processes.

The PV is an elastic medium and, because a free particle distorts the PV, the sudden appearance or disappearance of a free particle will initiate a corresponding phonon disturbance in that vacuum. In the rest frame of the particle the static distortion force is [3]

$$F(r) = \frac{e_*^2}{r^2} - \frac{mc^2}{r}\,, \tag{7}$$

where m is the particle mass and the first and second forces are the polarization and curvature force respectively. (In the laboratory frame these opposing forces lead to the particle's de Broglie radius [4, Append. A].) The two forces on the right side of (7) are equal at the Compton radius ($r_c = e_*^2/mc^2$) of the particle, the positive polarization force dominating inside this radius ($r < r_c$) and the negative curvature force outside ($r > r_c$). These opposing forces result in a harmonic-oscillator-type disturbance within the PV, the effective "spring constant" of which is easy to derive from (7):

$$\Delta F(x) = \frac{e_*^2}{(r_c + x)^2} - \frac{mc^2}{r_c + x} = \\ = \frac{e_*^2}{r_c^2}\left[-\frac{x}{r_c} + 2\left(\frac{x}{r_c}\right)^2 - \cdots\right] \approx -\frac{e_*^2}{r_c^3}\,x = -g_c x\,, \tag{8}$$

where x is the excursion of the disturbance about its equilibrium position at $x = 0$, and where the particle Compton relation $e_*^2/r_c^2 = mc^2/r_c$ is used in deriving the second expression. For small excursions ($x/r_c \ll 1$) the force reduces to the final expression where $g_c \equiv e_*^2/r_c^3$ is the desired "spring constant".

Using $r_a = r_c$ and $g_a = g_c$ and the Compton radius (it is $r_c = e_*^2/mc^2$) of the free particle (the lepton) in (4) and (5) leads to

$$\hbar\omega_k = \frac{e_*^2}{r_c}\,\frac{\sin(kr_c/2)}{1/2} \approx e_*^2 k \tag{9}$$

and

$$\frac{v_k}{c} = \cos\left(\frac{kr_c}{2}\right) \approx 1 - \frac{1}{2}\left(\frac{kr_c}{2}\right)^2 = 1 - \frac{1}{2}\left(\frac{e_*^2 k/2}{mc^2}\right)^2 \tag{10}$$

to second order in $kr_c/2$. The "spring constant" (g_c) and scaling factor ($k_c = 1/r_c$) tie the m-phonons to the m-lepton that created them, where the prefix "m" stands for the lepton mass in (10). Inserting (9) and (10) into (6) yields

$$U_k = \frac{e_*^2}{r_c}\,\frac{\sin(kr_c/2)}{1/2} \cdot c\cos(kr_c/2) \cdot N_k \tag{11}$$

$$\approx e_*^2 k \cdot c\left[1 - \frac{1}{2}\left(\frac{e_*^2 k/2}{mc^2}\right)^2\right] \cdot N_k \tag{12}$$

for the mean power flux of the lepton-induced neutrino. The magnitude of N_k varies with the needs of the decay or capture process to conserve momentum and energy (and spin, although spin is not included in the present discussion). That is, the PV absorbs the unbalanced momentum and energy of the process.

Using $r_c = e_*^2/mc^2$, (11) and (12) can be put in the more convenient form

$$U_k = mc^2\,\frac{\sin(m_k c^2/2mc^2)}{1/2} \cdot c\cos(m_k c^2/2mc^2) \cdot N_k \tag{13}$$

$$\approx m_k c^2 \cdot c\left[1 - \frac{1}{2}\left(\frac{m_k c^2}{2mc^2}\right)^2\right] \cdot N_k \tag{14}$$

where $m_k \equiv e_*^2 k/c^2$ is a ficticious or effective mass. It is clear from (14) that m_k cannot vanish for then the packet flux U_k would also vanish. The bracket shows that the packet propagates at somewhat less than the speed of light.

It is instructive at this point to compare the particle and phonon-packet models of the neutrino. In the particle model described by (1) and (2), the energy and velocity of the neutrino are

$$E'_\nu = cp'_\nu = m'_\nu c^2 \cdot \beta\gamma \tag{15}$$

and

$$\frac{v'_\nu}{c} = 1 - \frac{1}{2}\left(\frac{m'_\nu c^2}{E'_\nu}\right)^2 \tag{16}$$

for $E'_\nu \gg m'_\nu c^2$. As discussed in the first paragraph, the particle mass m'_ν is a variable mass and, in order to make the equations fit the experimental data, mass and flavor mixing (see below) must be brought *ad hoc* into the particle model, destroying the particle description of the neutrino in the process. From (14) for the packet model

$$E_k = m_k c^2 \cdot N_k \tag{17}$$

and

$$\frac{v_k}{c} = 1 - \frac{1}{2}\left(\frac{m_k c^2}{2mc^2}\right)^2 \tag{18}$$

for small $m_k c^2$. Equation (17) shows that the neutrino energy E_k is the product of the phonon energy $m_k c^2$ and the number of phonons N_k in the packet. Equation (18) shows that the neutrino velocity is determined solely by the neutrino mass m_k and its corresponding lepton mass m.

The three types (or flavors) of neutrinos are the electron (ν_e), muon (ν_μ), and tau (ν_τ) neutrinos and, in the particle model, each flavor is assumed to have one or a combination of three masses (m_1, m_2, m_3) [1, p. 452]. The corresponding three-neutrino mixing (or flavor oscillation) is a phenomenon in which a neutrino created with a particular flavor is later measured to have a different flavor due to a mismatch between the flavor and mass eigenstates of the three neutrinos. In the packet model each neutrino has its own mass as seen in (17) and (18), leading to the more straightforward flavor-oscillation process described below.

The harmonic (quadratic) approximation [2, p. 12] to the Hamiltonian for a linear lattice chain leads to the calculations in equations (3) through (14). For a three-dimensional lattice, the addition of the anharmonic cubic term [2, pp. 130–136] to the quadratic Hamiltonian, along with the effects of the selection rules, lead to a three-phonon process

$$(\mathbf{k}, \mathbf{p}) + (\mathbf{k}', \mathbf{p}') \Longleftrightarrow (\mathbf{k}'', \mathbf{p}'') \tag{19}$$

that can be tied to the three-neutrino mixing phenomenon, where $\mathbf{k}$ and p, etc., are the wavenumber vector and polarization of the three phonons. That is, the only allowed transitions are those in which two phonons combine to give a third, or vise versa. In addition, conservation of energy requires that

$$\hbar\omega_{\mathbf{k},\mathbf{p}} + \hbar\omega_{\mathbf{k}',\mathbf{p}'} = \hbar\omega_{\mathbf{k}'',\mathbf{p}''} \tag{20}$$

and the conservation of wave vector for a *continuous* medium gives

$$\mathbf{k} + \mathbf{k}' = \mathbf{k}'' , \tag{21}$$

where, although the PV is discontinuous at the Planck level ($l \sim r_*$), it is effectively continuous at lengths $l \sim r_c \gg r_*$ where the observed particle Compton radius r_c is concerned. When the phonons are traveling the same straight line, the $\mathbf{k}$s in (19)–(21) can be replaced by their magnitudes. To illustrate the "physical" meaning of (19), consider the equation going from left to right, where the $\mathbf{k}$ and $\mathbf{k}'$ phonons combine to produce the phonon $\mathbf{k}''$: as $\mathbf{k}$ propagates, it distorts the medium in such a fashion as to create an effective "diffraction grating" off of which $\mathbf{k}'$ reflects, destroying the $\mathbf{k}$ and $\mathbf{k}'$ phonons while creating the $\mathbf{k}''$ phonon [2, p. 133].

Equations (19)–(21) are the foundation of the phonon-packet description of flavor mixing which involves three packets (one for each type of neutrino) of the form found in (14). For example, employing (19) from right to left, the neutrino described in (3) through (14) can change into two different neutrinos according to a given probability law [2, eqn.(3.1.6)]. Ignoring polarization and assuming the phonons travel the same straight line, (20) and (21) reduce to

$$m_k c^2 + m'_k c^2 = m''_k c^2 \tag{22}$$

and

$$k + k' = k'' , \tag{23}$$

which are the same equation as $m_k c^2 = e_*^2 k$, etc.. Thus the effective masses of the neutrinos drop out of the mixing process; i.e. there is no mass mixing in the packet description of flavor mixing.

In summary, the ease with which the phonon-packet model of the neutrino, based on the negative-energy PV, describes and explains the experimental data makes a compelling case for that model and for a negative-energy vacuum state. With the inclusion of flavor oscillations and variable neutrino masses, on the other hand, the free-particle model appears to be an exercise more in curve fitting than physical modeling.

Submitted on November 14, 2008 / Accepted on December 01, 2008

References

1. Giunti C., Kim C.W. Fundamentals of neutrino physics and astrophysics. Oxford Univ. Press, Oxford, UK, 2007.
2. Ziman J.M. Electrons and phonons: the theory of transport phenomena in solids. Oxford Press, Oxford, UK, 1972.
3. Daywitt W.C. The planck vacuum. *Progress in Physics*, 2009, v. 1, 20.
4. Daywitt W.C. The source of the quantum vacuum. *Progress in Physics*, 2009, v. 1, 27.

Black Holes and Quantum Gravity from a Planck Vacuum Perspective

William C. Daywitt

National Institute for Standards and Technology (retired), Boulder, Colorado, USA

E-mail: wcdaywitt@earthlink.net

This note explores the question of whether or not the Planck vacuum theory can explain black holes and quantum gravity. It is argued that black holes do not physically exist in nature and that the term "quantum gravity" makes no sense. The importance of the Planck vacuum in constraining the n-ratio in the Schwarzschild line element is noted.

The Planck vacuum (PV) [1] is an omnipresent degenerate gas of negative-energy Planck particles (PP) characterized by the triad (e_*, m_*, r_*), where e_*, m_*, and r_* $(\lambda_*/2\pi)$ are the PP charge, mass, and Compton radius respectively. The vacuum is held together by van der Waals forces. The charge e_* is the bare (true) electronic charge common to all charged elementary particles and is related to the observed electronic charge e through the fine structure constant $\alpha = e^2/e_*^2$ which is a manifestation of the PV polarizability. The PP mass and Compton radius are equal to the Planck mass and length respectively. The particle-PV interaction is the source of the gravitational $(G = e_*^2/m_*^2)$ and Planck $(\hbar = e_*^2/c)$ constants, and the Compton relations $(r_* m_* c^2 = r_c mc^2 = e_*^2)$ relating the PV and its PPs to the observed elementary particles, where the charged elementary particles are characterized by the triad (e_*, m, r_c), m and r_c being the mass and Compton radius $(\lambda_c/2\pi)$ of the particle (particle spin is not yet included in the theory). A feedback mechanism in the particle-PV interaction leads to the Lorentz transformation. The zero-point random motion of the PP charges e_* about their equilibrium positions within the PV, and the PV dynamics, are the source of the quantum vacuum [2]. Neutrinos appear to be phonon packets that exist and propagate within the PV [3].

General relativity describes the spacetime-curvature aspects of the PV [1]. So it is natural to assume that this vacuum state has something to do with black holes, "tunnels in spacetime", and "wormholes connecting different universes" [4, p. 642] if such things do indeed exist.

The Einstein metric equation, and the "Schwarzschild" line element outside a static sphere of mass m, expressed in terms of the PV parameters, are [1]

$$G_{\mu\nu} = \frac{8\pi T_{\mu\nu}}{c^4/G} = \frac{8\pi T_{\mu\nu}}{m_* c^2/r_*} \tag{1}$$

and

$$ds^2 = -\left[1 - 2n_r\right] c^2 dt^2 + \frac{dr^2}{\left[1 - 2n_r\right]} + r^2\, d\Omega^2, \tag{2}$$

where the n-ratio is

$$n_r \equiv n_r(m/r) \equiv \frac{mc^2/r}{c^4/G} = \frac{mc^2/r}{m_* c^2/r_*} \tag{3}$$

with $0 \leqslant n_r < 1$. Here $d\Omega^2 \equiv d\theta^2 + \sin^2\theta\, d\phi^2$.

The force mc^2/r is the distortion or curvature force the mass m exerts on the PV at a distance r from the center of the mass [1]. This curvature force is always smaller than the ultimate curvature force $c^4/G = m_* c^2/r_*$. As $r \to \infty$ the n-ratio vanishes where the metric bracket $[1 - n_r]$ is unity and the spacetime is flat. At the surface of the sun, a white dwarf, or a neutron star, n_r is roughly 0.00001, 0.001, and 0.5 respectively. Only at $m_* c^2/r_*$ is n_r equal to one. Thus the n-ratio is limited to $n_r < 1$ by the nature of the PV.

The metric structure of (2) leads to a black hole with its event horizon at $n_r = 1/2$ and to the corresponding "Schwarzschild radius" $R_s = 2Mc^2/(m_* c^2/r_*)$ [4, pp. 630–636]. From here such ideas as "tunnels" and "wormholes" arise. However, (2) is apparently incorrect [5–8]. For a point mass m at $r = 0$, the original and correct Schwarzschild line element [5] is

$$ds^2 = -\left[1 - 2n(R)\right] c^2 dt^2 + \frac{dR^2}{\left[1 - 2n(R)\right]} + R^2\, d\Omega^2, \tag{4}$$

where

$$R = r[1 + 8n_r^3]^{1/3} \tag{5}$$

and where (4) is only valid for $r > 0$. The metric bracket is now

$$1 - 2n(R) = 1 - \frac{2n_r}{[1 + 8n_r^3]^{1/3}}\,, \tag{6}$$

which is monotonically decreasing from 1 at $n_r = 0$ to $0.0385\ldots$ at $n_r = 1$. Thus, in the allowable range of n_r, the line element ds in equation (4) is well behaved. Again the metric bracket is unity as $r \to \infty$ where both n_r and $n(R)$ vanish.

The velocity of a radial photon starting from infinity and heading toward $r = 0$ can be found by setting $d\Omega^2 = 0$ and $ds = 0$ in (4). Its velocity dr/dt relative to its velocity (c) at infinity is easily shown to be

$$\beta(n_r) = \left(1 + 8n_r^3\right)^{2/3} \left[1 - \frac{2n_r}{\left(1 + 8n_r^3\right)^{1/3}}\right], \tag{7}$$

which yields $\beta(0) = 1$ as it should, and $\beta(1) \approx 1/6$ for a PP $(n_r = 1)$ positioned at $r = 0$.

From the two preceding paragraphs it is clear that nothing singular happens to the Schwarzschild line element of (4) in the allowed range of n_r. Furthermore, the PV theory does not

need to explain the black hole or its "tunneling" and "wormhole" attributes since the black hole does not exist.

The metric gravity discussed above deals with what happens when the curvature force mc^2/r of an isolated mass perturbs the PV. If "electromagnetics" is what happens when the polarization force e_*^2/r^2 of an isolated bare charge e_* perturbs the PV, then it can be shown that electromagnetics leads to the Maxwell equations, the relativistic electric and magnetic fields of a moving charge, and the Lorentz transformation [1]. Both of these phenomena deal with a *single* force acting on the PV. In either case, the terms "quantum gravity" or "quantum electromagnetics" make no sense because the word "quantum" applies to what happens when both forces, mc^2/r and e_*^2/r^2, perturb the PV simultaneously and lead to the Planck constant

$$r_c mc = \frac{e_*^2}{c} = \hbar \tag{8}$$

at $r = r_c$ where the two forces are equal. The standard name for this dual-force perturbation is, of course, "quantum electrodynamics" when dealing with an electron containing both mass and charge. In summary, the search for a theory of "quantum gravity" appears to make no sense.

Submitted on November 14, 2008 / Accepted on December 01, 2008

References

1. Daywitt W.C. The planck vacuum. *Progress in Physics*, 2009, v. 1, 20.
2. Daywitt W.C. The source of the quantum vacuum. *Progress in Physics*, 2009, v. 1, 27.
3. Daywitt W.C. The neutrino: evidence of a negative-energy vacuum state. *Progress in Physics*, 2009, v. 2, 3.
4. Carroll B.W., Ostlie D.A. An introduction to modern astrophysics. Addison-Wesley, San Francisco–Toronto, 2007.
5. Schwarzschild K. On the gravitational field of a mass point according to Einstein's theory. *Sitzungsberichte der Königlich Preussischen Akademie der Wissenschaften zu Berlin*, *Phys.-Math. Klasse*, 1916, 189.
6. Abrams L.S. Black holes: the legacy of Hilbert's error. *Can. J. Phys.*, 1989, v. 67, 919.
7. Crothers S.J. On the general solution to Einstein's vacuum field and its implications for relativistic degeneracy. *Progress in Physics*, 2005, v. 1, 68.
8. Rabounski D. On the current situation concerning the black hole problem. *Progress in Physics*, 2008, v. 1, 101.

On the Generalized Maxwell Equations and Their Prediction of Electroscalar Wave

Arbab I. Arbab and Zeinab A. Satti

Department of Physics, Faculty of Science, University of Khartoum, P.O. 321, Khartoum 11115, Sudan
Department of Physics and Applied Mathematics, Faculty of Applied Sciences and Computer, Omdurman Ahlia University, P.O. Box 786, Omdurman, Sudan

E-mail: aiarbab@uofk.edu; arbab_ai@yahoo.com

We have formulated the basic laws of electromagnetic theory in quaternion form. The formalism shows that Maxwell equations and Lorentz force are derivable from just one quaternion equation that only requires the Lorentz gauge. We proposed a quaternion form of the continuity equation from which we have derived the ordinary continuity equation. We introduce new transformations that produces a scalar wave and generalize the continuity equation to a set of three equations. These equations imply that both current and density are waves. Moreover, we have shown that the current can not circulate around a point emanating from it. Maxwell equations are invariant under these transformations. An electroscalar wave propagating with speed of light is derived upon requiring the invariance of the energy conservation equation under the new transformations. The electroscalar wave function is found to be proportional to the electric field component along the charged particle motion. This scalar wave exists with or without considering the Lorentz gauge. We have shown that the electromagnetic fields travel with speed of light in the presence or absence of free charges.

1 Introduction

Quaternions are mathematical construct that are generalization of complex numbers. They were introduced by Irish mathematician Sir William Rowan Hamilton in 1843 (Sweetser, 2005 [1]). They consist of four components that are represented by one real component (imaginary part) and three vector components (real part). Quaternions are closed under multiplication. Because of their interesting properties one can use them to write the physical laws in a compact way. A quaternion $\widetilde{A}$ can be written as $\widetilde{A} = A_0 + A_1 i + A_2 j + A_3 k$, where $i^2 = j^2 = k^2 = -1$ and $ij = k$, $ki = j$, $jk = i$, $ijk = -1$. A_0 is called the scalar component and A_1, A_2, A_3 are the vector components. Each component consists of real part and imaginary part. The real part of the scalar component vanishes. Similarly the imaginary part of the vector component vanishes too. This is the general prescription of quaternion representation.

In this paper we write the Maxwell equations in quaternion including the Lorentz force and the continuity equation. We have found that the Maxwell equations are derived from just one quaternion equation. The solution of these equations shows that the charge and current densities are waves traveling with speed of light. Generalizing the continuity equation resulted in obtaining three equations defining the charge and current densities. Besides, there exists a set of transformation that leave generalized continuity equation invariant. When these transformations are applied to the energy conservation law an electroscalar wave propagating with speed of light is obtained. Thus, the quaternionic Maxwell equation and continuity equation predict that there exist a scalar wave propagating with speed of light. This wave could possibly arise due to vacuum fluctuation. Such a wave is not included in the Maxwell equations. Therefore, the existence of the electroscalar is a very essential integral part of Maxwell theory. Expressions of Lorentz force and the power delivered to a charge particle are obtained from the quaternion Lorentz force.

Moreover, the current and charge density are solutions of a wave equation travelling with speed of light. Furthermore, we have shown that the electromagnetic field travels with speed of light in the presence and/or absence of charge. However, in Maxwell theory the electromagnetic field travels with speed of light only if there is no current (or free charge) in the medium. We have found here two more equations relating the charge and current that should supplement the familiar continuity equation. These two equations are found to be compatible with Maxwell equations. Hence, Maxwell equations are found to be invariant under these new transformations. This suggests that the extra two equations should be appended to Maxwell equations. Accordingly, we have found an electroscalar wave propagating at the speed of light. The time and space variation of this electroscalar wave induce a charge density and current density even in a source free. The electroscalar wave arises due to the invariance of the Maxwell equations under the new set of transformations. We have shown that such a scalar wave is purely electric and has no magnetic component. This is evident from the Poynting vector that has only two components, one along the particle motion and the other along the electric field direction. We re-

mark that Maxwell equations are still exact and need no modifications. They steadily predict the existence of the a electroscalar wave if we impose the new transformation we obtained in this work.

2 Derivation of Maxwells' equations

The multiplication of two quaternions is given by

$$\begin{aligned}&\widetilde{A}\,\widetilde{B} = (A_0, \vec{A})\,(B_0, \vec{B}) = \\ &= (A_0 B_0 - \vec{A}\cdot\vec{B},\, A_0\vec{B} + \vec{A}\,B_0 + \vec{A}\times\vec{B})\,. \end{aligned} \tag{1}$$

We define the quaternion D'Alembertian operator as

$$\widetilde{\Box}^2 \equiv -|\nabla|^2 = -\widetilde{\nabla}\widetilde{\nabla}^* = \frac{1}{c^2}\frac{\partial^2}{\partial t^2} - \vec{\nabla}\cdot\vec{\nabla}\,, \tag{2}$$

where Nabla and its conjugate are defined by

$$\widetilde{\nabla} = \left(\frac{i}{c}\frac{\partial}{\partial t},\, \vec{\nabla}\right), \qquad \widetilde{\nabla}^* = \left(\frac{i}{c}\frac{\partial}{\partial t},\, -\vec{\nabla}\right). \tag{3}$$

The wave equation of the quaternionic vector potential $\widetilde{A} = (i\frac{\varphi}{c}\,, \vec{A})$ has the form

$$\widetilde{\Box}^{\,2}\widetilde{A} = \mu_0\widetilde{J}, \qquad \widetilde{J} = (ic\rho\,, \vec{J})\,. \tag{4}$$

where ρ is the charge density.

The electric and magnetic fields are defined by (Jackson, 1967 [2])

$$\vec{E} = -\left(\vec{\nabla}\varphi + \frac{\partial\vec{A}}{\partial t}\right), \qquad \vec{B} = \vec{\nabla}\times\vec{A}\,. \tag{5}$$

Using Eqs. (1)–(3), the scalar part of Eq. (4) now reads

$$\begin{aligned}&-\frac{i}{c}\vec{\nabla}\cdot\left(\vec{\nabla}\varphi + \frac{\partial\vec{A}}{\partial t}\right) + \frac{i}{c}\frac{\partial}{\partial t}\left(\frac{1}{c^2}\frac{\partial\varphi}{\partial t} + \vec{\nabla}\cdot\vec{A}\right) - \\ &\qquad - \vec{\nabla}\cdot\left(\vec{\nabla}\times\vec{A}\right) = ic\mu_0\rho\,. \end{aligned} \tag{6}$$

Using Eq. (5) the above equation yields

$$\vec{\nabla}\cdot\vec{B} = 0\,, \tag{7}$$

$$\frac{1}{c^2}\frac{\partial\varphi}{\partial t} + \vec{\nabla}\cdot\vec{A} = 0\,, \tag{8}$$

and

$$\vec{\nabla}\cdot\vec{E} = \frac{\rho}{\varepsilon_0}\,, \tag{9}$$

where $c = \frac{1}{\sqrt{\varepsilon_0\mu_0}}$. This is the Gauss Law and is one of the Maxwell equations.

The vector part of the Eq. (4) can be written as

$$\begin{aligned}&-\frac{i}{c}\left(\vec{\nabla}\times\vec{E} + \frac{\partial\vec{B}}{\partial t}\right) + \left(\vec{\nabla}\times\vec{B} - \frac{1}{c^2}\frac{\partial\vec{E}}{\partial t}\right) - \\ &\qquad - \vec{\nabla}\left(\frac{1}{c^2}\frac{\partial\varphi}{\partial t} + \vec{\nabla}\cdot\vec{A}\right) = \mu\vec{J}\,. \end{aligned} \tag{10}$$

This yields the two equations

$$\vec{\nabla}\times\vec{E} + \frac{\partial\vec{B}}{\partial t} = 0 \tag{11}$$

and

$$\vec{\nabla}\times\vec{B} - \frac{1}{c^2}\frac{\partial\vec{E}}{\partial t} = \mu_0\vec{J}\,. \tag{12}$$

Eqs. (7), (9), (11) and (12) are the Maxwell equations.

By direct cancelation of terms, Eqs. (6) and (10), yield the wave equations of the scalar potential φ and the vector potential $\vec{A}$, viz., $\Box^2\varphi = \frac{\rho}{\varepsilon_0}$ and $\Box^2\vec{A} = \mu_0\vec{J}$.

We thus see that we are able to derive Maxwell equations from the wave equation of the quaternion vector potential. In this formalism only Lorentz gauge is required by the quaternion formulation to derive Maxwell equations. This would mean that Lorentz gauge is more fundamental. It is thus very remarkable that one are able to derive Maxwell equations from just one quaternion equation. Notice that with the 4-vector formulation Maxwell equation are written in terms of two sets of equations.

3 The quaternionic Lorentz force

The quaternionic Lorentz force can be written in the form

$$\left.\begin{aligned}&\widetilde{F} = q\,\widetilde{V}(\widetilde{\nabla}\widetilde{A})\,,\quad \widetilde{V} = (ic\,,\vec{v})\,,\quad \widetilde{F} = \left(i\frac{P}{c}\,,\ \vec{F}\right)\\ &\widetilde{A} = \left(\frac{i\varphi}{c}\,,\vec{A}\right),\ \widetilde{\nabla} = \left(\frac{i}{c}\frac{\partial}{\partial t}\,,\vec{\nabla}\right)\end{aligned}\right\}, \tag{13}$$

where P is the power. The scalar part of the above equation can be written in the form

$$\begin{aligned}&-iqc\left[\left(\vec{\nabla}\cdot\vec{A} + \frac{1}{c^2}\frac{\partial\varphi}{\partial t}\right) + \frac{\vec{v}}{c^2}\cdot\left(\vec{\nabla}\varphi + \frac{\partial\vec{A}}{\partial t}\right)\right] - \\ &- q\,\vec{v}\cdot\vec{\nabla}\times\vec{A} = i\frac{P}{c}\,. \end{aligned} \tag{14}$$

Upon using Eqs. (5) and (8), one gets

$$q\,\vec{v}\cdot\vec{\nabla}\times\vec{A} = 0 \quad\Rightarrow\quad \vec{v}\cdot\vec{B} = 0\,, \tag{15}$$

and

$$P = q\,\vec{v}\cdot\vec{E}\,. \tag{16}$$

This is the usual power delivered to a charged particle in an electromagnetic field. Eq. (15) shows that the charged particle moves in a direction normal to the direction of the magnetic field.

Now the vector component of Eq. (13) is

$$\begin{aligned}&q\left[-\frac{\partial\vec{A}}{\partial t} - \vec{\nabla}\varphi + ic\,\vec{\nabla}\times\vec{A} - \frac{\vec{v}}{c^2}\frac{\partial\varphi}{\partial t} - \right.\\ &\left. - \vec{v}(\vec{\nabla}\cdot\vec{A}) + \vec{v}\times\left(\frac{i}{c}\frac{\partial\vec{A}}{\partial t} + \frac{i}{c}\vec{\nabla}\varphi + \vec{\nabla}\times\vec{A}\right)\right] = \vec{F}\,. \end{aligned} \tag{17}$$

This yields the two equations

$$\vec{F} = q\,\left(\vec{E} + \vec{v}\times\vec{B}\right), \tag{18}$$

and

$$\vec{B}_m \equiv \vec{B} = \frac{\vec{v}}{c^2}\times\vec{E}\,. \tag{19}$$

Eq. (18) is the familiar Lorentz force. Eq. (19) gives a new relation between the magnetic field of a moving charge due to an electric field. Thus, we are able to derive the power and the Lorentz force on a charged particle. This new magnetic field may be interpreted as the magnetic field seen in a frame moving with velocity $\vec{v}$ when $\vec{B}=0$ in the rest frame. It is thus an apparent field. This equation is compatible with Eq. (15), since $\vec{v}\cdot\vec{B}_m = \vec{v}\cdot(\frac{\vec{v}}{c^2}\times\vec{E}) = 0$, by vector property. Moreover, we notice that $\vec{E}\cdot\vec{B}_m = \vec{E}\cdot(\frac{\vec{v}}{c^2}\times\vec{E}) = 0$. This clearly shows that the magnetic field produced by the charged particle is perpendicular to the electric field applied on the particle. Thus, a charged particle when placed in an external electric field produces a magnetic field perpendicular to the direction of the particle motion and to the electric field producing it. As evident from Eq. (19), this magnetic field is generally very small due to the presence of the factor c^2 in the dominator. Hence, the reactive force arising from this magnetic field is

$$\vec{F}_m = q\,\vec{v}\times\vec{B}_m\,, \tag{20}$$

which upon using Eq. (19) yields

$$\vec{F}_m = q\,\vec{v}\times\left(\frac{\vec{v}}{c^2}\times\vec{E}\right). \tag{21}$$

Using Eq. (16) and the vector properties, this can be casted into

$$\vec{F}_m = \frac{P}{c^2}\,\vec{v} - \frac{v^2}{c^2}\,q\,\vec{E}\,. \tag{22}$$

This reactive force acts along the particle motion (longitudinal) and field direction. The negative sign of the second term is due to the back reaction of the charge when accelerates by the external electric field. The total force acting on the charge particle is $\vec{F}_{\rm total} = q(\vec{E} + \vec{v}\times\vec{B}_{\rm total})$, $\vec{B}_{\rm total} = \vec{B} + \vec{B}_m$, $\vec{F}_{\rm total} = q\big(1-\frac{v^2}{c^2}\big)\vec{E} + q\,\vec{v}\times\vec{B} + \frac{P}{c^2}\,\vec{v}$. Notice that when $v \ll c$, this force reduces to the ordinary force and no noticeable difference will be observed. However, when $v \approx c$ measurable effects will be prominent.

4 Continuity equation

The quaternion continuity equation can be written in the form

$$\widetilde{\nabla}\,\widetilde{J} = 0\,, \qquad \widetilde{J} = \left(i\rho c\,,\vec{J}\right), \tag{23}$$

so that the above equation becomes

$$\widetilde{\nabla}\,\widetilde{J} = \left[-\left(\vec{\nabla}\cdot\vec{J} + \frac{\partial\rho}{\partial t}\right), \frac{i}{c}\left(\frac{\partial\vec{J}}{\partial t} + \vec{\nabla}\rho\,c^2\right) + \vec{\nabla}\times\vec{J}\right] = 0\,. \tag{24}$$

which yields the following three equations

$$\vec{\nabla}\cdot\vec{J} + \frac{\partial\rho}{\partial t} = 0\,, \tag{25}$$

and

$$\vec{\nabla}\rho + \frac{1}{c^2}\frac{\partial\vec{J}}{\partial t} = 0\,, \tag{26}$$

so that

$$\vec{\nabla}\times\vec{J} = 0\,. \tag{27}$$

Using the Stockes theorem one can write Eq. (27) to get, $\int\vec{J}\cdot d\vec{\ell} = 0$. Eqs. (26) and (27) are new equations for a flow. Eq. (27) states that a current emanating from a point in spacetime does not circulate to the same point. In comparison with a magnetic field, we know that the magnetic field lines have circulation.

Now take the dot product of both sides of Eq. (26) with $d\vec{S}$, where S is a surface, and integrate to get

$$\int\vec{\nabla}\rho\cdot d\vec{S} + \int\frac{1}{c^2}\frac{\partial\vec{J}\cdot d\vec{S}}{\partial t} = 0\,, \tag{28}$$

or

$$\int\vec{\nabla}\rho\cdot d\vec{S} + \frac{1}{c^2}\frac{\partial I}{\partial t} = 0\,, \qquad I = \int\vec{J}\cdot d\vec{S}\,. \tag{29}$$

But from Stokes' theorem $\int\vec{A}\cdot d\vec{S} = \int\vec{\nabla}\times\vec{A}\cdot d\vec{\ell}$. Therefore, one gets

$$\int\vec{\nabla}\rho\cdot d\vec{S} = \int\vec{\nabla}\times(\vec{\nabla}\rho)\cdot d\vec{\ell} = 0\,, \quad \vec{A} = \vec{\nabla}\rho\,. \tag{30}$$

This implies that $\frac{\partial I}{\partial t} = 0$ which shows that the current is conserved. This is a Kirchoff-type law of current loops. However, Eq. (25) represents a conservation of charge for electric current.

Eq. (27) suggests that one can write the current density as

$$\vec{J} = \vec{\nabla}\Lambda\,, \tag{31}$$

where Λ is some scalar field. It has a dimension of Henry (H). It thus represent a magnetic field intensity. We may therefore call it a magnetic scalar. Substituting this expression in Eq. (26) and using Eq. (42), one yields

$$\nabla^2\Lambda - \frac{1}{c^2}\frac{\partial^2\Lambda}{\partial t^2} = 0\,. \tag{32}$$

This means that the scalar function $\Lambda(r,t)$ is a wave traveling with speed of light.

Now taking the divergence of Eq. (26), one gets

$$\vec{\nabla}\cdot\vec{\nabla}(\rho\,c^2) + \frac{\partial\,\vec{\nabla}\cdot\vec{J}}{\partial t} = 0\,, \tag{33}$$

which upon using Eq. (25) becomes

$$\nabla^2(\rho\,c^2) + \frac{\partial\,\frac{-\partial\rho}{\partial t}}{\partial t} = 0\,, \tag{34}$$

or

$$\frac{1}{c^2}\frac{\partial^2\rho}{\partial t^2}-\nabla^2\rho=0\,, \tag{35}$$

which states the the charge scalar (ρ) is a field propagating with speed of light.

Now take the curl of Eq. (27) to get

$$\vec{\nabla}\times(\vec{\nabla}\times\vec{J})=\vec{\nabla}(\vec{\nabla}\cdot\vec{J})-\nabla^2\vec{J}=0\,, \tag{36}$$

and upon using Eq. (25) and (26) one gets

$$\vec{\nabla}\left(-\frac{\partial\rho}{\partial t}\right)-\nabla^2\vec{J}=\frac{\partial(-\vec{\nabla}\rho)}{\partial t}-\nabla^2\vec{J}=$$
$$=\frac{\partial\frac{1}{c^2}\frac{\partial\vec{J}}{\partial t}}{\partial t}-\nabla^2\vec{J}=0\,, \tag{37}$$

which states that the current density satisfies a wave that propagate with speed of light, i.e.,

$$\frac{1}{c^2}\frac{\partial^2\vec{J}}{\partial t^2}-\nabla^2\vec{J}=0\,. \tag{38}$$

Therefore, both the current and charge densities are solutions of a wave equation traveling with a speed of light. This is a remarkable result that does not appear in Maxwell initial derivation. Notice however that if we take $\frac{\partial}{\partial t}$ of Eq. (12) and apply Eqs. (11) and (9), we get

$$\frac{1}{c^2}\frac{\partial^2\vec{E}}{\partial t^2}-\nabla^2\vec{E}=-\frac{1}{\varepsilon_0}\left(\vec{\nabla}\rho+\frac{1}{c^2}\frac{\partial\vec{J}}{\partial t}\right). \tag{39}$$

Now take the curl of both sides of Eq. (12) and apply Eqs. (11) and (7), we get

$$\frac{1}{c^2}\frac{\partial^2\vec{B}}{\partial t^2}-\nabla^2\vec{B}=\mu_0\big(\vec{\nabla}\times\vec{J}\big)\,. \tag{40}$$

The left hand side of Eqs. (39) and (40) is zero according to Eqs. (26) and (27). Therefore, they yield electric and magnetic fields travelling with speed of light. However, Maxwell equations yield electric and magnetic fields propagating with speed of light only if $\vec{J}=0$ and $\rho=0$ (free space). Because of Eqs. (26) and (27) electromagnetic field travels with speed of light whether the space is empty or having free charges. It seems that Maxwell solution is a special case of the above two equations. Therefore, Eqs. (39) and (40) are remarkable.

Now we introduce the new gauge transformations of $\vec{J}$ and ρ as:

$$\rho'=\rho+\frac{1}{c^2}\frac{\partial\Lambda}{\partial t}\,,\qquad \vec{J}'=\vec{J}-\vec{\nabla}\Lambda\,, \tag{41}$$

leaving Eqs. (25) - (27) invariant, where Λ satisfies the wave equation

$$\frac{1}{c^2}\frac{\partial^2\Lambda}{\partial t^2}-\nabla^2\Lambda=-\left(\vec{\nabla}\cdot\vec{J}+\frac{\partial\rho}{\partial t}\right). \tag{42}$$

These transformations are similar to gauge transformations endorse on the vector potential ($\vec{A}$) and the scalar potential (φ) leaving $\vec{E}$ and $\vec{B}$ invariant. It is interesting to see that the current $\vec{J}$ and density ρ are not unique, however. van Vlaenderen and Waser arrived at similar equations, but they attribute the Λ field to a longitudinal electroscalar wave in vacuum. Thus, even if there is no charge or current density present in a region, the scalar field Λ could act as a source for the electromagnetic field. Such a term could come from quantum fluctuations of the vacuum. This is a very intriguing result. Notice from Eq. (41) that the scalar wave (Λ) distribution induces a charge density, $\rho_{\mathrm{vacuum}}=\frac{1}{c^2}\frac{\partial\Lambda}{\partial t}$, and a current $\vec{J}_{\mathrm{vacuum}}=-\vec{\nabla}\Lambda$. It may help understand the Casimir force generated when two uncharged metallic plates in a vacuum, placed a few micrometers apart, without any external electromagnetic field attract each other(Bressi, *et al.*, 2002 [18]). Notice that this vacuum current and density satisfy the continuity equations, Eqs. (25)–(27). Note that these vacuum quantities could be treated as a correction of the current and charge, since in quantum electrodynamics all physical quantities have to be renormalized. It is interesting that the Maxwell equations expressed in Eqs. (39) and (40), are invariant under the transformation in Eq. (41) provided that $\vec{E}'=\vec{E}$, $\vec{B}'=\vec{B}$. It is thus remarkable to learn that Maxwell equations are invariant under the transformation,

$$\left.\begin{array}{ll}\rho'=\rho+\dfrac{1}{c^2}\dfrac{\partial\Lambda}{\partial t}\,, & \vec{J}'=\vec{J}-\vec{\nabla}\Lambda\\ \vec{E}'=\vec{E}, & \vec{B}'=\vec{B}\end{array}\right\}. \tag{43}$$

We notice from Eq. (42) that the electroscalar wave propagates with speed of light if the charge is conserved. However, if the charge is not conserve then Λ will have a source term equals to the charge violation term. In this case the electroscalar wave propagates with a speed less than the speed of light. Hence, charge conservation can be detected from the propagation speed of this electroscalar wave.

5 Poynting vector

The Poynting theorem, which represents the energy conservation law is given by (Griffiths, 1999 [4])

$$\frac{\partial u}{\partial t}+\vec{\nabla}\cdot\vec{S}=-\vec{J}\cdot\vec{E}\,, \tag{44}$$

where $\vec{S}$ is the Poynting vector, which gives the direction of energy flow and u is the energy density. However, in our present case we have

$$\frac{\partial u_{\mathrm{total}}}{\partial t}+\vec{\nabla}\cdot\vec{S}_{\mathrm{total}}=-\vec{J}'\cdot\vec{E}\,', \tag{45}$$

where $\vec{S}_{\mathrm{total}}=\vec{S}_{\mathrm{em}}+\vec{S}_m$ is the total Poynting vector, $\vec{S}_{\mathrm{em}}=$ $=\frac{\vec{E}\times\vec{B}}{\mu_0}$, and $u_{\mathrm{total}}=\frac{1}{2}\,\varepsilon_0\,E^2+\frac{1}{2\mu_0}(\vec{B}+\vec{B}_m)^2$. Because of Eqs. (15) and (19), the cross term in the bracket vanishes. Hence,

$$u_{\mathrm{total}}=\frac{1}{2}\,\varepsilon_0\left(1+\frac{v^2}{c^2}\right)E^2+\frac{B^2}{2\mu_0}-\frac{1}{2}\,\varepsilon_0\left(\frac{\vec{v}}{c}\cdot\vec{E}\right)^2. \tag{46}$$

This implies that the excessive magnetic field of the charged particles contributes an energy, $u_m = \frac{1}{2}\,\varepsilon_0 \frac{v^2}{c^2}\,E^2 \times$ $\times \left(1 - (\hat{n}\cdot\hat{e})^2\right)$, where $\hat{n}$ and $\hat{e}$ are two unit vectors along the motion of the particle and the electric field. This contribution is generally very small, viz., for $v \ll c$. When the charged particle moves parallel to the electric field, i.e., $\hat{n}\cdot\hat{e} = 1$, its energy density contribution vanishes.

Using Eq. (19), one finds

$$\vec{S}_m = \frac{\vec{E}\times\vec{B}_m}{\mu_0} = \frac{\vec{E}}{\mu_0}\times\left(\frac{\vec{v}\times\vec{E}}{c^2}\right) = \\ = \left(\varepsilon_0 E^2\right)\vec{v} - \left(\vec{E}\cdot\vec{v}\right)\varepsilon_0\,\vec{E}\,. \quad (47)$$

Using the vector identity, $\vec{\nabla}\cdot\left(f\vec{A}\right) = \left(\vec{\nabla}f\right)\cdot\vec{A} + \left(\vec{\nabla}\cdot\vec{A}\right)f$ (Gradstein and Ryzik, 2002 [5]) and Eq. (19), the energy conservation law in Eq. (47) reads

$$\frac{\partial u_{\mathrm{total}}}{\partial t} + \vec{\nabla}\cdot\left(\vec{S}_{\mathrm{em}} + \left(\varepsilon_0 E^2\right)\vec{v}\right) = \\ = -\vec{E}\cdot\vec{\nabla}\left(\Lambda - \varepsilon_0(\vec{E}\cdot\vec{v})\right). \quad (48)$$

The left hand side of the above equation vanishes when

$$\Lambda = \varepsilon_0\left(\vec{E}\cdot\vec{v}\right). \quad (49)$$

Thus, this scalar wave is not any arbitrary function. It is associated with the electric field of the electromagnetic wave. It is thus suitable to call this an electroscalar wave. Eq. (48) with the condition in Eq. (49) states that when Λ is defined as above, there is no work done to move the free charges, and that a new wave is generated with both energy density and having energy flow along the particle direction. Hence,

$$\frac{\partial u_{\mathrm{total}}}{\partial t} + \vec{\nabla}\cdot\left(\vec{S}_{\mathrm{em}} + \left(\varepsilon_0 E^2\right)\vec{v}\right) = 0\,. \quad (50)$$

In such a case, we see that no electromagnetic energy is converted (into neither mechanical energy nor heat). The medium acts as if it were empty of current. This shows that the scalar wave and the charged particle propagate concomitantly. However, in the de Broglie picture a wave is associated with the particle motion to interpret the wave particle duality present in quantum mechanics. Eq. (50) shows that there is no energy flow along along the magnetic field direction. Therefore, this electroscalar wave is a longitudinal wave. The transmission of such a wave does cost extra energy and it avails the electromagnetic energy accompany it. Notice that this scalar wave can be used to transmit and receive wireless signals (van Vlaenderen and Waser, 2001 [6]). It has an advantage over the electromagnetic wave, since it is a longitudinal wave and has no polarization properties. We will anticipate that this new scalar wave will bring about new technology of transmission that avails such properties.

We have seen that recently van Vlaenderen, 2003 [7], showed that there is a scalar wave associated with abandonment of Lorentz gauge. He called such a scalar field, S. We have shown that without such abandonment one can arrive at the same conclusion regarding the existence of such a scalar wave. We have seen that the scalar wave associated with the current $\vec{J}$ travels along the current direction. However, van Vlaenderen obtain such a scalar wave with the condition that $\vec{J} = \vec{B} = 0$. But our derivation here shows that this is not limited to such a case, and is valid for any value of $\vec{E}, \vec{B}$, and $\vec{J}$. We can obtain the scalar wave equation of van Vlaenderen if we apply our transformation in Eq. (41) to Maxwell equations.

Van Vlaenderen obtained a scalar field for $\vec{E} = 0$ and $\vec{B} = 0$. See, Eq. (25) and (26). These equations can be obtained from from Maxwell and continuity equation by requiring an invariance of Maxwell equations under our transformation in Eq. (41) without requiring $\vec{E} = \vec{B} = 0$. Therefore, our Eq. (42) is similar to van Vlaenderen equation, viz., Eq. (35).

Wesley and Monstein [9] claimed that the scalar wave (longitudinal electric wave) transmission has an energy density equals to $\frac{1}{2\mu_0}\,S^2$. However, if the violation of Lorentz condition is very minute then this energy density term will have a very small contribution and can be ignored in comparison with the linear term in the Poynting vector term. Notice, however, that in such a case the van Vlaenderen prediction will be indistinguishable from our theory with a valid Lorentz condition. Hence, the existence of the electroscalar wave is not very much associated with Lorentz condition invalidation. Ignatiev and Leus [10] have confirmed experimentally the existence of longitudinal vacuum wave without magnetic component. This is evident from Eq. (47) that the energy flows only along the particle motion and the electric field direction, without trace to any magnetic component. van Vlaenderen proposed source transformations to generalize electrodynamic force and power of a charge particle in terms of a scalar wave S. Therefrom, he obtain a Poynting vector due to this scalar to be $-\frac{S}{\mu_0}\vec{E}$. These transformations coincide with our new transformation that arising from the invariance of the continuity equations under these transformation. Hence, Eq. (35) of van Vlaenderen would become identical to our Eq. (43), by setting $\Lambda = \frac{S}{\mu_0}$, but not necessarily limited to $\vec{B} = 0$, as he assumed.

We summarize here the quaternion forms of the physical laws which we have studied so far we:

- Maxwell equation: $\widetilde{\square}^2\widetilde{A} = \mu_0\widetilde{J}$;
- Lorentz force: $\widetilde{F} = q\widetilde{V}(\widetilde{\nabla}\widetilde{A})$;
- continuity equation: $\widetilde{\nabla}\widetilde{J} = 0$.

6 Conclusion

I think that a new and very powerful idea drives this work, namely, that all events are nicely represented as a quaternion. This implies that any collection of event can be generated by an appropriate quaternion function. Scalar and vector mix

under multiplication, so quaternions are mixed representation. Every event, function, operator can be written in terms of quaternions. We have shown in this paper that the four Maxwell equations emerge from just one quaternion equation. Moreover, Lorentz force and the power delivered by a charged particle stem from one quaternion equation. The quaternion form of the continuity equation gives rise to the ordinary continuity equation, in addition to two more equations. The invariance of Maxwell equations under our new transformation shown in Eq. (43) ushers in the existence of new wave. This wave is not like the ordinary electromagnetic wave we know. It is a longitudinal wave having their origin in the variation of the electric field. It is called an electroscalar wave, besides that fact that it has a dimension of magnetic field intensity. Thus, in this paper we have laid down the theoretical formulation of the electroscalar wave without spoiling the beauty of Maxwell equations (in addition to Lorentz force). This scalar wave is not like the scalar potential which is a wave with a source term represented by the density that travels at a speed less than that of light. If the electroscalar wave is found experimentally, it will open a new era of electroscalar communication, and a new technology is then required. We remark that one does not need to invalidate the Lorentz condition to obtain such wave as it is formulated by some authors. In this work, we have generalize the continuity equation to embody a set of three equations. These equations imply that both current and density are waves traveling at a speed of light. Urgent experimental work to disclose the validity of these predictions is highly needed.

Acknowledgements

This work is supported by the University of Khartoum and Ahlia University research fund. We appreciate very much this support. Special thanks go to F. Amin for enlightening and fruitful discission.

Submitted on November 28, 2008 / Accepted on December 05, 2008

References

1. Sweetser D.B. Doing physics with quaternions. MIT, 2005. Accessed online: http://world.std.com/∼sweetser/quaternions/ps/book.pdf
2. Jackson J.D. Classical electrodynamics. John Wiley and Sons, 1967.
3. Bressi G., Carugno G., Onofrio R., and Ruoso G. *Phys. Rev. Lett.*, 2002, v. 88, 041804.
4. Griffiths D.J., Introduction to electrodynamics. Prentice-Hall Inc., 1999.
5. Gradstein I.S. and Ryzik I.M Vector field theorem. Academic Press, San Diego (CA), 2002.
6. Van Vlaenderen K.J. and Waser A. *Hadronic Journal*, 2001, v. 24, 609.
7. Van Vlaenderen K.J. arXiv: physics/0305098.
8. Waser A. Quaternions in electrodynamics. AW-verlag, 2000.
9. Monstein C. and Wesley J.P. *Europhysics Letters*, 2002, v. 59, 514.
10. Ignatiev G.F. and Leus V.A. In: *Instantaneous Action at a Distance in Modern Physics: Pro and Contra*, Nova Science, Hauppage (NY), 1999, 203.

On the New Gauge Transformations of Maxwell's Equations

Arbab I. Arbab

Department of Physics, Faculty of Science, University of Khartoum, P.O. 321, Khartoum 11115, Sudan
Department of Physics and Applied Mathematics, Faculty of Applied Sciences and Computer, Omdurman Ahlia University, P.O. Box 786, Omdurman, Sudan

E-mail: aiarbab@uofk.edu; arbab_ai@yahoo.com

We have found new gauge transformations that are compatible with Maxwell's equations and Lorentz gauge. With these transformations, we have formulated the electrodynamic equations that are shown to be invariant. New generalized continuity equations are derived that are also compatible with Maxwell's equations. Moreover, we have shown that the electromagnetic wave travels with speed of light in vacuum or a medium with free charge or current if the generalized continuity equations are satisfied. Magnetic monopoles don't show up in ordinary experiments because the Lorentz force acting on the magnetic charge is zero.

1 Introduction

Maxwell's equations describing the electric ($\vec{E}$) and magnetic ($\vec{B}$) fields reveal that when these fields are written in terms of a vector and scalar potentials, the equations of motion of these potential are generally solutions of wave equation with a source term. However, there is no unique way to define these potentials. A set of new potentials satisfying the Lorentz gauge can be solutions as well. Thus, Maxwell's equations are also invariant under these gauge transformations. Maxwell's equations are invariant under Lorentz transformation. Since the motion of charged particles is governed by the continuity equation, Maxwell's equations determine the motion of the charged particles in conformity with this equation.

Using quaternions, we have recently shown that Maxwell's equations can be written as a single quaternionic equation (Arbab and Satti, 2009 [1]). It is a wave equation. This immediately shows that the electromagnetic fields are waves. Similarly, by writing the continuity equation in a quaternionic form, we have shown that this equation yields three set of equations. We call these equations the generalized continuity equations (GCEs). Besides, we have found that the magnetic field arised from the charge motion (with speed $\vec{v}$) acted by an electric field is given by $\vec{B} = \frac{\vec{v}}{c^2} \times \vec{E}$. Because of this feature, the magnetic monopoles postulated by Dirac (Dirac, 1931 [2]) couldn't show up, because the Lorentz force component acting on this magnetic charge vanishes (Moulin, 2001 [3], Wolfgang, 1989 [4]). Hence, magnetic monopole can only be detected indirectly.

In the present paper, we have introduced new gauge transformations that leave Maxwell's equations, Lorentz gauge and the continuity equations invariant. Moreover, we know that according to Maxwell's theory the electromagnetic fields travel with speed of light in vacuum, i.e., when no free charge or current exists. However, in our present formulation, we have shown that the electromagnetic fields travel with speed of light in vacuum or free charged medium if the GCEs are satisfied.

2 Continuity equation

The flow of any continuous medium is governed by the continuity equation. The quaternionic continuity equation reads, (Arbab and Satti, 2009 [1]),

$$\tilde{\vec{\nabla}}\,\tilde{J} = \left[-\left(\vec{\nabla}\cdot\vec{J} + \frac{\partial\rho}{\partial t} \right) \frac{i}{c} \left(\frac{\partial \vec{J}}{\partial t} + \vec{\nabla}\rho c^2 \right) + \vec{\nabla}\times\vec{J} \right] = 0\,, \quad (1)$$

where

$$\tilde{\vec{\nabla}} = \left(\frac{i}{c}\frac{\partial}{\partial t}, \vec{\nabla} \right), \qquad \tilde{J} = \left(i\rho c, \vec{J} \right). \quad (2)$$

This implies that

$$\vec{\nabla}\cdot\vec{J} + \frac{\partial\rho}{\partial t} = 0\,, \quad (3)$$

$$\vec{\nabla}\rho + \frac{1}{c^2}\frac{\partial\vec{J}}{\partial t} = 0\,, \quad (4)$$

and

$$\vec{\nabla}\times\vec{J} = 0\,. \quad (5)$$

We call Eqs. (3)–(5) the *generalized continuity equations* (GCEs). Equation (5) states the current density $\vec{J}$ is irrotational.

In a covariant form, Eqs. (3)–(5) read

$$\partial_\mu J^\mu = 0\,, \qquad N_{\mu\nu} \equiv \partial_\mu J_\nu - \partial_\nu J_\mu = 0\,. \quad (6)$$

Notice that the tensor $N_{\mu\nu}$ is an antisymmetric tensor. It is evident from Eq. (6) that Eqs. (3)–(6) are Lorentz invariant. Now differentiate Eq. (3) partially with respect to time and use Eq. (4), we obtain

$$\frac{1}{c^2}\frac{\partial^2\rho}{\partial t^2} - \nabla^2\rho = 0\,. \quad (7)$$

Similarly, take the divergence of Eq. (4) and use Eq. (3), we obtain

$$\frac{1}{c^2}\frac{\partial^2 \vec{J}}{\partial t^2} - \nabla^2 \vec{J} = 0\,, \tag{8}$$

where $\rho = \rho(\vec{r}, t)$ and $\vec{J} = \vec{J}(\vec{r}, t)$. Therefore, both the current density and charge density satisfy a wave equation propagating with speed of light. In covariant form, Eqs. (7) and (8) now read

$$\Box^2 J^\nu \equiv \partial_\mu \partial^\mu J^\nu = 0\,. \tag{9}$$

We remark that the GCEs are applicable to any flow whether created by charged particles or neutral ones.

3 Maxwell's equations

We have recently shown that quaternion equation (Arbab and Satti, 2009 [1])

$$\tilde{\Box}^2 \tilde{A} = \mu_0 \tilde{J}\,, \qquad \tilde{A} = \left(i\frac{\varphi}{c},\ \vec{A}\right) \tag{10}$$

yields the Maxwell's equations (Arbab and Satti, 2009 [1])

$$\vec{\nabla}\cdot\vec{E} = \frac{\rho}{\varepsilon_0}\,, \tag{11}$$

$$\vec{\nabla}\times\vec{E} + \frac{\partial \vec{B}}{\partial t} = 0\,, \tag{12}$$

$$\vec{\nabla}\times\vec{B} - \frac{1}{c^2}\frac{\partial \vec{E}}{\partial t} = \mu_0 \vec{J}\,, \tag{13}$$

and

$$\vec{\nabla}\cdot\vec{B} = 0\,. \tag{14}$$

The electric and magnetic fields are defined by the vector potential (A) and the scalar potential (φ) as follows

$$\vec{E} = -\vec{\nabla}\varphi - \frac{\partial \vec{A}}{\partial t}\,, \qquad \vec{B} = \vec{\nabla}\times\vec{A}\,, \tag{15}$$

such that the Lorentz gauge

$$\vec{\nabla}\cdot\vec{A} + \frac{1}{c^2}\frac{\partial \varphi}{\partial t} = 0\,, \tag{16}$$

is satisfied. We know that the electric and magnetic fields are invariant under the following gauge transformations

$$\vec{A}' = \vec{A} - \vec{\nabla}\chi\,, \qquad \varphi' = \varphi + \frac{\partial \chi}{\partial t}\,. \tag{17}$$

The invariance of the Lorentz gauge implies that

$$\frac{1}{c^2}\frac{\partial^2 \chi}{\partial t^2} - \nabla^2 \chi = 0\,. \tag{18}$$

The 4-vector potential, A_μ, can be written as

$$A_\mu = \left(\frac{\varphi}{c}, -\vec{A}\right)\,. \tag{19}$$

In a covariant form, Eq. (17) becomes

$$A'_\mu = A_\mu + \partial_\mu \chi\,. \tag{20}$$

Eq. (15) can be written in a covariant form as

$$F_{\mu\nu} = \partial_\mu A_\nu - \partial_\nu A_\mu\,. \tag{21}$$

In a covariant form, Maxwell's equations, Eqs. (11)–(14), read

$$\partial_\mu F^{\mu\nu} = \mu_0 J^\nu, \qquad \partial_\mu F_{\nu\lambda} + \partial_\nu F_{\lambda\mu} + \partial_\lambda F_{\mu\nu} = 0\,. \tag{22}$$

Notice however that if we take $\frac{\partial}{\partial t}$ of Eq. (12) and apply Eqs. (13) and (14), we get

$$\frac{1}{c^2}\frac{\partial^2 \vec{B}}{\partial t^2} - \nabla^2 \vec{B} = \mu_0\left(\vec{\nabla}\times\vec{J}\right)\,. \tag{23}$$

Now take the curl of both sides of Eq. (12) and apply Eqs. (11) and (13), we get

$$\frac{1}{c^2}\frac{\partial^2 \vec{E}}{\partial t^2} - \nabla^2 \vec{E} = -\frac{1}{\varepsilon_0}\left(\vec{\nabla}\rho + \frac{1}{c^2}\frac{\partial \vec{J}}{\partial t}\right). \tag{24}$$

We remark that, according to our GCEs, the electric and magnetic waves propagate with speed of light whether $\vec{J} = \rho = 0$ or not, as long as Eqs. (4) and (5) are satisfied.

In a covariant form, Eqs. (23) and (24) read

$$\Box^2 F_{\mu\nu} = \mu_0\left(\partial_\mu J_\nu - \partial_\nu J_\mu\right)\,. \tag{25}$$

This can be casted in the form

$$\partial^\alpha\left(\mu_0^{-1}\partial_\alpha F_{\mu\nu} + g_{\nu\alpha}J_\mu - g_{\mu\alpha}J_\nu\right) \equiv \partial^\alpha \mathcal{C}_{\alpha\mu\nu} = 0\,, \tag{26}$$

where

$$\mathcal{C}_{\alpha\mu\nu} = \mu_0^{-1}\partial_\alpha F_{\mu\nu} + g_{\nu\alpha}J_\mu - g_{\mu\alpha}J_\nu\,, \tag{27}$$

where $g_{\mu\nu}$ is the metric tensor. Notice that the current tensor $\mathcal{C}_{\alpha\mu\nu}$ is antisymmetric in the indices μ, ν and is a conserved quantity. Likewise the total momentum and energy of the electrodynamics system (fields + particles) is conserved, we found here that the total current of the system, one arising from the electromagnetic fields and the other from the particles motion, is conserved. The first term in Eq. (27) represents the electromagnetic current, the second term represents the electronic current and the last term represents the vacuum current (with negative sign) as suggested by Eq. (28).

4 New gauge transformations

Now we introduce the current density transformations (CDTs) for $\vec{J}$ and ρ, viz.,

$$\rho' = \rho + \frac{1}{c^2}\frac{\partial \Lambda}{\partial t}\,, \qquad \vec{J}' = \vec{J} - \vec{\nabla}\Lambda\,, \tag{28}$$

leaving the generalized continuity equations (GCEs) invariant. In a covariant form, Eq. (28) reads

$$J_\mu{}' = J_\mu + \partial_\mu \Lambda \,. \tag{29}$$

Applying this transformation in Eq. (6), one finds that

$$\partial_\mu (J^\mu + \partial^\mu \Lambda) = \partial_\mu J^{\mu\,\prime} = 0 \,, \qquad N'_{\mu\nu} = N_{\mu\nu} \,. \tag{30}$$

It is thus evident that the GCEs are invariant under the CDTs. Moreover, the application of the current transformation in the continuity equation, Eq. (3), yields

$$\frac{1}{c^2}\frac{\partial^2 \Lambda}{\partial t^2} - \nabla^2 \Lambda = -\left(\vec{\nabla}\cdot\vec{J} + \frac{\partial \rho}{\partial t}\right) \,. \tag{31}$$

We thus that $\vec{J}$ and ρ in the GCEs are not unique and any new set of $\vec{J}'$ and ρ' will lead to the same GCEs provided that Λ is gauged by Eq. (31). Since the right hand side of Eq. (31) vanishes, Λ is a solution of a wave equation traveling with speed of light in vacuum. This equation is similar to Eq. (18). Notice also that Eqs. (23) and (24) are invariant under the following CDTs

$$\rho' = \rho + \frac{1}{c^2}\frac{\partial \Lambda}{\partial t} \,, \quad \vec{J}' = \vec{J} - \vec{\nabla}\Lambda \,, \quad \vec{E}\,' = \vec{E}, \quad \vec{B}\,' = \vec{B} \,. \tag{32}$$

In a covariant form, these read

$$J'_\mu = J_\mu + \partial_\mu \Lambda \,, \qquad F'_{\mu\nu} = F_{\mu\nu} \,. \tag{33}$$

Now let us introduce new gauge transformations (NGTs) as follows

$$\vec{A}\,' = \vec{A} + \alpha \vec{J} \,, \;\; \varphi' = \varphi + \alpha \rho\, c^2 \,, \;\; \alpha = \mu_0 \lambda^2 \,, \;\; \lambda = \text{const.} \tag{34}$$

In a covariant form, Eq. (34) reads

$$A'_\mu = A_\mu + \alpha\, J_\mu \,, \tag{35}$$

so that the electromagnetic tensor

$$F'_{\mu\nu} = F_{\mu\nu} + \alpha\,(\partial_\mu J_\nu - \partial_\nu J_\mu) \,, \tag{36}$$

using Eq. (6), is invariant under the NGTs and hence, Maxwell's equations are invariant too. Moreover, notice that the Lorentz gauge

$$\vec{\nabla}\cdot\vec{A} + \frac{1}{c^2}\frac{\partial \varphi}{\partial t} = 0 \,, \qquad \text{or} \qquad \partial_\mu A^\mu = 0 \,, \tag{37}$$

is also invariant under the NGTs provided that the continuity equation, Eq. (3), is satisfied. The covariant derivative is defined by

$$D_\mu = \partial_\mu - \frac{ie}{\hbar}\, A_\mu \,. \tag{38}$$

The quantum electrodynamics Lagrangian of a particle of spinor ψ is given by

$$\mathcal{L} = \overline{\psi}\,(i\hbar\, c\, \gamma^\mu\, D_\mu - mc^2)\psi - \frac{1}{4\mu_0} F_{\mu\nu} F^{\mu\nu} \,. \tag{39}$$

so that the Eq. (39) is invariant under the local gauge transformation of the spinor ψ (Bjorken, 1964 [5]). In terms of this derivative, one has

$$F_{\mu\nu} = D_\mu A_\nu - D_\nu A_\mu \,, \tag{40}$$

and Maxwell's equations become

$$D_\mu F^{\mu\nu} = \mu_0 J^\nu, \quad D_\mu F_{\nu\lambda} + D_\nu F_{\lambda\mu} + D_\lambda F_{\mu\nu} = 0 \,. \tag{41}$$

Upon using Eq. (6), Eq. (41) is invariant under NGTs. Applying the NGTs into the above Lagrangian yields

$$\mathcal{L}' = \mathcal{L} + \alpha\, J_\mu J^\mu \,. \tag{42}$$

The current density is defined by $J^\mu = ec\,\overline{\psi}\gamma^\mu\psi$. This extra interaction term has already appeared in the Fermi theory of beta decay. It is written in the form $\frac{G_F}{\sqrt{2}} J_\mu J^\mu$, i.e., $\alpha = \frac{G_F}{\sqrt{2}}$, where G_F is the Fermi constant. We anticipate that this term is related to the mass of the photon (propagator). This term term couldn't be added to the initial Lagrangian because, it breaks the ordinary gauge invariance. However, the NGTs could rise to the mass of the photon. It is something like Higg's mechanism that gives the elementary particles their masses. Such a term may be related to an interaction of two electrons closed to each other like in Cooper pairs in superconductivity. The behavior of superconductors suggests that electron pairs are coupling over a range of hundreds of nanometers, three orders of magnitude larger than the lattice spacing. These coupled electrons can take the character of a boson and condense into the ground state.

5 Symmetrized Maxwell's equation

Dirac was the first to suggest the possibility of a particle that carries magnetic charge. At the present time there is no experimental evidence for the existence of magnetic charges or monopoles. This can be formulated in the context of Maxwell's equations. Maxwell's equations can be written in a symmetric form by invoking the idea of monopole. Let us denote the magnetic charge by q_m and its density and current by ρ_m and J_m, so that symmetrized Maxwell's equations are written as follows

$$\vec{\nabla}\cdot\vec{E} = \frac{\rho_e}{\varepsilon_0} \,, \tag{43}$$

$$\vec{\nabla}\times\vec{E} = -\mu_0 \vec{J}_m - \frac{\partial \vec{B}}{\partial t} \,, \tag{44}$$

$$\vec{\nabla}\times\vec{B} = \mu_0 \vec{J}_e + \frac{1}{c^2}\frac{\partial \vec{E}}{\partial t} \,, \tag{45}$$

and

$$\vec{\nabla}\;\cdot\;\vec{B} = \mu_0 \rho_m \,. \tag{46}$$

Lorentz force will have the form (Moulin, 2001 [3])

$$F = q_e(\vec{E} + \vec{v}\times\vec{B}) + q_m(\vec{B} - \frac{\vec{v}}{c^2}\times\vec{E}) \,. \tag{47}$$

But since (Arbab and Satti, 2009 [1])

$$\vec{B} = \frac{\vec{v}}{c^2} \times \vec{E} \tag{48}$$

the Lorentz force does not affect the magnetic charge whether it exists or not. Hence, the magnetic monopole does not manifest its self via Lorentz force. The magnetic field generated by the charged particle is in such a way that it does not influence the magnetic charge. Note also that the magnetic field created by the charged particle does not do work because $\vec{v} \cdot \vec{B}$. The above symmetrized Maxwell's equations have the duality transformations, i.e., $\vec{E} \to \vec{B}$, $\vec{B} \to -\vec{E}$.

Using the vector identity $\vec{\nabla} \cdot (\vec{A} \times \vec{C}) = \vec{C} \cdot (\vec{\nabla} \times \vec{A}) - - \vec{A} \cdot (\vec{\nabla} \times \vec{C})$, it is interesting to notice that the divergence of Eq. (48) vanishes, viz.,

$$\vec{\nabla} \cdot \vec{B} = \vec{\nabla} \cdot \left(\frac{\vec{v}}{c^2} \times \vec{E} \right) = \\ = \frac{1}{c^2} \left[\vec{E} \cdot (\vec{\nabla} \times \vec{v}) - \vec{v} \cdot (\vec{\nabla} \times \vec{E}) \right] = 0, \tag{49}$$

for a motion with constant velocity, where $\vec{\nabla} \times \vec{v} = 0$ and $\vec{v}$ is perpendicular to $\vec{\nabla} \times \vec{E}$.

6 The Biot-Savart law

We can now apply Eq. (48) to calculate the magnetic field acted on the electron in Hydrogen-like atoms. This magnetic field is produced by the moving electron due to the presence of an electric field created by the nucleus at a distance r, as seen by the electron. Therefore,

$$\vec{B} = \frac{\vec{v}}{c^2} \times \vec{E}\,, \tag{50}$$

where $\vec{E}$ is the electric produced by the nucleus at the electron site. The magnetic field due to a single moving charged particle (q) is given by the Biot-Savart law as

$$\vec{B} = \frac{\mu_0}{4\pi} \frac{q\,\vec{v} \times \vec{r}}{r^3}\,. \tag{51}$$

Comparing Eq. (50) with Eq. (51) and using the fact that $\mu_0 \varepsilon_0 c^2 = 1$, one gets

$$\vec{E} = \frac{q}{4\pi\varepsilon_0} \frac{\vec{r}}{r^3} \tag{52}$$

which is the familiar definition of the electric field of a single charged particle. Hence, Eq. (50) is one variant of Biot-Savart law. This law was not included in the original formulation of Maxwell's theory. Hence, Maxwell's equations were missing this law and thus were incomplete.

Since the electric field produced by the nucleus is perpendicular to the electron velocity, Eq. (50) yields

$$B = \frac{v}{c^2} E\,. \tag{53}$$

But for Hydrogen-like atoms

$$E = \frac{1}{4\pi\varepsilon_0} \frac{Ze}{r^2}\,, \tag{54}$$

so that one has

$$B = \frac{Zev}{4\pi\varepsilon_0 r^2}\,. \tag{55}$$

In terms of the orbital angular momentum (L) where $L = mvr$, one has

$$\vec{B} = \frac{Ze}{4\pi\varepsilon_0 mr^3} \vec{L}\,. \tag{56}$$

However, this is the same equation that is obtained using the Biot-Savart law. This is a remarkable result, and suggests that the relation $\vec{B} = \frac{\vec{v}}{c^2} \times \vec{E}$ is truly fundamental in electrodynamics. This term gives rise to the spin-orbit interaction described by

$$E_{\text{int}} = \frac{1}{4\pi\varepsilon_0} \frac{Ze^2}{m_e^2 c^2 r^3}\, \vec{S} \cdot \vec{L}\,. \tag{57}$$

A factor of $1/2$ correcting the above expression is introduced by Thomas leading to

$$E_{\text{int}} = \frac{1}{8\pi\varepsilon_0} \frac{Ze^2}{m_e^2 c^2 r^3}\, \vec{S} \cdot \vec{L}\,. \tag{58}$$

We now use the Biot-Savart law to demonstrate that $\vec{\nabla} \cdot \vec{B} = 0$. This law is written in the form

$$\vec{B} = \frac{\mu_0}{4\pi} \int \frac{\vec{J}(\vec{r}\,') \times (\vec{r} - \vec{r}\,')}{|\vec{r} - \vec{r}\,'|^3}\, d^3 r'\,. \tag{59}$$

Using the vector identity $\vec{\nabla} \cdot (\vec{A} \times \vec{C}) = \vec{C} \cdot (\vec{\nabla} \times \vec{A}) - - \vec{A} \cdot (\vec{\nabla} \times \vec{C})$, one has

$$\vec{\nabla} \cdot \int \left(\frac{\vec{J}(\vec{r}\,') \times (\vec{r} - \vec{r}\,')}{|\vec{r} - \vec{r}\,'|^3} \right) d^3 r' = \\ = \int \frac{(\vec{r} - \vec{r}\,')}{|\vec{r} - \vec{r}\,'|^3} \cdot \left(\vec{\nabla} \times \vec{J} \right) d^3 r' - \int \vec{J} \cdot \left(\vec{\nabla} \times \frac{(\vec{r} - \vec{r}\,')}{|\vec{r} - \vec{r}\,'|^3} \right) d^3 r'. \tag{60}$$

Because of Eq. (5) and the fact that the curl of any pure radial function is zero, i.e. $\vec{\nabla} \times (f(r)\,\hat{r}) = 0$, the first and the second term vanish, so that above equation yields

$$\vec{\nabla} \cdot \vec{B} = 0\,. \tag{61}$$

Now let us calculate the magnetic field at a distance r from the wire produced by an infinitely long wire carrying a current I . Using Ampere's law, this is given by

$$B = \frac{\mu_0 I}{2\pi r}\,. \tag{62}$$

However, using Eqs. (50) and (51) and the fact that $I\,t = q$ and $\vec{v}$ is perpendicular to $\vec{r}$, one finds that the magnetic

field sets up at a point P at a distance r is *not* instantaneous, but reaches after a passage of time

$$\Delta t = \frac{2r}{v}\,. \tag{63}$$

Placing a detector at a distance r from the wire, one can measured this time experimentally. $2\,r$ is the round trip distance covered by the mediator (photon) traveling with speed v to send the magnetic induction at a point P. This exhibits the causal behavior associated with the wave disturbance. This shows that an effect observed at the point r at time t is caused by the action of the source a distant r away at an earlier or retarded time $t' = t - r/c$.The time r/c is the time of propagation of the disturbance from the source to the point r. Because of this Maxwell's equations satisfy the causality principle. Notice that this magnetic field is not changing with time. This may help understand that photons are emitted and absorbed by electron continuously, asserting that the electromagnetic interaction is exchanged by a mediator, as advocated by the quantum field theory.

7 Concluding remarks

We have shown in this paper the importance of the new gauge transformations, and how they leave Maxwell's equations invariant. These are the continuity equations, the current-density transformations and the current-gauge field transformations. According to Noether's theorem, invariance of a Lagrangian under any transformation will give rise to a conserved quantity. Hence, we trust that there must be some deep connections of these transformations with other electrodynamics phenomena. We emphasize here how the relation $\vec{B} = \frac{\vec{v}}{c^2} \times \vec{E}$ is important in calculating magnetic fields produced by moving charged particle. This equation was missing in the derivation of Maxwell's equations. Note that this field is always perpendicular to the velocity of the particle, i.e., $\vec{v} \cdot \vec{B} = 0$. We have also found that $\vec{B} = \frac{\vec{v}}{c^2} \times \vec{E}$ is equivalent to Biot-Savart law. Thus, the quaternionic form of Maxwell's equations generalizes the ordinary Maxwell's equations and unified the Biot-Savart law with other electromagnetic laws. The magnetic charge (monopole) proposed by Dirac could exist in principle, but it doesn't feel the electromagnetic force. The generalized continuity equations are in agreement with Newton's second law of motion. Moreover, we have obtained the Euler and energy conservation equations from the quaternionic Newton's law. Application of these new gauge transformations in quantum field theory will be one of our future endeavor.

Acknowledgments

I would like to thank F. Amin for the enlightening and stimulating discussion.

Submitted on December 06, 2008 / Accepted on December 13, 2008

References

1. Arbab A.I. and Satti Z.A. *Progress in Physics*, 2009, v. 1, 8.
2. Dirac P.A.M. *Proc. Roy. Soc.*, 1931, v. A133, 60.; Dirac P.A.M. *Phys. Rev.*, 1948, v. 74, 817.
3. Moulin F. *Nuovo Cimento*, 2001, v. 116B, 869.
4. Wolfgang R. *Am. J. Phys.*, 1989, v. 57, 993.
5. Bjorken J.D. and Drell S.D. *Relativistic Quantum Mechanics*, McGraw-Hill Book Company, 1964.

Introducing the Table of the Elements of Anti-Substance, and the Theoretical Grounds to It

Albert Khazan
E-mail: albkhazan@.gmail.com

Herein we study how the Hyperbolic Law acts in the Periodic Table of Elements, in each of the four quadrants of the plane "molecular mass X — contents of element Y". It is shown that the symmetry of the equation $Y = K/X$ is permitted only in the 1st and 2nd quadrants. The negative numerical values on the X-axis, and also $K < 0$, testify that the 2nd quadrant should contain the elements and compounds of anti-substances.

1 Introduction

As can be seen in [1–4], our method has produced hyperbolas located in the first quadrant. At the same time, their second branches have not been investigated from the point of view of the hyperbolic law in the Periodic Table of Elements.

Its essence is reflected in the fact that in any chemical compound with molecular mass X referred to one gram-atom of a defined element K, its maintenance Y represents the equilateral hyperbola $Y = K/X$ whose top is located on the valid axis located in a corner at 45 degrees with respect to the abscissa in the positive direction.

2 Mathematical substantiation. A principle of symmetry

For any element $K > 0$ there is only one hyperbola consisting of two branches (in the first and the third quadrants). Hyperbolas with various values K cannot be imposed against each other. At each point of a hyperbola, there are coordinates according to the equation $XY = K$ where X and Y can have not only positive values, but also negative values. If we identify the set of hyperbolas at various values K, they can wholly fill the area of the rectangular corner XOY (the first quadrant). In mathematics, the two branches of an equilateral hyperbola are symmetric with respect to each other. The valid axis passes through the tops located in the first and third quadrants, and also through the center of symmetry. The normal to it is an imaginary axis, and also an axis of symmetry around which it is possible to combine both quadrants.

3 The comparative analysis of equilateral hyperbolas in the first and third quadrants

Let's consider the hyperbolas of Beryllium, Chromium, Mercury, and the last element identified by us, which we shall call 155 and which is represented in Fig. 1. Apparently, the ordinate of the curves is equal to unity, while the abscissa is 600. The tops of the curves are on the valid axis which is perpendicular to the imaginary axis, while their curvature decreases with the growth of molecular mass. These properties have been considered in detail in our previous works for the first quadrant, in which $Y = K/X$ (where $X > 0, Y > 0$).

If these hyperbolas are constructed in the coordinates $X < 0, Y < 0$, (at $K > 0$), they will take the place of the second branches and settle down in the third quadrant. Hence, the properties of these equilateral hyperbolas, proceeding from mathematical concepts, except for one, can be completely found. It is impossible to combine these curves in two quadrants as the axes X and Y have different names and, accordingly, we see that the scales are caused by chemical conditions.

This discrepancy can be excluded if we take advantage of the factor of scaling $M = 20.2895$ described in a previous work [1]. In a Fig. 2 the same hyperbolas in the coordinates transformed by means of M are shown: $X' = X/M$, $Y' = YM$. Apparently, the form and properties of the hyperbolas after transformation remain unchanged and prove the mathematical principles.

If now around an imaginary axis we make the third and the first quadrants overlap, it is possible to see that there is nearly full concurrence among the curves and valid axes (Fig. 3). However, there is some increase in the ordinates because the abscissa in Fig. 2 possesses a slightly higher value than that of the ordinate, which is easy to notice from the position of circles designating the second branches. It has no basic value since the initial scales of the coordinate axes are naturally various upon their schematic construction. Therefore, the corner of the valid axis seems to be less than 45 degrees though its equation is given by the equality $Y = X$. This fact is due to the scale of coordinate axes only. At identical values of X and Y, the tangent of the corner of an inclination of the valid axis of an equilateral hyperbola is equal to 1, while, at the same time, its top is defined as a root square of K and corresponds to the equality $X_0 = Y_0$.

It is necessary to note also that all the established laws apply extensively to adjacent hyperbolas of the kind given by $Y = 1 - KX$ [2].

4 Discussion of results

On the basis of our results, it is possible to draw a conclusion that the properties of hyperbolas described by $K = XY$, which is in first quadrant, prove to be true. The same holds for those in the third quadrant, where $K = (-X)(-Y)$. Hence,

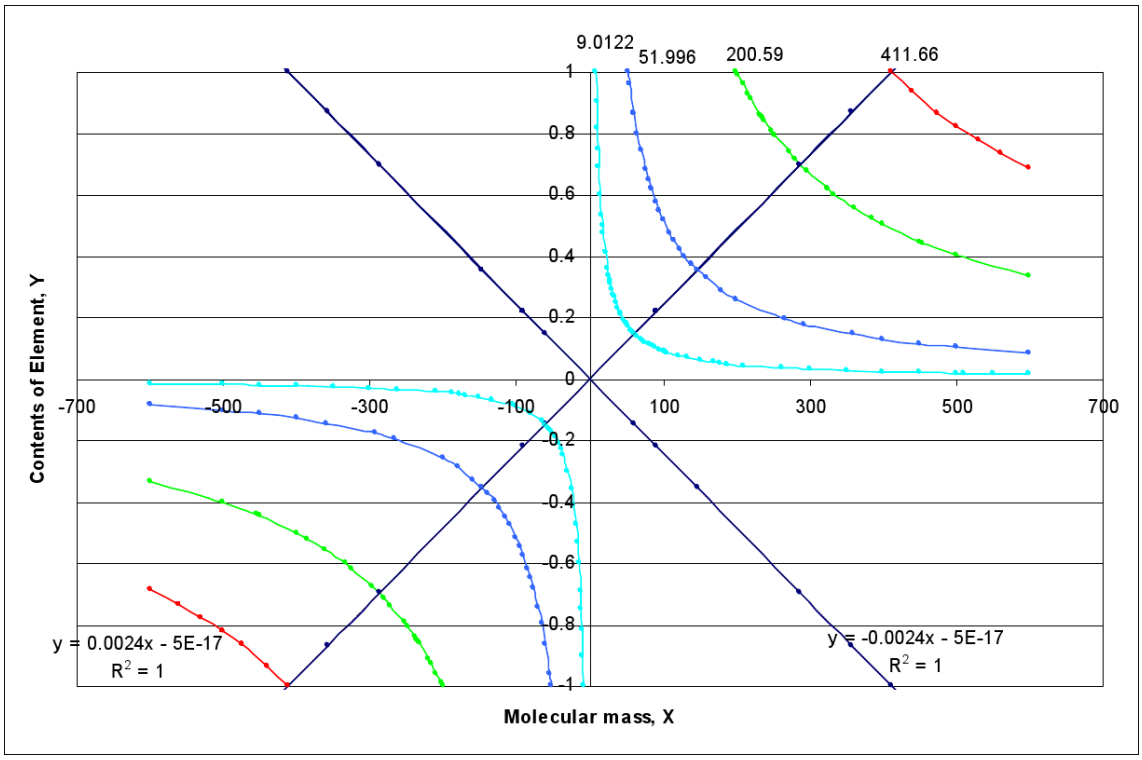

Fig. 1: Dependence of the contents of Be, Cr, Hg, No. 155 from molecular mass of the compounds.

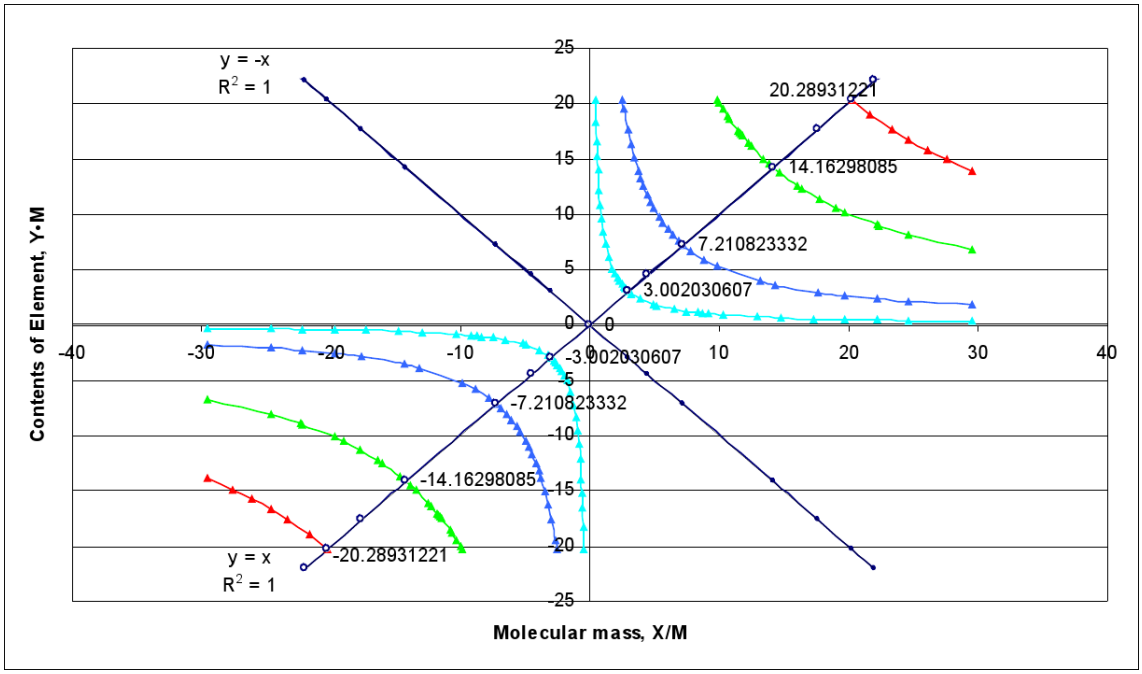

Fig. 2: Dependence of the contents of Be, Cr, Hg, No. 155 from molecular mass of the compounds, using the scaling coefficient M.

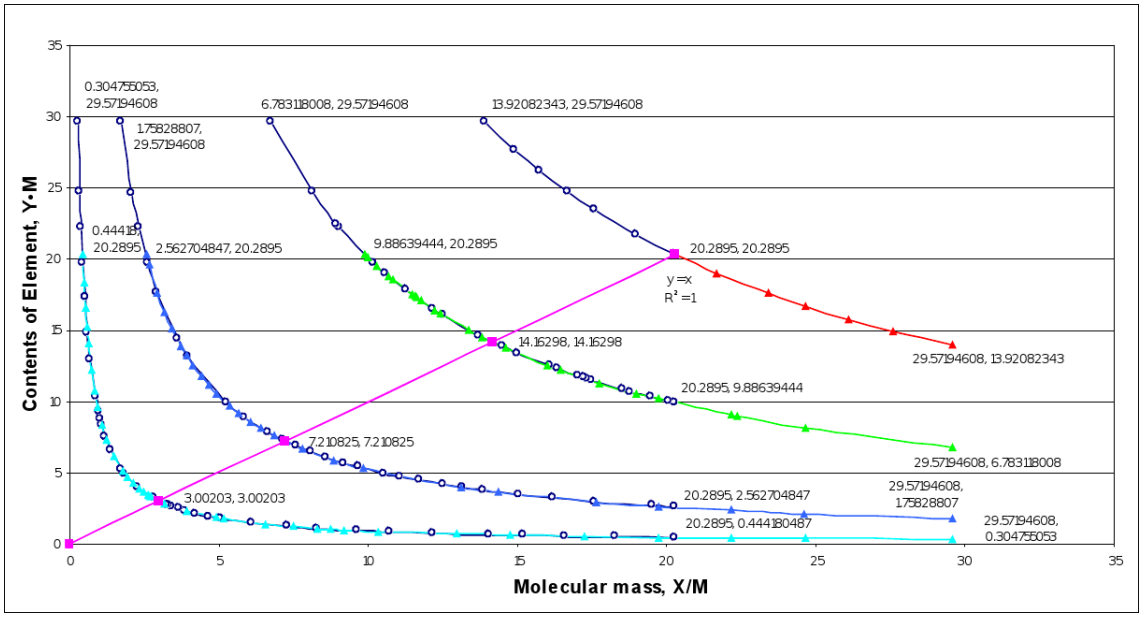

Fig. 3: The scale of the axes X and Y are numerically like each other, while the divisions of the scales are different. So, if a division is 3.075 in the axis X, while it is 1.75 in the axis Y. Under 60, the corner of the real axis gives 45°.

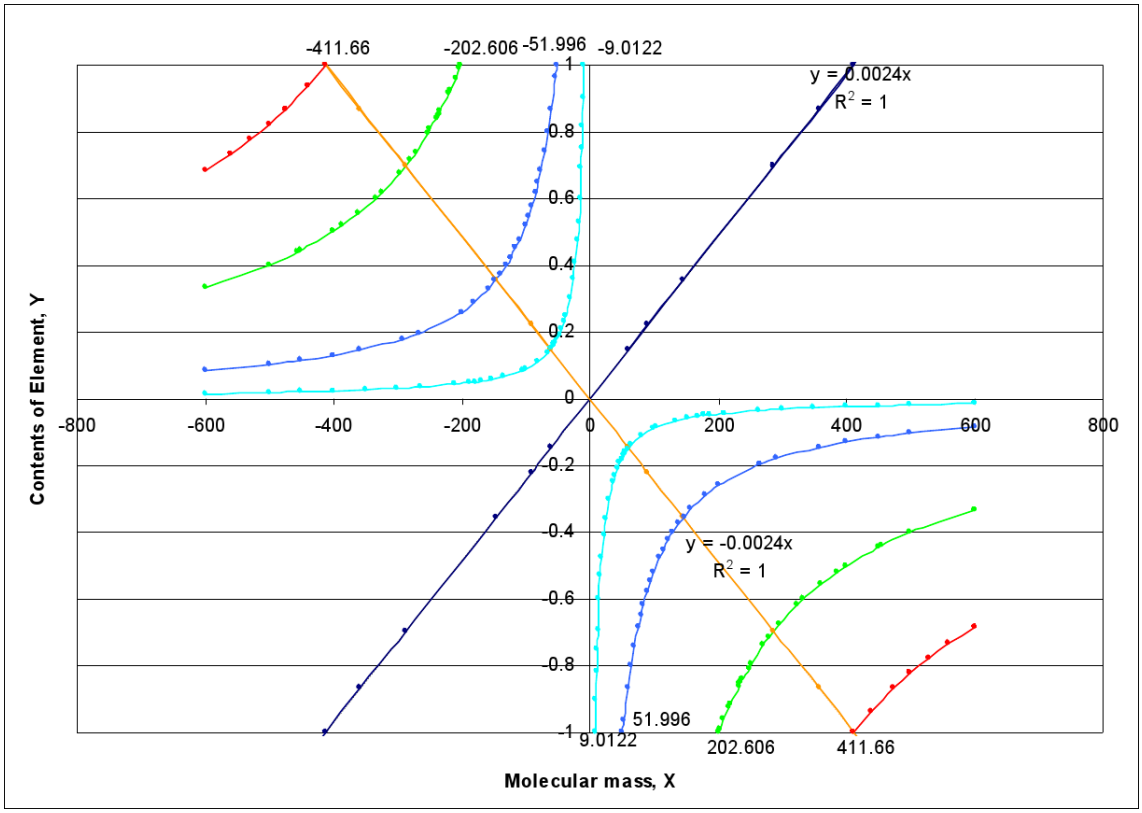

Fig. 4: Dependence of the contents of Be, Cr, Hg, No. 155 from molecular mass of the compounds in the 2nd and 4th quadrants.

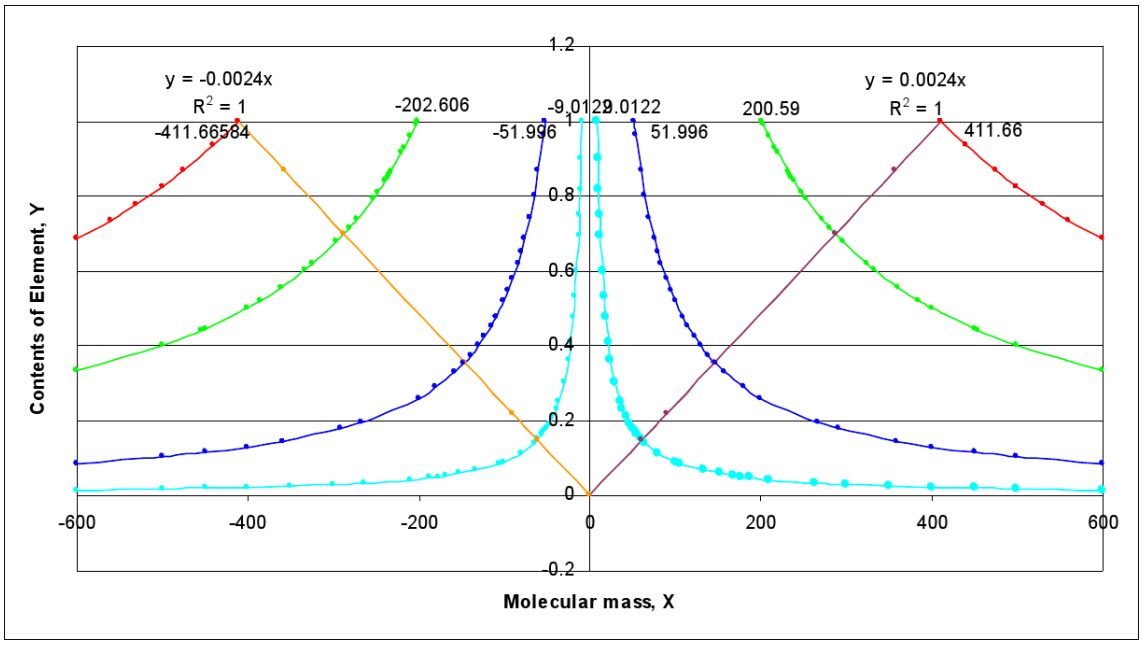

Fig. 5: Dependence of the contents of Be, Cr, Hg, No. 155 from molecular mass of the compounds in the 1st and 2nd quadrants.

1 H -	2A 2											3A 13	4A 14	5A 15	6A 16	7A 17	2 He -
3 Li -	4 Be -	3B 3	4B 4	5B 5	6B 6	7B 7	8	9	10	1B 11	2B 12	5 B -	6 C -	7 N -	8 O -	9 F -	10 Ne -
11 Na -	12 Mg -											13 Al -	14 Si -	15 P -	16 S -	17 Cl -	18 Ar -
19 K -	20 Ca -	21 Sc -	22 Ti -	23 V -	24 Cr -	25 Mn -	26 Fe -	27 Co -	28 Ni -	29 Cu -	30 Zn -	31 Ga -	32 Ge -	33 As -	34 Se -	35 Br -	36 Kr -
37 Rb -	38 Sr -	39 Y -	40 Zr -	41 Nb -	42 Mo -	43 Tc -	44 Ru -	45 Rh -	46 Pd -	47 Ag -	48 Cd -	49 In -	50 Sn -	51 Sb -	52 Te -	53 I -	54 Xe -
55 Cs -	56 Ba -	57-71	72 Hf -	73 Ta -	74 W -	75 Re -	76 Os -	77 Ir -	78 Pt -	79 Au -	80 Hg -	81 Tl -	82 Pb -	83 Bi -	84 Po -	85 At -	86 Rn -
87 Fr -	88 Ra -	89-103	104 Rf -	105 Db -	106 Sg -	107 Bh -	108 Hs -	109 Mt -	110 Ds -	111 Rg -	112 Uub -	113 Uut -	114 Uuq -	115 Uup -	116 Uuh -	117 Uus -	118 Uuo -

Lantanoids (upper row) and Actinoids (lower row)

57 La -	58 Ce -	59 Pr -	60 Nd -	61 Pm -	62 Sm -	63 Eu -	64 Gd -	65 Tb -	66 Dy -	67 Ho -	68 Er -	69 Tm -	70 Yb -	71 Lu -
89 Ac -	90 Th -	91 Pa -	92 U -	93 Np -	94 Pu -	95 Am -	96 Cm -	97 Bk -	98 Cf -	99 Es -	100 Fm -	101 Md -	102 No -	103 Lr -

8th period

119 -	120 -	121 -	122 -	123 -	124 -	125 -	126 -	127 -	128 -	129 -	130 -	131 -	132 -	133 -	134 -	135 -	136 -
137 -	138 -	139 -	140 -	141 -	142 -	143 -	144 -	145 -	146 -	147 -	148 -	149 -	150 -	151 -	152 -	153 -	154 -
155 -																	

s-block	alkaline metals and alkaline earth metals
d-block	transit metals
p-block	metals, metaloids and non-metals
f-block	lantanoids, actinoids
Short dash is signed in the Table for anti-elements	

Table 1: Eight periods of the Table of Substance and Anti-Substance.

the action of the Hyperbolic Law covers also an area of negative values of coordinate axes covering 155.

We recall the construction of hyperbolas at $K < 0$ (Fig. 4). Therefore, it has been established that in the second and the fourth quadrants of the hyperbolas, the same laws hold, which have also been established by us for the first and the third quadrants. It is caused by the fact that the equilateral hyperbolas have equal parameters on the module, but opposite in sign, namely, they are mutually interfaced and so possess identical properties. Therefore, proceeding from the chemical concepts, they can be symmetric only after changing the scale of the axes X, Y. Thus, referring to their congruence, unlike other mathematical conditions: curves coincide in the field of action of the factor M. Outside, its one hyperbola is generated as the abscissa increases, while the second corresponds to the increase in ordinate, not changing the direction of a curve. As it has appeared, absolute symmetry is available only on the axes X and Y.

Because in the third and fourth quadrants, a negative ordinate (a degree of transformation of a substance) cannot occur in Nature, we shall consider only quadrants 1 and 2.

From Fig. 5 it is seen that for $K > 0$ and $K < 0$ the congruence of hyperbolas and their valid axes are imposed against each other.

Corresponding to such symmetry, there is a question about the observation of chemical conditions. In the first quadrant, they have been considered in detail and do not cause doubts. In the second case (at $K < 0$) the abscissa is negative, and the ordinate is positive. Here the degree of transformation Y defined as the mass of an element (of one gram-atom), with respect to the corresponding molecular mass, is given by $Y = K/(-X)$, or, in other words, $K = (-X)Y$. From the point of view of mathematics, this result is fair. At the same time, physicists are in need of further necessary elaboration from the point of view of chemistry.

5 Substances and anti-substances

It is known that a Substance consists of atoms containing protons, neutrons, and electrons. An Anti-Substance differs only by the prefix "anti". In terms of chemical condition, all substances are divided into simple and complex (chemical compounds). They can be organic and inorganic.

As the Hyperbolic Law in the Periodic Table has been proved for hyperbolas of the first quadrant, there arises an idea to apply it also to the second quadrant. As the basis for this purpose, the quadrants are symmetric and the maintenance of elements in connection (Y) has a positive value. The difference consists only in those abscissas with opposite signs. But it is possible only when the molecular mass of a chemical compound has a minus sign. If, in the first quadrant, we arrange all possible hyperbolas around 155 inclusively, nothing prevents us from making the same apply to the second quadrant. Hence, in it there are substances with a minus sign, i.e., anti-substances constructed of anti-particles (similar to the substances in the first quadrant). With respect to mass, they are similar to a proton, neutron and, electron, only with an opposite (minus) sign.

From this it follows that it is possible to construct Table 1 (similar to the Periodic Table [3]) for the elements of anti-substances. For example, the known synthesized elements (their hyperbolas are more exact): anti-hydrogen, anti-deuterium, and anti-helium occupy symmetric places in both quadrants.

6 Conclusions

On the basis of symmetry with application of the Hyperbolic Law in the Periodic Table of Elements, the existence of anti-substances has been indirectly proved. As well, the construction of the various hyperbolas in the second quadrant and in the Table has been shown to be similar to that of the Periodic Table of Substances. It is clear that the third and fourth quadrants cannot be (directly) applied to calculation in the field of chemistry because the negative degree of transformation of substances does not exist.

Hence, it is now possible to draw a conclusion that the Hyperbolic Law established by us in the Periodic Table of Elements is generally true for the characteristics of not only substances, but also those of anti-substances. It also allows us to calculate all nuclear masses up to the last element (anti-element).

Submitted on December 04, 2008 / Accepted on December 23, 2008

References

1. Khazan A. Upper limit in the Periodic System of Elements. *Progress in Physics*, 2007, v. 1, 38–41.
2. Khazan A. Effect from Hyperbolic law in the Periodic Table of Elements. *Progress in Physics*, 2007, v. 2, 83–86.
3. Khazan A. Upper limit of the Periodic Table and synthesis of super heavy elements. *Progress in Physics*, 2007, v. 2, 104–109.
4. Khazan A. The rôle of the element Rhodium in the hyperbolic law of the Periodic Table of Elements. *Progress in Physics*, 2008, v. 3, 56–62.

Aspects of Stability and Quantum Mechanics

Robert Carroll

University of Illinois, Urbana, IL 61801, USA
E-mail: rcarroll@math.uiuc.edu

We comment on some work of Ruslov and Vlasenko indicating how stable Hamiltonian systems can be quantized under certain assumptions about the perturbations.

1 Introduction

In [7] we indicated some results of Rusov and Vlasenko [56, 57] involving Hamiltonian stability and quantization which we summarize here with a somewhat different interpretation. In [56, 57] (which are the same modulo typos and conclusions) one indicates how the work of Chetaev [9–11] (based in particular on classical results of Poincaré [52] and Lyapunov [39]) allow one to relate stability of classical systems to quantum mechanics in certain situations. We review here some of the arguments (cf. also [7, 55, 60] for additional material on the Poincaré-Chetaev equations).

One recalls that holonomic systems involve an agreement of the degrees of freedom with the number of independent variables. Then following [9] consider a holonomic system with Hamiltonian coordinates

$$\frac{dq_j}{dt} = \frac{\partial H}{\partial p_j};\ \frac{dp_j}{dt} = -\frac{\partial H}{\partial q_j} \tag{1.1}$$

and think of perturbations $(\mathbf{1A})$ $q_j = q_j(t) + \xi_j$ and $p_j = p_j(t) + \eta_j$. Denoting then $q_j \sim q_j(t)$ and $p_j \sim p_j(t)$ one has

$$\left.\begin{aligned} \frac{d(q_j+\xi_j)}{dt} &= \frac{\partial H(t, q_i+\xi_i, p_i+\eta_i)}{\partial p_j} \\ \frac{d(p_j+\eta_j)}{dt} &= -\frac{\partial H(t, q_i+\xi_i, p_i+\eta_i)}{\partial q_j} \end{aligned}\right\}. \tag{1.2}$$

Expanding and using (1.1) gives

$$\left.\begin{aligned} \frac{d\xi_j}{dt} &= \sum\left(\frac{\partial^2 H}{\partial p_j \partial q_i}\,\xi_i + \frac{\partial^2 H}{\partial p_j \partial p_i}\,\eta_i\right) + X_j \\ \frac{d\eta_j}{dt} &= -\sum\left(\frac{\partial^2 H}{\partial q_j \partial q_i}\,\xi_i + \frac{\partial^2 H}{\partial q_j \partial p_i}\,\eta_i\right) + Y_j \end{aligned}\right\}, \tag{1.3}$$

where the X_j, Y_j are higher order terms in ξ, η. The first approximations (with $X_j = Y_j = 0$) are referred to as Poincaré variational equations. Now given stability questions relative to functions Q_s of (t, q, p) one writes

$$x_s = Q_s(t, q_i+\xi_i, p_i+\eta_i) - Q_s(t, q_i, p_i) = \\ = \sum\left(\frac{\partial Q_s}{\partial q_i}\xi_i + \frac{\partial Q_s}{\partial p_i}\eta_i\right) + \cdots \tag{1.4}$$

which implies

$$\frac{dx_s}{dt} = \sum\left(\frac{\partial Q'_s}{\partial q_i}\xi_i + \frac{\partial Q'_s}{\partial p_i}\eta_i\right) + \cdots \tag{1.5}$$

where

$$Q'_s = \frac{\partial Q_s}{\partial t} + \sum\left(\frac{\partial Q_s}{\partial q_i}\frac{\partial H}{\partial p_i} - \frac{\partial Q_s}{\partial p_i}\frac{\partial H}{\partial q_i}\right). \tag{1.6}$$

Given $1 \leqslant s \leqslant 2k$ and $1 \leqslant i, j \leqslant k$ one can express the ξ_i, η_i in terms of x_s and write $(\mathbf{1B})$ $(dx_s/dt) = X_s$ (normal form) with $X_s(0) = 0$. For equations $(\mathbf{1B})$ with $1 \leqslant s \leqslant n$, for sufficiently small perturbations ϵ_j, ϵ'_j one assumes there exists some system of initial values x_{s0} with $\sum x_{s0}^2 < A$ for an arbitrarily small A (with perturbations ϵ_j, $\epsilon'_j \leqslant E_j$, E'_j). Further for arbitrarily small E_j, E'_j one assumes it is possible to find A as above such that there exists one or more values ϵ_j, ϵ'_j with absolute values $\leqslant E_j$, E'_j. Under these conditions the initial values of x_s play the same role for stability as the ϵ_j, ϵ'_j and one assumes this to hold. One assumes also convergent power series for the X_s etc. Then Lyapunov stability means that for arbitrary small A there exists λ such that for all perburbations x_{s0} satisfying $\sum x_{s0}^2 \leqslant \lambda$ and for all $t \geqslant t_0$ one has $\sum x_s^2 < A$ (i.e. the unperturbed motion is stable). Next one considers $t \geqslant t_0$ and $\sum x_s^2 \leqslant H$ and looks for a sign definite (Lyapunov) function V (with $V' = \partial_t V + \sum_1^n X_j(\partial V/\partial x_j)$ then sign definite of opposite sign or zero). If such a function exists the unperturbed motion is stable (see [9] for proof).

We pick up the story now in [10] where relations between optics and mechanics are also illuminated (but not considered here). Take a holonomic mechanical system with coordinates q_i and conjugate momenta p_i with n degrees of freedom. Assume the holonomic constraints are independent of time and the forces acting on the system are represented by a potential function $U(q_i)$. Let $(\mathbf{1C})$ $T = \frac{1}{2}\sum_{i,j} g_{ij}p_i p_j$ denote the kinetic energy where the $g_{ij} = g_{ji}$ are not dependent explicitly on time. Hamilton's equations have the form

$$2T = \sum g_{ij}\frac{\partial S}{\partial q_i}\frac{\partial S}{\partial q_j} = 2(U+E) \tag{1.7}$$

where E represents a kinetic energy constant (the sign of U is changed in Section 2). Here the integral of (1.7) is $(\mathbf{1D})$ $S(q_i, \alpha_i) + c$ with the α_i constants and $(\mathbf{1E})$ $||\partial^2 S/\partial q_i \partial \alpha_j|| \neq 0$ while $(\mathbf{1F})$ $E = E(\alpha_i)$. According to the Hamilton-Jacobi theory the general solution of the motion equations is given via $(\mathbf{1G})$ $p_i = \partial S/\partial q_i$ and $\beta_i = -t(\partial E/\partial \alpha_i) + \partial S/\partial \alpha_i$ where the β_i are constants. In order to determine a stable

solution one looks at the Poincaré variations

$$\left.\begin{aligned}\frac{d\xi_i}{dt} &= \sum_j \left(\frac{\partial^2 H}{\partial q_j \partial p_i}\,\xi_j + \frac{\partial^2 H}{\partial p_j \partial p_i}\,\eta_j\right)\\ \frac{d\eta_i}{dt} &= -\sum \left(\frac{\partial^2 H}{\partial q_j \partial q_i}\,\xi_j + \frac{\partial^2 H}{\partial p_j \partial q_i}\,\eta_j\right)\end{aligned}\right\}, \tag{1.8}$$

where H should be defined here via $(\mathbf{1H})$ $H = T - U$. For a stable unperturbed motion the differential equations for Poincaré variations (1.8) must be reducible by nonsingular transformation to a system of linear differential equations with constant coefficients all of whose characteristic values must be zero (recall that the Lyapunov characteristic value $X[f]$ of f is $X[f] = -\overline{\lim_{t\to\infty}}[\log(|f(t)|)/t]$ — cf. [39,40]). In such perturbed motion, because of $(\mathbf{1G})$ one has (recall $p_i \sim \partial S/\partial q_i$)

$$\eta_i = \sum_j \frac{\partial^2 S}{\partial q_i \partial q_j}\,\xi_j \;\; (i = 1, \cdots, n)\,. \tag{1.9}$$

Hence

$$\frac{d\xi_i}{dt} = \sum_{j,s} \xi_s \frac{\partial}{\partial q_s}\left(g_{ij}\frac{\partial S}{\partial q_j}\right) \;\; (i = 1, \cdots, n)\,. \tag{1.10}$$

Note here that (1.8) involves $\sum g_{ij}p_i p_j - U$ so

$$(\bigstar)\;\; \frac{\partial H}{\partial p_i} = \sum g_{ij}p_j; \quad \frac{\partial H}{\partial q_j} = \sum \frac{\partial g_{ij}}{\partial q_j}\,p_i p_j - \frac{\partial U}{\partial q_j}$$

and (1.10) says

$$(\bigstar\bigstar)\;\; \frac{d\xi_i}{dt} = \sum \xi_s \left(\frac{\partial g_{ij}}{\partial q_s}\frac{\partial S}{\partial q_j} + g_{ij}\frac{\partial^2 S}{\partial q_s \partial q_j}\right) = \\ = \sum \xi_s \frac{\partial g_{ij}}{\partial q_s}\frac{\partial S}{\partial q_j} + \sum g_{ij}\eta_j\,.$$

The second term here is $[\partial^2 H/\partial p_i \partial p_j]\,\eta_j$ and we want to identify the term $\xi_s(\partial g_{ij}/\partial q_s)(\partial S/\partial q_j)$ with $\partial^2 H/\partial q_s \partial p_i \xi_s$. However we can see that $\partial U/\partial p_i = 0$ so $\xi_s(\partial^2 H/\partial q_s \partial p_i) = \xi_s(2\partial^2 T/\partial q_s \partial p_i) = \xi_s(\partial g_{ij}/\partial q_s)p_j$ confirming (1.10). Here the q_i, α_i are represented by their values in an unperturbed motion. Now for a stable unperturbed motion let (1.10) be reducible by a nonsingular linear transformation $(\mathbf{1I})$ $x_i = \sum \gamma_{ij}\xi_j$ with a constant determinant $\Gamma = ||\gamma_{ij}||$. If ξ_{ir} $(r = 1, \cdots, n)$ are a normal system of independent solutions of (1.10) then $(\mathbf{1J})$ $x_{ir} = \sum_j \gamma_{ij}\xi_{jr}$ will be the solution for the reduced system. For a stable unperturbed motion all the characteristic values of the solutions x_{ir} $(i = 1, \cdots, n)$ are zero and consequently

$$||x_{sr}|| = C^* = ||\gamma_{sj}||\,||\xi_{jr}|| = \\ = \Gamma\, C \exp\left[\int \sum \frac{\partial}{\partial q_i}\left(g_{ij}\frac{\partial S}{\partial q_j}\right) dt\right]. \tag{1.11}$$

Consequently for a stable perturbed motion (cf. [9,39,40])

$$\sum \frac{\partial}{\partial q_i}\left(g_{ij}\frac{\partial S}{\partial q_j}\right) = 0\,. \tag{1.12}$$

2 Stability approach

Following Rusov and Vlasenko one writes an integral of the Hamilton-Jacobi (HJ) equation in the form $(\mathbf{2A})$ $S = f(t, q_i, \alpha_i) + A$ $(i = 1, \cdots, n)$ with the α_i arbitrary constants. The general solution is then $(\mathbf{2B})$ $p_i = \partial S/\partial q_i$ with $\beta_i = \partial S/\partial \alpha_i$ where the β_i are new constants of integration. The canonical equations of motion are $dq_i/dt = \partial H/\partial p_i$ and $dp_i/dt = -\partial H/\partial q_i$ where H is the Hamiltonian and under perturbations of the α_i, β_i one writes $\xi_i = \delta q_i = q_i - q_i(t)$ and $\eta_i = \delta p_i = p_i - p_i(t)$ and derives equations of first approximation

$$\left.\begin{aligned}\frac{d\xi_i}{dt} &= \sum \frac{\partial^2 H}{\partial q_j \partial p_i}\,\xi_j + \sum \frac{\partial^2 H}{\partial p_j \partial p_i}\,\eta_j\\ \frac{d\eta_i}{dt} &= -\sum \frac{\partial^2 H}{\partial q_j \partial q_i}\,\xi_j - \sum \frac{\partial^2 H}{\partial p_j \partial q_i}\,\eta_j\end{aligned}\right\} \tag{2.1}$$

as in (1.8). By differentiating in t one obtains then $(\mathbf{2C})$ $C = \sum(\xi_s\eta_s' - \eta_s\xi_s')$ where C is a constant. Also for given ξ_s, η_s there is always at least one solution ξ_s', η_x' for which $C \neq 0$. Stability considerations (as in form. 1.1) then lead via $(\bigstar)$ $\eta_i = \sum(\partial^2 S/\partial q_i \partial q_j)\xi_j$ and $(\mathbf{2D})$ $H = \frac{1}{2}\sum g_{ij}p_i p_j + U = T + U$ to

$$\frac{d\xi_i}{dt} = \sum \xi_s \frac{\partial}{\partial q_s}\left(g_{ij}\frac{\partial S}{\partial q_j}\right) \tag{2.2}$$

(note in Section 1 $H \sim T - U$ following [10] but we take now $U \to -U$ to agree with [56, 57] — the sign of U is not important here). According to [56, 57], based on results of Chetaev [10] (as portrayed in Section 1), it results that $L = \sum(\partial/\partial q_i)[g_{ij}(\partial S/\partial q_j)] = 0$ (as in form. 1.12) for stability (we mention e.g. [9–11,39,40,45] for stability theory, Lyapunov exponents, and all that).

REMARK 2.1. One also notes in [56, 57] that a similar result occurs for $(\bullet\bullet)$ $U \to U^* = U + Q$ for some natural Q and the stability condition (1.12) itself provides the natural introduction of quantization (see below). The perturbation relation in (1.9) is irrelevant to this feature (which we did not realize previously) and the quantum perturbations introduced via Q will satisfy the Heisenberg uncertainty principle as desired (cf. [3]). ■

Now one introduces a function $(\mathbf{2E})$ $\psi = A\exp(ikS)$ in (1.12) where k is constant and A is a real function of the coordinates q_i only. There results

$$\frac{\partial S}{\partial q_j} = \frac{1}{ik}\left(\frac{1}{\psi}\frac{\partial \psi}{\partial q_j} - \frac{1}{A}\frac{\partial A}{\partial q_j}\right) \tag{2.3}$$

so that (1.12) becomes

$$\sum_{i,j} \frac{\partial}{\partial q_i}\left[g_{ij}\left(\frac{1}{\psi}\frac{\partial \psi}{\partial q_j} - \frac{1}{A}\frac{\partial A}{\partial q_i}\right)\right] = 0\,. \tag{2.4}$$

On the other hand for the perturbed motion (with $U \to$

$\to U^* = U + Q$) the HJ equation can be written in the form

$$\frac{1}{2k^2}\sum_{i,j} g_{ij}\left[\frac{1}{\psi}\frac{\partial\psi}{\partial q_i} - \frac{1}{A}\frac{\partial A}{\partial q_i}\right]\left[\frac{1}{\psi}\frac{\partial\psi}{\partial q_j} - \frac{1}{A}\frac{\partial A}{\partial q_j}\right] = \\ = \partial_t S + U + Q \quad (2.5)$$

with $\partial_t S$ obtained via (**2E**). Adding (2.4) and (2.5) yields

$$\frac{1}{2k^2\psi}\sum_{i,j}\frac{\partial}{\partial q_i}\left(g_{ij}\frac{\partial\psi}{\partial q_j}\right) - \frac{1}{2k^2 A}\sum_{i,j}\frac{\partial}{\partial q_i}\left(g_{ij}\frac{\partial A}{\partial q_j}\right) - \\ - \frac{1}{k^2 A}\sum_{i,j} g_{ij}\frac{\partial A}{\partial q_j}\left(\frac{1}{\psi}\frac{\partial\psi}{\partial q_i} - \frac{1}{A}\frac{\partial A}{\partial q_i}\right) - \\ - \frac{1}{ikA\psi}\left[A\,\partial_t\psi - \psi\,\partial_t A\right] - U - Q = 0 \quad (2.6)$$

as a necessary stability condition (in the first approximation). Note (2.6) will not contain Q if A is defined via

$$\frac{1}{2k^2 A}\sum_{i,j}\frac{\partial}{\partial q_i}\left(g_{ij}\frac{\partial A}{\partial q_j}\right) + \\ + \frac{i}{kA}\sum_{i,j} g_{ij}\frac{\partial A}{\partial q_j}\frac{\partial S}{\partial q_i} - \frac{1}{ikA}\,\partial_t A + Q = 0 \quad (2.7)$$

which means

$$\left.\begin{aligned} Q &= -\frac{1}{2k^2 A}\sum_{i,j}\frac{\partial}{\partial q_i}\left(g_{ij}\frac{\partial A}{\partial q_j}\right) \\ \partial_t A &= -\sum_{i,j} g_{ij}\frac{\partial A}{\partial q_j}\frac{\partial S}{\partial q_i} \end{aligned}\right\}. \quad (2.8)$$

A discussion of the physical content of (2.8) appears in [56, 57] and given (2.8) the stability condition (2.6) leads to

$$\frac{i}{k}\,\partial_t\psi = -\frac{1}{2k^2}\sum_{i,j}\frac{\partial}{\partial q_i}\left(g_{ij}\frac{\partial\psi}{\partial q_j}\right) + U\psi \quad (2.9)$$

which is of course a SE for $k = 1/\hbar$ (this is the place where quantum mechanics somewhat abruptly enters the picture — see Remark 2.1). In fact for kinetic energy (**2F**) $T = \frac{1}{2m}\left[p_1^2 + \right.$ $\left. + p_2^2 + p_3^2\right]$ (2.9) leads to

$$Q = -\frac{\hbar^2}{2m}\frac{\Delta A}{A};\;\; \partial_t A = -\frac{1}{m}\sum\frac{\partial A}{\partial x_j}\,p_j;\;\; k = \frac{1}{\hbar} \quad (2.10)$$

and (2.9) becomes (note $A = A(q)$)

$$i\hbar\,\partial_t\psi = -\frac{\hbar^2}{2m}\Delta\psi + U\psi\,. \quad (2.11)$$

Going backwards now put the wave following function $\psi = A\exp(iS/\hbar)$ in (2.11) to obtain via (1.12) and (2.8) the Bohmian equations

$$\left.\begin{aligned} \partial_t A &= -\frac{1}{2m}\left[A\Delta S + 2\nabla A\cdot\nabla S\right] = -\nabla A\cdot\frac{\nabla S}{m} \\ \partial_t S &= -\left[\frac{(\nabla S)^2}{2m} + U - \frac{\hbar^2}{2m}\frac{\nabla A}{A}\right] \end{aligned}\right\}, \quad (2.12)$$

where the quantum potential QP is naturally identified.

If one writes now $P = \psi\psi^* = A^2$ then (2.12) can be rewritten in a familiar form

$$\left.\begin{aligned} &\partial_t P = -\nabla P\cdot\frac{\nabla S}{m} \\ &\partial_t S + \frac{(\nabla S)^2}{2m} + U - \\ &\qquad - \frac{\hbar^2}{4m}\left[\frac{\Delta P}{P} - \frac{1}{2}\frac{(\nabla P)^2}{P^2}\right] = 0 \end{aligned}\right\}. \quad (2.13)$$

That P is indeed a probability density is "substantiated" via a least action of perturbation principle attributed to Chetaev [11, 56, 57] which involves (**2G**) $\int Q|\psi^2|dV = \min$ where dV is a volume element with $\int|\psi|^2 dV = 1$ and this condition is claimed to be necessary for stability (one assumes that the influence of perturbative forces generated by Q is proportional to the density of trajectories $|\psi|^2 = A^2$ and dV cannot be a phase space volume element as stated in [56,57]). Write now, using (**2D**)

$$Q = -\partial_t S - U - T = -\partial_t S - U - \frac{1}{2}\sum g_{ij}\frac{\partial S}{\partial q_i}\frac{\partial S}{\partial q_j}\,. \quad (2.14)$$

Then if (**2E**) holds one can show that

$$\frac{1}{2}\sum g_{ij}\frac{\partial S}{\partial q_i}\frac{\partial S}{\partial q_j} = -\frac{1}{2k^2\psi^2}\sum g_{ij}\frac{\partial\psi}{\partial q_i}\frac{\partial\psi}{\partial q_j} + \\ + \frac{1}{2k^2 A^2}\sum g_{ij}\frac{\partial A}{\partial q_i}\frac{\partial A}{\partial q_j} + \frac{ik}{2k^2 A^2}\sum g_{ij}\frac{\partial A}{\partial q_i}\frac{\partial S}{\partial q_j}\,. \quad (2.15)$$

Then for the first term on the right side substitute its value from the first stability condition (2.4), then insert this relation into (2.15) and put the result into the equation (2.14) corresponding to the variational principle; the result is then (2.6) and consequently the resulting structure expression and the necessary condition for stability coincide with (2.8) and (2.9). This leads one to conclude that stability and (Bohmian) quantum mechanics are two complementary procedures of Hamiltonian theory. The authors cite an impressive list of references related to experimental work related to the analysis in [56,57].

3 The quantum potential

From Sections 1–2 we have seen that a stable Hamiltonian system as indicated gives rise to a quantum Schrödinger equation with quantum potential Q. It seems therefore appropriate to examine this in the light of other manifestations of the QP as in e.g. [3–6, 16–19, 24, 26–28, 30, 36, 37, 53]. We note that following [4] one can reverse some arguments involving the exact uncertainty principle (cf. [3,26–28,53]) to show that any SE described by a QP based on $|\psi|^2 = P$ can be modeled on a quantum model of a classical Hamiltonian H perturbed by a term H_Q based on Fisher information, namely

$$H_Q = \frac{c}{2m}\int\frac{(\nabla P)^2}{P}\,dx = \frac{c}{2m}\int P(\delta p)^2, \quad (3.1)$$

where $\delta p = \nabla P/P$. This does not of course deny the presence of "related" $x \sim q$ oscillations $\delta x \sim \delta q$ and in fact in Olavo [49] (cf. also [3]) Gaussian fluctuations in δq are indicated and related to δp via an exact uncertainty relation $(\mathbf{3A})$ $\overline{(\delta p)^2 \cdot (\delta q)^2} = \hbar^2/4$. We note that the arguments establishing exact uncertainty stipulate that the position uncertainty must be entirely characterized by $P = |\psi|^2$ (cf. [3,26–28,53]). Thus the quantum potential generates the quantum perturbations δp and these are essentially unrelated to the $\delta p \sim \eta_i$ of (1.9).

REMARK 3.1. We recall here [29] (cf. also [54]) were it is shown that quantum mechanics can be considered as a classical theory in which a Riemannian geometry is provided with the distance between states defined with natural units determined via Planck's constant (which is the inverse of the scalar curvature). ■

REMARK 3.2. In [2] one shows that non-relativistic quantum mechanics for a free particle emerges from classical mechanics via an invariance principle under transformations that preserve the Heisenberg inequality. The invariance imposes a change in the laws of classical mechanics corresponding to the classical to quantum transition. Some similarities to the Nottale theory of scale relativity in a fractal spacetime are also indicated (cf. [3, 8, 47, 48]). There are relations here to the Hall-Reginatto treatment which postulates that the non-classical momentum fluctuations are entirely determined by the position probability (as mentioned above). In Brenig's work one derives this from an invariance principle under scale transformations affecting the position and momentum uncertainties and preserving the Heisenberg inequality. One modifies the classical definition of momentum uncertainty in order to satisfy the imposed transformation rules and this modification is also constrained by conditions of causality and additivity of kinetic energy used by Hall-Reginatto. This leads to a complete specification of the functional dependance of the supplementary term corresponding to the modification which turns out to be proportional to the quantum potential. ■

REMARK 3.3. We note that in work of Grössing (cf. [6, 24]) one deals with subquantum thermal oscillations leading to momentum fluctuations $(\mathbf{3B})$ $\delta p = -(\hbar/2)(\nabla P/P)$ where P is a position probability density with $-\nabla \log(P) = \beta \nabla \mathcal{Q}$ for $\mathcal{Q}$ a thermal term (thus $P = c\exp(-\beta \mathcal{Q})$ where $\beta = 1/kT$ with k the Boltzman constant). This leads also to consideration of a diffusion process with osmotic velocity $\mathbf{u} \propto -\nabla \mathcal{Q}$ and produces a quantum potential

$$Q = \frac{\hbar^2}{4m}\left[\nabla^2 \tilde{\mathcal{Q}} - \frac{1}{D}\,\partial_t \tilde{\mathcal{Q}}\right] \tag{3.2}$$

where $\tilde{\mathcal{Q}} = \mathcal{Q}/kT$ and $D = \hbar/2m$ is a diffusion coefficient. Consequently (cf. [6] one has a Fisher information $(\mathbf{3C})$ $F \propto \beta^2 \int \exp(-\beta \mathcal{Q}(\nabla \mathcal{Q})^2 d^3x$. As in the preceeding discussions the fluctuations are generated by the position probability density and one expects a connection to (Bohmian) quantum mechanics (cf. [3, 12, 18, 19]). ■

REMARK 3.4. There is considerable literature devoted to the emergence of quantum mechanics from classical mechanics. There have also been many studies of stochastic and hydrodynamic models, or fractal situations, involving such situations and we mention in particular [1, 3–6, 8, 12, 13, 18–20, 23, 24, 26–28, 36, 37, 42–44, 46–49, 53, 58, 59, 61]; a survey of some of this appears in [3]. For various geometrical considerations related to the emergence question see also [14, 15, 25, 30–35, 51, 62] and in connection with chaos we cite e.g. [1, 25, 38, 41, 50, 51, 62, 63]. ■

Submitted on December 12, 2008 / Accepted on December 23, 2008

References

1. Benenti G., Casati G., and Strini G. Principles of quantum computation and information. Vols. 1 and 2. World Scientific, 2007.
2. Brenig L. *Jour. Phys. A*, 2007, v. 40, 4567–4584; arXiv: quant-ph/0608025.
3. Carroll R. Fluctuations, information, gravity and the quantum potential. Springer, 2006; On the quantum potential. Arima Publ., 2007.
4. Carroll R. *Teor. i Mat. Fiz.*, 2007, v. 152, 904–914.
5. Carroll R. *Prog. in Phys.*, 2007, v. 4, 22–24 and 2008, v. 1, 21–24 (preprinted in arXiV: math-ph/0703065 and 0710.4351); *Prog. in Phys.*, 2008, v. 2, 89–90 (preprinted in arXiv: math-ph/0712.3251).
6. Carroll R. arXiv: math-ph/0807.1320 and 0807.4158.
7. Carroll R. arXiv: math-ph/0808.2965.
8. Célérier M. and Nottale L. *Jour. Phys. A*, 2004, v. 37, 931; arXiv: hep-th/0112213 and 0210027.
9. Chetaev N. The stability of motion (Ustoichevost dvizhenia). Permagon, 1961; Theoretical mechanics. Mir-Springer, 1989.
10. Chetaev N. *Soviet Applied Math. and Mech.*, 1958, v. 22, 487–489.
11. Chetaev N. *Soviet Applied Math. and Mech.*, 1956, v. 20, 309–314; 1959, v. 23, 425–433; 1960, v. 24, 6–19, 23–32, 33–34.
12. Crowell L. Quantum fluctuations of spacetime. World Scientific, 2005.
13. Davidson M. *Jour. Math. Phys.*, 1979, v. 20, 1865–1869; arXiv: quant-ph/0112063, 0112076, 0112114, 0112099, 0112157, 0211097, and 0602211; *Annales L. de Broglie*, 2004, v. 29, 661–680.
14. Elitzur A., Dolev S., and Kolenda N. (Eds.). Quo vadis quantum mechanics. Springer, 2005.
15. Elze H. arXiv: gr-qc/0512016; quant-ph/0710.2765.
16. Frieden B. and Gatenby R. Exploratory data analysis using Fisher information. Springer, 2007.
17. Frieden B. Physics from Fisher information. Cambridge Univ. Press, 1998; Science from Fisher information. Springer, 2004.

18. Garbaczewski P. *Entropy*, 2005, v. 7, 253–299; *Jour. Stat. Phys.*, 2007, v. 123, 315–355.
19. Garbaczewski P. arXiv: cond-mat/0202463, 0211362, 0510533, 0706248, 0604538, and 0703147; quant-ph/0612151.
20. Gell-man M. and Tsallis C. Non-extensive entropy. Oxford Univ. Press, 2004.
21. de Gosson M. arXiv: quant-ph/0808.2774; Maslov classes, metaplectic representations, and Lagrangian quantization. Akad. Verlag, 1997.
22. de Gosson M. and Luef F. *Phys. Lett. A*, 2007, v. 364, 453–457.
23. Granik A. arXiv: quant-ph/0801.3311.
24. Grössing G. *Phys. Lett. A*, 2008, v. 372, 4556–4562; *Found. Phys. Lett.*, 2004, v. 17, 343–362; arXiv: quant-ph/0201035, 0205047, 0404030, 0410236, 0508079, and 0806.4462.
25. Gutzwiller M. Chaos in classical and quantum mechanics. Springer, 1990.
26. Hall M. and Reginatto M. *Jour. Phys. A*, 2002, v. 35, 3289–3303; *Fortschr. Phys.*, 2002, v. 50, 646–651; arXiv: quant-ph/0201084.
27. Hall M., Kumar K., and Reginatto M. *Jour. Phys. A*, 2003, v. 36, 9779–9794.
28. Hall M. arXiv: gr-qc/0408098, quant-ph/0007116; *Jour. Phys. A*, 2004, v. 37, 7799 and 9549 (preprinted in arXiv: quant-ph/0404123 and 0406054).
29. Heslot A. *Amer. Jour. Phys.*, 1983, v. 51, 1096–1102; *Phys. Rev. D*, 1985, v. 31, 1341–1348.
30. Hiley B. Quo vadis quantum mechanics. Springer, 2005, pp. 299–324.
31. Holland P. The quantum theory of motion. Cambridge Univ. Press, 1993.
32. 't Hooft G. arXiv: hep-th/0707.4568, quant-ph/0604008.
33. Isidro J., Santander J., and de Cordoba P.F. arXiv: hep-th/0808.2351 and 0808.2717; gr-qc/0804.0169.
34. Isidro J. arXiv: hep-th/0110151, 0204178, 0304175, 0407161, 0411015, and 0510075; quant-ph/0307172, 0310092, and 0407159.
35. Isidro J. and de Gosson M. arXiv: hep-th/0608087; quant-ph/0608093.
36. Kaniadakis G. arXiv: quant-ph/0112049.
37. Kaniadakis G. and Scarfone A. arXiv: cond-mat/0303334.
38. Klages R. Microscopic chaos, fractals, and transport in non-equilibrium statistical mechanics. World Scientific, 2007.
39. Lyapunov A. The general problem of stability of motion. Gostekhizdat, 1950; Princeton Univ. Press, 1947.
40. Malkin I. Theory of stability of motion. Gostekhizdat, 1952; Some problems in the theory of nonlinear oscillations. Gostekhizdat, 1956.
41. Magnitskij N. and Sidorov S. New methods for chaotic dynamics. World Scientific, 2006.
42. Nasiri S. arXiv: quant-ph/0511125.
43. Nasiri S., Sobouti Y., and Taati F. arXiv: quant-ph/0605129.
44. Nelson E. Quantum fluctuations. Princeton Univ. Press, 1985; Dynamical theory of Brownian motion. Princeton Univ. Press, 1967.
45. Nemytskii V. and Stepanov V. Qualitative theory of differential equations. Dover, 1989.
46. Nottale L. Fractal space-time and microphysics: Toward a theory of scale relativity. World Scientific, 1993.
47. Nottale L., Célérier M., and Lehner T. arXiv: hep-th/0407093.
48. Nottale L. and Célérier M. arXiv: quant-ph/0711.2418.
49. Olavo L. *Physica A*, 1999, v. 262, 197–214; 1999, v. 267, 260–302; *Phys. Rev. E*, 2001, v. 64, 036125.
50. Ott E. Chaos in dynamical systems. Cambridge Univ. Press, 2002.
51. Pettini M. Geometry and topology in Hamiltonian dynamics and statistical mechanics. Springer, 2007.
52. Poincaré H. New methods of celestial mechanics. Vols. 1–3. Dover, 1957.
53. Reginatto M. arXiv: quant-ph/9909065; gr-qc/0501030; *Phys. Rev. A*, 1998, v. 58, 1775–1778.
54. Rowe D., Ryman A., and Rosensteel G. *Phys. Rev. A*, 1980, v. 22, 2362–2373.
55. Rumyantsev V. *Soviet Applied Math. and Mech.*, 1996, v. 60, 899–909; 1994, v. 58, 373–386.
56. Rusov V. arXiv: quant-ph/0804.1427.
57. Rusov V. and Vlasenko D. arXiv: quant-ph/08064050.
58. Schuch D. *Inter. Jour. Quant. Chem.*, 1989, v. 23, 59–72; 1992, v. 42, 663–683.
59. Soubouti Y. and Nasiri S. *Inter. Jour. Mod. Phys. B*, 1993, v. 7, 3255–3272.
60. Stanuykovitch P., Kolesnikov S., and Moskovkin V. In: *Problems of Space, Time, and Matter Theory*, Atomizdat, 1968.
61. Tsekov R. *Jour. Phys. A*, 1995, v. 28, L557–L561; 2007, v. 40, 10945–10947; arXiv: quant-ph/07111442, 0803.4409, and 0808.0326.
62. Wyatt R. Quantum dynamics with trajectories. Springer, 2005.
63. Zaslavsky G. Hamilton chaos and fractional dynamics. Oxford Univ. Press, 2005.

On the Physical Model of the Phenomena Registered in the Experiments by Shnoll's Group and Smirnov's Group

Sergey A. Vasiliev

Scientific Research Institute of Exploration Geophysics VNII Geofizika (retired), Moscow 107140, Russia
Permanent address: 38 Nazliu Str., Palio Faliro, Athens 17564, Greece
E-mail: disput22@gmail.com

The study of experimental data leads to the conclusion about the existence of the fields of the Earth as not being of clear physical nature. The structure and properties of these fields on the Earth's surface are studied. These fields turn out to be related to the motions of matter and, in particular, to the internal motions of the Earth itself. Therefore, the fields may include precursors to earthquakes that conform to experiments. The disclosed statistical relations of seismicity with the planet configurations, sunrises and sunsets, and with the pulsar impact becomes logical. Other planets, the Sun and the Moon must possess the same fields.

1 Introduction

Nearly thirty years ago, Meidav and Sadeh [1] discovered the effect of pulsar CP1133 on seismicity that triggered the professionals' interest. Ya. B. Zeldovich immediately apprehended the potential meaning of this phenomenon. According to him, even if that message would be by ten per cent true, he would only engage himself with this issue. According to Weber, the energy of the pulsar gravitational waves is many orders of magnitude lower than that required for the detected pulsar effect on seismicity. The interest in this phenomenon gradually shrank to a nullity, mainly because this phenomenon had not acquired any reasonable interpretation. At about the same time, Ben-Menachem, the famous seismologist, detected a correlation between seismicity and sunrises-sunsets that could not be explained as well. As a consequence, the above Ben-Menachem's discovery was overridden, although he insisted that his experimental results were correct. Recently, Georgian seismologists have found a correlation between the planets' configuration and earthquakes [2]. Moreover, as it turned out, some distant planets rather than neighboring planets play a part in this correlation. T. Chernoglazova has disclosed a strong correlation between earthquakes and the coverings of the planets and the Sun by the Moon (in the sky). A. Ya. Lezdinsh has advanced further. He forecasts the epicenter, the time and the magnitude of the earthquakes at the same time for Kamchatka Peninsula by using the correlation between earthquakes and stellar bodies' positions relative to the Earth and the local horizon plane [3]. This method comes first in the open competition among many methods of earthquake forecast (with maximal magnitude error 0.4 point). At rises and settings, the upper and the lower culminations of the Sun, the Moon and the planets, Smirnov's detector (a specific gyroscope on a magnetic suspension) changes its average angular spin rate by 0.7–1.5% for a short period of time (generally, 1.5–3 minutes) [4–8]*. For instance, at the rises of Jupiter the gravitational effect on the detector is one and half billion times weaker than that of an observer moving around the detector†. However, the device responded to the planet but no to the observer. As in Refs. [1, 2, 3], here we again observe an effect of the planets on the motions in the Earth's region with a lack of the effective energy for such an event, and against all else, much more powerful effects. Smirnov's detector produces as well the anomalous signals, the strong earthquakes precursors for 2–10 days before strong earthquakes [9]. They are quite distinct from other signals due to their unusually high amplitude and extended duration (refer to Figs. 4 and 5 in Ref. [9]). Since Smirnov's detector indicates direction to the signal source as well, the perspective appears to find epicenters of the future strong earthquakes up to thousand kilometers off the detector that demands the labor-consuming but necessary forecast finalizing technique. Smirnov's and Shnoll's detectors respond to the same astronomical phenomena, but Shnoll's one shows variations not in angular velocity but in the G histogram shapes representing macroscopic fluctuations of the rates of physical processes‡. In their experiments, Shnoll's group [10–15] has studied G histograms for processes of different physical nature and different energy saturation, from radioactive decays and chemical reactions to the noises in gravitational antennas. Despite of the great differences in energy saturation of the above processes (forty orders of magnitude) their G histograms taken at the same time tend to look alike§. The effects of the Sun and the Moon on the G histograms have been disclosed. To put it differently, again a certain distant impact on the processes is disclosed in the absence of any accordance between the impact energy and the energies of the processes. According

*Developed by Kurchatov Institute of Atomic Energy and MEPHI.

†For proper calculation of the gravitational effect of planets, account must be taken of free falling of the Earth in an external gravity field.

‡Developed by Institute of Theoretical and Experimental Biophysics, Russian Academy of Science.

§More precisely, a probability increase of similar histograms occurrence is observed. For brevity's sake, this will be referred to as occurrence of similar histograms.

to S. E. Shnoll, the G histograms' shape variations are generated by space-time fluctuations, because, as pointed out, it is the only common factor for such different processes [14]. S. E. Shnoll has drawn attention to the important fact of the energy-free nature of the considered impacts [15]:

> "... The energy variation range for the processes under study equals tens of orders of magnitude. It is therefore clear that the "external force" that causes synchronous alteration of the histogram shapes is of the non-energy nature."

Recently, responding to my request, V. A. Zubov et al. (2008, Germany) have accordingly adjusted the technique of their experiments. As a consequence, their direct physical experiment has confirmed, at last, a significant impact of planets on the living matter on the Earth [20]. For instance, during the upper culmination of the Jupiter, the abrupt pulse variations in the mean molecular weight of potato biomatrix clusters, in terms of the number of the various clusters and their energy irradiation, were observed [20]:

> "During the Jupiter upper culmination the reliable picture of its effect on the potato biomatrix is disclosed. ... the Jupiter effect is unexpectedly strong during its culmination ... the commensurability of the planet and the Moon effects follows from the experimental data".

At least an approximate explanation of the above referred phenomena is in order. A physical model is created below as a logical consequence of the accumulated experimental material. The model allows us to approach the understanding of many of the described, seemingly paradoxical, facts. As long as the detectors are located on the Earth, as the unique planet, the effects of that can be studied in any direction relative to its center, whereas the effects of the other planets, the Sun and the Moon may be investigated on the Earth's orbit only. Shnoll's detector has been used in observations in various geographical regions, including the North Pole and Antarctica regions. Therefore our searching is based on the investigations of Shnoll's detector data and the corresponding impacts, mainly, of the Earth. This paper is based on the Refs. [16, 17].

2 Shnoll's detector data and the principles of their physical modeling

Initially the duration Dt of the histograms G was 1 hour. Presently, it has been reduced to less than a second. Let us denote the histogram with duration Dt confined to the time moment t as $G(t)$*. Let us denote the corresponding histograms from detectors A and B as $G_A(t)$ and $G_B(t)$, respectively. Using the detectors' data, observers can plot the graph of the probability of occurrence of the similar histogram shapes $G_B(t+\delta t^*)$ and $G_A(t)$ depending on the time shift δt^* and then seek a narrow peak (or peaks) of the probability increase and determine such time shift δt, at which a maximum peak occurs. (The peak width is usually equal to a few of the histograms durations Dt.) In what follows, the regularities of appearance of the similar histograms $G_B(t+\delta t)$ and $G_A(t)$ at the above maxima are studied depending on the time shift δt and on the detectors' locations. Let us conditionally denote the similarity of histograms as $G_B(t+\delta t) \approx G_A(t)$, and the coincidence of the histogram shapes as $G_B(t+\delta t) = G_A(t)$. The above equalities refer to the similarity of two histograms taken at the maxima of the aforesaid peaks, in the presence of these peaks, but not with respect to a random similarity of any pair of histograms. For brevity's sake only, the histograms $G_B(t+\delta t)$ and $G_A(t)$ similar at the above maxima denoted below shall simply be referred to as "similar histograms". A series of the cycles and the regularities in the occurrence of similar histograms has been determined. To understand the physical meaning of these cycles and regularities, the physical principles of their modeling should be established (listed below as enumerated notes).

Note 1: As mentioned above, the histogram shape varies with distance effects, at least, of the Sun and the Moon. In physics, the substance that transmits a distance effect is called a "field". Thus let us consider that the histogram shape is changed by some field† F (probably, of electromagnetic or gravitational origin). The field F may be multi-component (i.e. is composed of the sub-fields F_1, F_2, F_3, etc.) and many various sources of the field F may exist. To interpret Shnoll's detectors data, the following postulated rules will be used. The character of the field F impact on the detector is mapped into the histogram shape. The identical histogram shapes (at the maxima of the mentioned peaks) correspond to the identical impact character of the field F_i (where $i = 1, 2, 3, \dots$) from a single source, the histogram shapes at the mentioned maxima are not identical but only similar due to the different effects of the fields from others sources and/or other field components from the same source. Disclosed repetitions of similar histograms correspond to repetitions of the impact character of some field component F_i or of some field F. If one of the Moon, the Sun, and the Earth possesses a field F_i, then all of them possess this field‡. ■

According to Note 1, if the impact of the mentioned component on the detector is much stronger than other impacts, almost an identical histogram shape with almost a hundred percent probability should be observed. The Earth is surrounded by different celestial bodies. Of them, the highest variable impact on the Earth is caused by the Sun and the Moon. Their maximal impact should be expected when they are in the ray aimed at the Earth. Actually, during solar eclipses, several Shnoll's detectors located in different geo-

*For example, the time moment t may be the middle or the beginning of the $G(t)$ histogram.

†In the articles by Shnoll's team, a cloudy notion of some "structures" affecting the histograms is used. This one is used instead of the field notion. This one is not explained [15].

‡The fact that this statement is true becomes clear from the sub-section "About the reasons of the field beginning...".

graphical locations, produce at the same moment almost identical histograms with nearly a hundred percent probability [14]. This confirms the principles postulated in Note 1 and indicates also that the statistical properties of the macroscopic fluctuations, displayed by the histograms, are not random at all, but that they are distantly generated by celestial bodies, i.e. by their some field F. Thus an intensification of the impact of the field F (relative to the background) is displayed by the histograms through probability increase in the maxima of the above peaks. Therefore, through the histograms, one can judge about the character and relative strength of the impact of the field F and can also grade it using the probabilities at the maxima of the peaks. Then the field conception will start to possess the quantitative character. As far as the author knows, such dynamic investigations have not been performed yet. It is useful to perform them through a quantitative study of time and space distribution of the relative impact force, induced by each field component F_i from each source. For this purpose, localized observations at very short distances between the Shnoll detectors are most suitable [11]. According to experimental results, during the solar eclipse the above-mentioned peak's width is much shorter than the eclipse duration. Consequently, interaction between the field F from the Sun and the Moon at their junction is of a strongly marked, very short, splash-like character. Similar events happen during full-moon and new moon times [14].

Note 2: If an impact character on the detector is constant in time, then (in the absence of other impacts), according to Note 1, it induces histograms $G(t)$, whose shape is independent of time: $G_B(t+\delta t^*) = G(t)$ at any δt^*. As a consequence, there is no peak of histogram similarity at some definite time shift δt^*. Therefore, when the character of impact gradually becomes constant, the histogram similarity peak smears out gradually and disappears. Therefore, *the Shnoll technique based on the separation of the histogram similarity peaks is unable to identify impacts of constant character*. In this case, the Shnoll technique *gives the impression of an impact's absence, although the detector itself records both changing and constant impacts*. In the case of constant impact, another technique is required to investigate the near-zero temporal frequencies against the parameter δt^*. When a constant impact is considered in the background of a multiplicity of other changing impacts on the detector, conclusions remain the same, but the histogram shapes become rather similar than coincidental (this, of course, if a constant impact still remains visible in the presence of the other impacts). ■

Let $\{\mathrm{V}_d^m\}$ be the detector's movement parameters, where $m = 0, 1, 2, 3, \ldots$ and V_d^m is the m-th time derivative of the detector's speed V_d, $\mathrm{V}_d^0 \equiv \mathrm{V}_d$. The same set $\{\mathrm{V}_S^m\}$ denotes the movement's parameters of any object S.

Note 3: It is not excluded that the character of the impact on the detector is defined by both the field F and orientation O of some detector motion parameters $\mathrm{V}_{d,a}^m$ (belonging to a set $\{\mathrm{V}_d^m\}$), to be called active, relative to a ray L by which the field F arrives (similar to the case of a magnetic field and a moving electrical charge). The *force and character of the impact* may depend, of course, on the values of the motion parameters. Apparently, the active parameters $\mathrm{V}_{d,a}^m$ represent acceleration and/or acceleration derivative, and/or rate, etc. Let the field F, whose impact character depends also on the orientation O, be called the *second-type field* F_2 and be distinguished from the *first-type field* F_1, whose impact character is independent of the direction of the detector's motion parameter. If there is a dependence of the impacts on the motion parameters, let us consider the following: the Earth's field impact depends on the parameters of the detector's motion relative to the Earth, while the Sun's field impact depends on the parameters of the detector's motion relative to the Sun, etc. To put it differently, the impact of a field from some source depends on the detector's motion parameters relative to this source. The following question arises: whether or not the first and the second-type fields exist? ■

Generally, the experimental data will be studied in reference to a geocentric (GSC) and heliocentric (HSC) systems of coordinates. The GSC does not rotate relative to "motionless" stars. In the GSC, the Earth spins. In the GSC, let us determine the latitude φ and longitude θ of the Earth's surface points relative to the geographical Earth poles in the usual manner, but the meridian $\theta = \text{const}$ and the parallel $\varphi = \text{const}$ do not rotate relative to "motionless" stars. Let two detectors A and B be fixed on the Earth's surface and at time t in GSC have longitudes $\theta_A(t)$ and $\theta_B(t)$ and latitudes $\varphi_A(t)$ and $\varphi_B(t)$, respectively. For definiteness, if the detectors are located at different rotating geographical meridians, let us consider that the detector A is positioned ahead of detector B relative to the Earth's rotation direction. In the GSC system, detectors rotate about the Earth axis, moving along a motionless parallel given by $\varphi = \text{const}$.

According to the experiment [10, 11, 14], as the detector slides along the a motionless parallel $\varphi = \text{const}$, its histograms change, but the following equalities, which express the *effect of local sidereal time*, according to the terminology of experimentalists, stand:

$$G_B(t+\delta t_{ST}) \approx G_A(t) \text{ at } \varphi_A(t) = \varphi_B(t) = \text{const}, \quad (1)$$

$$G_B(t) \approx G_A(t) \text{ at } \theta_A(t) = \theta_B(t)\,, \quad (2)$$

$$G_A(t+T_{ST}) \approx G_A(t)\,, \quad (3)$$

where T_{ST} is the sidereal day, $\delta t_{ST} = t_{ST,A} - t_{ST,B}$, $t_{ST,A}$ and $t_{ST,B}$ are the local *sidereal* times at the locations of the detectors A and B, respectively. Sidereal day, T_{ST}, is the period of rotation of the Earth and the detectors in the GSC system about the Earth axis. In particular, in the GSC, at the moment $(t+T_{ST})$, the detector A returns to the same location, where it was at time t. In the GSC, when the detector is fixed at a geographical point on the Earth's surface, its parameters V_d^m are the same with the respective parameters $\mathrm{V}_d^{SPIN,m}$ of

the detector's fixation point's rotary (spin) motion about the Earth axis:

$$\mathrm{V}_d^m = \mathrm{V}_d^{SPIN,m}. \quad (4)$$

Obviously, the directions (and the values) of the parameters V_d^m of the detectors' rotary motion relative to the "motionless" stars are also repeated with the same period T_{ST} in the GSC system. The velocity V_d and its even order derivatives are directed along the tangent to the local parallel at the detector's location point. The odd-order derivatives of the rate V_d (including acceleration V_d^1) are directed along the local normal to the Earth's axis dropped from the detector's location point to the Earth axis. Therefore, in the GSC system, directions of the parameters V_d^m do not change along the meridians. In the GSC, the local sidereal times $t_{ST,A}$ and $t_{ST,B}$ unambiguously characterize the angle of detectors' rotation about the Earth axis relative to their initial position at the moment $t_{ST,A} = t_{ST,B} = 0$. In the GSC, the difference, δt_{ST}, represents a period of time, after which detector B arrives at the same place, where detector A was at the moment t. Therefore, by virtue of Note 1, the equalities (1)–(3) mean:

Statement 1: There are some fields F, whose summarized impact character at the Earth's surface points depends on the point location in the GSC, but not on time (equalities (1) and (3), and changes in the GSC along the motionless parallels and is constant along the motionless meridians of the Earth (formula 2). ■

For example, the effects (1)–(3) may be explained by the existence of the Earth's own field of the first type, not rotating in the GSC and changing along the motionless parallels but being constant along the motionless meridians of the Earth. The effects (1) and (3) may also be explained by the existence of an external field of the second type F_{2ext}, whose rays L_{2ext} are mutually parallel, and the field itself is constant at the Earth's orbit. According to Note 3, this shall lead to repetitions in the impact character of the field F_{2ext}, when the directions and magnitudes of the vectors V_d^m are repeated. By analogy, according to Note 3, the effect (2) can be caused by the Sun's field F_{2S}, of the second type, because the directions of the Sun rays and the parameters V_d^m along the Earth meridian do not virtually change, and, therefore, the angles between them do not change along this meridian as well. As can be seen, the use of only the local sidereal time effects gives multiple interpretations.

Just as the above, the effect of the *local solar time* has also been discovered experimentally [14] and is split into three equalities (detectors A and B are again fixed at the Earth's surface)

$$G_B(t + \delta t_S) \approx G_A(t) \text{ at } \varphi_A(t) = \varphi_B(t) = \text{const}, \quad (5)$$

$$G_B(t) \approx G_A(t) \text{ at } \theta_A(t) = \theta_B(t), \quad (6)$$

$$G_A(t + T_S) \approx G_A(t), \quad (7)$$

where T_S is the solar day; $\delta t_S = t_{S,A} - t_{S,B}$, $t_{S,A}$ and $t_{S,B}$ are the local *solar* times at the locations of the detectors A and B, respectively. The solar day, T_S, is the period of repetitions of the upper culmination of the Sun. By analogy, the effects of the local lunar time, the local planetary time, etc. may be introduced, but these effects have not been studied experimentally by Shnoll's group. Since the effects (5) and (7) include the local solar time, they obviously relate to the impacts of the Sun. Due to the Earth's motion along its orbit, the direction from the Earth to the Sun changes slightly, approximately by a degree per day. Therefore, the solar day is approximately 4 minutes longer than the sidereal day. The parameters V_d^m of the detector's motion relative to the Sun, i.e., in the HSC system, are composed of the detector's rotation relative to the Earth's axis (spin) and of its motion together with the Earth along its orbit. As a consequence, in the HSC system

$$\mathrm{V}_d^m = \mathrm{V}_d^{SPIN,m} + \mathrm{V}_d^{ORB,m}, \quad (8)$$

where $\mathrm{V}_d^{ORB,m}$ are the orbital motion parameters of the Earth and the detector. Despite the almost full coincidence of the formulae (1)–(3) and (5)–(7), their physical meaning is significantly different. Obviously, the orientation of the parameters $\mathrm{V}_d^{ORB,m}$ in relation to the Sun's ray, L_S, passing through the detector, does not change with time*. The orientation of parameters $\mathrm{V}_d^{SPIN,m}$ relative to the ray L_S, after a solar day T_S, is repeated with high accuracy. This repetition would have been exact, if the angle of the Earth axis to the ray L_S did not change during a solar day T_S, but as is known, it changes a little — by one fourth of a degree per day, approximately. Thereafter, the parameters of the spin motion of the detectors A and B at the times t and $t + \delta t_S$, respectively, have an almost equal orientation relative to the ray L_S. Therefore, by virtue of Note 3, the effects (5) and (7) can be explained by the existence of the Sun's field F_{2S} of the second type, almost or exactly cylindrically symmetrical relatively to the axis passing through the Earth's orbit center, and almost or exactly perpendicular to its plane. If, indeed, such the field F_{2S} does exist, its impact should be repeated almost or exactly everytime, when the orientation of the parameters $\mathrm{V}_d^{SPIN,m}$ relative to the ray L_S is repeated. This is really what happens according to the relations (5) and (7). The same effects could be explained in other ways. For example, by the repetitions of the total impact of the Sun's and Earth's fields, resulting from the repetitions of the angles between the solar ray L_S and the ray L_E of the Earth's own field radiated from the Earth's center or from its rotation axis. It is seen here again that the use of only the local solar time effects gives multiple interpretations.

Which field existence could be determined unambiguously? Let us answer this question using some other experiments. Experiments using collimators have the decisive meaning for answering the above question. As it turns out, the theoretical

*Within the accuracy of the Earth's orbit deviations from a circular orbit.

study of the experiments with collimators predicts many of the effects (1)–(3) and (5)–(7) as well as the results of other experiments. The study is based on the discovery and using of the significant differences of the physical meaning of experimental results obtained by using detectors of different types.

3 The particular rôle of the Shnoll radiation detectors

The effects of the local time (1)–(3), (5)–(7) are confirmed experimentally by the histograms records of processes of different physical nature. For example, there is a version of Shnoll's detector D_α based on the histograms recording of the quantity of the moving α-particles emitted by the compact radioactive source Plutonium-239 (^{239}Pu). Another version of the detector D_{noise} is based on the histograms recording of the noises in semiconductors. Seemingly, it's all the same, which physical process is used, because processes of different physical nature display similar histograms at the same time (see Introduction). Therefore, in the works of Shnoll's group, no difference is made between the physical meaning of the experimental results obtained by the detectors D_α and D_{noise}. However, in practice, the difference is considerable. Without the understanding of this, it is difficult to correctly understand the many valuable experimental results of Shnoll's group. This difference is essentially used below.

The motion parameters V_α^m of the α-particles emitted in different directions are differently oriented in space and, therefore, they are differently affected by the fields of the second type. If fields represented by F_2 exist, the histograms of the α-particles emitted in different directions should be different, i.e., at the level of macroscopic fluctuations an impression of the space anisotropy should be formed. The phenomenon described is, indeed, observed in the experiments with the collimators, which cut off pencils of the α-particles' emission directions [13, 14]. According to the results of all experiments with the collimators, S. E. Shnoll comes to a conclusion [14]:

> "... the shape of histograms depends on the α-particles' emission direction in relation to a particular point of the celestial sphere".

Theoretically, the impact character of the type-two field F_2 on any detector should be depended on the orientation O of the active detector motion parameters $\mathrm{V}_{d,a}^m$ relative to the ray L_2, by which the impact of the field F_2 comes to the detector. However, the points of the Earth equator are rotated by the Earth about its axis at the linear speed $V^{EQV} = 0.465$ km/s. The average speed of the Earth's orbital motion equals $V^{ORB} = 29.765$ km/s. The average kinetic energy of the α-particles emitted by Plutonium-239 equals 5.15 MeV, which corresponds to the α-particle emission speed of $V_\alpha = 15760$ km/s. Obviously, the speeds V^{EQV} and V^{ORB} are negligibly small in comparison with the speed V_α. The act of the α-particle irradiation is so short (tiny parts of a second) that for the acceleration and acceleration derivatives the ratios are very much not in favour of these motions of the Earth. Therefore, I conclude:

> Actually, the impact character of the type-two field F_2 on the detectors D_α is independent of the parameters $\mathrm{V}_d^{SPIN,m}$ and $\mathrm{V}_d^{ORB,m}$. This character depends only on the field F_2 and directions of the α-particles emission (used in the detector D_α) relative to the ray L_2.

In the collimator detector $D_{\alpha K}$, all parameters V_α^m of the α-particles motion are directed along the collimator. Hence, firstly, the detectors D_α are, in fact, inapplicable to the study of the effects on the histogram shapes of the directions and magnitudes of the vectors $\mathrm{V}_d^{SPIN,m}$ and $\mathrm{V}_d^{ORB,m}$. Secondly, the collimator detectors $D_{\alpha K}$ are almost the ideal tool for disclosing the second-type field and for the study of its impact character dependence on the angles between the motion parameters and ray L_2. General scheme of experiments for the disclosing of the field F_2 is simple: the collimator detector $D_{\alpha K}$ voluntarily, but periodically, with some period T, changes its direction relative to the ray L_2. Then, at each repetition of the orientation of the detector $D_{\alpha K}$ relative to the ray L_2, the repetitions of the impact character of the field F_2 and of the histogram similarity must be observed. Here it's all the same, either the collimator is fixed relative to the local horizon plane (LHP) and changes its direction periodically due to the Earth rotation or the detector direction is changed by an experimenter. To determine the direction, for instance, of the ray L_{2ext} of the field F_{2ext}, the collimator $D_{\alpha K}$ should periodically circumscribe a round cone with some cone axis O_K and some constant angle γ_K between the axis and generator of this cone. When the direction of the axis O_K approaches to an unknown direction of the ray L_{2ext}, the peak at the point $\delta t = T$ must gradually spread and disappear completely, when the directions of the axis O_K and ray L_{2ext} coincide. Indeed, when the axis O_K is parallel to the ray L_{2ext}, the angle between the ray L_{2ext} and the collimator is not changed if the latter circumscribes a round cone. Therefore, the impact character of the field F_{2ext} on the collimator's α-particles is permanently constant. Then according to Note 2, the narrow similarity peak disappears. The experiments with rotating collimators have been run in [13]. However, since the above specific rôle of the detectors $D_{\alpha K}$ has been unclear, it has also been impossible to understand what we are to do with the collimators and how we should understand the results of the experiments with the rotated collimators. Therefore, firstly, insufficient attention has been paid to the experiments with the rotated detectors $D_{\alpha K}$. As a result, such experiments has been run very little. Secondly, the results of these experiments have caused bewilderment among their authors [13]:

> "Despite the fact that the results obtained are quite clear, they cause natural bewilderment ... Apparently, explanation of these phenomena requires changes in the general physical concept".

The bewilderment was caused by dependence of the histogram shape on the collimator's direction, disclosed in [13]. Thirdly, the authors of the experiments have come to the main conclusion of the article [13] that the said angular dependence "*point to the sharp anisotropy of the space*". Fourthly, by means of the experiments with the detectors D_α, the impact character and histogram shape dependencies on the directions of the impacted object's motion parameters has not been investigated.

The bewilderment is resolved, if we take into consideration the angular dependence of the type- two field impacts on the moving α-particles, whose existence may be discovered just in the experiments with the rotated collimators. Obviously, not every angular dependence is equivalent to the space anisotropy. Therefore, the problem about the space anisotropy requires further development. If S. E. Shnoll is correct in the statement that changes in the histogram shape are induced by the fluctuations of the space-time properties [14], it is most likely, that the matter is thus: the type-two fields generate the space-time fluctuations; but in the near-Earth region the space is isotropic, and the small space fluctuations are anisotropic (more precisely, they depend on the angles between directions in the space and the ray of any type-two field). By the concourse of the circumstances, the experiments with the rotated collimators [13] coincide with the particular version of the above general scheme of the experiments for the detection of the field F_2 with the following particular parameters: the collimator circumscribes a round cone; the axis O_K is parallel to the Earth axis; $\gamma_K = 90^\circ$ (i.e. the collimator rotated in the local parallel plane $\varphi = \text{const}$); $T = \frac{1}{4}T_{ST}, \frac{1}{3}T_{ST}, \frac{1}{2}T_{ST}, T_{ST}$. These experiments are suitable for the disclosure of the type-two fields of the Sun, the Earth and the sources external to the Solar System. The experiments for the determination of the direction of the ray of the external field F_2 have not been carried out.

Note 4 (on the technology of the experiments): In the plate-type detectors $D_{\alpha P}$, the point-like radioactive source is located so close to the plate P detecting the α-particles that nearly half of all α-particles are detected. In this case, the α-particles are detected at once upon the setting of directions of the emission. This is equivalent to the integral detection of the α-particles by the many differently directed collimator detectors $D_{\alpha K}$. The central direction of the α-particles' entrapment coincides with the line perpendicular to the plate. Let's draw the perpendicular line through the plate center. By symmetry, the directional diagram of the detector $D_{\alpha P}$ is symmetrical relative to this perpendicular line. Therefore, the direction of this perpendicular line characterizes the directivity of the detector $D_{\alpha P}$ and its orientation in space. This perpendicular line we shall name the axis of the detector $D_{\alpha P}$ and we shall denote it as $O_{\alpha P}$. In the experiments, the plate P was always fixed horizontally relative to LHP and, consequently, was turned about the Earth axis together with LHP and the parameters $\mathrm{V}_d^{SPIN,m}$. Hence:

> During the Earth rotation, the spatial orientations of the detector $D_{\alpha P}$, LHP and parameters $\mathrm{V}_d^{SPIN,m}$ are always changed synchronously and equally.

Primarily, the effects of the local time (1)–(3), (5)–(7) was disclosed by the plate-type detector $D_{\alpha P}$ and then confirmed by the noise detector D_{noise}. ■

4 The disclosure and the cylindrical symmetry properties of the type two field F_2

Let F_{2ext} be some second-type field, external in relation to the Solar System, whose ray L_{2ext} and the field F_{2ext} itself are constant within the spatial area covered by the Solar System during the entire period of the experiments. How can we disclose the field F_{2ext} and determine the direction of its ray? In accordance with the above-mentioned general scheme, we should change the direction of the collimator $D_{\alpha K}$ relative to "motionless" stars almost voluntarily but periodically, with a voluntarily chosen period T. Then the collimator's orientation (and the parameters V_α^m of the motion of the α-particles) relative to an unknown but constant direction of the ray L_{2ext} will be repeated with the period T. This will induce the similarity between the histograms $G_K(t)$ of the detector $D_{\alpha K}$ separated in time by period T, i.e., the following equality will be fulfilled:

$$G_K(t+T) \approx G_K(t)\,, \tag{9}$$

which usually has a clear narrow peak by the parameter δt^*. This similarity will be the indicator of the existence of the field F_{2ext}. In realized collimator experiences, the axis O_K is parallel to the Earth axis and, hence, has constant orientation relative to the system of "motionless" stars (which is accurate to small deviations). Therefore these experiences are suitable for the detection of the field F_{2ext}. These experiences were performed at the periods $T = \frac{1}{4}T_{ST}, \frac{1}{3}T_{ST}, \frac{1}{2}T_{ST}, T_{ST}$. For all the mentioned periods, the delineated (by δt^*) narrow peak of the histogram similarity (9) was disclosed [13]. Hence, *the field F_{2ext} exists**. Taking into account the physical model developed here, it is useful to determine the direction of the ray L_{2ext} and the force of the field F_{2ext}, making clear, first of all, whether it comes from the Galactic Plane or from some external source relative to the Galaxy. Many fields, such F_{2ext}, may indeed occur†. Therefore, one may

*At time T_{ST}, the detector returns to the same point in the GSC system. Therefore, if $T = T_{ST}$, the histogram similarity (9) is also caused by the Earth's field of the first type (see below). At $T = \frac{1}{4}T_{ST}, \frac{1}{3}T_{ST}$, the only parameter, which is repeated with the period T, is the collimator orientation relative to "motionless" stars and the ray L_{2ext}. Hence, at $T = \frac{1}{4}T_{ST}, \frac{1}{3}T_{ST}$ the histogram similarity (3) unambiguously occurs due to the existence of the field F_{2ext} that makes sense of the experiments with $T = \frac{1}{4}T_{ST}, \frac{1}{3}T_{ST}$.

†During a single day, the direction of the ray from remote planets relative to "motionless" stars is almost not changed.

expect to get an interesting and informative investigation result.

If the detectors A and B from equalities (1)–(3) and (5)–(7) are the plate-type detectors, $D_{\alpha P}$, let us denote them as $D_{\alpha PA}$ and $D_{\alpha PB}$, respectively. When they are the noise detectors, D_{noise}, let us denote them as D_{noiseA} and D_{noiseB}.

> The existence of the field F_{2ext} explains the effects (1) and (3) in the experiments with the detectors $D_{\alpha P}$, since the orientation of the detector $D_{\alpha PA}$, in relation to the ray L_{2ext}, is repeated after the period T_{ST}, and the orientation of the detector $D_{\alpha PB}$ in relation to the ray L_{2ext} at the moment $t + \delta t_{ST}$ repeats the orientation of the detector $D_{\alpha PA}$ at the moment t (see Note 4 and Section 3).

If we do not neglect the orbital motion, the existence of the field F_{2ext} cannot explain the effects (1) and (3) in the experiments with the noise detector D_{noise} as, by virtue of equality (8), in the times δt_{ST} and T_{ST} there are no the corresponding repetitions of the directions of the detector's parameters V_d^m relative to the ray L_{2ext} because of the Earth's orbital motion. Probably, the effects (1) and (3) are generated in the noise detector by any other field (about this, see Section 5 "The disclosure and constancy of the type-one field F_1 along meridians").

By analogy, the disclosure of the type-two field F_{2S} of the Sun requires a periodical, with voluntarily chosen period T, variation of the orientation of the collimator $D_{\alpha K}$ in relation to the solar ray L_S passing through the detector $D_{\alpha K}$. But in practice, the period of the previous experiments may be used. For example, at $T = \frac{1}{4} T_{ST}$ the collimator is rotated in the plane of the local parallel (and, therefore, in the plane of the local celestial equator) with quadruplicated angular velocity of the Earth. Therefore the collimator almost exactly repeats its orientation in relation to the ray L_S in one forth of the solar day T_S. Indeed, in the experiments, the similarity of the histograms $G_K(t + \frac{1}{4} T_S)$ and $G_K(t)$ have been determined [13]:

$$G_K \left(t + \frac{1}{4} T_S \right) \approx G_K(t) \,. \tag{10}$$

In the time interval $\frac{1}{4} T_S$, nothing but ψ_α^m is repeated where ψ_α^m are the angles between the parameters V_α^m of the motion of α-particles and the solar ray L_S. As a consequence, the effect (10) is the result of the Sun's field impact, moreover, of the type-two field F_{2S}, because its impact depends on the above angles. The same is also confirmed experimentally at the repetition of the above angles during the time intervals $\frac{1}{3} T_S$, $\frac{1}{2} T_S$, and T_S. Thus:

> The Sun's field of the second type F_{2S} and the active motion parameters exist.

Which ones are the active motion parameters? This has not been determined experimentally. At the time lapse of 529600 minutes, i.e., at the time of an integer number of the solar days nearest to the sidereal year $T_{SID} = 525969$ min, the orientations of the detectors $D_{\alpha P}$ and $D_{\alpha K}$ relative to the direction to the Sun are also repeated, and the histogram similarity should occur, too. The required experiments were performed with the plate-type detector $D_{\alpha P}$. The experiments demonstrate [14] the presence of the effect that is the additional confirmation of the existence of the field F_{2S}. The histogram similarity after the time lapse of 529600 minutes was detected accurate to within a minute. At the time of a solar day T_S, the orientation of the detector $D_{\alpha PA}$ relative to the ray L_S is repeated. Under the condition $\varphi_A(t) = \varphi_B(t) =$ const, the orientation of the detector $D_{\alpha PB}$ relative to the ray L_S at the moment $t + \delta t_S$ repeats the orientation of the detector $D_{\alpha PA}$ at the moment t.

> Therefore, the existence of the type-two field F_{2S} of the Sun must lead to the effects (5) and (7) in the experiments with the detectors $D_{\alpha P}$ but only under the condition that the field F_{2S} is accurately, or sufficiently accurately, cylindrically symmetrical about the Earth's orbital axis, at least, in the orbital plane.*

The last condition is fulfilled because the effects (5) and (7) are indeed observed in the experiments with the detector $D_{\alpha P}$. Why is this condition fulfilled? The fact is that the experiment has confirmed (see below) the cylindrical symmetry of the type-two field of the Earth relative to the Earth's rotation axis. As a consequence, the Sun's field F_{2S} should be cylindrically symmetrical about the Sun's rotation axis. The rotation axis of the Sun is approximately normal to the Earth's orbit plane that leads to a sufficiently low deviation of the field F_{2S} from the cylindrical symmetry about the Earth's orbital axis. It is easier to study the field of the second type in the example of the Earth, because in relation to it the experiments are more accessible (with the reason presented below).

> The field F_{2S} induces all effects (5) and (7), and in the experiments with the noise detectors.

Indeed, in the period of a Sun's day T_S, the orientation of the moving parameters $\mathrm{V}_d^m = \mathrm{V}_d^{SPIN,m} + \mathrm{V}_d^{ORB,m}$ of the detector D_{noiseA} relative to the solar ray L_S is repeated. Under the condition $\varphi_A(t) = \varphi_B(t) =$ const, the orientation of the moving parameters of the detector D_{noiseB} relative to the solar ray L_S at moment $t + \delta t_S$ repeats the moving parameters orientation of the detector D_{noiseA} that the last had relative to the ray L_S at the moment t. In this reason, the effects (5) and (7) arise as it will be shown shortly.

Does the Earth has its own field F_{2E} of the second type, cylindrically symmetrical relative to the Earth's rotation axis? The presence of the field F_{2E} may be checked experimentally, for whose purpose let us compose an appropriate experiment.

*The impact character of the field F_{2S} depends on both the said orientations and the field F_{2S} itself. If the field F_{2S} does not possess the said symmetry, it changes along the Earth's orbit, which prevents the occurrence of the effects (5) and (7).

By virtue of the cylindrical symmetry, the field F_{2E}, if it exists, comes from, as it were, from the Earth axis by the ray L_E perpendicular to the Earth axis (in the Earth's areas outlying from its poles). Let us use the noise detector D_{noise}. Then the impact character of the field F_{2E} on the detector should depend on the orientation of the active motion parameters $\mathrm{V}^m_{d,a}$ of the detector relative to the ray L_E passing through the detector. According to Note 3, the motion parameters should be considered in the GSC system.

> In the framework of Shnoll's technique, it is useless to fix a detector D_{noise} on the rotating Earth surface.

This is because in this case they will be moved in the GSC system along the motionless parallels $\varphi = \text{const}$ and have constant orientation and magnitudes of its parameters $\mathrm{V}^m_{d,a}$ relative to the ray L_E passing through the detector. Hence, the impact character of the field F_{2E} on each detector will be constant in time.

> Then, by virtue of Note 2, the Shnoll technique may not determine the existence of the field F_{2E}.*

Therefore, let us detach some detectors from the Earth's surface and begin to move them in the GSC system not in parallel to the motionless parallels $\varphi = \text{const}$. Then in the GSC system, every detector $D_{noise,n}$ $(n = 1, 2, 3, \ldots, N)$ has time-dependent active motion parameters $\mathrm{V}^m_{d,a,n}(t)$. The detector D_n crosses the motionless parallel $\varphi = \text{const}$ at some point Q_n, at some moment of time t_n. Vectors $\mathrm{V}^m_{d,a,n}(t_n)$ are the active motion parameters of the detector $D_{noise,n}$ at the moments t_n of the intersections by the detector of the motionless parallel $\varphi = \text{const}$, that is at the point Q_n. Let the following condition be observed: the points Q_n do not coincide among themselves; the magnitudes and orientations of the active motion parameters $\mathrm{V}^m_{d,a,n}(t_n)$ relative to the ray L_E passing through the detector $D_{noise,n}$ are the same for all detector $D_{noise,n}$. Under the condition, despite the differences between the points Q_n, the field F_{2E} impact character on all detectors at the moments of their crossing of the parallel $\varphi = \text{const}$ must be the same that should generate the appropriate histograms similarity. The histogram of the detector $D_{noise,n}$ timed to moment t will be denoted as $G_n(t)$. As a consequence, the following equality must be observed:

$$G_1(t_1) \approx G_2(t_2) \approx G_3(t_3) \approx \cdots \approx G_N(t_N)\,. \qquad (11)$$

The particular case of the above described experiment with two detectors, that were detached from the Earth's surface and placed on board of the same aircraft flying to the north at a constant speed relative to the Earth's rotating surface, was performed in [12]. In principle, the detectors may be placed on board of different aircrafts, which fly differently, providing that the above conditions is observed. In [12], one detector was located northward from another. In the GSC system, the aircraft is shifted eastward by the Earth rotation. Therefore, in the GSC system, the detectors cross the parallel $\varphi = \text{const}$ at some different points Q_1 and Q_2. Obviously, the above conditions is observed. As a result, in these different points of the parallel, the expressed peak of the histograms $G_1(t_1)$ and $G_2(t_2)$ similarity (11) was really detected, i.e.:

$$G_1(t_1) \approx G_2(t_2)\,, \qquad (12)$$

or, in other words:

> This fact experimentally confirms existence of the field F_{2E} of the Earth.†

If only the field F_{2E} does not change along the meridians, the similar histograms would occur equiprobably at different time shifts within the value $t_2 - t_1$, and the histogram similarity peak (12) would smears out and disappears (see Note 2). Hence, the field F_{2E} changes along the meridians. Not simple but useful is to broaden the experiment, as it is described above, for studying of the impacts' dependence on the values and directions of the detector motion parameters relative to the Earth's axis and the ray L_E passing through the detector.

> It is much simpler to perform these investigations in a laboratory by moving the detector relative to a rotating massive body, because the last must, as it will be seen, also generate the second type field and, since it is clear now how the detector should be moved to study the field impact.

By the opinion of experimenters, this experiment "confirms the hypothesis that the local time effect is induced by systematic motion in a heterogeneous alternating space" [12]. Contrary to the above opinion, this experiment bears no relation to the local time effect, but represents a new, long-awaited result [16], which experimentally confirms the existence of the Earth's field F_{2E} of the second type. The above experiment would relate to the local time effects, if the second detector in GSC enters the same point of the same motionless parallel, where the first detector has occurred before, i.e. if points Q_1 and Q_2 are the same, as required by the local sidereal time effect. By analogy, there is no relation to the local solar time effect.

5 The disclosure and constancy of the type-one field F_1 along the meridians

As is obvious, many in the effects (1)–(3) and (5)–(7) are explainable as results of the disclosure of the type-two fields. However, the existence of the type-two fields cannot explain

*The same also relates to detectors D_α with the orientation fixed relative to the LHP system, because in this case the detector orientation relative to the ray L_E do not change along the parallels.

†Obviously, $t_2 = t_1 + (t_2 - t_1) = t_1 + \tau$, where $\tau \equiv t_2 - t_1$. At any moment t_1, the first detector crosses some parallel $\varphi = \text{const}$. Therefore, in the formula (12), the value t_1 can be changed by the current time t and present it as $G_1(t) \approx G_2(t + \tau)$. In [12], the value τ is constant. The same experiment could be performed with detectors $D_{\alpha K}$ observing constancy of the collimator direction relative to the ray L_E (and in a sufficient resolution power by time).

synchronism along the meridian (2), (6) in the experiments with the detector $D_{\alpha P}$. Actually, as is easy to see, the orientations of the plate-type detectors $D_{\alpha PA}$ and $D_{\alpha PB}$ (perpendicular to the plate) change along the meridians relative to the rays L_S, L_E, L_{2ext} and any other system of the ray mutually parallel within the bounds of the Earth. At the same time, the impact character of the type-two fields on the detectors $D_{\alpha PA}$ and $D_{\alpha PB}$ depends on the above orientations. Therefore, in the experiments with the detectors $D_{\alpha PA}$ and $D_{\alpha PB}$, the type-two fields of the Earth, the Sun and any other external source of them associated with the ray, mutually parallel within the Earth, may not generate the synchronism (2) and (6) on the Earth meridians. By analogy, regarding the orbital motion of the Earth, the existence of the type-two fields may not explain the effects (1) and (3) in the experiments with the noise detector D_{noise}. Hence:

> The different field does exist, the impact character of which is independent of the above orientations.

This field must affect the histograms of any Shnoll detector independently on the orientation of the parameters of its motion or the motions of the α-particles (for example, on the detectors $D_{\alpha P}$, $D_{\alpha K}$ and D_{noise}). The character of its impact depends exclusively on the field itself, on the detector location in this field and, probably, on the magnitudes of the above motion parameters. By definition, this is *the field F_1 of the first type*. The constancy lines of its impact character are the Earth meridians despite of the Earth's motion in space. Hence, this is the self-field F_{1E} of the Earth. If the field F_{1E} impact character would not vary and along the Earth parallels $\varphi = \text{const}$, it would be constants on the Earth's surface. Then there would be no reason for the raise of the probability of the similar histograms occurrences when two detectors are located on the same meridian. But, still, the indicated raise is observed. Hence, the field F_{1E} changes along the Earth parallels $\varphi = \text{const}$.

According to Note 1, the Sun must have its own field F_{1S} of the first type, the impact character of which in the HSC system is constant along of the Sun's meridians, but changes along its parallels motionless in the HSC system. The field F_{1S} should change along the Earth's orbit. If the field F_{1S} is static at a time in the HSC system, the character of its impact on the Earth should depend only on the Earth's location along the Earth's orbit. In the sidereal year T_{SID}, the Earth repeats its location in its orbit. A sidereal year is not equal to an integer of a sidereal day $T_{ST} = 1436$ min since in the sidereal year the Earth makes not an integer of its turnovers about of the Earth axis. Therefore, the detector's motion parameters and the motion parameters of the α-particles, if the detector is the radiation detector, at the moments $t + T_{SID}$ and t are directed differently. It is simple to convince ourselves that the angular difference in the directions on the equator attains approximately 90°. Despite of the indicated difference in the directions, if the Sun has a static field F_{1S}, the impact character of the field F_{1S} on the detectors D_{noiseA} and $D_{\alpha PA}$ should repeat in the sidereal year T_{SID}. Hence, the histogram similarity should be observed at the time T_{SID} under the effect of the field F_{1S} on the detectors. During the searching by S. E. Shnoll's group at about a year's cycle, the required experiment has been carried out but only with the detector $D_{\alpha PA}$ and with the use of many moments of a time t during several sidereal years [14]. In the experiments of Shnoll's group [14], the expressed peak of the similarity among the histograms divided by the interval $T_{SID} = 525969$ min has really been detected to one minute, which in addition experimentally confirms the existence of the first-type fields (of celestial bodies), their variability along motionless parallels and their *static character at a time*.

As we have illustrated earlier, in the GSC system at $\varphi_A(t) = \varphi_B(t) = \text{const}$, the detector D_{noiseB} at the moment $t + \delta t_{ST}$ and the detector D_{noiseA} at the moment $t + T_{ST}$ arrive at the same point where the detector D_{noiseA} was at the moment t and, therefore, arrive at the same point of the field F_{1E}. For this reason, the effects (1) and (3) should be in the experiments with the noise detectors as it is observed. Synchronism along the meridian is observed on the noise detectors. But the magnitudes of the motion parameter $\mathrm{V}_d^{SPIN,m}$ of the noise detector D_{noise} change along the Earth meridians — from zero value at the Earth poles to a maximum value on the Earth equator. Therefore field F_{1E} can generate synchronism along the meridian with the noise detectors only during the event when only the impact force, but not the impact character, of the first-type field F_1 depends on the magnitudes of the detector's motion parameters.

The effects (1) and (3) with the noise detectors are generated also by the exterior field F_{2ext} if it is possible to neglect the active parameters of the orbital motion. Indeed, in this case only the spin motion parameter $\mathrm{V}_d^{SPIN,m}$ of the noise detector D_{noise} relative to the Earth's center plays a rôle. These parameters of the noise detector D_{noiseA} repeat their orientation relative to the ray L_{2ext} at the time T_{ST}. A detector D_{noiseB} at the moment $t + \delta t_{ST}$ repeats the orientation of the parameter $\mathrm{V}_d^{SPIN,m}$ of the detector D_{noiseB}, which it previously had at the moment t. This way, it reduces to the effects (1) and (3). At any fixed moment t, the direction of each parameter $\mathrm{V}_d^{SPIN,m}$ does not change along the meridians. Therefore the field F_{2ext} should generate synchronism along the meridians (2) in the experiments with the noise detector D_{noise} but only if the impact force, but not the impact character, of the second-type field F_2 depends on the magnitudes of the detector's motion parameters (varying along the meridians). The ray coming from each point of the Sun (as well as the ray L_{2ext} of the external field) is practically mutually parallel in the Earth's limit (to five thousandth of a grade). Therefore the Sun's field F_{2S} also generates synchronism along the meridians in the experiments with the noise detector D_{noise} but only under the last condition.

Thus, in all cases, for the appearance of the above syn-

chronism on the noise detectors it is necessary that only the impact force, but not the impact character, of the considered fields depends on the magnitudes of the detector's motion parameters. Synchronism along the meridians on the noise detectors is observed. Hence:

> At least for one of the fields F_1 and F_2, only the impact force, but not the impact character, depends on the magnitudes of the detector's motion parameters.

Now, let's ask ourselves whether it is possible to neglect the active parameters of the orbital motion? Probably — yes, if all active parameters are derivatives of the acceleration. In fact, the first derivative $\mathrm{V}_d^{ORB,2}$ of the detector's orbital acceleration with respect to the Sun makes only five ten-thousandth of the first derivative $\mathrm{V}_d^{SPIN,2}$ of the detector's rotational acceleration with respect to the Earth axis. With respect to the derivatives and the motion relative to the galactic center, a relation is not for the benefit of the latest. From the current experiments with the noise detector, it is not possible to draw a single one-valued conclusion concerning the rôle of the orbital motions as the active parameters have not been discovered.

6 About the reasons of the occurrence of the fields of the first and the second types

The field F_{2E} of the Earth is cylindrically symmetrical relative to the Earth axis. The Earth axis is the axis of its rotation. Hence the field F_{2E} is inseparably linked to the Earth rotation about its axis. If we stop the Earth rotation, the Earth axis loses its physical meaning and disappears and, consequently, the field cylindrically symmetrical relative to the Earth rotation axis loses its sense too. At the stopped Earth rotation, the field no longer has reason to be cylindrically symmetrical relative to the Earth axis. In this case, any other field may exist (with other properties) but not the above field F_{2E}. Consequently:

> The field F_{2E} arises as the result of the Earth rotation*.

The spatial distribution of the impact character of the field F_{1E} (as well as that of the field F_{2E}) is determined by the Earth's rotational characteristics — by its meridians $\theta = \text{const}$ and parallels $\varphi = \text{const}$. In fact, impact character of the field F_{1E} is constant along the Earth meridians $\theta = \text{const}$ and changes along the Earth parallels $\varphi = \text{const}$. So the field F_{1E} is also inseparably linked to the Earth rotation about its axis. At the stopped Earth rotation, the Earth poles, its meridians and parallels lose their physical meaning and disappear and, consequently, the field F_{1E} inseparably linked to the Earth meridians and parallels loses its physical meaning, too. At the stopped Earth rotation, the field has no reason to be linked to the Earth meridians and parallels. In this case, any other field (with others properties) may exist, not the above field F_{1E}. Hence:

> The field F_{1E} also arises as a result of the Earth rotation.

The origination of the field as a result of a material body's rotation may be checked by laboratory experiment. In one of the preceding paper of the author (2004), it is noted:

> "If a sphere or a disk first is rotated and then is stopped in a laboratory, the field generated by the rotation first will appear and then will disappear. Our interest is to register this phenomenon by the Shnoll detector and then study, in a laboratory, the characteristics of this field, its relations with rotation if, of course, the Shnoll detector will be sensitive enough, because the laboratory body mass is negligibly small compared with the masses of planets".

Based on the theory developed here, it is interesting to ask ourselves the following question: what must occur when the body is rotated in a laboratory with the angular velocity ω? As a result of a body's rotation, the fields of the first type, F_{1B}, and the second type, F_{2B}, must be generated. Let the position and the orientation of the detector $D_{\alpha P}$ be constant relative to a body's axis. When $\omega = \text{const}$, the fields F_{1B}, F_{2B} and their the impacts character on the motionless detector are constant in time. At $\omega = \text{const}$, by virtue of Note 2, the Shnoll technique gives no ability to detect impacts of the fields F_{1B}, F_{2B}, and

> An impression of the absence of the impact arises, although the detector itself registers the impacts of alternate and constant character.

If the impact character depends on ω value, upon multiple repetitions of the angular velocity with the period T, the impact character must repeat multiply, too†. Accordingly, the peak of similarity of the detector histograms $G(t)$ separated in time by the period T should occur: $G(t + \delta t) \approx G(t)$ at $\delta t = T$. The first appropriate experiment has already been performed with the detector $D_{\alpha P}$ [18]. The Shnoll detector had been found to be sensitive enough. The rotating massive body was accelerated from the angular velocity $\omega_{min} = 10\,\pi$ rad/s (300 rpm) to $\omega_{max} = 100\,\pi$ rad/s (3000 rpm). The acceleration and deceleration times were about one minute, and the rotation at the constant angular velocity $\omega = \omega_{max}$ lasted for about three minutes. This repeated many times every 5 minutes of the slow rotation at $\omega = \omega_{min} = \text{const}$. Finally, the process periodically repeated every 10 minutes. During

*The Earth rotation forms and, most likely, generates the field F_{2E}. The point is that in all cases known in physics, if the field is formed by some motion, then it is also generated by this motion. These are intimately related to cases of the formation and generation of the magnetic field by moving electric charges, or to cases of the formation and generation of the so-called gravimagnetic, or co-gravitational fields of moving masses. For the consideration below of the field's dependence on motion, it does not matter, that the field is generated or formed by motion. It is important only that the field arises in the definite form as a result of the motion.

†If the impact character is independent of ω, at its voluntary changes the former false impression will be created.

the acceleration, the value of ω was increased from ω_{min} to ω_{max}, and during the deceleration the value of ω was decreased from ω_{max} to ω_{min}. As a consequence, the angular velocity ω multiply repeated, approximately, at the periods $T = 3 - 5$ min and $T = 5 - 7$ min. According to the developed theory, the similarity peaks of the histograms should be observed at these periods. More similar histograms should be observed at $T = 5$ min. But the greatest number of ω repetitions happens within the period $T = 10$ min, where the maximal peak of the histogram similarity should be expected. In accordance with the developed theory, in the first experiment the impression was created [18]:

> "... that the recording system is sensitive not to the presence or absence of the rotor's centrifuge rotation, but to its acceleration or deceleration".

Secondly, the similarity peak of the histograms was detected within the interval $\delta t = 3 - 7$ min with the maximum at the time shift δt about $\delta t = 5$ min (see Fig. 10a in Ref. [18]). In accordance with the process' cyclicity, the highest peak is observed for the shear $\delta t = 10$ min (see Fig. 10a in Ref. [18]). Despite the obviousness, the authors of the work [18] have spoken about the appearance of the "*five-minute period instead of expected ten-min period*". They came to the inexact conclusion because of the application of the Fourier transform to the curve of numbers of the similar histograms with respect to the shear δt between histograms (see Fig. 10b in [18]). However, the maximum at the shear $\delta t = 10$ min already indicates the maximal repetition of the histogram shape separated by the interval $\delta t = 10$ min. Therefore, to detect repetition of the histogram shape in the interval $\delta t = 10$ min no Fourier transform is needed. The Fourier transform indicates another: it indicates that at the time 5 minute the peaks on the above curve repeat. These peaks are present at $\delta t = 5$, 10 and 15 min. As a result, the Fourier transform mixes the physically miscellaneous peaks and gives the spectrum its maximum at the frequency corresponding to the period of the peaks' repetition 5 min. This has no relation to the sought interval of the histogram shape repetition*. Moreover, it may be shown that in the considered experiment, the quasistationary rotation takes place, i.e., the angular acceleration is so low that it does not affect the instantaneous linear velocity, acceleration and accelerational derivative of the rotating body's points. Indeed, let point M rotate at a variable angular velocity ω. Then it is clear that vectors of its linear velocity v, linear acceleration a and accelerational derivative a' in time are defined by the expressions:

$$\mathrm{v} = \big[\omega, \mathrm{r}\big] , \tag{13}$$

$$\mathrm{a} \equiv \mathrm{v}' = \big[\omega, \big[\omega, \mathrm{r}\big]\big] + \big[\omega', \mathrm{r}\big] , \tag{14}$$

$$\mathrm{a}' \equiv \mathrm{v}'' = \big[\omega, \big[\omega, \big[\omega, \mathrm{r}\big]\big]\big] + \big[\omega, \big[\omega', \mathrm{r}\big]\big] + 2\big[\omega', \big[\omega, \mathrm{r}\big]\big] + \big[\omega'', \mathrm{r}\big] , \tag{15}$$

where ω is the angular velocity vector, "prime" is signed for time derivative, square brackets denote vector cross-product, and r is the radius-vector of the point M relative to the axis of rotation. For the stationary rotation case, $|\omega'| = |\omega''| = 0$. Therefore, linear parameters v, a, a' of the stationary rotation are described by the first summands in the right part of the formulas (13)–(15). The rest summands containing ω' and ω'' values describe the correction arising from the rotation's unevenness. For the purpose of estimation, let us suggest that $|\omega'| = \frac{\omega_{max} - \omega_{min}}{60 \text{ sec}} = \frac{3\pi}{2}$ rad/s^2. For example, at $\omega = \omega_{max}$, we get

$$\big|\big[\omega, \big[\omega, \mathrm{r}\big]\big]\big| = (\omega_{max})^2 \, |\mathrm{r}| = (10000\,\pi) \times \pi |\mathrm{r}| , \tag{16}$$

$$\big|\big[\omega', \mathrm{r}\big]\big| = \frac{3\pi}{2} \, |\mathrm{r}| . \tag{17}$$

Therefore, the second sum in (14) is $\frac{10000 \times 2\,\pi}{3} = 20943$ times smaller in absolute magnitude than the first summand, and may be neglected. The linear acceleration a is determined by the first summand and equals that of the stationary case. As is estimated, the same is true for other values of ω and a'. Therefore, it shall be reasonably assumed that the results of this experiment indicate the effects of rotation, but not acceleration or deceleration of rotation. Thus:

> The experiment confirms formation of the field as a result of the body's rotation and discloses the presence of the impact character dependence on the angular velocity. Hence, at least for one of the fields F_1 and F_2, the impact character depends on the magnitudes of the motion parameters of the field source, and, by the principles of relativity and reciprocity, also from the magnitudes of the motion parameters of the detector.

Then we obtain the analogy of an electromagnetic field impact on an electric charge — the electric field's impact does not depend on the velocity of the charge, and a magnetic field's impact depends on the magnitude and direction of the velocity of the charge. If we trust this analogy, there should expectedly be a mutual induction of fields F_1 and F_2. The axis $O_{\alpha P}$ of the detector $D_{\alpha P}$ has been directed to the body's rotational axis in the above circumscribed experiment. In another experiment, the detector has been turned on. Its axis was parallel to the body's rotational axis. As a result, the produced histograms, which form a response to the body's rotation, has disappeared [18]. The impact character of the field F_1 does not depend on the turns of the axis $O_{\alpha P}$ of the detector $D_{\alpha P}$. Therefore the effects of its action cannot disappear at the turns of the detector $D_{\alpha P}$. At the turns of the detector $D_{\alpha P}$, the action of only the field F_2 varies. Hence,

*If a multitude of other variable impacts did not interfere, obviously, the similarity peaks would also be observed at $\delta t = 20, 30, 40$ min, etc. (see Note 1). In this case, the Fourier transform would have physical meaning and give the peak at the frequency corresponding to the period 10 min. The cut-off of the transformed curve at time $\delta t = 26$ min and the said interference, naturally, do not render the peak at the above frequency possible, and simply mix the physically miscellaneous peaks.

the response of the detector in the first experiment is the result of the impact of the field F_2. Consequently:

> The impact character of the field F_2 depends on the magnitudes of the motion parameters of the source and the receiver, and the impact character of the field F_1 does not depend on these magnitudes. Only the impact force of the field F_1 can depend on these magnitudes.

And, the impact of the field F_2 of a rotating body disappears or the impact character of the field F_2 does not depend on the motion parameters of the source when the detector axis $O_{\alpha P}$ is parallel to the rotating body axis. These conclusions are obtained by the supposition that the detector records directly the fields F_1 and F_2 generated by the rotation. However, in it there is some doubt. The rotating body mass is very small in comparison with the masses of the planets. Probably, the rotating body generates the fields $F_1$and F_2 so weakly, that the detector is not capable of registering them. On the contrary, the speed of the variations (changing) of these fields in the experiments are unusually great on planetary scales, i.e., in comparison with the speed of the variations (changing) of such fields of the Earth, or of the remote planets. Therefore, probably, there are enough strong fields of an induction (induced by weak, but sufficiently fast varying fields of the rotating body) which are registered with the detector. Then essential conclusions can vary. Therefore:

> In the development based on such experiences, it is useful experimentally "to study in a laboratory the performance of the investigated field", especially by the collimator detector $D_{\alpha K}$, to investigate in a laboratory the relation between the field's impact force and character on the location and the motion parameters of the source and the detector, to study the effects of the local-time type and a possible mutual induction of fields F_1 and F_2.

In order to detect the field's existence at $\omega = \text{const}$, it is possible to move the detector.

The formation of the field F_{2E} as a result of the Earth rotation gives birth to consequences chain. The field F_{2E} of the entire Earth formed by rotation should be composed of the elementary fields F_{2P} of the material points P of the Earth. The material points P move around the axis of the Earth. Hence, the whole field F_{2E} is composed of its elementary components F_{2P} arising as a result of the cyclic motions of the material points P around the Earth axis (similar to how a magnetic field is generated by the motion of an electric charge). At any fixed moment of time t, a (sample) material point P is located not at all points of its cyclic orbit around the Earth axis, but at some fixed point K of its orbit. At the moment t, at the point K, the field F_{2P} is formed, naturally, not due to the general characteristics of the motion of the material point P on its whole orbit, but due to the local characteristics of its motion at the point K at the moment t, i.e., at least due to some active, parameter $\mathrm{V}^m_{P,a}$ of the motion of the point P from the set $\{\mathrm{V}^m_P\}$, where $m = 0, 1, 2, 3, \ldots$; V^m_P is the m-th derivative of the velocity V_P of the material point P, $\mathrm{V}^0_P \equiv \mathrm{V}_P$. The significant task for the physical experiment is to find out what the parameters of the motion of the (sample) material point are active and how the field F_{2P} depends on them. Now, in general terms, the following can be said: if some component of the field arises as a result of a motion, then its intensity must depend on the motion's intensity, i.e., on the value of the active parameter $\mathrm{V}^m_{P,a}$, and, for the total field F_{2E} of the entire Earth, on the angular velocity of the Earth rotation. The Earth is moving along its orbit around the Sun. Therefore, the motion of the material points P along the Earth orbit must lead to the formation of some field F^{ORB}_{2E}which we shall denote as the *orbital* field of the Earth. We will distinguish it from the Earth's field formed due to its self-rotation about its axis, which is called the *spin* field and denoted as F^{SPIN}_{2E}. Analogously to the orbital motion, the internal motions of the material points of the Earth (the motions of tectonic plates, subcortical melt, water flows, etc.) must lead to the formation of the field F^{IN}_{2E}, which we will denote as the field of the internal motions of the Earth. The Earth is only one of many planets. Then the said must be true for other planets, their satellites, the Sun, the Moon and for other celestial bodies, because all of them consist of material points, have orbital, spin and internal motions, i.e., all celestial bodies must have orbital, spin fields and fields formed by their internal motions. This is in accordance with NOTE 1. Any sample (a motionless one included) of matter consists of physical material particles (molecules, atoms, etc.) which are mobile. Hence, any sample of matter has the same fields. By the same logic, the same consequences chain for the field F_{1E} are obtained. In particular, the field F_{1E} of the entire Earth is composed of elementary field F_{1P} of the material points P of the Earth. Consequently, the above conclusions about relation between the *type-two* fields and the motions of their sources are also true for the *type-one* field. Then the Earth has a spin field, F^{SPIN}_{1E}, and an orbital field, F^{ORB}_{1E}, of the first type, as well as the type-one field F^{IN}_{1E} formed by the internal motions of the Earth. The impact character of the field $F_P = F_{1P} + F_{2P}$ depends on the magnitudes of the active parameters of the motion of the material point P, since for the entire Earth it depends on ω.

7 Conclusions and discussion

From the experimental material accumulated by Shnoll's group, the following physical model is logically succeeded. The Shnoll detector records the fields of two types. The impact character of the second-type field F_2 displayed by the histogram shape depends on the orientation of the active parameters of motion of the object relative to the ray by which the impact arrive at the object. The impact character of the first-type field F_1 does not depend on the above orientation. The motion of the material particles P leads to the simulta-

neous formation of the type-one field F_{1P} and type-two field F_{2P} of the particles. Therefore, the fields F_{1P} and F_{2P} may be considered as the components of the single field $F_P = F_{1P} + F_{2P}$. The intensity of the fields F_{1P} and F_{2P} should depend on the intensity of the motions, i.e., on the active parameters of motion of the particles P. The impact character of the field $F_P = F_{1P} + F_{2P}$ depends on them, too. The material particles of the Earth are moving around the Earth axis and, as a result, form the Earth's total *spin* fields of the first type, F_{1E}^{SPIN}, and the second type, F_{2E}^{SPIN}. In the geocentric coordinate system, GCS, (non-rotating relative to "motionless" stars), the impact character of the field F_{1E}^{SPIN} is constant along the motionless meridians $\theta = \text{const}$ of the Earth but changes along its motionless parallels $\varphi = \text{const}$. The field F_{2E}^{SPIN} is cylindrically symmetrical about the rotation axis of the Earth. Its impact character is constant along the parallels $\varphi = \text{const}$ and changes along the meridians $\theta = \text{const}$. The motion of the Earth's particles, as of a single whole, along the Earth's orbit forms *orbital* fields of the Earth of the first type, F_{1E}^{ORB}, and the second type, F_{2E}^{ORB}.

> The motion of tectonic plates, subcortical melt, water flows, etc. form the fields F_{1E}^{IN} and F_{2E}^{IN} of the Earth's internal motions of both types.

The measure of the relative strength of the considered fields may be the probability of the appearance of similar histograms by the considered field effect. This allows a change over from a qualitative estimation to a quantitative estimation of the field. The Earth is only one of many planets. Other planets, their satellites, the Sun, the Moon and other celestial bodies must have the same fields. The study of the results of the experiments performed with the Shnoll detector has allowed us to uncover the existence of the first and second-type fields of the Earth and the Sun, as well as the field F_{2ext} of the second type external to the Solar system, the ray of which is reciprocally parallel within the Earth's orbit. Any sample (including a motionless one) of matter consists of mobile material particles (molecules, atoms, etc.) and possesses the same fields. According to S. E. Shnoll's opinion [14], his detector, per se, detects fluctuations of local space-time properties. If S. E. Shnoll is right, the physical nature of the above-studied field F displays itself in the form of fluctuations of local space-time properties (just as the gravitational field displays itself in the form of space-time distortion). Then the statistical properties of the body's internal motions should affect the statistical character of the space-time fluctuations, induced by this body. The inverse effect should also take place, i.e., there should be an interaction between the statistical phenomena in the body and in space-time. The studied aggregate field $F = F_1 + F_2$ of the Sun, the Earth, the Moon, planets, and other material bodies should also depend on the microscopic motions of microscopic particles, for instance, on temperature and spin motions of their atoms. Therefore, the aggregate field F of any material body should depend not simply on its mass, but also on its substance, structure and processes occurring in it.

One would think, that it doesn't matter which Shnoll detector is used, since the histograms of the processes of different physical natures are similar and changed synchronously. Nevertheless, in this paper a different physical meaning of the experimental data of the detectors of the different types is determined: the noise detector D_{noise} indicates dependence of the impact character on the active vectorial parameters of the motions of the detector and the points of the Earth, but the detectors D_α, based on the α-decay registration, indicates dependence of the impact character on the active vectorial parameters of the motion of α-particles. Correspondingly, if the dependence of the impact character and the histogram shapes on the directions of motion parameters or on the spatial orientation of the detector is studied, the method for the interpretation of the experiments with the detector D_α must always be different from the method for the interpretation of the experiments with the detector D_{noise}, which has not been taken into account in the works [10–14]. Taking into account the last conclusion, the system of experimental data of the Shnoll detector and the specific rôle of the experiments with the rotating collimator $D_{\alpha K}$, cutting off the pencils of α-particles, become clear. In the framework of the developed physical model, the effects of local time (1), (3), (5), (7) and near-year cycle with the period of 529600 minutes, observed on detectors D_α, are the theoretical consequences of the experiments resulting from performance of the rotated collimator $D_{\alpha K}$, in which the Sun's second-type field F_{2S} and the external field F_{2ext} has been disclosed. Naturally, this is the reason for the recommendation to use the detectors D_α and $D_{\alpha K}$ for studying of the angular diagram of the type-two field impact upon their laboratory generation. In particular, as described in this paper, with the detectors D_α and $D_{\alpha K}$ rotating on different planes, it is desirable to study the character and relative strength of the impact, and the directions of the ray of the type-two field. The laboratory experiments may allow us more reliably to determinate the details of the properties of the fields of both types. For instance, the already performed laboratory experiment has confirmed the theory's conclusions about the field generation by rotation and has disclosed the disappearance of the response of the plate-type detector $D_{\alpha P}$ to the body's rotation within the detector's orientation along the rotational axis [18]. This is in accordance with an experiment, in which the collimator is parallel to the Earth's rotational axis. The Moon rotates about its axis 28 times slower than the Earth. Therefore, the detection and study of the Moon's type-two field may answer the following question: what changes, if the rotational velocity is strongly decreased?

In the nearest future, the influence of macroscopic internal motions of the Earth on the aggregate two-component field F_E of the Earth may gain direct practical importance for the purpose of the detection of hidden water flows, motions of tectonic plates and subcortical melt, forecasting of strong

earthquakes, etc. According to seismology, earthquakes happen as a result of collision in the Earth's crust of large plates floating on the underlying melt. Let us briefly consider earthquakes themselves. During an earthquake, a short-term (pulse) motion and displacement of large masses of the Earth's crust arise. Then, by virtue of our theory, a pulse change of the field of the mentioned masses arises and, therefore, a pulse change of the Earth's field $F_E^{IN} = F_{1E}^{IN} + F_{2E}^{IN}$ arises too. That is why the Smirnov (and Shnoll) detectors should detect earthquakes, being integral recorders of the motions and displacements of masses. The precursors' appearance in indications of the Smirnov detector before 2–10 days of the earthquakes means, apparently, that some pulse changes in the motions or displacements of the large masses of the Earth's crust or subcortical melt happen also and 2–10 days prior to a strong earthquake that may be, for example, due to the mechanism in which the mentioned plates come into sufficiently rigid contact and, as a result, they are sufficiently abruptly decelerated. Therefore, the presence of earthquake precursors in the field F_E is not surprising and seems logical. However, the precursors' strength is unexpected. The Smirnov detector goes off scale, and it requires us to reduce the detector's sensitivity. Now the precursors of strong earthquakes are separated exactly by anomalously high amplitudes (and with the duration increased, approximately, up to 12–13 minutes). The reason of the mentioned anomalous strength of the precursors' amplitudes may be due to the induction of a strong field due to relatively quick changes in the motions and positions of the tectonic plates or melt. Frequently, in physics, the following rule of reciprocity is true: if some physical process generates or changes some field then, vice versa, this field or its changes may influence the behavior of this process. As a result of the seismic motions, the aggregate two-component field is formed and changed. Seemingly, the reciprocity rule is realized in the connection between such fields and earthquakes, i.e., the fields affect the Earth's seismicity. Moreover, if planets, the Sun and the Moon affect the motions on the Earth via their own aggregate two-component field F, which has been disclosed by the Smirnov detector, then there are serious foundations for the supposition that they also affect the Earth's internal motions related to the earthquakes. This is directly confirmed by the detected correlation between microseismicity and planetary motions. In favor of the same, the old data of Ben-Menachem state the correlation between microseismicity and sunrises and sunsets. According to the Smirnov detector's data, the strong splashes of the field F of the Sun and planets occur exactly at risings, settings and culminations. (Incidentally, the Sun's gravitational impact is minimal exactly at sunrises and sunsets.) This also explains the Jupiter splash affecting in living matter immediately at its upper culmination. Actually, the system of such splashes is much wider. In particular, the strong short-term splashes happen at pair-wise connections between planets, the Sun and the Moon on the coelosphere and at their crossing of their network's definite lines, which will be discussed in a separate paper. Therefore, a strong correlation between earthquakes and the connection between the Moon and planets, observed by T. Chernoglazova, becomes natural. The data on the effects of the pulsar on the Earth's seismicity indicate a noticeable long-range action of the considered fields. Generally, the outlined effects of planets and the pulsar on seismicity and terrestrial motions indicate the existence of the long-range action fields.

However, astrophysics firmly states one's position: *planets are unable to impact the Earth*. These are not mere words. Actually, the total energy flow of a field (known or still unknown to us) through its frontal area must be constant and must be spread throughout the frontal area. The frontal area increases with respect to r^2 (in the case of its spherical shape, where r is the distance from the point-source of the field). Finally, the energy-flux density of the field together with the field intensity should decrease with respect to $1/r^2$ or faster. The corresponding numerical estimates lead astrophysics to the said position. However, astrophysics keeps back the following: *the position is correct for the class of energy fields*. Scientific experiments and observations demonstrate the impact of planets and pulsars on the Earth. Therefore, the dilemma arises: either astrophysics is right in the class of energy fields, then consequently there are the fields outside this class (by definition, they are the energy-free fields) or astrophysics is not right. The known physical laws do not prohibit the existence of the energy-free impacts and fields. Moreover, from physics it is known that energy-free impacts exist. These energy-free impacts do not change the energy of the process but merely control its development, for example, turning on and off energy transforms from one of its kind to another [16]. As is mentioned in the Introduction, S. E. Shnoll has disclosed some universal, remote non-energy impact synchronously affecting on processes of different physical nature. That is, some substance — some physical field — does exist, which is transferring these non-energetic impacts. In order not to conflict with the mentioned position of astrophysics and the conservation law of energy, this field itself must be of non-energetic nature. Though the above idea about a non-energetic field is unusual, it should be seriously investigated, as it is the result of experiments and generally recognized scientific views of astrophysics.

At the same time, the developed theory here does not disclose the physical nature of the fields. This theory is valid independently of whether the fields are energetic or energy-free, electromagnetic, gravitational or of any other physical nature. This theory just gives the field properties as the logical consequence of the experimental material and independently of their physical nature. Therefore, as A. A. Artamonov has reasonably noted, this theory may be included as an independent block for any future theory attempting to explain the properties and the physical nature of the considered fields.

In the interrelation between the considered fields and seismicity, significant are not only new prospects in the forecasts

of earthquakes. Most likely, higher importance is attributed to the renovated view on the physical model of evolution and the interdependence between seismic processes themselves and the surrounding cosmos [19]. The renovated view arises also on geopathogenic zones, as on the zones of anomalies of the considered fields since, according to the above theory and other observations, these fields affect the state of living systems, that will be discussed in a special paper.

Acknowledgements

The author is thankful to the following persons: A. S. Alekseev, the full member of Russian Academy of Sciences, A. V. Nikolaev, the corresponding member of Russian Academy of Sciences, V. (N.) P. Tataridou, and also Dr. A. D. Gruzdev. Essential discussions of the problem with these persons have led to valuable advices and their supporting the author's investigations.

Submitted on October 19, 2008 / Accepted on January 09, 2009

References

1. Sadeh Dror and Meidav Meir. Periodisities in seismic response caused by pulsar CP1133. *Nature*, 1972, v. 240, November 17, 136–138.
2. Kiladze R.I., Kachakhidze M.K., Kachakhidze N.K., Kukhnanidze V.D., Ramishvili G.T. Seaching for possible connections between strong earthquakes and astronomic phenomena on the example of seismically active region in Caucasus. *Vulkanologia i Seismologia*, 2005, no. 3, 78–84 (*in Russian*).
3. Lezdinsh A.Ya. Astroseismology. *The Earth Planet System*, *Proceedings of XVI-th Scientific Seminar*, Moscow State University, Moscow, 2008, 221–225 (*in Russian*).
4. Bogdanovich B.Yu., Shchedrin I.S., Smirnov V.N., Egorov N.V. Specific method of mass rotation — the instrument for astrophysical investigations. Preliminary analytical estimates of changes in kinetic energy of rotating mass on coordinate-time position of the Sun and the Moon. *Scientific Session MEPHI-2003*, Moscow, MEPHI, 2003, v. 7, 45–48 (*in Russian*); http://library.mephi.ru/data/scientific-sessions/2003/7/045.html
5. Bogdanovich B.Yu., Egorov N.V., Smirnov V.N. Recording of some phenomena by spatial-temporal geometrizer. *Scientific Session MEPHI-2005*, Moscow, MEPHI, 2005, v. 7, 59 (*in Russian*); http://library.mephi.ru/data/scientific-sessions/2005/t7/0-1-24.doc
6. Bogdanovich B.Yu., Egorov N.V., Kulago A.P., Smirnov V.N. Recording of various orbital configurations of planets in the Solar System by the gravitational interactions detector. *Scientific Session MEPHI-2006*, Moscow, MEPHI, 2006, v. 7, 1–5 (*in Russian*); http://library.mephi.ru/data/scientific-sessions/2006/t7/0-6-5.doc
7. Bogdanovich B.Yu., Smirnov V.N. The peculiarities of experimental works in studies of gravitational interactions. *Inzhenernaya Fizika*, 2006, no. 4, 10–14 (*in Russian*).
8. Smirnov V.N. Gravitational disturbances and physical peculiarities of rotating gyroscope. *Inzhenernaya Fizika*, 2006, no. 5, 22–24 (*in Russian*).
9. Smirnov V.N., Egorov N.V. and Shchedrin S.I. A new detector for perturbations in gravitational field. *Progress in Physics*, 2008, v. 2, 129–133.
10. Shnoll S.E., Kolombet V.A., Pozharskyi E.V., Zenchenko T.A., Zvereva I.M., Kondratov A.A. On realization of discrete states during fluctuations in macroscopic processes. *Physics-Uspekhi*, 1998, v. 168, no. 5, 1129–1140.
11. Panchelyuga V.A., Shnoll S.E. On the dependence of a local-time effect on spatial direction. *Progress in Physics*, 2007, v. 3, 51–54.
12. Panchelyuga V.A. and Shnoll S.E. A study of a local time effect on moving sources of fluctuations. *Progress in Physics*, 2007, v. 3, 55–56.
13. Shnoll S.E., Rubinshtein I.A., Zenchenko K.I., Shlehtarev V.A., Kaminsky A.V., Konradov A.A., Udaltsova N.V. Experiments with rotating collimators cutting out pencil of α-particles at radioactive decay of 239-Pu evidence sharp anisotropy of space. *Progress in Physics*, 2005, v. 1, 81–84.
14. Shnoll S.E. Changes in the fine structure of stochastic distributions as consequence of space-time fluctuations. *Progress in Physics*, 2006, v. 6, 39–45.
15. Shnoll S.E. Macroscopic fluctuations — possible consequence of time-space fluctuations. Arithmetical and cosmophysical aspects. *Rossiyskii Khimicheskii Zhurnal*, 2001, v. XLV, no. 1, 12–15 (*in Russian*).
16. Vasiliev S.A. On some field of the Earth in view of its internal motions. *Degassing of the Earth: Geodynamics, Geofluids, Oil, Gas, and Their Parameters*, *Proceedings of the Conference*, Moscow, April 22–25, 2008, GEOS Publishing House, Moscow, 576–579 (*in Russian*).
17. Vasiliev S.A. On two-component field of the Earth and stellar bodies. *The Earth Planet System*, *Proceedings of XVI-th Scientific Seminar*, Moscow State University, Moscow, 2008, 98–119 (*in Russian*).
18. Panchelyuga V.A., Shnoll S.E. Experimental study of quickly rotating massive body influence on the shape of distribution functions amplitudes of α-decay rate fluctuations. *Hypercomplex Numbers in Geometry and Physics*, 2006. v. 3, no. 1, 102–115.
19. Nikolaev A.V. The pattern of geophysics in XXI century. In: *Problems of Geophysics in XXI Century*, collected papare, book 1, 2003, Moscow, Nauka Publishing House, 7–16 (*in Russian*).
20. Zubov V.A. et al. Private communications. Germany, 2008.

Beta Decay and Quark-Antiquark Non-Parity in Collision-Induced Gravity

Gary C. Vezzoli

Department of Science and Mathematics, Lebanon College, Hanover Street, Lebanon, NH 03766, USA
Senior Research Consultant Physicist, Institute for the Basic Sciences, West Windsor, VT 05089, USA

E-mail: vezzoli2005@yahoo.com

The quark-antiquark interaction, with non-conservation of parity, associated with neutrino-nucleon inelastic scattering, and electron/positron decay consequent to nuclear transmutation and re-materialization, are invoked as the phenomena responsible for heat carry-off. The mechanism is applied to collision-induced gravity, including quantitative justification, using Feynman parton theory. The application to heat dissipation necessarily involves the tri-quark current that associates with weak interactions.

1 Introduction

Parity refers to the operation of studying a system or a sequence of events reflected in a mirror plane [1]. In chemistry and biology, the term "chirality" is used, instead of parity, and refers to a structure that is different from its mirror reflection, and from this property, very important criteria of handedness and broken symmetry arise [2]. In physics, a deeper understanding of the meaning of parity (often called space parity) refers to every real object or process having a mirror image that *obeys the same physical laws* as the original object. It was originally assumed that parity is conserved upon collisions, and this implied that elementary particles have antiparticles, such as neutrinos and antineutrinos, such that the antiparticle subscribed to the *same* physical laws as the particle. This all changed with the publishing of Lee and Yang's seminal work [3] that argued that parity was *not* conserved in weak interactions. One such interaction is radioactive decay, described to arise from what is referred to as the "weak force", contrasting the strong force and electromagnetism both of which are shown to conserve parity in interaction with matter. Experiments by Wu et al. [4] involving the direction of beta decay emitted from Co^{60} in a magnetic field (thus relative to the associated applied magnetic field vector) confirmed that in beta decay, parity is *not* conserved. The relationship between *gravitating* bodies is also a manifestation of weak interactions. In both a field-based wave-mechanical model of gravity, and a particle-based collision-induced model of gravity [5, 6], parity is thus interpreted to be non-conserved.

The theoretical analysis [6], which was based on the interpretations from super K data that the neutrino oscillations between flavors could only occur if the neutrino had a rest mass, was cast in terms of a net transfer of *linear* momentum, but since it is now known that the neutrino always possesses left-handed helicity, and since it is reported that upon inelastic collision between a neutrino at $v \sim c$, and a proton or a neutron, the flavor of the neutrino has a very high probability to change — thus the spin magnetic moment property of the particle changes — the analysis is broadened herein to include *total* angular momentum. The nucleon's spin properties, the neutrino's spin properties, and the neutrino's essentially linear velocity at collision, all then demand the consideration of spin angular momentum *and* linear angular momentum; however, since quark properties must also be considered in an inelastic interaction with protons or neutrons, the orbital angular momentum must also be treated in a full analysis.

A major element of a collision-induced gravity model that has not been yet explained is how the heat generated in the inelastic collision is carried-off from the local neighborhood of the 3D coordinates of the collision. Without fully explaining heat carry-off, such a model is not complete. The major purpose of this current work is to propose to an international forum of readers, a model for the phenomenological basis of this removal of heat, so as to receive feedback and stimulate further work.

In the interest of simplicity in basic modeling, the collision-induced mathematical analysis did *not* treat the effect of a change-in-flavor of the neutrino (flux) consequent to a neutrino-nucleon inelastic collision due, for example, to a collision with nucleons of the moon during a total solar eclipse, which would then generate a change in the collision cross-section that could affect a subsequent collision with another mass body (such as an interaction with a gravity measuring experimental apparatus located at an Earth laboratory). As a more comprehensive knowledge of the properties of the neutrino is emerging, it seems *unlikely* that a collision of a neutrino with a mass particle would *not* cause a change in flavor. Although the original model [6] has been successful [7] in generating the total solar eclipse (occurring March 1997 in China) gravitational anomaly dip signal detected by Wang et al. [8], and elaborated upon by Yang and Wang [9], adjustment parameters are employed to reproduce the signal, especially in the central region of the signal, but the fundamental *functional* basis for these collision-related parameter adjustments is not yet established.

In wave mechanics terms, and in a particle approach, when the spatial coordinates are reflected from coordinates x, y, z through the origin to position $-x$, $-y$, $-z$, non-conservation of parity means that what is physically expected/observed at x, y, z is *not* the same as what is expected/

observed at $-x$, $-y$, $-z$. In the model/theory of collision-induced gravity this has profound importance, and herein is applied to explain the process of heat carry-off after the inelastic scattering net-transfer-of momentum interaction that the collision model invokes as the fundamental cause of gravity. Without solving the heat-carry-off problem, the collision model suffers vulnerability to a potentially critical weakness.

In our original theoretical work [6] we utilized 10^{-38} cm^2 for the collision cross-section of the neutrino with the neutron, as well as for the collision cross-section with the proton — a value now supported by other studies [10] that relate to the Feynman parton model, and about one order of magnitude higher than the values of sigma arising from earlier work [11]. This is an extremely small collision cross-section, and implies a very enormous flux density of particles such that the neutrino could be considered a realistic candidate for the particle that carries the gravity interaction property. The paradox is that even though experiments such as those conducted in the Super K project or related works, report that it is exceedingly difficult to detect a neutrino (as with scintillator counter devices), these calculations and the interpretations of experiments, do not consider that the neutrino is taking part in gravity interactions, and thus is implicitly detected. If the neutrino is indeed responsible for collision-induced gravity, then the equipment and experiment that is being utilized to detect its collisions with nucleons — such as the 50000 gallons of nuclide treated water, and the associated scintillation counters — is itself detecting neutrinos by virtue of the gravitational interactions related to the experiment as a whole.

2 Initial hypothesis

My own interpretation of very important and unique experimental work of the collimated free-falling neutron experiments at Grenoble [12] is that gravitational interactions must be quantized. And my own hypothesis as to the origin of that quantization, and also the origin of the phenomenon that explains the carry-off of heat generated from an inelastic scattering interaction (in which although momentum *is* conserved, energy is *not* — because of the involved heat), is cast in terms of the quantum mechanics of neutrino-nucleon inelastic collision, and this necessarily must involve the quark constituents of the nucleon. (If this were not so, then I see no way in which gravity can be quantized, and no way that collision-induced gravity could pass all of the scrutinizing tests necessary for embracing a model/theory as viable in modern physics.) Thus the hypothesis must include that the quark-antiquark interaction is involved in the heat carry-off phenomenon.

3 Related original experimental results

For the details regarding experimental findings, including the non-constancy of G, that are not explicable through field theory, including General Relativity, see [8, 9, 13–16]. The original data for my own experimental work, measuring a gravitational anomalous dip ($\sim$35 sec) on 18 May 2001 (16:10 hrs EDT) during the lineup of Earth-Sun-Jupiter's magnetosphere, and Saturn is given in Fig. 1 [16]. This signal was measured using two close-proximity dual-cable suspended Newton cradle pendula. The inter-pendula distance was interrogated with a 100 mw He-Ne cw laser. A change in the very short length-scale inter-pendula distance caused a change in the scattered laser radiation which was detected by a light-detecting diode. The output of the diode detector was fed into a Goerz 7800 chart recorder in the Y vs t mode, and also into a computer using an analogue-to-digital converter. All apparatus was mounted on an optical bench floating on inner tubes, and within a screened enclosure to preclude stray signals. Isolation transformers and RC filters were employed to minimize effects of transients. The operational amplifiers were employed on an offset scale for highest sensitivity so that the magnitude of the dip in gravity, which is shown in Fig. 1, is a relative measurement in arbitrary units. To my best estimate, the decrease in gravity due to the syzygy is of the order of a few microgals (see caption to Fig. 1). At the time of the measurement of the anomalous dip shown in Fig. 1, by use of a telescope attached to the experimental apparatus, I could clearly see the two pendula separating slightly due to the weakened gravity because of the presence of the Sun, Jupiter's magnetosphere, and Saturn that had moved between the deep space source of neutrinos and the Earth-laboratory.

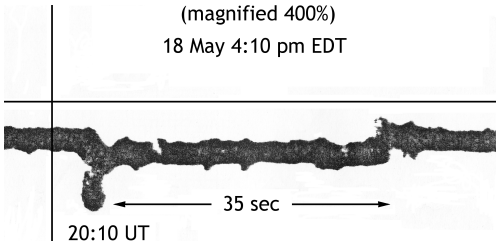

Fig. 1: Original raw data [16] of anomalous dip in gravity detected by use of laser scattering between two gravitating dual-cable suspended pendula, during the planetary line-up/syzygy of 18 May 2001: Earth/Sun/Jupiter's-magnetosphere/Saturn. The leading edge of the signal when expanded is a parabolic dip very similar to the initial parabolic dip detected by Wang et al. [8] for the 1997 total solar eclipse in China. The trailing edge is a parabolic bump, not analogous to any reported data known to the author. I interpret the above signal as due to occulting by the chromosphere-photosphere 1000 km zone of the Sun associated with an enormous change in temperature (from 10,000 to 1,000,000 degrees) and a major change in density, characteristic of the corona region.

The work of Refs. [8, 9, 13–16] strongly argue that G is *not* a constant, and this has been readily shown by the work of Gershteyn et al. at the Massachusetts Institute of Technology, reporting [17] that G varies at least 0.054% as a function of the orientation of the vector between the two gravitating

Cavendish spheres and the direction to large stars, and also that G is periodic with the sidereal year This histogram periodicity can only develop, in my judgment, if gravity is based on external impinging particles such that once per sidereal year the bulk of the Earth is interrupting the flux of gravity-bearing particles some of which never reach the measuring instrumentation (the Cavendish spheres). More precise examination of data of highly controlled robotically measured experiments such as that of Ref. [17] should be capable of measuring indications of periodicity of G on a monthly and daily basis as well. My own work determined the value of G (measured in 2007 in New England) as $G = 6.692 \pm 0.10 \times 10^{-11}$) cubic meters per kg sec^2 [18]. This work was accomplished with a fixed 16 pound spherical composite non-conducting resting mass located on a micro-moveable track, and a close-proximity 3 gram cork pendulum suspended from a nylon fiber. The inter-mass distance was interrogated by a HeNe cw laser, the radiation of which was scattered by the gravitating masses, and detected by a light-detecting diode and/or a solar cell, the output of which was fed into an oscilloscope.

The spatial and temporal patterns of the scattered laser light were measured as the massive sphere was slowly moved, by a servo-mechanism, toward the oscillating cork pendulum, which caused the frequency of oscillation of the cork pendulum to change slightly. By measuring this change in frequency (Δf) as a function of distance between the gravitating masses, we could determine the change in interacting energy, and determine the change in the associated force between the gravitating masses. We tested for any charge concentrations on the gravitating masses, and observed none. The theoretical analysis for the massive-sphere/pendulum interaction can employ either a Newtonian approach or a Lagrangian approach, yielding the same results. From these analyses we could extract the value of G. Our work also showed that our value of G changed somewhat if a film of water replaced air as the inter-mass medium, and changed again, if the temperature of that water was altered from 22°C to about 60°C.

Both our work and the highly accurate laser-cooling interferrometric Pb micro-mass work of Fixler et al. at Stanford (published earlier in 2007), giving $G = 6.693 \times 10^{-11}$ [19], is at significant variance from the accepted averaged value of 6.67, and thus indicates that corrections must be made to those determinations based on using the standard accepted value of G. As a function of collision parameters [6], G is expected to change with time, and with location of the position of measurement in the galaxy, and in the universe.

Our earlier measurements showed that G changes as a function of temperature according to $G = G_0(1 + aT)$, where a is a micro-valued constant in accord with measurements taken much earlier in England, and also changed as a function of phase (increasing as ice melts to water) and as a function of shape (increasing as a loop of 1 mil diameter Cu wire underwent multi-convolutions of the loop to approximate a sphere such as a spool of wool) [16,18].

4 Theoretical discussion

The parton model, advanced by Richard Feynman, postulates that the nucleon is composed of point-like constituents, referred to as partons. The partons share the total momentum of the nucleon by constituting variable fractions of the total momentum, designated (within the Feynman model) by the variable x. The probability, $f(x)$, of the parton to carry momentum does *not* depend upon the process in which it is engaged, or the nucleon energy, but is an intrinsic property. This, in my own interpretation, is fundamental to collision-induced gravity — namely that the carrying and transferring of momentum is an intrinsic property of the neutrino-nucleon interaction, and this is why, at least in part, the gravitation interaction is weak. The partons are composed of the three quarks (referred to as the valence quarks), but also includes the quark-antiquark pairs emerging from vacuum point energy, explicable by the uncertainty principle as well as involving gluons which are quanta of the strong force of quark interactions. The question naturally arises of how a *weak force* non-parity-conserving interaction can affect *strong* force quanta. Because the momenta of quarks (and of gluons) are added to give proton momentum, and from implication of the collision-induced gravity theory, I wish to postulate herein that there exists a constraint, and although strong forces/interactions are necessary to break quark-quark bonds and break apart the nucleus, weak forces are sufficient to change, for example, a d-quark (down-quark) to u-quark (up quark) which involve a transmutation of a neutron to a proton, and which gives rise to a quark-antiquark interaction, otherwise quantum mechanical selection rules could not emerge. Justification for this postulate is given subsequently.

It is thus proposed herein, based on my own interpretation of what is necessitated and implied in collision-induced gravity model and theory, that

> ... the within-nucleon transition of a d-quark to a u-quark, or the reverse, is associated with the formation of an antiquark, without the requirement of GeV energies necessary to break apart the nucleus.

(Because of the broken parity, I believe that further analysis and research must be conducted to determine/understand any thermal properties that might be associated with the antiquark).

The laws of quantum mechanics as applied to the wave function that is associated with the quark-antiquark system, imply that for a quark and antiquark, having angular momentum, L, the parity is established by:

$$P = (-1)(L + 1),$$

where L is an integer. Thus, in an even function, parity is conserved, but if the applicable function is an odd function, then parity is *not* conserved.

The amount of orbital angular momentum, L, and the spin angular momentum, S, of the quark-antiquark system is constrained by quantum mechanics as integers. Parity (P) depends only upon relative orbital angular momentum between objects, however, charge conjugation (C) depends upon both the orbital angular momentum and the combined spin states of the quark and antiquark. If the sum of $L+S$ is an odd integer, then the wave function changes sign when charge conjugation is effectuated upon a collision between a neutrino and a nucleon. From the analysis, there are a set of allowed states $J(PC)$ for a quark and an antiquark in net spin 0 and 1 coupled to orbital angular momentum, L, and total spin $J=L+S$. It is within the context of allowed $J(PC)$ states whereby gravity is, I believe, quantized.

Since the neutron is believed to be spherically symmetric, having a much simpler topology than the proton (which appears to be peanut or torus shaped depending upon respectively whether the quark spin aligns with the proton spin or opposite to it), and since the magnetic moment of the neutron is opposite in direction to that of the highest magnetic moment neutrino flavor — the tau neutrino which has a magnetic moment two orders of magnitude higher than the electron neutrino and/or the muon neutrino — the neutrino-neutron inelastic interaction is first analyzed herein. (I believe that the change of shape of the proton, associated with the alignment relationship of the spin of the quark emphasizes the importance of the quark-antiquark interaction, as related to gravitation.)

The inelastic scattering interaction between the neutrino and the neutron can be described as:

$$\nu(0)+\mathrm{n}(0) \longrightarrow \mathrm{p}^{+}+\mathrm{e}^{-}+\nu_{[\mathrm{anti}]}(0),$$

where ν refers to the neutrino, p refers to the proton, e refers to the electron, 0 means charge neutrality, and $^{+}$ and $^{-}$ refer to positive and negative charge, and "anti" refers to an anti-particle. The above represents a nuclear transmutation creating an element of atomic number $Z+1$, from an element of atomic number, Z, however the transiently created element having $N-1$ neutrons, yet essentially unchanged atomic weight A. This process must be associated with the creation of heat, and kinetic energy cannot be conserved. This neutrino-interaction generating a $Z+1$ atom must decay to the stable Z atomic number atom, and the created heat cannot be allowed to build up, thus must be transported from the system. The reverse-direction reaction, namely

$$\mathrm{p}^{+}+\mathrm{e}^{-}+\nu_{[\mathrm{anti}]}(0) \longrightarrow \mathrm{n}(0)+\nu(0)$$

must also be valid in the description of collision-induced gravity*. This then indicates that if the neutrino or the antineutrino perturbs the proton, then the electron can become unstable and collapse into the proton, and combine with the proton to form a neutron (by changing the direction of one quark).

The reaction that then represents the decay of the unstable $Z+1$ state is normally written:

$$^{A}_{Z}X_{N} \longrightarrow {}^{A}_{Z-1}Y_{N+1}+\mathrm{e}^{+}+\nu\,,$$

where X and Y designate different elemental atoms that differ by one proton, or by a single quark in the up-flavor (X), rather than the down-flavor (Y).

The equivalent reaction for the decay of the unstable state after the interaction between the neutrino and the proton is written as:

$$^{A}_{Z}X_{N} \longrightarrow {}^{A}_{Z+1}Y_{N-1}+\mathrm{e}^{-}+\boldsymbol{\nu}\,,$$

where $\boldsymbol{\nu}$ represents the antineutrino. The above represents beta decay.

> In summary of the above, it is postulated that the generated heat is carried off by the neutrino, and the antineutrino, ejected with changed energy, that are produced, respectively, in the above nuclear decay reactions, and do so according to quantum mechanical selection rules that emerge from the quark-antiquark non-conservation of parity interaction.

It is herein proposed that the Feynman work indicating that the cross-section for the neutrino-nucleon interaction can be described through the quark distribution functions, $d\sigma/dxdy$, which expressed in terms of momentum of the u-quark and the d-quark, is fundamental to explain collision-induced gravity. The work clearly shows that more momentum is transferred by quarks than be antiquarks.

The calculation yields that

$$\sigma_{\nu}=1.56\left(Q\pm\frac{Q}{3}\right)\times 10^{-38}\ \mathrm{cm}^{2}/\mathrm{GeV},$$

where Q represents the momentum integral (for the integrated cross-section). This gives sigma $\nu=0.74\pm 02\times 10^{-38}$ cm^2/GeV for the neutrino, and for the antineutrino, sigma $\nu_{[\mathrm{anti}]}=0.28\pm 0.01\times 10^{-38}$ cm^2/GeV. Therefore σ is linearly *energy dependent for both the neutrino and the anti-neutrino*, and, thus, so is the heat carry-off phenomenon. This also suggests that more heat is carried off by neutrinos than antineutrinos, and this must be because of the structural differences between the proton and the neutron, and differences in their collision cross-sections with respect to neutrinos.

The implication of a collision-induced gravity is that since gravity is statistical, and that the net change of momentum involves a flux of externally impinging particles, and certainly more than a single proton or neutron, and thus a collective effect of protons and neutrons interacting with external particles (neutrinos), such interactions will always be at least slightly different regarding the number of total particles involved. This implies that no two measurements, taking place

*Otherwise, if the inelastic collision with the neutrino, only involved neutrons, then hydrogen (consisiting of one proton, one electron, and zero neutrons) would not be observed to possess weight.

at two different time, of any experimental parameter will ever yield exactly the same value — this possibly related to some of the physical roots of the Uncertainty principle. Both the entity being measured, and the entity doing the measuring, are constantly changing to at least some infinitesimal level because of the stochastic properties of a particle-based gravity. This implies, for example, that typical Poisson statistics are not simply an instrument to assess statistical error in measurements, and standard deviation, but are a fundamentally related to the statistical properties of gravity.

Before this paper can attain closure, it is necessary to furnish scholarly support for my postulate that the quark-antiquark interaction (necessary for establishing the quantum mechanical selection rules that give rise to heat carry-off) can arise from weak interactions. As a career condensed matter basic research physicist, who for the past ten years has been working in gravitation measurements, and interpretations thereof aimed at an understanding of the fundamental cause of gravity — not being a theoretical particle physicist — I had to recruit the assistance from others upon realizing reaching a potential impasse in endeavoring to explain heat carry off — that impasse being explaining how a weak interaction can affect the tri-quark current. I was graciously assisted [20], and the following italicized material is a condensed version of this assistance which is highly cogent to my work.

> The non-conservation of parity of hadronic interactions is closely related to the interaction current of neutrino couplings. Key to understanding this relationship is the unification between leptonic neutrinos and gluons. This manifests at *lower* energy values of particle couplings and is observed in decay patterns of the high-quark meson complexes, such as the top- and bottom-quarks, but these are resonant energies of the up-quark and the down-quark. The proton-neutron interconversion acts to cause a mixing of wave functions and the exchange of a mesonic mediator. This is known as Yukawa coupling, and it is the Yukawa meson that carries the antiquark which couples to an up-quark of the proton. These couplings necessarily relate to the Heisenberg zero-point energy (ZPE) metric background.

In our measurement of G, cited earlier herein, the method which we employed, involving ultra-close-length/scale gravitating bodies, interrogated by cw laser scattering (as a function of the temperature of the coupling medium of air or water), inescapably had to involve the Casimir effect and ZPE — albeit a classical or mixed version of the Casimir effect. It seems that fundamental studies of the physics of the quark-antiquark interaction must involve ZPE.

> The net result is that the strong gluonic coupling can be assumed by the weak antineutrino coupling in terms of a neutral weak-interaction current. The current arises from the triquark complex of a nucleon, and thus can re-circulate; therefore the original nucleon (such as the neutron in the $\nu + \mathrm{n}$ inelastic interaction) can be re-materialized. The associated long decay times are ideal for heat carry-off. The significant point to this is that the quark-antiquark coupling (designated ud') is transmuted into a temporary diquark selfstate (designated ud) following a simple exchange of the state-antistate couplings of the neutral pions (designated dd' and uu').

My experimental results indicate that as related to gravitational interactions, the above couplings collectively are associated with time-constants, or relaxation times, of the order of a fraction of a millisecond. The results of the above analysis, and the available CERN Proton Synchrotron data on the neutrino and the antineutrino, and on the quark and the antiquark, indicate that the input-output physics of the neutrino-nucleon inelastic scattering process yields only a relatively small fraction of the input energy being converted to heat. This is because of values of masses and velocities before and after the inelastic collision do not change substantially. I estimate that the maximum heat energy would be about 15% of the input neutrino energy, and this depends upon the exit velocity of the antineutrino. Detailed quantitative calculated results giving the heat carry-off in electron volts, as a function of input energy in electron volts, will be eventually forthcoming as theoretical intra-nucleus thermodynamic codes become more detailed and comprehensive.

5 Conclusion and interpretation

I conclude that my conjecture/postulate that for d-quark/u-quark neutrino-inelastic- collision-induced transmutations, and consequent quark-antiquark interactions, the strong gluon energies are *not* required for neutral currents, and the weak gluon-neutrino interaction is sufficient, is supported by current accepted theory. Although the above analysis includes very complex internal nuclear processes, and although as scientists we search for elegant simplicity in explanations of nature, it seems to me that to provide an understanding of the heat carry-off phenomenon in inelastic neutrino-nucleon scattering, the invoking of these very complex workings within the nucleon is necessary.

Acknowledgements

The author wishes to express appreciation to Dr. W. Stanley, Professor X. Yang, and members of the Yahoo physics group forums for years of valuable discussions that relate to this work. Gratitude is also expressed to the administration and faculty of Lebanon College who have been supportive of my research, and to Sandra Smalling who has edited and assembled graphics related to thousands of items of data and thousands pages of publications and reports. Appreciation is

also extended to Dr. John Gedye (dec), Frank Lucatelli, Dr. Robert Zamenhof, Robert Morgan, Professor C. Blatchley, Mr. Julian Leon, Ms. Leanne Mortell, Dr. Richard Chrystal, Dr. Traci Jensen, and Dr. Dave Spero for intensive discussions and/or administrative support over the course of the past ten years.

Submitted on January 05, 2009 / Accepted on January 09, 2008

References

1. Bertulani C. Nuclear physics. Princeton University Press, 2007, p. 8, 9, 195, 196. See also Kaku M. and Thompson J. Beyond Einstein. Anchor, Random House, New York, 1995.
2. The new physics. Edited by P. Davies, Cambridge University Press, 1989, p. 400–405.
3. Lee T. and Yang C. *Phys. Rev.*, 1956, v. 104, 256–259.
4. Wu C. et al. *Phys. Rev.*, 1957, v. 105, 1413–1416.
5. The original work on push gravity is attributed to le Sage, and analyzed by Laplace.
6. Stanley W. and Vezzoli G. Induced gravity model based on external impinging neutrinos: calculation of G in terms of collision phenomena and inferences to inertial mass and atomic quantization. arXiv: astro-ph/0102109.
7. Stanley W. and Vezzoli G. Unpublished manuscript.
8. Wang Q., Yang X., Wu C., Guo H., Liu H., and Hua C. Precise measurement of gravity variation during a total solar eclipse. *Phys. Rev. D.*, 2000, v. 62, 041101R.
9. Yang X. and Wang Q. Gravity anomaly during the Mohe total solar eclipse and new constraint on gravitational shielding parameter. *Astrophysics and Space Science*, 2002, v. 285, 245–253; also: Yang X. Private communications. 2005–2007.
10. Kudryabtsev V. Lectures "The Development of Particle Physics". *Phys. Lett.*, 1986, v. 170B, 79–89. This work treats the Feynman parton theory.
11. Work originally done at Princeton University, 1959.
12. Nesvishevsky V.N. et al. Quantum states of neutrons in Earth's gravitational field. *Nature*, 2002, v. 413, 297–299.
13. Alais M. Movement of paracanonical pendulum and total solar eclipse of 30 June 1954, 1957. *Proceedings of the French Academy of Sciences*, 1959, v. 18, 46–49.
14. Saxl E. and Allen M. 1970 solar eclipse as "seen" by a torsion pendulum. *Phys. Rev. D*, 1971, v. 3(4), 823–825.
15. Mishra D. and Rao M. Total solar eclipse of October 224, 1995 in Dhorajii, Saurashtra. *Current Science*, 1997, v. 72(11), 783–786.
16. Vezzoli G. C. Gravitational data during the syzygy of May 18, 2001 and related studies. *Infinite Energy*, 2004, v. 9(53), 18–27.
17. Gershteyn M. et al. *Gravitation and Cosmology*, 2002, v. 3(32) 243–247. This work is regarded by the author as of profound significance, and relates to analogous sidereal year, lunar month, and solar day, periodicity in properties of radioactive decay of Pu-239, observed and reported by S. E. Schnol' for decades; see Letters authored by myself and Schnol' in *Progress in Physics*, 2008, v. 2. I have observed similar diurnal periodicity in related experiments using Po-210 during Jupiter eclipsing quasar J0842+1835, 7–11 Sept 2002 (see Ref. 16).
18. Vezzoli G.C. Experimental research incondensed matter physics arguing for modifications in mainstream concepts: considerations of the significance of a physics of collisions, shape and spin, regarding charge as a paradigm, relationship to subtle energy physics and far-from-equilibrium physics as well as zero point energy. *Infinite Energy*, 2007.
19. Fixler J. et al. Atom interferometer measurement of the Newtonian constant of gravity. *Science*, 2007, v. 315, 74–77.
20. John Shadow (Moderator: Yahoo Groups, Theoretical Physicist); Hans Schatten (Theoretical Physicist) and Tony Bedmenseder (Quantum Relativity Theoretical Physicist). Private communications.

The Mass of the Universe and Other Relations in the Idea of a Possible Cosmic Quantum Mechanics

Ioannis Iraklis Haranas* and Michael Harney†

*Department of Physics and Astronomy, York University, 314A Petrie Building, North York, Ontario, M3J-1P3, Canada
E-mail: ioannis@yorku.ca

†841 North 700 West, Pleasant Grove, Utah, 84062, USA
E-mail: michael.harney@signaldisplay.com

Recent observations confirm that galactic red-shifts might be quantized and hint a possible new form of quantum mechanics, which could probably explain these observed properties of the galaxies. This brief note investigates some expressions for the mass of the universe M_U, which were obtained with the help of the definition of the new cosmic Planck's constant $\hbar_g$.

Introduction

After it was found that the recession velocities for single and double galaxies appear to be quantized [1] then a new quantum of action was also derived to yield [2, 3]:

$$\hbar_g = \frac{\left(1+\sqrt{3}\right)^2 M}{H} V^2 \cong 7.0\times10^{74}\ \text{erg}\times\text{s}, \qquad (1)$$

where $V = 12$ km/s, $M = 10^{44}$ g, and $H = 1.7\times10^{-18}$ s^{-1}. Using Weinberg's relation for the mass of an elementary particle [4] we can now expect to obtain the mass of the universe if Planck's constant in (2) has been substituted by the new maximum value of the new cosmic quantum of action $\hbar_g$ [5]. Therefore we have

$$M_U = \left[\frac{\hbar_g^2 H}{Gc}\right]^{1/3}. \qquad (2)$$

If we now solve for the new defined quantum of action $\hbar_g$ in equations (2), and also use (1) we obtain that the mass of the universe is given by:

$$M_U = \left(1+\sqrt{3}\right)^4 \left[\frac{v^4}{GHc}\right]. \qquad (3)$$

Relation (3) was obtained after treating the universe as the "ultimate superparticle" following Weinberg's idea [4], and using his relation for the mass of an elementary particle. If now assume that velocity v corresponds to the radial velocity of the individual "particle" galaxies we can further assume that their velocities are those of the expansion of the universe's horizon, and will be equal to speed of light c, so that we obtain:

$$M_U = \left(1+\sqrt{3}\right)^4 \left[\frac{c^3}{GH}\right]. \qquad (4)$$

Substituting for the known values of constants in (4), and using $H = 1.7\times10^{-18}$ s^{-1} we obtain for the mass of the universe to be

$$M_U = 1.326\times10^{58}\ \text{g}. \qquad (5)$$

The mass of the universe found here is actually higher than the universes's actuall mass of 7.5×10^{55} g as given in [6] That could also be due to the contribution of the numerical term that enters the calculations from the definition of the cosmic $\hbar_g$. Since not all the objects in the universe are within such a great cosmic distances to allow $v \approx c$, this could also mean that the cosmic quantum mechanics idea could apply to the universe at very early times when the objects were closer together. To ensure numerically the value of the mass of the universe from (3) a galaxy would have to have a radial velocity $v = 0.254c = 7.640\times10^9$ cm/s. Objects of this redshift are observationally quite frequent. Quasistellar objects or quasars hold the record for redshifts up to $z = 5$ [7]. Therefore it could be that at those cosmic distances that quasars exist qualifies them for possible candidates of cosmic quantum mechanics, which somehow could be effecting their physics. Now suppose that this superparticle universe contains a number of particles in an Euclidean sphere of radius c/H_0 then, following Narlikar [8] we have that:

$$N = \frac{c^3}{2m_pGH}. \qquad (6)$$

Using (6) and (4) we can also obtain for the mass of the universe:

$$M_U = \left(1+\sqrt{3}\right)^4 [2m_pN] = 1.86\times10^{58}\ \text{g}, \qquad (7)$$

and where m_P is the mass of the proton, 1.672×10^{-24} g, and $N \approx 10^{80}$ is the total number of particles in the universe.

Let us now consider relation (4) and from that let us try to obtain the mass of the "super-particle" universe at very early times, and near Planck time. For that a very early Hubble constant should be taken into account. Since the age of the universe in general is equal to the inverse of the Hubble constant, then $\frac{1}{H_p} = t_p = \frac{\hbar}{m_{pl}c^2}$ we finally have after simplifying that

$$M_U = \left(1+\sqrt{3}\right)^4 m_{pl} = 1.114\times10^{-3}\ \text{g}. \qquad (8)$$

Now let us define the maximum value of the cosmological constant Λ which is defined below [9]

$$\Lambda_{max} = \frac{c^3}{G\hbar} \approx 10^{66}\ \mathrm{cm}^{-2} \quad (9)$$

and occurs during the quantum era of the early universe and using (1) we can now obtain the corresponding $\Lambda_{max}(\hbar_g)$ under cosmic quantum mechanics and so we have

$$\Lambda_{max}(\hbar_g) = \frac{c^3}{G\hbar_g} = 5.782\times10^{-37}\ \mathrm{cm}^{-2}. \quad (10)$$

Using now (10) together with (4) we can also write for the mass of the universe

$$M_U = \left(1+\sqrt{3}\right)^4 \left[\frac{\Lambda_{max}(\hbar_g)}{H}\right]\hbar_g = \\ = 1.894\times10^{-17}\hbar_g = 1.325\times10^{58}\ \mathrm{g}. \quad (11)$$

From the above we see that the mass of the universe becomes a multiple of the cosmic $\hbar_g$, or in other words the mass of the universe is now quantized in units of the cosmic $\hbar_g$. That could probably indicate that if cosmic quantum mechanics is in effect in the universe, basic quantities like mass, energy, or angular momentum could also be quantized, in an analogy with ordinary quantum mechanics.

Next if we try to obtain the cosmic quantum mechanical equivalent of Planck time by again substituting $\hbar \to \hbar_g = 7\times10^{74}$ ergs we have:

$$t_{pl_{cos}} = \sqrt{\frac{\hbar_g G}{c^5}} = 4.383\times10^{7}\ \mathrm{s}. \quad (12)$$

This period is well into the radiation era of the universe which lies between $10\ \mathrm{s} \leqslant t \leqslant 10^{12}$ s [10]. Next we can obtain the possible maximum cosmic Planck time for $\hbar_g = 2.228\times10^{94}$ ergs

$$t_{pl_{cos}} = \sqrt{\frac{\hbar_g G}{c^5}} \approx \frac{1}{H_0} = 2.472\times10^{17}\ \mathrm{s}. \quad (13)$$

The time found in (13) is almost the value of the Hubble constant today. This is the matter era of the universe. For the value of time in (13) a temperature close to the microwave background should be calculated. Therefore we have:

$$T = \frac{1.5\times10^{12}}{t^{2/3}} = 3.808\ \mathrm{K}. \quad (14)$$

Next a relation can be derived which connects the mass of the "super-particle universe" to its gravitational energy under the cosmic $\Lambda_{max}(\hbar_g)$. In general the energy of a hadron particle is given by [11]:

$$E_{grav} = \frac{Gm^3c^2}{\hbar^2} \cong NH_0. \quad (15)$$

Therefore (4) becomes:

$$M_U = \left(1+\sqrt{3}\right)^4 \left[\frac{\Lambda_{max}(\hbar_g)}{H_0^2}\right] E_{grav}(\hbar_g) = \\ = 1.114\times10^{1} E_{grav}(\hbar_g) = 1.894\times10^{57}\ \mathrm{g}. \quad (16)$$

Conclusions

A relation for the mass of the universe has been derived in the grand scheme of a possible quantum mechanics, an idea that emanates from a probable redshift quantization in observational data. The mass of the universe has been found to depend on three fundamental quantities: i.e. the speed of light, the gravitational constant, and the Hubble parameter. Its numerical value is almost two hundred times higher than the actual mass of the universe. From that another expression for the mass of the universe at very early times has also been retrieved. The mass of the universe at Planck time seems to be slightly larger than the Planck mass by a factor of a hundred. Next making use of a max quantum cosmic cosmological term (lambda) we obtained the mass of the universe, which now appears quantized in the units of cosmic $\hbar_g$. Also the Planck cosmic quantum mechanical time equivalent was obtained for the two different values of $\hbar_g$. The first lies in the radiation era of the universe, and the second in the matter era, being almost the same in magnitude with today's Hubble parameter, from which a temperature of 3.8 K is obtained. Finally the mass of universe was obtained in relation to its gravitational energy. Hence it might be that a relation between ordinary and cosmic quantum mechanics based on the results found might exists, a relation between microcosm and macrocosm an idea, which had been suspected for long.

Submitted on December 13, 2008 / Accepted on January 09, 2009

References

1. Cocke W. and Tifft W. *Astrophysical Journal*, 1984, v. 287, 492.
2. Dersarkissian M. *Lett. Nuovo Cimento*, 1984, v. 40, 390.
3. Dersarkissian M. *Lett. Nuovo Cimento*, 1985, v. 43, 274.
4. Weinberg S. Gravitation and cosmology. John Wiley, New York, 1972.
5. Haranas I. *Journal of Theoretics*, 2001, v. 3, no. 2, 2001.
6. Padmanabhan T. Structure formation in the Universe. Cambridge University Press, Cambridge, 1993.
7. Antwrp.gsfc.nasa.gov/apod/ap981211.html
8. Narlikar J. Introduction to cosmology. Cambridge University Press, Cambridge, 1993, p. 272.
9. Sivaram C. and de Sabbata V. *Astrophysics and Space-Science*, 1991, v. 176, 145–148, 1991.
10. Ohanian H.C. and Ruffini R. Gravitation and space-time. 2nd edition, Norton & Co., 1994.
11. Johri V.B. The early Universe. Hadronic Press, Instituto Per La Ricerca Di Base, Italy, 1996, p. 33.

A Planck Vacuum Cosmology

William C. Daywitt

National Institute for Standards and Technology (retired), Boulder, Colorado, USA

E-mail: wcdaywitt@earthlink.net

Both the big-bang and the quasi-steady-state cosmologies originate in some type of Planck state. This paper presents a new cosmological theory based on the Planck-vacuum negative-energy state, a state consisting of a degenerate collection of negative-energy Planck particles. A heuristic look at the Einstein field equation provides a convincing argument that such a vacuum state could provide a theoretical explanation for the visible universe.

1 Introduction

Cosmology, taken as a whole, is the study of the origin and evolution of the universe [1, p. 1144]. The universe is the visible (observable by whatever means) universe that exists in free space. At present there are two major competing cosmologies that theoretically describe the real observed universe, the big-bang cosmology [2] and the quasi-steady-state cosmology [3], the big-bang cosmology being considered by most cosmologists as the major one of the two. Both cosmologies claim some type of Planck state as the origin for their calculations; in the big-bang case it is a point source at time zero in which an explosion takes place, subsequently creating the expanding universe; while in the quasi-steady-state case a background field called the "creation field" creates free Planck particles (PP) on a quasi-continuous basis that immediately decay into a large number of particles, subparticles and fields.

The present paper presents a new cosmological model called the Planck-vacuum (PV) cosmology. The PV (briefly described in Appendix A) is an omnipresent negative-energy state that is assumed to be the Planck state that is the foundation for the visible universe, its expansion, and also its eventual contraction. The addition of the PV to the visible universe in a cosmological model requires a name to distinguish the combination from the visible universe of standard cosmology. The name used here is "cosmos" and includes, correspondingly, the PV and the visible universe. As might be expected, this new model differs significantly from the two models mentioned in the preceding paragraph.

We begin with a brief look at the standard Einstein metric equation

$$G_{\mu\nu} = \frac{8\pi G}{c^4} T_{\mu\nu} = \frac{8\pi}{m_* c^2 / r_*} T_{\mu\nu} \qquad (1)$$

where $G_{\mu\nu}$ and $T_{\mu\nu}$ are the Einstein and energy-momentum tensors, and G and c are the gravitational and speed-of-light constants. The force $m_* c^2 / r_*$ in the denominator of the final expression is the ultimate curvature force that can be applied to the spacetime of General Relativity or to the PV [4]. Compared to this force, the relative curvature force the sun, a white dwarf, or a neutron star exert on spacetime and the PV is 0.00001, 0.001, and 0.5 respectively. With the help of Appendix A, the Einstein equation can also be expressed in the form

$$\frac{G_{\mu\nu}/6}{1/r_*^2} = \frac{T_{\mu\nu}}{\rho_* c^2} \qquad (2)$$

where r_* is the Compton radius of the PP and ρ_* is its mass density. The ratio $1/r_*^2$ can be thought of as the PP's Gaussian curvature. In this latter form both sides of the equation are dimensionless. As the curvature force, the mass density, and the Gaussian curvature are intimately related to the PPs in the negative-energy PV, it is easy to conclude that the Einstein equation and General Relativity must also be intimately related to that vacuum state.

The PV-cosmology modeling begins in the next section which concerns the expansion of the cosmos. Since little is known about the PV at the present time, however, the calculations in that section and the one following it are a bit sketchy and of a cursory nature.

The PV cosmology must address the question of how PPs from the PV are injected into free space to populate the visible universe with the particles and fields upon which the larger components of the universe are built. A scenario for this injection process that somewhat parallels the quasi-steady-state theory of PP creation is presented in Section 3, the main difference being that in the quasi-steady-state model the PPs evolve from "creation fields" while in the present theory they spring directly from the negative-energy PV state.

A comments Section 4 closes the main text of the paper. Appendix A gives a brief description of the PV theory to date and Appendix B compares the PV to the cosmological-constant term in the Einstein field equation.

2 Cosmological expansion

The mass density of the degenerate PV state in the PV cosmology is roughly equal to the PP mass density

$$\rho_* \equiv \frac{m_*}{4\pi r_*^3/3} \approx 10^{94} \ [\mathrm{gm\ cm^{-3}}] \qquad (3)$$

where m_* and r_* are the PP mass and Compton radius respectively. If we somewhat arbitrarily take the universal

mass density as $\rho_m \sim 10^{-30}$ [gm cm^{-3}], then the ratio $\rho_m/\rho_* \sim 10^{-124}$ is vanishingly small. Thus it is unreasonable to expect that the visible universe can effect the expansion or contraction of the cosmos as it does for the universe in the big-bang and quasi-steady-state cosmologies. This fact leads to the conclusion that the expansion of the universe must be determined by that of the PV itself.

The expansion of a homogeneous and isotropic universe is characterized by the expansion factor S $(= S(t))$ in the Robertson-Walker line element [3, p. 111]

$$ds^2 = c^2dt^2 - S^2\left[\frac{dr^2}{1-kr^2} + r^2d\theta^2 + r^2\sin^2\theta\, d\phi^2\right] \quad (4)$$

where (t, r, θ, ϕ) are comoving coordinates, and where $k=+1$, $k=-1$, and $k=0$ denote a universe with a positive, negative, or zero curvature respectively. The Robertson-Walker metric is used to determine the "kinematic" properties of the universe for any given S, the dynamics of the expansion only appearing implicitly in the time dependence of S. For example, (4) can be used to derive the standard expressions for the redshift z [3, pp.112-113] and the Hubble constant H [3, pp.118–119]:

$$1 + z = \frac{1}{S} \quad (5)$$

$$H = \frac{\dot{S}}{S} \quad (6)$$

without specifying the particular dynamics of the expansion. Thus these relations are equally valid in the big-bang, quasi-steady-state, and PV cosmological models.

To determine the dynamics of the expansion factor in the big-bang and quasi-steady-state cosmologies, some form of the Einstein equation (2) is used. Both models start by calculating the Einstein tensor $G_{\mu\nu}$ from the metric coefficients of the Robertson-Walker line element (4). The standard big-bang cosmology then assumes various energy-momentum tensors for the right side of (2) to derive the Friedmann equations for S in the various phases of the expanding universe [2, pp.48–50]. An early version of the quasi-steady-state model modifies the numerator on the right side of (2) to include a "creation field" for generating PPs, then derives Friedmann-like equations for the expansion-factor dynamics [3, pp.322–324]. As the expansion-factor dynamics in the PV-cosmology model is determined by the expansion of the PV itself, however, it isn't clear what part the Einstein and Friedmann-like equations may or may not play in the research surrounding the PV cosmology.

There is no compelling evidence that the constants governing the fundamental laws of physics were once different from their present values [1, p. 1056]. This statement bares significantly on the nature of the PV expansion — it implies, in effect, that the PV expands by an increase in its content rather than a change in its properties. Assume that the number density of the PPs in the PV decreases as the PV expands for example. Then the density of the virtual fields of the quantum vacuum [5] would also decrease because the PV is the source of the quantum vacuum [6]. This in turn would decrease the magnitude of the dominant Bethe term [7, p. 208] in the $2S_{1/2} - 2P_{1/2}$ Lamb shift of atomic hydrogen as the Bethe term is proportional to the density of the virtual fields [5, p. 91]. Thus the 2S-2P transition frequency of the atom would decrease as the PV expands, contradicting the assumption in the first sentence of the paragraph.

3 Planck Particle creation

It is assumed that a sufficiently stressed PV will release one or more of its PPs into the visible universe in a manner resembling a mini-big-bang outburst. "[This] requirement is in agreement with observational astrophysics, which in respect of high-energy activity is all of explosive outbursts, as seen in the QSOs, the active galactic nuclei, etc. The profusion of sites where X-ray and γ-ray activity is occurring are in the present [quasi-steady-state] theory sites where the creation of matter is currently taking place" [3, p. 340]. It is then assumed that the new free-space PP decays into a number of secondary particles. The lifetime of the free PP is assumed to be governed by the time required ($t_* = r_*/c \sim 10^{-44}$ sec) for the internal PP fields (traveling at the speed of light) to decay within the confines of the PP Compton radius r_*.

It is too early in the PV-cosmology theory to present any substantial analysis concerning the details of the activity mentioned in the previous paragraph. We are left, then, with a heuristic description of the PP-creation process in terms of the Einstein field equation. Taking the (covariant) divergence of (2) gives

$$G^{\mu\nu}_{\ ;\nu} \equiv 0 \qquad \Longrightarrow \qquad T^{\mu\nu}_{\ ;\nu} = 0 \quad (7)$$

showing that the standard Einstein equation provides no mechanism for creating PPs due to the vanishing divergence of the energy-momentum tensor. Assume that at some point x^α $(\alpha = 0, 1, 2, 3)$ in empty spacetime ($T^{\mu\nu} \approx 0$ before x^0) a PP is ejected from the PV into the free space of the visible universe. In the standard action (see Appendix A)

$$\mathcal{A} = \frac{1}{2c}\left(\frac{\rho_* c^2}{1/r_*^2}\right)\int \frac{R}{6}\sqrt{-g}\, d^4x + m_a c\int ds_a \quad (8)$$

whose variation yields (2), the world lines are considered to be continuous in the full range $0 < |x^\alpha| < \infty$. At the point x^α where a PP is created, however, the PP world line begins. It is possible to modify (8) in that case so its variation leads to the modified Einstein equation [3, p. 323]

$$\frac{G^{\mu\nu}/6}{1/r_*^2} = \frac{T^{\mu\nu}_{(m_*)} + \mathcal{T}^{\mu\nu}_{(pv)}}{\rho_* c^2} \quad (9)$$

where, as interpreted here, the calligraphic tensor in the nu-

merator at the right is associated with processes taking place within the PV.

The free-PP creation represented by (9) is explained physically as an interchange of energy and momentum between the PV and the PP injected into the visible universe. The divergence of (9) now leads to

$$T^{\mu\nu}_{(m_*);\nu} = -\mathcal{T}^{\mu\nu}_{(pv);\nu} \tag{10}$$

which is meaningful only if the right side of the equation leads to a positive free-space PP energy [3, p. 325]; i.e. only if the 0-0 component of the PV energy-momentum tensor is negative. That this tensor component is negative follows from the fact that the PV state is a negative-energy state. Thus we have

$$T^{00}_{(m_*)} = -\mathcal{T}^{00}_{(pv)} = +\rho_* c^2 \tag{11}$$

as

$$\mathcal{T}^{00}_{(pv)} = -\rho_* c^2 \tag{12}$$

since the PP mass-energy density of a PP *within* the PV is $-\rho_* c^2$.

4 Sundary comments

It is assumed that the origin of the light nuclei and the cosmic microwave background in the PV-cosmology model are essentially the same as those discussed in the quasi-steady-state model [3, pp.350-358].

Both the big-bang and the quasi-steady-state cosmologies are based on field theory, the big-bang cosmology on the quantum field theory of the early universe [2] and the quasi-steady-state cosmology on the so-called "creation fields". The choice of a field-theoretic approach reflects, of course, the current paradigm that fields are the fundamental building blocks of the particles and subparticles out of which the observed universe is constructed. With the advent of the PV theory, however, these fields now have a charged source (the PPs within the PV) as their origin. It is this charged source that is the foundation of the PV cosmology presented here.

The action integrals in (A8) of the appendix tie the creation field $\mathcal{C}_\mu$ of the quasi-steady-state theory [3, p. 321] directly to the PPs in the PV.

The calculations in Appendix B show that the PV cannot be identified with the cosmological-constant term in the Einstein field equation.

Appendix A: The Planck Vacuum

The PV [4] is a uni-polar, omnipresent, degenerate gas of negative-energy PPs which are characterized by the triad (e_*, m_*, r_*), where e_*, m_*, and r_* $(\lambda_*/2\pi)$ are the PP charge, mass, and Compton radius respectively. The vacuum is held together by van der Waals forces. The charge e_* is the bare (true) electronic charge common to all charged elementary particles and is related to the observed electronic charge e through the fine structure constant $\alpha = e^2/e_*^2$ which is a manifestation of the PV polarizability. The PP mass and Compton radius are equal to the Planck mass and length respectively. The particle-PV interaction is the source of the gravitational $(G = e_*^2/m_*^2)$ and Planck $(\hbar = e_*^2/c)$ constants, and the string of Compton relations

$$r_* m_* = \cdots = r_c m = \cdots = e_*^2/c^2 = \hbar/c \tag{A1}$$

relating the PV and its PPs to the observed elementary particles, where the charged elementary particles are characterized by the triad (e_*, m, r_c), m and r_c being the mass and Compton radius $(\lambda_c/2\pi)$ of the particle (particle spin is not yet included in the theory). The zero-point random motion of the PP charges e_* about their equilibrium positions within the PV, and the PV dynamics, are the source of the quantum vacuum [6] [5]. Neutrinos appear to be phonon packets that exist and propagate within the PV [8].

The Compton relations (A1) follow from the fact that an elementary particle exerts two perturbing forces on the PV, a curvature force mc^2/r and a polarization force e_*^2/r^2:

$$\frac{mc^2}{r} = \frac{e_*^2}{r^2} \qquad \Longrightarrow \qquad r_c = \frac{e_*^2}{mc^2} \tag{A2}$$

whose magnitudes are equal at the particle's Compton radius r_c.

Equating the first and third expressions in (A1) leads to $r_* m_* = e_*^2/c^2$. Changing this result from Gaussian to MKS units yields the free-space permittivities [4]

$$\epsilon_0 = \frac{1}{\mu_0 c^2} = \frac{e_*^2}{4\pi r_* m_* c^2} \quad [\mathrm{mks}] \tag{A3}$$

where $\mu_0/4\pi = r_* m_*/e_*^2 = r_c m/e_*^2 = 10^{-7}$ in MKS units. Converting (A3) back into Gaussian units gives

$$\epsilon = \frac{1}{\mu} = \frac{e_*^2}{r_* m_* c^2} = 1 \tag{A4}$$

for the permittivities.

A feedback mechanism in the particle-PV interaction leads to the Maxwell equations and the Lorentz transformation. General Relativity describes the spacetime-curvature aspects of the PV. The ultimate curvature force [4]

$$\frac{c^4}{G} = \frac{m_* c^2}{r_*} \tag{A5}$$

that can be exerted on spacetime and the PV is due to a free PP, large astrophysical objects exerting a curvature force equal to Mc^2/R, where M and R are the mass and radius of the object. Equation (A5) leads to the important ratio

$$\frac{c^4}{8\pi G} = \frac{1}{6}\,\frac{\rho_* c^2}{1/r_*^2} \tag{A6}$$

where $\rho_* \equiv m_*/(4\pi r_*^3/3)$ is the PP mass density and $1/r_*^2$ is its Gaussian curvature.

Using (A6), the Einstein-Hilbert action $\mathcal{A}_g$ can be expressed as

$$\mathcal{A}_g = \frac{c^3}{16\pi G}\int R\,\sqrt{-g}\,d^4x = \\ = \frac{1}{2c}\left(\frac{\rho_* c^2}{1/r_*^2}\right)\int \frac{R}{6}\,\sqrt{-g}\,d^4x \tag{A7}$$

leading to the total PP-creation action [3, p. 321]

$$\mathcal{A} = \frac{1}{2c}\left(\frac{\rho_* c^2}{1/r_*^2}\right)\int \frac{R}{6}\sqrt{-g}\,d^4x + m_a c\int ds_a + \\ + \frac{f}{2c}\int C_\mu C^\mu \sqrt{-g}\,d^4x - \int C_\mu\, da^\mu, \tag{A8}$$

which includes the usual inertial second term, and the third and fourth creation-field terms containing C_μ. The effect of the PV PPs on this equation is clearly evident in the parenthesis of the first term which is the ratio of the PP's mass-energy density to its Gaussian curvature.

Appendix B: Cosmological constant

The Einstein equation including the cosmological constant Λ is

$$\frac{(G_{\mu\nu} + \Lambda g_{\mu\nu})/6}{1/r_*^2} = \frac{T_{\mu\nu}}{\rho_* c^2}, \tag{B1}$$

which can be expressed as

$$\frac{G_{\mu\nu}/6}{1/r_*^2} = \frac{T_{\mu\nu} + \mathcal{T}_{\mu\nu}}{\rho_* c^2}, \tag{B2}$$

where

$$\mathcal{T}_{\mu\nu}^{(vac)} \equiv -\frac{1}{6}\frac{\rho_* c^2}{1/r_*^2}\,\Lambda g_{\mu\nu} \tag{B3}$$

leads to

$$\rho_{vac} c^2 \equiv \frac{\mathcal{T}_{00}}{g_{00}} = -\frac{1}{6}\frac{\rho_* c^2}{1/r_*^2}\,\Lambda \tag{B4}$$

which is often seen as the "vacuum energy".

From (B4)

$$\frac{\rho_{vac}}{\rho_*} = -\frac{1}{6}\frac{\Lambda}{1/r_*^2} \tag{B5}$$

the ratio being negative for a positive Λ. If the vacuum density ρ_{vac} is identified as the PP mass density ρ_*, then

$$\Lambda = \frac{6}{r_*^2} \approx 2.3 \times 10^{66}\,[\mathrm{cm}^{-2}]\,. \tag{B6}$$

As Λ should be close to zero, it is clear that the PV is not related to the cosmological constant.

Submitted on December 31, 2008 / Accepted on January 13, 2009

References

1. Carroll B.W., Ostlie D.A. An introduction to modern astrophysics. Addison-Wesley, San Francisco—Toronto, 2007.
2. Kolb E.W, Turner M.S. The early universe. Westview Press, 1990.
3. Narlikar J.V. An introduction to cosmology. Third edition, Cambridge Univ. Press, Cambridge, UK, 2002.
4. Daywitt W.C. The planck vacuum. *Progress in Physics*, 2009, v. 1, 20.
5. Milonni P.W. The quantum vacuum — an introduction to quantum electrodynamics. Academic Press, New York, 1994.
6. Daywitt W.C. The source of the quantum vacuum. *Progress in Physics*, 2009, v. 1, 27.
7. Grandy W.T. Jr. Relativistic quantum mechanics of leptons and fields. Kluwer Academic Publishers, Dordrecht-London, 1991.
8. Daywitt W.C. The neutrino: evidence of a negative-energy vacuum state. *Progress in Physics*, 2009, v. 2, 3.

An Alternative Hypothesis for Special Relativity

Horst Eckardt

Alpha Institute for Advanced Study (AIAS) and Telesio-Galilei Association (TGA)
E-mail: horsteck@aol.com

An alternative theory being analogous to Einstein's special theory of relativity is presented. While Einstein based his theory on the relativity principle of motion and constancy of the velocity of light, this theory assumes an absolute frame of reference and a general length contraction. Both concepts are taken from general relativity and applied to an asymptotically flat space. This results in a transformation group being different from the Lorentz transformation and a Eucledian addition theorem of velocitites. The results are in accordance with experiments and long known discrepancies between special relativity and experimental findings are resolved as well as paradoxa being introduced by Einstein's original theory. Physical facts being unintelligible before can be interpreted in the light of the alternative theory.

1 Introduction

The theory of special relativity of Albert Einstein is essentially based on the constancy of the velocity of light in all inertial frames of reference. Einstein introduced this as a physical principle or axiom in order to explain the negative outcome of the experiments of Michelson and Morley who tried to prove the existence of a drift velocity of the earth in a hypothetical ether. However, in the last years a number of experiments came up showing that the velocity of light is not an incontrovertible constant. For example Nimtz [5, 6] has realised a transfer of information by microwaves by speeds faster than light. His explanations are wound and based on quantum effects (tunnelling) which should not appear in systems with exclusively macroscopic dimensions. Most convincing would be an explanation by classical physics which is also the basis of electromagnetic signal transmission. Another important development is the re-interpretation of the Michelson-Morley experiments [10, 11] which show that they had not been evaluated in the right way. When doing this, earlier inconsistencies are resolved and an absolute motion of the earth against the space background is detected. This revolutionary insight has not been recognized in the scientific public so far. Therefore re-thinking about the concepts of special relativity is required.

A second fundament of modern physics is the principle of relativity. Besides the reasonable assumption that laws of nature work in the same way in all reference frames not being accelerated to one another, it is postulated that the transformation between reference frames is always of the same form. It is assumed that all frames of reference be of equal kind. This consideration does not take into account that the universe is structured by masses which define reference points for physical processes. The whole universe is impleted with gravitational and electromagnetic fields. This also holds for the "empty" ranges between galaxies and galaxy clusters since the particle density is non-vanishing in interstellar space to today's knowledge. So we can say that in certain areas of the cosmos we can neglect the influence of cosmic fields, but normally we use the visible beacons (earth, sun, centers of galaxies) to define reference frames. The cosmos as a whole is described by general relativity and Mach's principle which states that the masses define the space. Without masses there is no space at all. Crothers [4] has pointed out that there is no smooth transition from general to special relativity:

> "Special Relativity is merely an augmentation to Minkowski space by the arbitrary insertion of mass and energy into Minkowski space with the constrained kinematic features of Minkowski space applied to those masses and energies".

This view is corroborated by newer advanced theories like Einstein-Cartan-Evans theory [18] where space is not empty but filled with the background or "vacuum" potential. Without potential there is no space, in accordance with Mach's principle. So it should become clear that general relativity (or any similar advanced theory) is necessarily required to define a basis for all physics. One can abstract then from these foundations and concentrate on other problems, for example experiments of particle collisions, without taking care of these basic premises. When it comes to define the frames of reference, however, the state of motion relative to the absolutely defined environment is important again.

All these arguments become much more intelligible if we assume that the space between massive particles has a state of motion. This sounds like introducing the old ether idea from the nineteenth century. Our knowledge has only little improved since then. The ether was abolished by Einstein, but indirectly re-introduced by himself in his theory of general relativity. It is possible to define an "objective" frame of reference constituted by existing masses. Considering Einstein-Cartan-Evans theory, space is not empty but itself a medium which for example has optical properties [18]. We can extend the comparison with usual media by assigning a state of

motion to the space itself. Masses "swim" in this space and therefore reflect its movement. Conversely, the fields created by the masses determine the surrounding space in a fed-back manner. Both entities cannot be considered independently from each other.

In Einstein-Cartan-Evans theory, the covariance principle is the most general description base of physics, indicating that all laws of nature are independent of the coordinate system or reference frame. Our physical environment is defined by the objectively existing structure which is defined by masses, charges and fields. These are adequately described in an objective manner by laws of nature being independent from subjective human receptions.

In this article we try to modify Einstein's axioms of special relativity in such a way that constancy of light velocity is not required to be introduced axiomatically. It will be shown that this is an artifact of measurement. Instead of this axiom we demand for an absolute frame of reference. As a consequence, we will arrive at transformation laws similar to Einstein's which depend on the absolute reference frame but change asymptotically to Einstein form in certain important application cases. In particular we will obtain a different addition theorem of velocities allowing for superluminal speed. The well known Lorentz transformation and symmetry will evolve not to be valid in our new framework. A more general four-dimensional affine transformation will take its place which has mathematical group properties as well. We will end with a short discussion of the experiments mentioned it this introduction in the light of the new theory.

2 Problems in experimental proofs of Special Relativity

In the well-known experiment of Michelson and Morley, which was repeated several times at the beginning of the twentieth century (see a review in [11]), it was apparently shown that the velocity of light c is the same in all directions relative to the earth orbit. This was considered to be a proof that this velocity is a general constant in nature under all circumstances. We will critically analyse this in the following.

Firstly we have to comment that this is valid only in special relativity, i.e. for unacceletated motion. In general relativity c depends on the gravitational field (or on all fields in case of unified field theories). This dependence is well proven experimentally. Therefore we should state that constancy of c is only valid in vacuo with neglection of all fields.

Secondly we inspect the way in which measurements of the speed of light were done. These were carried out by interferometers where the runtime of light rays was compared between rays having been reflected in different directions. If there is a directional dependence on propagation speed, a characteristic interferometric pattern should occur if the apparatus is rotated. Within assumed experimental uncertainties, no such pattern was observed. Since the length of the apparatus was not changed it was concluded that the velocity of light was the same in all directions. What not has been considered in this explanation is the effect of length contraction. According to Einstein's special relativity, the measured length changes with the same factor as the measured time, if the frame of reference is changed by modifying relative speed between observer and object. For the experiments of Michelson-Morley type this means that the run-time of light as well as the interferometer length change, as soon as the apparatus is rotated relative to a hypothetical absolute direction of motion ("ether wind"). The compression factor is the same for length and time, therefore we obtain for two directions with length l and l' and run-time t and t':

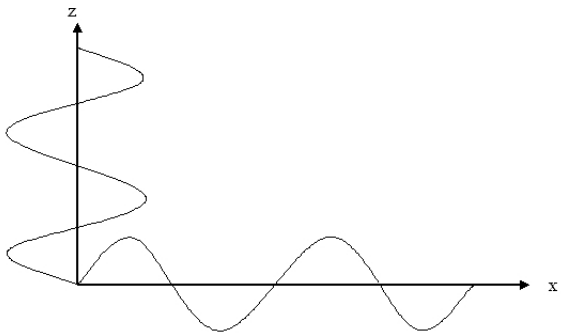

Fig. 1: Length contraction in experiments of Michelson Morley type.

$$c = \frac{l}{t} = \frac{l'}{t'} = \text{const.} \qquad (1)$$

According to Fig. 1 the number of wave trains is the same irrespective of the compression factor. No wonder the value of c is constant. This type of experiments does not prove the details of the Lorentz transformation.

The re-evaluation of experiments of Michelson-Morley type by Cahill et al. [10, 11] has revealed that the evaluation of experimental data was done by erroneously assuming no length contraction. As explained above, taking length contraction into account leads to a meaningless null experiment. This is the outcome of modern laser interferometer spectroscopy in vacuo. However, the older experiments were performed by interferometers in air or helium. Therefore the refraction index is different from unity (although nearby). Doing the evaluation with respection of length contraction as well as refractive index effects leads indeed to a non-null result. Surprisingly, all the older experiments, evaluated in this way, then prove a velocity of the earth orbit relative to the space background of 365 km/s within error bars, see Fig. 2 taken from [10, 11]. This is the most significant experimental hint for the physical relevance of a background field. However, it must be added that the most precise value in Fig. 2, measured from the constant background radiation by the COBE satellite, is controversial. Robitaille [17] has argued that the background radiation is an earth-made effect due to the black body radiation of the oceans. Further satellite missions will clear this up.

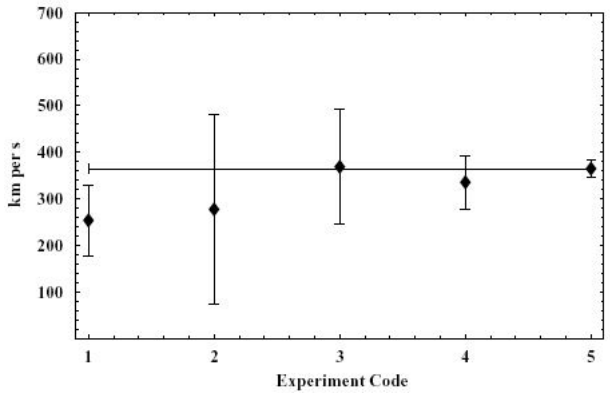

Fig. 2: Speed of earth orbit (reproduction from [10]) in km/s, determined from various Michelson interferometer experiments (1)–(4) and COBE (5): (1) Michelson-Morley (noon observations), (2) Michelson-Morley (18h observations), (3) Illingworth, (4) Miller, Mt.Wilson, and finally in (5) the speed from the COBE satellite observation of the CBR (Constant Background Radiation) microwave spectrum dipole term.

A third problem concerns the interpretation of length contraction and time dilation. Originally Einstein believed that these changes are virtual, i.e. are only measured values of an observer moving relative to another system. The scales of the real objects never change. Later after upcoming of general relativity it became clear that scales have to change in reality because the gravitational field is real in the sense that it evokes real, measurable forces. So it was implicitly assumed that also the scale changes of special relativity have to be real. This however is a severe philosophical problem since two observers measuring the same object would obtain different values for identical physical properties of the object. This discrepancy has not been addressed in literature until today and reflects inconsistencies in the transition from general to special relativity.

3 Length contraction

Since length contraction is the central property of this theory as well as Einstein's special relativity, we will give an explanation how this can be interpreted as a geometric property of fast moving circular or spherical objects. We assume a simple model of matter where atoms are built from an atomic nucleus and orbiting electrons moving in spherical orbits. An observer may travel relative to such an atom with velocity $-v$, and the orbital tangential velocity of an electron may be v_e (near to speed of light). Then the observer sees the electron moving on a curve which is a cycloid or trochoid, see Fig. 3. The form of the curve depends on the ratio of radii a/b, where a is the radius of the "rolling" circle and b is the radius of the path of the electron. For the uniform velocity v we have

$$v = \omega a \tag{2}$$

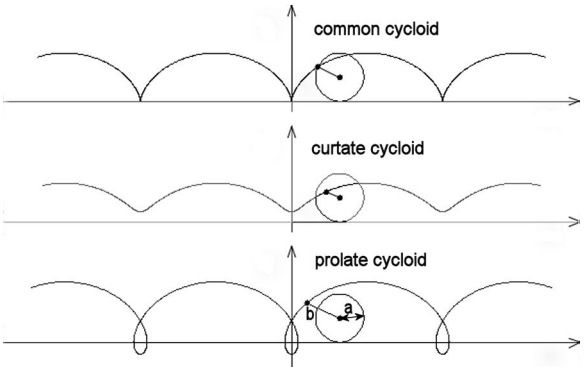

Fig. 3: Several forms of trochoids, also called common cycloid, curtate cycloid and prolate cycloid [19].

with ω being the angular velocity of angle ϕ rotating in time t:

$$\phi = \omega t\,. \tag{3}$$

For the x and y coordinates the parameter form of the cycloid is given by

$$x = a\phi - b\sin\phi\,, \tag{4}$$

$$y = a - b\cos\phi\,. \tag{5}$$

In the rest frame of the atom we have

$$v_e = \omega b \tag{6}$$

for the rotating electron. This equation determines the angular velocity ω. The same ω has to be used in formula (2). The roll radius a is determined then by the relative velocity v. If an observer tries to measure the diameter of a moving atom, he will see the reduced thickness of the cycloidal loop. For $v = v_e$ we obtain $a = b$, the diameter goes to zero. For $v > v_e$ there is only an unharmonic wave left and there is no measurable diameter of an atomic structure.

The diameter can be calculated quantitatively as follows. The x values for the diameter are defined by a vertical tangent of the cycloid, i.e.

$$\frac{dx}{d\phi} = 0\,, \tag{7}$$

which is according to Eq. (4):

$$a - b\cos\phi_0 = 0 \tag{8}$$

or

$$\phi_0 = \arccos\left(\frac{a}{b}\right). \tag{9}$$

Inserting ϕ_0 into (4) gives for the x values where the diameter is being measured

$$x_0 = a\,\arccos\left(\frac{a}{b}\right) - b\,\sqrt{1-\frac{a^2}{b^2}}\,. \tag{10}$$

Since we have

$$x\left(\phi = 0\right) = 0 \tag{11}$$

the value x_0 describes the radius of the atom measured from an observer frame with relative speed v. The well-known square root term is contained in this expression. To obtain this term exclusively we have to tentatatively modify Eq. (4) by replacing a by another parameter a_1. Then we obtain from (10):

$$x_0 = a_1 \arccos\left(\frac{a}{b}\right) - b\sqrt{1-\frac{a^2}{b^2}} \qquad (12)$$

and in the limit $a_1 \to 0$ the observed radius of the atom becomes

$$r = |x_0| = b\sqrt{1-\frac{a^2}{b^2}}\,, \qquad (13)$$

which with help of (2) and (6) can be rewritten to

$$r = b\sqrt{1-\frac{v^2}{v_e^2}}\,, \qquad (14)$$

which is the experimentally found expression for length contraction. So at least qualitatively we can explain length contraction from the geometric effect of relative circular motion.

4 Special Relativity according to Einstein

We describe shortly the axiomatic foundation of special relativity as given by H. Ruder [1]. All physical conclusions follow from the Lorentz transformation. This can be derived from three postulates or axioms:

1. Homogeneity and isotropy of space;
2. Principle of relativity;
3. Constancy of light velocity.

The first axiom is foundational for all physics. The three-dimensional space free of masses has no places which are singled out from others and all directions are equivalent. From classical mechanics we know that these properties lead to the conservation laws of energy and angular momentum. Both statements are equivalent. Therefore axiom 1 is unsurrendable.

The relativity principle states that all inertial frames are equivalent for describing the laws of physics. A difference by measurement is not detectable. The prerequisite is that a global, absolute reference frame does not exist. This is at variance with general relativity as well as newer experiments explained in section 2. The relativity principle would be valid only if space were exactly homogeneous, i.e. free of matter. Then, according to general relativity and Mach's principle, the space would not exist at all. Therefore the relativity principle is a simplifying assumption which we will abandon in the following.

In the same way we do not claim absolute constancy of light velocity (c) in all reference frames. From general relativity it follows that this velocity is not constant but dependent on the strength of the gravitational and other fields. One has to negate this assumption even in special relativity as soon as optical refraction plays a role where the transmission speed of waves is $v = c/n$ with n being the index of refraction. c can only be considered to be a value of light propagation in vacuo with absence of fields of every kind. Another way of circumventing the a priori assumption of a constant c is to measure the transformation law for the proper time of fast moving systems. In this way the well-known Myon experiment can be interpreted for example [1]. It comes out that the transformation law can be cast in a mathematical form containing a constant c which "may have something to do" with light propagation in vacuo. We conclude that only the first axiom has withstood a critical analysis.

5 Modified Special Relativity according to this hypothesis

We will derive now the alternative theory resting upon the three fundamental assumptions:

1. Homogeneity and isotropy of space;
2. Existence of an absolute frame of reference;
3. Physical length contraction.

The first axiom has already been discussed. The second can be constituted by the fact that a more general theory, which does not presuppose inertial systems, allows a referencing system bound to the masses of the universe. Therefore it makes no sense to ignore this fact. If an absolute frame of reference is of physical relevance, it will have an effect. This is not so obvious from general relativity, because the gravitational field is no more effective outside the range of galaxies. It would be more plausible to have a principle of close-ranging or local interaction. In this class of principles belong the ether theories. Already Einstein talked of an "ether space" which was immaterial to his opinion. Sometimes new ether theories come up as for example by Schmelzer [2] where the ether has the property of mediating the principle "actio = reactio". An absolute frame of reference can be related to this ether. It is analogous to a medium for sound waves and the concept of non-homogeneity and the refraction index of wave propagation are applicable. This shows that an ether concept can be added to general relativity, if not already existing in it. An attempt to incorporate it into technical applications was made by Meyl [3].

The ether concept is not necessary when we base our considerations on a unified field theory like Einstein-Cartan-Evans theory [18]. Then space itself is a medium which shows optical properties and a local structure which is defined by the vacuum or background potential. The new interpretation of Michelson-Morley experiments is compatible with this concept.

As a third prerequisite we assume length contraction first introduced by Fitzgerald and Lorentz. As explained above this contraction is required to give consistent results of the

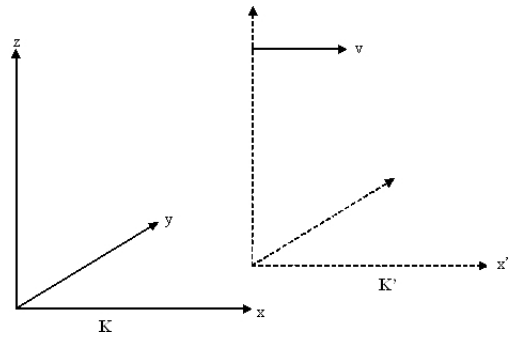

Fig. 4: Reference frames at rest (K) and with relative motion (K').

interferometric experiments. If a body moves with velocity v relative to the background, all lengths are shortened by a factor of

$$\gamma = \sqrt{1 - \frac{v^2}{c^2}}. \tag{15}$$

This contraction is real and not an artifact of measurement. According to the considerations above this is an effect of relative motion. This factor also appears in electrodynamics where it describes the transformation law between electromagnetic fields. Matter exists on an electromagnetic basis. Consequently, this factor also appears in relativistic quantum mechanics. We will see in the next section that length contraction has an effect on time measurements so that local ("proper") times of moving systems are impacted in the same way.

6 Derivation of the alternative theory

6.1 The transformation equations

In the following we will derive the transformation law between different reference frames. We will first give the transformation law of special relativity in the most general case as described in [1]. The result of the first axiom can be used directly because it is identical in Einstein's and our theory. We define a coordinate system K at rest and a system K' moving with velocity v relative to K. The system K is the absolute rest frame as for example measured by experiment. Coordinate axes are chosen so that all axes between K and K' are in parallel, and motion is in x direction of system K. Then we can restrict consideration to one dimension. According to [1] the transformation law between K and K' then has the general form

$$x' = b(v)(x - vt) \tag{16}$$

$$x = b'(v')(x' + v't') \tag{17}$$

where $b(v)$ and $b'(v')$ are functions of the velocity. The second axiom has already been respected by assuming K to be at absolute rest. It should be noted that v is not an arbitrary relative velocity between any two frames but the velocity between the rest frame and another one.

Since the relativity principle is not valid it makes a difference if we transform from the resting to the moving system or backward. The functions b and b' therefore are different. b is defined by length contraction according to the third axiom. Since length contraction is real there is no symmetry between both systems. All length scales in moving systems are larger than in the rest system. The length l of a moving system measured from the rest system then is

$$l_0 = l\sqrt{1 - \frac{v^2}{c^2}}\,. \tag{18}$$

All scales are shrinking, i.e. for measuring the same length (the measured value read from a scale) in K' more scale units have to be used than in K if measurement is done when K' flies by in K. The length Δl (in units of K or K' respectively) transforms then as

$$\Delta l' = \frac{\Delta l}{\sqrt{1 - \frac{v^2}{c^2}}} \tag{19}$$

and the function b from (16) is defined by

$$b = \frac{1}{\sqrt{1 - \frac{v^2}{c^2}}}\,. \tag{20}$$

By backtransformation from K' to K we have to obtain the original length again, therefore

$$b' = b^{-1} = \sqrt{1 - \frac{v^2}{c^2}}\,. \tag{21}$$

If K' moves with v, observed from K, then K moves with $-v$ observed from K'. This is the only place where the relativity principle remains valid. The sign of v however does not play a role in (20). The reversal of the sign of v has already been taken into account in Eqs. (16, 17). Therefore we can assume $v = v'$ in the following.

As already mentioned, the length contraction also leads to a change in time scales as we can see from insertion of (16) into (17) (or vice versa) with regard of b and b':

$$t' = bt = \frac{t}{\sqrt{1 - \frac{v^2}{c^2}}}\,. \tag{22}$$

In total we arrive at the complete non-symmetric set of transformation equations

$$x' = \frac{x - vt}{\sqrt{1 - \frac{v^2}{c^2}}}\,, \tag{23}$$

$$t' = \frac{t}{\sqrt{1 - \frac{v^2}{c^2}}}\,, \tag{24}$$

$$x = (x' + vt') \sqrt{1 - \frac{v^2}{c^2}}\,, \tag{25}$$

$$t = t' \sqrt{1 - \frac{v^2}{c^2}}\,. \tag{26}$$

So far we have considered only two inertial frames with one of them being at (absolute) rest. In case of several frames moving arbitrary to one another, none of them can be assumed to be the rest frame. Let us define two frames K' and K'' whose coordinate origins move with speeds v_1 and v_2 relative to the rest frame K. then we have for the length contraction in both frames:

$$\Delta l' = \frac{\Delta l}{\sqrt{1 - \frac{v_1^2}{c^2}}}\,, \tag{27}$$

$$\Delta l'' = \frac{\Delta l}{\sqrt{1 - \frac{v_2^2}{c^2}}}\,. \tag{28}$$

Setting them in relation to each other directly gives

$$\frac{\Delta l'}{\Delta l''} = \sqrt{\frac{c^2 - v_2^2}{c^2 - v_1^2}} \tag{29}$$

or

$$\Delta l'' = \Delta l' \sqrt{\frac{c^2 - v_1^2}{c^2 - v_2^2}}\,. \tag{30}$$

Only in case $v_1 << v_2$ this approximately results in the expression being know from special relativity:

$$\Delta l'' = \frac{\Delta l'}{\sqrt{1 - \frac{v_2^2}{c^2}}}\,, \tag{31}$$

where v_2 is approximately the relative velocity between frames K' and K''. To derive the complete transformation law between K' and K'' we first write the transformation of both frames from the rest frame:

$$x' = \frac{x - v_1 t}{\sqrt{1 - \frac{v_1^2}{c^2}}}\,, \tag{32}$$

$$t' = \frac{t}{\sqrt{1 - \frac{v_1^2}{c^2}}}\,, \tag{33}$$

$$x'' = \frac{x - v_2 t}{\sqrt{1 - \frac{v_2^2}{c^2}}}\,, \tag{34}$$

$$t'' = \frac{t}{\sqrt{1 - \frac{v_2^2}{c^2}}}\,. \tag{35}$$

Mutual insertion then gives the direct transformation

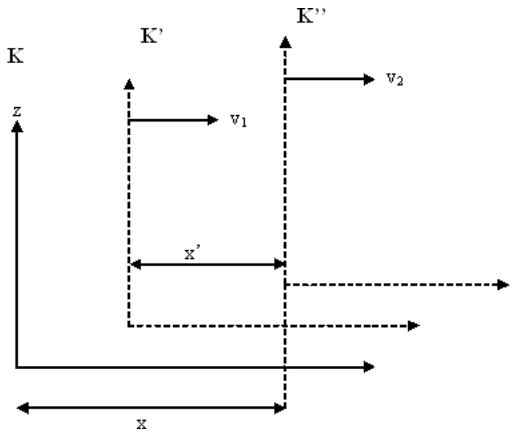

Fig. 5: Reference frames for addition theorem of velocities.

$K' \to K''$ as well as the reverse transformation $K'' \to K'$:

$$x'' = (x' - (v_2 - v_1)t') \sqrt{\frac{c^2 - v_1^2}{c^2 - v_2^2}}\,, \tag{36}$$

$$t'' = t' \sqrt{\frac{c^2 - v_1^2}{c^2 - v_2^2}}\,, \tag{37}$$

$$x' = (x'' + (v_2 - v_1)t'') \sqrt{\frac{c^2 - v_2^2}{c^2 - v_1^2}}\,, \tag{38}$$

$$t' = t'' \sqrt{\frac{c^2 - v_2^2}{c^2 - v_1^2}}\,. \tag{39}$$

Thus we have arrived at the general transformation laws between arbitrary frames of reference. For the back transformation the square root terms change to their inverse, and the sign of the vt term changes. These expressions cannot be reduced to a simple dependence on the speed difference $v = v_2 - v_1$. They depend on the absolute speeds of the inertial systems against the rest frame. Space and time coordinates transform with the same factor.

6.2 The addition theorem of velocities

We consider three coordinate systems K, K' and K'' . Frame K' is moving with velocity v_1 relative to the rest frame K and K'' with velocity v_2 relative to K'. We will compute now with which velocity v_3 then K'' moves relative to K (Fig. 5). At time $t = t' = t'' = 0$ all three coordinate origins shall coincide, so we have

$$x = v_3 t\,, \tag{40}$$

$$x' = v_2 t'\,. \tag{41}$$

The transformation equations (25–26) then with (41)

yield the connection between $x(x', t')$ and $t(t')$:

$$x = (x' + v_1 t')\sqrt{1 - \frac{v_1^2}{c^2}} = (v_2 t' + v_1 t')\sqrt{1 - \frac{v_1^2}{c^2}}\,, \quad (42)$$

$$t = t'\sqrt{1 - \frac{v_1^2}{c^2}}\,. \quad (43)$$

By applying (40) the resulting velocity of K'' is

$$v_3 = \frac{x}{t} = v_1 + v_2\,. \quad (44)$$

This is the addition theorem. The velocities add as vectors, in contrast to special relativity where we have the Einsteinian addition theorem (see Table 1). According to the latter, the sum of two velocities cannot exceed velocity of light. In this theory velocities add as vectors as in the Galilean transformation. The experimental consequences will be discussed in the subsequent section.

Now let's consider how velocities transform between frames directly. We assume that in K' and K'' the same movement (for example of a mass) is measured locally by the velocities

$$v' = \frac{x'}{t'} \quad (45)$$

and

$$v'' = \frac{x''}{t''}\,. \quad (46)$$

By inserting (36, 37) into (46) we find

$$v'' = v' - (v_2 - v_1)\,. \quad (47)$$

Velocities transform according to the Galilean transformation. In particular there is no limiting velocity.

7 Consequences

7.1 Comparison with Special Relativity

Both theories show a high degree of similarity, but there are some essential differences (see Table 1). In Einsteinian relativity the transformations are the same in both directions which is a consequence of the relativity principle. In the alternative theory the contraction factor reverses. This follows from the fact that this theory is based on an absolute frame of reference. This will be further discussed below.

There is a principal difference in the time transformations. In the alternative theory time is stretched by the same factor as length. In Einstein's relativity there is an additional term containing the space coordinate. So there is a coupling between space and time which ensures the basic axiom of constancy of c. In our theory space and time are decoupled, leading to a different metric. The coupling between space and time coordinates can be interpreted as follows. Consider two clocks in the rest frame, one at the coordinate origin and the other at location $x = x_0$, $y = 0$, $z = 0$. In Einstein's theory clocks must be synchronized. When the first clock registers an event at $x = 0$, $t = 0$, this will be seen at x_0 only after a delay which for light signals is $t_0 = x_0/c$. This delay of the measuring process is "built in" into special relativity and explains the appearance of the term $(v/c^2)x'$ in the time transformation $t(t')$ in Table 1.

This Theory	Special Relativity
Coordinate Transformation	
$x' = \dfrac{x - vt}{\sqrt{1 - \frac{v^2}{c^2}}}$	$x' = \dfrac{x - vt}{\sqrt{1 - \frac{v^2}{c^2}}}$
$x = (x' + vt')\sqrt{1 - \dfrac{v^2}{c^2}}$	$x = \dfrac{x' + vt'}{\sqrt{1 - \frac{v^2}{c^2}}}$
$y' = y$	$y' = y$
$z' = z$	$z' = z$
$t' = \dfrac{t}{\sqrt{1 - \frac{v^2}{c^2}}}$	$t' = \dfrac{t - \frac{v}{c^2}x}{\sqrt{1 - \frac{v^2}{c^2}}}$
$t = t'\sqrt{1 - \dfrac{v^2}{c^2}}$	$t = \dfrac{t' + \frac{v}{c^2}x'}{\sqrt{1 - \frac{v^2}{c^2}}}$
Addition Theorem of Velocities	
$v_3 = v_1 + v_2$	$v_3 = \dfrac{v_1 + v_2}{1 + \frac{v_1 v_2}{c^2}}$

Table 1: Comparison of theories.

In contrast to this, the alternative theory does not make any assumptions about measuring processes. Since there is no upper limit of relative velocities, it should be possible to construct an apparatus which measures a global time without significant delay. Such experiments have been discussed in section 1. Alternative methods of clock synchronization have been introduced by Tangherlini [7–9] who proposed a concept of a preferred frame similar to this work. He based his work (already done before 1958 [7]) on a partially instantaneous synchronization of clocks and arrived at transformation equations similar, but not identical, to ours. This corroborates that the measuring term x_0/c built into Einstein's theory is artificial. Tangherlini was not aware at that time of the anisotropy of c found experimentally in later years, for example by Cahill. Therefore he assumed full Lorentz invariance (i.e. isotropy) in each inertial frame. He *defined* the special form of time transformation so that it was consistent with his assumptions on clock synchronization. This is an essential difference to our work where the time transformation follows *by calculation* from the space transformation. Tangherlini obtained different values of c in each frame and a non-linear, direction dependent formula which relates these values to one another. In contrast, our calculation gives a vectorial addition

of all speeds including the signal transmission speed and relative frame speed. This is because we do not assume Lorentz invariance in each frame as Tangherlini did. Compared with the experiments of Cahill, our results are in accordance with them, but Tangherlini's are not.

Also in special relativity there is no real need for integrating signal transmission times into the transformation formulas. In addition, there are signal transmission speeds smaller than c, therefore it cannot be seen why experiments carried out with transmission velocity c should play a dominant role. If the space distance between clocks is known (and it can be measured of course), there is no problem to calculate the time of events at the other clock positions. This is like introducing time zones around the globe. We exactly know what time it is in other parts of the world without making any measurement. Occurrence of events at the same time can be defined by using the time of the rest frame.

While the Lorentz transformation represents a rotation in fourdimensional space, the transformation introduced by this theory has lower symmetry, it can be considered to be an affine mapping, i.e. a translation with stretching of scales. The transformation exhibits group properties as does the Lorentz transformation. This is shown in Appendix A in detail. We therefore conclude that the transformation introduced in this work can be used similarly to the Lorentz transformation as a basic property of higher developed theories, for example general relativity.

7.2 Comparison with known problems of Einsteinian theory

There are several interpretation problems in conventional special relativity. When comparing two frames being in motion to one another, the length rods of the other system appear shortened, seen from the system where the observer resides. This follows from the symmetry of the transformation law (Lorentz transformation). When the speed of one system is adopted to that of the other system, the difference in rod length disappears. At least Einstein has assumed that the scale change is a measuring artifact and not real.

Time dilation is regarded differently. In the well known twin paradoxon it is assumed that the integral taken over the coordinate time is identical to the real elapsed time, the scale change is considered to be a real effect as is done in general relativity. There is a contradiction in the interpretation. Contrary to this, the alternative theory assumes the scale changes always to be real. Since all length changes are related to the rest frame, there is no "symmetry" between measurements when one moving system measures quantities in another. For the twin paradoxon this means that the twin having higher absolute speed ages faster than the other one. Both twins can calculate the age of the other twin and come to the same result. All contradictions are removed.

The change of the time coordinate deserves further comments. As is generally known the Lorentz transformation is a rotation in four dimensions, therefore the length of vectors is an invariant as can be expressed by

$$x^2 + y^2 + z^2 - c^2t^2 = x'^2 + y'^2 + z'^2 - c^2t'^2. \qquad (48)$$

From this the differential invariance condition of the Minkowski metric follows:

$$dx^2 + dy^2 + dz^2 - c^2dt^2 = dx'^2 + dy'^2 + dz'^2 - c^2dt'^2. \qquad (49)$$

To the knowledge of the author, experimental tests of special relativity, however, are not based on the invariance principle but on the coordinate transformations where the proper time of a moving system is computed by integrating the equation

$$d\tau = dt\sqrt{1 - \frac{v^2}{c^2}}\,. \qquad (50)$$

Considering the time transformation for special relativity in Table 1, this equation should generally read

$$d\tau = \left(dt - \frac{v}{c^2}\,dx\right)\sqrt{1 - \frac{v^2}{c^2}}\,. \qquad (51)$$

It is questionable if this formula ever has been tested experimentally. Experimenters always used setups where the simplified Eq. (50) was sufficient. These types of checks of special relativity have been made with very high precision. For testing the Lorentz transformation thoroughly, however, use of Eq. (51) would be required.

We conclude this section with a hint to relativistic mechanics which is also based on Eq. (50). Therefore the alternative theory gives the same results as special relativity, as far as the lab system can be identified within sufficient precision with the absolutely resting system. When experiments with light are performed, this is the case. Relativistic mechanics would look differently if experiments were performed in a fast moving lab relative to earth.

7.3 Comparison with newer experiments and final remarks

As a last point we bring to mind the experiments of Cahill et al. [10, 11] mentioned in sections 1 and 2. The authors stress that older experiments of Michelson-Morley type were two-way experiments, that means the distances in the interferometer were passed twice by light rays, in contrary directions. Thus a lot of information gets lost, and such experiments in vacuo are even meaningless as already mentioned. With use of modern electronics, one-way experiments have been carried out by Cahill et al. It could be shown that light velocity is indeed different in both directions compared to the motion of the earth relative to the space background. Even fluctuations in the background velocity were found. There is a full analogy to sound waves in media, with effects of speeds relative to the observer and of the refraction index. Similar experiments were carried out be de Witte [12]. Further independent

confirmations are required. There are certain measurements of Marinov [15, 16] which seem not to be consistent with Cahill's results, but it is not clear if the evaluation method of Marinov is compatible with that of Cahill and this work.

The concept of the refraction index can be used to produce superluminal processes by deploying special optical media with a refraction index $n < 1$. Obviously, the experiments of Nimtz [5, 6], who has transmitted audio data with superluminal speed, can be explained in this way. Since the input data (a symphony of Mozart) was recognized as such after the transmission, it is clear that useful signals can be transmitted with such a speed. The old argument that a "phase velocity" $v > c$ cannot transport any information no longer holds. Thus our above statements are corroborated that a global time can be defined experimentally. Thornhill [14], and later Cahill [13], have further shown that Maxwell's equations, which are taken as an irrevocable proof that the Lorentz transform is incorporated in nature, can be formulated Galilei-invariant. Advanced theories like Einstein-Cartan-Evans theory [18] introduced a background potential and optical properties of space itself. Einstein's area is overcome. We conclude with a citation from Cahill [13]:

> "The Special Relativity formalism asserts that only relative descriptions of phenomena between two or more observers have any meaning. In fact we now understand that all effects are dynamically and observationally relative to an ontologically real, that is, detectable dynamical 3-space. Ironically this situation has always been known as an "absolute effect". The most extraordinary outcome of recent discoveries is that a dynamical 3-space exists, and that from the beginning of Physics this has been missed — that a most fundamental aspect of reality has been completely overlooked".

Appendix A: Proof of group properties

The transformation equations can be written in vector form with four-dimensional vectors and a transformation matrix:

$$\begin{pmatrix} x'' \\ y'' \\ z'' \\ t'' \end{pmatrix} = \begin{pmatrix} \alpha & 0 & 0 & -\alpha\beta \\ 0 & 1 & 0 & 0 \\ 0 & 0 & 1 & 0 \\ 0 & 0 & 0 & \alpha \end{pmatrix} \begin{pmatrix} x' \\ y' \\ z' \\ t' \end{pmatrix} \tag{A-1}$$

with

$$\alpha := \sqrt{\frac{c^2 - v_1^2}{c^2 - v_2^2}}\,, \qquad \beta := v_2 - v_1\,. \tag{A-2}$$

This is — in contrast to the Lorentz transformation — not a rotation in 4-space but a linear transformation (stretching) with a translation. The determinant is α^2, not unity as for the Lorentz transformation. Straight lines remain in parallel. The inverse transformation of (A-1) is

$$\begin{pmatrix} x' \\ y' \\ z' \\ t' \end{pmatrix} = \begin{pmatrix} \alpha^{-1} & 0 & 0 & \alpha^{-1}\beta \\ 0 & 1 & 0 & 0 \\ 0 & 0 & 1 & 0 \\ 0 & 0 & 0 & \alpha^{-1} \end{pmatrix} \begin{pmatrix} x'' \\ y'' \\ z'' \\ t'' \end{pmatrix} \tag{A-3}$$

as can be verified by multiplication of both matrices. To compare this with the Lorentz transformation we rewrite above Eqs. (A-1, A-3) with Minkowski coordinates, i.e. with an imaginary time coordinate:

$$\begin{pmatrix} x'' \\ y'' \\ z'' \\ ict'' \end{pmatrix} = \mathbf{T} \begin{pmatrix} x' \\ y' \\ z' \\ ict' \end{pmatrix} \tag{A-4}$$

with

$$\mathbf{T} = \begin{pmatrix} \alpha & 0 & 0 & i\alpha\beta \\ 0 & 1 & 0 & 0 \\ 0 & 0 & 1 & 0 \\ 0 & 0 & 0 & \alpha \end{pmatrix} \tag{A-5}$$

and

$$\alpha := \sqrt{\frac{c^2 - v_1^2}{c^2 - v_2^2}}\,, \qquad \beta := \frac{v_2 - v_1}{c}\,. \tag{A-6}$$

Then we have in analogy to above:

$$\mathbf{T}^{-1} = \begin{pmatrix} \alpha^{-1} & 0 & 0 & -i\alpha^{-1}\beta \\ 0 & 1 & 0 & 0 \\ 0 & 0 & 1 & 0 \\ 0 & 0 & 0 & \alpha^{-1} \end{pmatrix} \tag{A-7}$$

The set of transformations $T(\alpha, \beta)$ is a commutative group. This is proven in the following by examining the group axioms.

1. Completeness
We define

$$\alpha_1 := \sqrt{\frac{c^2 - v_1^2}{c^2 - v_2^2}}\,, \qquad \beta_1 := \frac{v_2 - v_1}{c}\,, \tag{A-8}$$

$$\alpha_2 := \sqrt{\frac{c^2 - v_3^2}{c^2 - v_4^2}}\,, \qquad \beta_2 := \frac{v_4 - v_3}{c}\,. \tag{A-9}$$

Then we find for the concatenation of two transformations by matrix multiplication:

$$T(\alpha_1, \beta_1)\, T(\alpha_2, \beta_2) = T(\alpha_1\alpha_2, \beta_1 + \beta_2)\,. \tag{A-10}$$

2. Neutral element
The neutral element of the group is the unit matrix.

3. Inverse element
For each $T(\alpha, \beta)$ there is an inverse transformation $T^{-1} = T(\alpha^{-1}, -\beta)$.

4. Associativity
The law of associativity for the matrix multiplication holds:

$$\begin{aligned} T(\alpha_1, \beta_1) \left[T(\alpha_2, \beta_2)\, T(\alpha_3, \beta_3) \right] = \\ = \left[T(\alpha_1, \beta_1)\, T(\alpha_2, \beta_2) \right] T(\alpha_3, \beta_3)\,. \end{aligned} \tag{A-11}$$

5. Commutativity
From Eq. (A-10) directly follows

$$T(\alpha_1, \beta_1)\, T(\alpha_2, \beta_2) = T(\alpha_2, \beta_2)\, T(\alpha_1, \beta_1). \tag{A-12}$$

So the group axioms have been proven.

Submitted on January 17, 2009 / Accepted on January 26, 2009

References

1. Ruder H. and M. Die Spezielle Relativitätstheorie. Viewег-Verlag, 1993.
2. Schmelzer I. General ether theory. arXiv: gr-qc/0001101.
3. Meyl K. Elektromagnetische Umweltverträglichkeit. Teil 3: Umdruck zum informationstechnischen Seminar. Indel-Verlag, 2003.
4. Crothers S.J. On certain conceptual anomalies in Einstein's theory of relativity. *Progress in Physics*, 2008, v. 1, 52–57.
5. Nimtz G. Tunneln mit Überlichtgeschwindigkeit. *DLR Nachrichten*, 1998, v. 90.
6. Nimtz G. Evanescent modes ar not necessarily Einstein causal. *The European Physical Journal*, 1999, v. B7, 523.
7. Tangherlini F.R. The velocity of light in uniformly moving frame. PhD Thesis, Stanford Univ., Sept. 1958, 135 pages.
8. Tangherlini F.R. An inroduction to the General Theory of Relativity. *Suppl. Nuovo Cim.*, 1961, Ser. X, v. 20, 1–86.
9. Malykin G.B. Frank Robert Tangherlini — the founder of an alternative relativistic kinematics (on the occasion of his 85th birthday). *Progress in Physics*, 2009, v. 1, L9–L14.
10. Cahill R.T., Kitto K. Michelson-Morley experiments revisited and the Cosmic Background Radiation preferred frame. *Apeiron*, 2003, v. 10(2), 104–117.
11. Cahill R.T. A new light-speed anisotropy experiment: absolute motion and gravitational waves detected. *Progress in Physics*, 2006, v. 4, 73–92.
12. Cahill R.T. The Roland De Witte 1991 experiment (to the memory of Roland De Witte). *Progress in Physics*, 2006, v. 3, 60–65.
13. Cahill R.T. Unravelling Lorentz covariance and the spacetime formalism, *Progress in Physics*, 2008, v. 4, 19–24.
14. Thornhill C.K. Real and apparent invariants in the transformation of the equations governing wave-motion in the general flow of a general fluid. *Proc. R. Soc. Lond. A*, 1993, 442, 495–504.
15. Marinov S. Measurement of the laboratory's absolute velocity. *General Relativity and Gravitation*, 1980, v. 12(1), 57–66.
16. Marinov S. Repetition of Silvertooth's experiment for measuring the aether drift. *Speculations in Science and Technology*, 1989, v. 12(3), 187–179.
17. Robitaille P.-M. On the origins of the CMB: insight from the COBE, WMAP, and Relikt-1 satellites. *Progress in Physics*, 2007, v. 1, 19–23.
18. Evans M.W. Generally covariant unified field theory. Abramis, 2005–2009, vols. 1–6; see also http://www.aias.us
19. http://en.wikipedia.org/wiki/Cycloid

On the Field of a Stationary Charged Spherical Source

Nikias Stavroulakis

Solomou 35, 15233 Chalandri, Greece
E-mail: nikias.stavroulakis@yahoo.fr

The equations of gravitation related to the field of a spherical charged source imply the existence of an interdependence between gravitation and electricity [5]. The present paper deals with the joint action of gravitation and electricity in the case of a stationary charged spherical source. Let m and ε be respectively the mass and the charge of the source, and let k be the gravitational constant. Then the equations of gravitation need specific discussion according as $|\varepsilon| < m\sqrt{k}$ (source weakly charged) or $|\varepsilon| = m\sqrt{k}$ or $|\varepsilon| > m\sqrt{k}$ (source strongly charged). In any case the curvature radius of the sphere bounding the matter possesses a strictly positive greatest lower hound, so that the source is necessarily an extended object. Pointwise sources do not exist. In particular, charged black holes do not exist.

1 Introduction

We recall that the field of an isotropic stationary spherical charged source is defined by solutions of the Einstein equations related to the stationary $\Theta(4)$-invariant metric

$$ds^2 = \left(f(\rho)\,dt + f_1(\rho)\,(x dx)\right)^2 - \\ - \left[\left(l_1(\rho)\right)^2 dx^2 + \frac{\left(\left(l(\rho)\right)^2 - \left(l_1(\rho)\right)^2\right)}{\rho^2}\,(x dx)^2\right], \quad (1.1)$$

($\rho = \|x\| = \sqrt{x_1^2 + x_2^2 + x_3^2}$, $l(0) = l_1(0)$). The functions of one variable $f(\rho)$, $f_1(\rho)$, $l_1(\rho)$, $l(\rho)$ are supposed to be C^∞ with respect to $\rho = \|x\|$ on the half-line $[0, +\infty[$ (or, possibly, on the entire real line $]-\infty, +\infty[$), but since the norm $\|x\|$ is not differentiable at the origin with respect to the coordinates x_1, x_2, x_3, these functions are not either. So, in general, the origin will appear as a singularity without physical meaning. In order to avoid the singularity, the considered functions must be smooth functions of the norm in the sense of the following definition.

Definition 1.1. A function of the norm $\|x\|$, say $f(\|x\|)$, will be called smooth function of the norm, if:

a). $f(\|x\|)$ is C^∞ on $\mathbb{R}^3 - \{(0,0,0)\}$ with respect to the coordinates x_1, x_2, x_3.

b). Every derivative of $f(\|x\|)$ with respect to the coordinates x_1, x_2, x_3 at the points $x \in \mathbb{R}^3 - \{(0,0,0)\}$ tends to a definite value as $x \to (0,0,0)$.

Remark 1.1. In [3], [4] a smooth function of the norm is considered as a function C^∞ on $\mathbb{R}$. However this last characterisation neglects the fact that the derivatives of the function are not directly defined at the origin.

The proof of the following theorem appears in [3].

Theorem 1.1. $f(\|x\|)$ is a smooth function of the norm if and only if the function of one variable $f(u)$ is C^∞ on $[0, \infty[$ and its right derivatives of odd order at $u = 0$ vanish.

This being said, a significant simplification of the problem results from the introduction of the radial geodesic distance

$$\delta = \int_0^\rho l(u)\,du = \beta(\rho), \quad (\beta(0) = 0),$$

which makes sense in the case of stationary fields.

Since $\beta(\rho)$ is a strictly increasing C^∞ function tending to $+\infty$ as $\rho \to +\infty$, the inverse function $\rho = \gamma(\delta)$ is also a C^∞ strictly increasing function of δ tending to $+\infty$ as $\delta \to +\infty$. So to the distance δ there corresponds a transformation of space coordinates:

$$y_i = \frac{\delta}{\rho}\,x_i = \frac{\beta(\rho)}{\rho}\,x_i, \quad (i = 1,2,3),$$

with inverse

$$x_i = \frac{\rho}{\beta(\rho)}\,y_i = \frac{\gamma(\delta)}{\delta}\,y_i, \quad (i = 1,2,3).$$

As shown in [4], these transformations involve smooth functions of the norm and since

$$x dx = \sum_{i=1}^3 x_i dx_i = \frac{\gamma\gamma'}{\delta}\,(y dy),$$

$$dx^2 = \sum_{i=1}^3 dx_i^2 = \left(\frac{\gamma'^2}{\delta^2} - \frac{\gamma^2}{\delta^4}\right)(y dy)^2 + \frac{\gamma'^2}{\delta^2}\,dy^2$$

by setting

$$F(\delta) = f(\gamma(\delta)), \quad F_1(\delta) = f_1(\gamma(\delta))\frac{\gamma(\delta)\gamma'(\delta)}{\delta},$$

$$L_1(\delta) = l_1(\gamma(\delta))\frac{\gamma(\delta)}{\delta},$$

and taking into account that

$$L(\delta) = l(\gamma(\delta))\,\gamma'(\delta) = 1$$

we get the transformed metric:

$$ds^2 = (Fdt + F_1(ydy))^2 - \\ - \left(L_1^2 dy^2 + \frac{1 - L_1^2}{\delta^2}(ydy)^2\right). \quad (1.2)$$

Then $\delta = \|y\|$ and the curvature radius of the spheres $\delta = $ $=$ const, is given by the function

$$G = G(\delta) = \delta L_1(\delta).$$

Moreover, instead of $h = \rho f_1$, we have now the function

$$H = H(\delta) = \delta F_1(\delta).$$

This being said, we recall [5] that, with respect to (1.1), the field outside the charged spherical source is defined by the equations

$$fl = c\,\frac{dg}{d\rho},$$

$$\frac{dg}{d\rho} = l\sqrt{1 - \frac{2\mu}{g} + \frac{\nu^2}{g^2}} = l\,\frac{\sqrt{g^2 - 2\mu g + \nu^2}}{g},$$

($\mu = \frac{km}{c^2}$, $\nu = \frac{\sqrt{k}}{c^2}|\varepsilon|$, $g^2 - 2\mu g + \nu^2 > 0$, where k is the gravitational constant, m and ε being respectively the mass and the charge of the source).

The function $h = \rho f_1$ does not appear in these equations. Every function $h = \rho f_1$ satisfying the required conditions of differentiability and such that $|h| \leqslant l$ is allowable.

We obtain a simpler system of equations if we refer to the metric (1.2). Then

$$F = c\frac{dG}{d\delta} = c\sqrt{1 - \frac{2\mu}{G} + \frac{\nu^2}{G^2}}, \quad (1.3)$$

$$\frac{dG}{d\delta} = \sqrt{1 - \frac{2\mu}{G} + \frac{\nu^2}{G^2}} = \frac{\sqrt{G^2 - 2\mu G + \nu^2}}{G}, \quad (1.4)$$

$$|H| \leqslant 1.$$

So our problem reduces essentially to the definition of the curvature radius $G(\delta)$ by means of the equation (1.4) the study of which depends on the sign of the difference

$$\nu^2 - \mu^2 = \frac{k}{c^4}\left(\varepsilon^2 - km^2\right).$$

A concise approach to this problem appeared first in the paper [1].

2 Source weakly charged ($\nu^2 < \mu^2$ or $|\varepsilon| < m\sqrt{k}$)

$G^2 - 2\mu G + \nu^2 = (G - \mu)^2 + \nu^2 - \mu^2$ vanishes for $G = $ $= \mu - \sqrt{\mu^2 - \nu^2}$ and $G = \mu + \sqrt{\mu^2 - \nu^2}$. Moreover $G^2 - $ $- 2\mu G + \nu^2 < 0$ if $\mu - \sqrt{\mu^2 - \nu^2} < G < \mu + \sqrt{\mu^2 - \nu^2}$ and $G^2 - 2\mu G + \nu^2 > 0$ if $G < \mu - \sqrt{\mu^2 - \nu^2}$ or $G > \mu + $ $+ \sqrt{\mu^2 - \nu^2}$. Since negative values of G are not allowed and since the solution must be topologically connected, we have to consider two cases according as

$$0 < G \leqslant \mu - \sqrt{\mu^2 - \nu^2}$$

or

$$\mu + \sqrt{\mu^2 - \nu^2} \leqslant G < +\infty.$$

The first case gives an unphysical solution, because G cannot be bounded outside the source. So, it remains to solve the equation (1.4) when G describes the half-line $\left[\mu + \sqrt{\mu^2 - \nu^2}, +\infty\right[$. The value $\mu + \sqrt{\mu^2 - \nu^2}$ is the greatest lower bound of the values of G and is not reachable physically, because F vanishes, and hence the metric degenerates for this value. However the value $\mu + \sqrt{\mu^2 - \nu^2}$ must be taken into account for the definition of the mathematical solution. So, on account of (1.4) the function $G(\delta)$ is defined as an implicit function by the equation

$$\delta_0 + \int_{\mu + \sqrt{\mu^2 - \nu^2}}^{G} \frac{u\,du}{\sqrt{u^2 - 2\mu u + \nu^2}} = \delta, \quad (\delta_0 = \text{const}),$$

or, after integration,

$$\delta_0 + \sqrt{G^2 - 2\mu G + \nu^2} + \\ + \mu \ln \frac{G - \mu + \sqrt{G^2 - 2\mu G + \nu^2}}{\sqrt{\mu^2 - \nu^2}} = \delta \quad (2.1)$$

with $G > \mu + \sqrt{\mu^2 - \nu^2}$.

We see that the solution involves a new constant δ_0 which is not defined classically. To given mass and charge there correspond many possible values of δ_0 depending probably on the size of the source as well as on its previous history, namely on its dynamical states preceding the considered stationary one. From the mathematical point of view, the determination of δ_0 necessitates an initial condition, for instance the value of the curvature radius of the sphere bounding the matter.

Let us denote by $E(G)$ the left hand side of (2.1). The function $E(G)$ is a strictly increasing function of G such that $E(G) \to +\infty$ as $G \to +\infty$. Consequently (2.1) possesses a unique strictly increasing solution $G(\delta)$ tending to $+\infty$ as $\delta \to +\infty$

The equation (2.1) allows to obtain two significant relations:

a) Since

$$\delta - G(\delta) = E(G) - G =$$
$$= \delta_0 + \mu \ln \frac{G - \mu + \sqrt{G^2 - 2\mu G + \nu^2}}{\sqrt{\mu^2 - \nu^2}} +$$
$$+ \sqrt{G^2 - 2\mu G + \nu^2} - G =$$
$$= \delta_0 + \mu \ln \frac{G - \mu + \sqrt{G^2 - 2\mu G + \nu^2}}{\sqrt{\mu^2 - \nu^2}} +$$
$$+ \frac{-2\mu + \frac{\nu^2}{G}}{1 + \sqrt{1 - \frac{2\mu}{G} + \frac{\nu^2}{G^2}}} \to +\infty \quad \text{as} \quad G \to +\infty,$$

it follows that $\delta - G(\delta) \to +\infty$ as $\delta \to +\infty$.

b) Since

$$\frac{\delta}{G(\delta)} = \frac{E(G)}{G} = \frac{\delta_0}{G} + \sqrt{1 - \frac{2\mu}{G} + \frac{\nu^2}{G^2}} +$$
$$+ \mu \frac{\ln G}{G} + \frac{\mu}{G} \ln \frac{1 - \frac{\mu}{G} + \sqrt{1 - \frac{2\mu}{G} + \frac{\nu^2}{G^2}}}{\sqrt{\mu^2 - \nu^2}} \to 1$$
$$\text{as} \quad G \to +\infty,$$

it follows that $\frac{\delta}{G(\delta)} \to 1$ as $\delta \to +\infty$.

Moreover from (2.1), it follows that the greatest lower bound $\mu + \sqrt{\mu^2 - \nu^2}$ of the values of $G(\delta)$ is obtained for $\delta = \delta_0$. The characteristics of the solution depend on the sign of δ_0.

Suppose first that $\delta_0 < 0$. Since function $G(\delta)$ is strictly increasing, we have $G(0) > \mu + \sqrt{\mu^2 - \nu^2}$, which is physically impossible, because the physical solution $G(\delta)$ vanishes for $\delta = 0$. Consequently there exists a strictly positive value δ_1 (the radius of the sphere bounding the matter) such that the solution is valid only for $\delta \geqslant \delta_1$. So, there exists no vacuum solution inside the ball $\|x\| < \delta_1$. In other words, the ball $\|x\| < \delta_1$ lies inside the matter.

Suppose secondly that $\delta_0 = 0$. Then

$$G(0) = \mu + \sqrt{\mu^2 - \nu^2} > 0,$$

which contradicts also the properties of the globally defined physical solution. Consequently there exists a strictly positive value δ_1 (the radius of the sphere bounding the matter) such that the solution is valid for $\delta \geqslant \delta_1$.

Suppose thirdly that $\delta_0 > 0$. Since

$$G(\delta_0) = \mu + \sqrt{\mu^2 - \nu^2}\,,$$

the derivative

$$G'(\delta_0) = \frac{\sqrt{(G(\delta_0))^2 - 2\mu G(\delta_0) + \nu^2}}{G(\delta_0)}$$

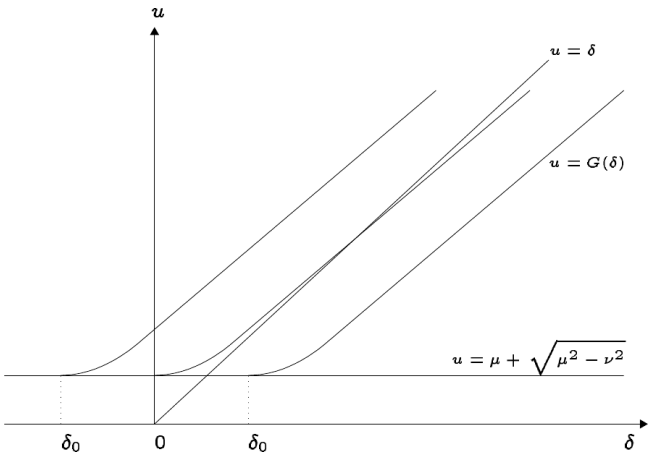

Fig. 1: Graph of G in the case where $\nu^2 < \mu^2$.

vanishes, so that $F(\delta_0) = c\,G'(\delta_0) = 0$. The vanishing of $F(\delta_0)$ implies the degeneracy of the spacetime metric for $\delta = \delta_0$ and since degenerate metrics have no physical meaning, there exists a value $\delta_1 > \delta_0$ such that the metric is physically valid for $\delta \geqslant \delta_1$. There exists no vacuum solution for $\delta \leqslant \delta_0$. The ball $\|x\| \leqslant \delta_0$ lies inside the matter.

From the preceding considerations it follows, in particular, that, whatever the case may be, a weakly charged source cannot be reduced to a point.

3 Source with $\mu^2 = \nu^2$ (or $|\varepsilon| = m\sqrt{k}$)

Since $\mu^2 = \nu^2$, we have $G^2 - 2\mu G + \nu^2 = (G - \mu)^2$, so that the equation (1.4) is written as

$$\frac{dG}{d\delta} = \frac{|G - \mu|}{G}\,.$$

Consider first the case where $G < \mu$. Then

$$\frac{dG}{d\delta} = \frac{G - \mu}{G} \quad \text{or} \quad \left(1 - \frac{\mu}{\mu - G}\right) dG = -\,d\delta\,,$$

whence

$$a_0 + G + \mu \ln \left(1 - \frac{G}{\mu}\right) = -\,\delta\,, \quad (a_0 = \text{const})\,.$$

If $G \to \mu$, then $\delta \to +\infty$, thus introducing a sphere with infinite radius and finite measure. This solution is unphysical. It remains to examine the case where $G > \mu$. Then

$$\left(1 + \frac{\mu}{G - \mu}\right) dG = d\delta\,,$$

whence

$$a_0 + G + \mu \ln \left(\frac{G}{\mu} - 1\right) = \delta\,, \quad (a_0 = \text{const})\,.$$

To the infinity of values of a_0 there correspond an infinity of solutions which results from one of them, for instance from

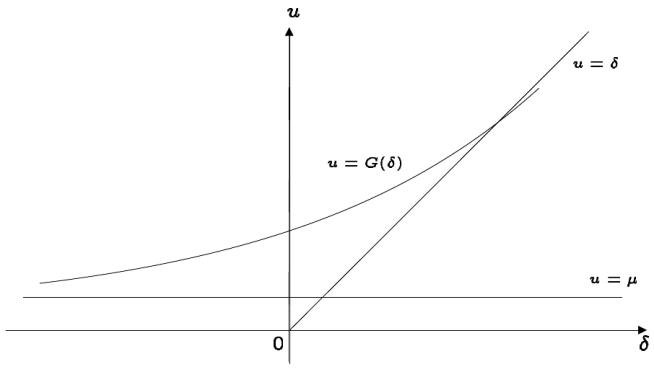

Fig. 2: Graph of G in the case where $\nu^2 = \mu^2$.

the solution obtained for $a_0 = 0$, by means of translations parallel to δ-axis.

For each value of a_0, we have $\delta \to +\infty$ as $G \to \mu$. The value μ is the unreachable greatest lower bound of the values of the corresponding solution $G(\delta)$ which is mathematically defined on the entire real line. If $\delta_1 > 0$ is the radius of the sphere bounding the matter, only the restriction of the solution to the half-line $[\delta_1, +\infty[$ is physically valid. In order to define the solution, we need the value of the corresponding constant a_0, the determination of which necessitates an initial condition, for instance the value $G(\delta_1)$. In any case, the values of $G(\delta)$ for $\delta \leqslant 0$ are unphysical.

Finally we remark that

$$\delta - G(\delta) \to +\infty \quad \text{and} \quad \frac{\delta}{G(\delta)} \to 1 \quad \text{as} \quad \delta \to +\infty.$$

4 Source strongly charged ($\nu^2 > \mu^2$ or $|\varepsilon| > m\sqrt{k}$)

Since $G^2 - 2\mu G + \nu^2 = (G - \mu)^2 + \nu^2 - \mu^2$, we have $G^2 - 2\mu G + \nu^2 > 0$ for every value of G. Regarding the function

$$\Phi(G) = 1 - \frac{2\mu}{G} + \frac{\nu^2}{G^2} = \frac{G^2 - 2\mu G + \nu^2}{G^2},$$

we have

$$\Phi(G) \to +\infty \text{ as } G \to 0 \quad \text{and} \quad \Phi(G) \to 1 \text{ as } G \to +\infty.$$

On the other hand the derivative

$$\Phi'(G) = \frac{2}{G^2}\left(\mu - \frac{\nu^2}{G}\right),$$

vanishes for

$$G = \frac{\nu^2}{\mu} = \frac{\varepsilon^2}{mc^2}$$

and moreover

$$\Phi'(G) < 0 \quad \text{for} \quad G < \frac{\nu^2}{\mu},$$

$$\Phi'(G) > 0 \quad \text{for} \quad G > \frac{\nu^2}{\mu}.$$

It follows that the function $\Phi(G)$ is strictly decreasing on the interval $]0, \frac{\nu^2}{\mu}[$, strictly increasing on the half-line $[\frac{\nu^2}{\mu}, +\infty[$, so that

$$\Phi\left(\frac{\nu^2}{\mu}\right) = 1 - \frac{\mu^2}{\nu^2} = 1 - \left(\frac{m\sqrt{k}}{\varepsilon}\right)^2$$

is the minimum of $\Phi(G)$.

The behaviour of the solution on the half-line $[\frac{\nu^2}{\mu}, +\infty[$ is quite different from that on the interval $]0, \frac{\nu^2}{\mu}[$. Several arguments suggest that only the restriction of the solution to the half-line $[\frac{\nu^2}{\mu}, +\infty[$ is physically valid.

a) Let δ_0 be the radius of the spherical source. In order to prove that the restriction of the solution to $]0, \frac{\nu^2}{\mu}[$ is unphysical, we have only to prove that $G(\delta_0) \geqslant \frac{\nu^2}{\mu}$. We argue by contradiction assuming that $G(\delta_0) < \frac{\nu^2}{\mu}$. Since $G(\delta)$ is unbounded, there exists a value $\delta_1 > \delta_0$ such that $G(\delta_1) = \frac{\nu^2}{\mu}$. On the other hand, since $G(\delta)$ satisfies the equation (1.4), namely

$$\frac{dG}{d\delta} = \sqrt{1 - \frac{2\mu}{G} + \frac{\nu^2}{G^2}} = \sqrt{\Phi(G)},$$

the function

$$F = c\frac{dG}{d\delta} = c\sqrt{\Phi(G)}$$

is strictly decreasing on the interval $]0, \frac{\nu^2}{\mu}[$, and strictly increasing on the half-line $[\frac{\nu^2}{\mu}, +\infty[$. Such a behaviour of the important function F, which is involved in the law of propagation of light, is unexplained. We cannot indicate a cause compelling the function F first to decrease and then to increase outside the spherical source. The solution cannot be valid physically in both intervals $]0, \frac{\nu^2}{\mu}[$ and $[\frac{\nu^2}{\mu}, +\infty[$, and since the great values of G are necessarily involved in the solution, it follows that only the half-line $[\frac{\nu^2}{\mu}, +\infty[$ must be taken into account. The assumption that $G(\delta_0) < \frac{\nu^2}{\mu}$ is to be rejected.

b) The non-Euclidean (or, more precisely, non-pseudo-Euclidean) properties of the spacetime metric are induced by the matter, and this is why they become more and more apparent in the neighbourhood of the spherical source. On the contrary, when δ (or G) increases the spacetime metric tends progressively to a pseudo-Euclidean form. This situation is expressed by the solution itself. In order to see this, we choose a positive value b_1 and integrate the equation (1.4) in the half-line $[b_1, +\infty[$,

$$b_0 + \int_{b_1}^{G} \frac{u\,du}{\sqrt{u^2 - 2\mu u + \nu^2}} = \delta\,, \quad (b_0 = \text{const}),$$

and then writing down the explicit expression resulting from the integration, we find, as previously, that

$$\delta - G(\delta) \to +\infty \quad \text{and} \quad \frac{\delta}{G(\delta)} \to 1 \text{ as } \delta \to +\infty.$$

But, since

$$L_1(\delta) = \frac{G(\delta)}{\delta} \to 1 \quad \text{and} \quad F = c\sqrt{\Phi(G(\delta))} \to c$$

as $\delta \to +\infty$, the metric (1.2) tends effectively to a pseudo-Euclidean form as $\delta \to +\infty$. Now, if δ decreases, the non-Euclidean properties become more and more apparent, so that the minimum $c\sqrt{1-\frac{\mu^2}{\nu^2}}$ of F, obtained for $G = \frac{\nu^2}{\mu}$, is related to the "strongest non-Euclidean character of the metric". For values of G less than $\frac{\nu^2}{\mu}$, the behaviour of the mathematical solution becomes unphysical. In fact, the metric loses progressively its non-Euclidean properties, and, in particular, for $G = \frac{\nu^2}{2\mu}$, we have

$$\Phi\left(\frac{\nu^2}{2\mu}\right) = 1 - \frac{4\mu^2}{\nu^2} + \frac{4\mu^2}{\nu^2} = 1,$$

hence $F\left(\frac{\nu^2}{2\mu}\right) = c$ and $\frac{dG}{d\delta} = 1$.

On account of $G = \delta L_1$, the last condition implies

$$1 = \frac{dG}{d\delta} = L_1 + \delta\,\frac{dL_1}{d\delta}$$

and since we have to do physically with very small values of δ (in the neighbourhood of the origin), we conclude that

$$L_1\left(\frac{\nu^2}{2\mu}\right) \approx 1.$$

and since $F\left(\frac{\nu^2}{2\mu}\right) = c$, the metric is almost pseudo-Euclidean, a phenomenon inadmissible physically in the neighbourhood of the source. So we are led to reject the restriction of the mathematical solution to the interval $[\frac{\nu^2}{2\mu}, \frac{\nu^2}{\mu}[$. For values less than $\frac{\nu^2}{2\mu}$, the function $F(G)$ increases rapidly and tends to $+\infty$ as G decreases, so that the restriction of the mathematical solution to the interval $]0, \frac{\nu^2}{2\mu}[$ is also physically inadmissible. It follows that the restriction of the solution to the entire interval $]0, \frac{\nu^2}{\mu}[$ is unphysical.

c) Another argument supporting the above assertion is given in [2].

Let δ_1 be the radius of the spherical source and assume that $G(\delta_1) > \frac{\nu^2}{\mu}$. A radiation emitted radially from the sphere bounding the matter is redshifted, and its redshift at the points of a sphere $\|x\| = \delta$ with $\delta > \delta_1$ is given by the formula

$$Z(\delta, \delta_1) = -1 + \frac{F(G(\delta))}{F(G(\delta_1))} = -1 + \sqrt{\frac{\Phi(G(\delta))}{\Phi(G(\delta_1))}}\,.$$

Suppose δ fixed and let us examine the variation of $Z(\delta, \delta_1)$ considered as function of δ_1. If δ_1 (or $G(\delta_1)$) decreases, $Z(\delta, \delta_1)$ increases and tends to its maximum, obtained for $G(\delta_1) = \frac{\nu^2}{\mu}$,

$$\max Z(\delta, \delta_1) = -1 + \sqrt{\frac{\Phi(G(\delta))}{1-\frac{\mu^2}{\nu^2}}}\,.$$

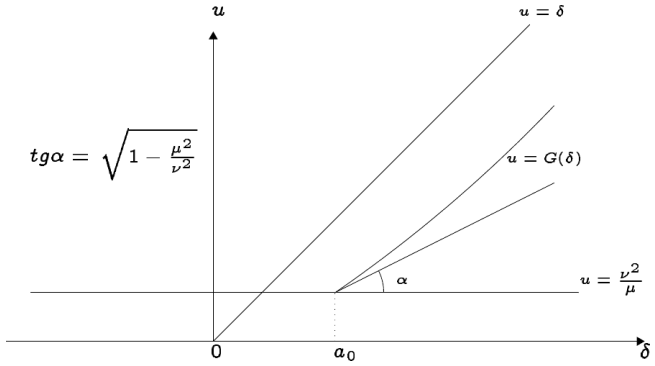

Fig. 3: Graph of G in the case where $\nu^2 > \mu^2$.

If $G(\delta_1)$ takes values less than $\frac{\nu^2}{\mu}$, the phenomenon is inverted: The redshift first decreases and then vanishes for a unique value $G(\delta_1) \in]\frac{\nu^2}{2\mu}, \frac{\nu^2}{\mu}[$ with $\Phi(G(\delta_1)) = \Phi(G(\delta))$. If $G(\delta_1)$ decreases further, instead of a redshift, we have a blueshift. This situation seems quite unphysical, inasmuch as the vanishing of the redshift depends on the position of the observer. In order to observe constantly a redshift, the condition $G(\delta_1) \geqslant \frac{\nu^2}{\mu}$ is necessary.

From the preceding considerations we conclude that the value

$$\frac{\nu^2}{\mu} = \frac{\varepsilon^2}{mc^2}$$

is the greatest lower bound of the curvature radius $G(\delta)$ outside the spherical strongly charged source. In particular, the curvature radius of the sphere bounding the matter is $\geqslant \frac{\varepsilon^2}{mc^2}$, so that a strongly charged source cannot be reduced to a point. Our study does not exclude the case where the solution $G(\delta)$ attains its greatest lower bound, namely the case where the curvature radius of the sphere bounding the matter is exactly equal to $\frac{\varepsilon^2}{mc^2}$. So, in order to take into account all possible cases, the equation (1.4) must be integrated as follows

$$a_0 + \int_{\nu^2/\mu}^{G} \frac{u\,du}{\sqrt{u^2 - 2\mu u + \nu^2}} = \delta\,, \quad (a_0 = \text{const})\,.$$

If $a_0 \leqslant 0$, there exists a value $\delta_1 > 0$ such that the solution is valid only for $\delta \geqslant \delta_1$.

If $a_0 > 0$, the solution is valid for $\delta \geqslant a_0$, only if the sphere bounding the matter has the curvature radius $\frac{\nu^2}{\mu}$. Otherwise there exists a value $\delta_1 > a_0$ such that the solution is valid for $\delta \geqslant \delta_1$.

The expression $\frac{\varepsilon^2}{mc^2}$ is also known in classical electrodynamics, but in the present situation it appears on the basis of new principles and with a different signification. Consider, for instance, the case of the electron. Then $\frac{|\varepsilon|}{m\sqrt{k}} = 2.02\times10^{21}$, so that the electron is strongly charged, and, from the point of view of the classical electrodynamics, is a spherical object with radius $\frac{\varepsilon^2}{mc^2} = 2.75\times10^{-13}$ cm.

Regarding the present theory, we can only assert that, if

the electron is a stationary spherical object, then it is a non-Euclidean ball such that the value 2.75×10^{-13} cm is the greatest lower bound of the possible values of the curvature radius of the sphere bounding it. The radius of the electron cannot be deduced from the present theory.

The proton is also strongly charged with $\frac{|\varepsilon|}{m\sqrt{k}}=1.1\times10^{18}$. The corresponding value $\frac{\varepsilon^2}{mc^2}=1.5\times10^{-16}$ cm is less than that related to the electron by a factor of the order 10^{-3}. So, if the proton is assumed to be spherical and stationary, it is not reasonable to accept that this value represents its radius. This last is not definable by the present theory.

Submitted on January 31, 2009 / Accepted on February 05, 2009

References

1. Stavroulakis N. Paramètres cachés dans les potentiels des champs statiques. *Annales Fond. Louis de Broglie*, 1981, v. 6 (4), 287–327.
2. Stavroulakis N. Particules et particules test en relativité générale. *Annales Fond. Louis de Broglie*, 1991, v. 16 (2), 129–175.
3. Stavroulakis N. Vérité scientifique et trous noires (deuxième partie) Symétries relatives au groupe des rotations. *Annales Fond. Louis de Broglie*, 2000, v. 25 (2), 223–266.
4. Stavroulakis N. Non-Euclidean geometry and gravitation. *Progress in Physics*, 2006, v. 2, 68–75.
5. Stavroulakis N. Gravitation and electricity. *Progress in Physics*, 2008, v. 2, 91–96.

Fractal Scaling Models of Resonant Oscillations in Chain Systems of Harmonic Oscillators

Hartmut Müller

Global Scaling Research Institute in memoriam Leonhard Euler, Munich, Germany
E-mail: info@globalscaling.de

Logarithmic scaling invariance is a wide distributed natural phenomenon and was proved in the distributions of physical properties of various processes — in high energy physics, chemistry, seismicity, biology, geology and technology. Based on the Gantmacher-Krein continued fraction method the present paper introduces fractal scaling models of resonant oscillations in chain systems of harmonic oscillators. These models generate logarithmic scaling spectra. The introduced models are not based on any statements about the nature of the link or interaction between the elements of the oscillating system. Therefore the model statements are quite generally, what opens a wide field of possible applications.

1 Introduction

Within the past 40 years many articles were published which show that logarithmic scaling invariance ("Scaling") is a wide distributed natural phenomenon.

In 1967/68 Feynman and Bjorken [1] discovered the scaling phenomenon in high energy physics, concrete in hadron collisions.

Simon E. Shnoll [2] found scaling in the distributions of macroscopic fluctuations of nuclear decay rates. Since 1967 his team discovers fractal scaling in the fluctuation distributions of different physical and chemical processes, as well as in the distributions of macroscopic fluctuations of different noise processes.

Within the fifties Beno Gutenberg and Charles Richter [3] have shown, that exists a logarithmic invariant (scaling) relationship between the energy (magnitude) and the total number of earthquakes in any given region and time period.

In 1981, Leonid L. Čislenko [4] published his extensive work on logarithmic invariance of the distribution of biological species, dependent on body size and weight of the organisms. By introducing a logarithmic scale for biologically significant parameters, such as mean body weight and size, Čislenko was able to prove that sections of increased specie representation repeat themselves in equal logarithmic intervals.

Knut Schmidt-Nielsen [5] (1984) was able to prove scaling in biological metabolic processes.

Alexey Zhirmunsky and Viktor Kuzmin [6] (1982) discovered process-independent scaling in the development stages of embryo-, morpho- and ontogenesis and in geological history.

In 1987–1989 we [7] have shown, that fractal scaling distributions of physical process properties can be understood as a consequence of resonant oscillations of matter. Based on a fractal scaling proton resonance model, we developed methods of optimization and prognostication of technical processes, which have got european and international patents [8].

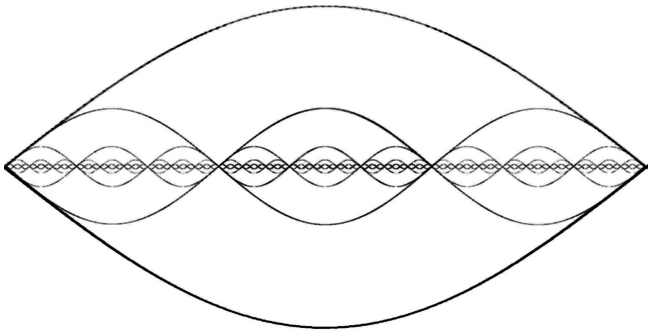

Fig. 1:

In the following we will show that Scaling is a fundamental property of any natural oscillation process. Therefore one can suspect, that natural oscillations of matter generate scaling distributions of physical properties in very different processes.

2 Fractal scaling as a fundamental property of resonant oscillations

A standing wave [9] in a homogeneous space arises only if in the direction of the wave penetration the space is finite and if the half wave length is equal to an integer part of the medium size L.

As a consequence we can find for any low enough resonant oscillation mode frequency f_0 a higher mode frequency f_1 with an integer relationship $n = f_1/f_0$. The frequencies of such resonant oscillation modes generate exponential series:

$$f_{n,p} = f_0 \cdot n^p. \qquad (1)$$

Fig. 1 illustrates the situation with $n = 3$ and $p = 0, 1, 2, \ldots$ for transversal oscillations.

Therefore, the complete resonant oscillation frequency spectrum can be represented as a set of logarithmic fractal spectra (1) with natural $n = 2, 3, 5, \ldots$ In this representation

the generation of the complete resonant oscillation frequency spectrum can be understood as an arithmetical task, what can be reduced to the fundamental theorem of arithmetic, that every natural number greater than 1 can be written as a unique product of prime numbers.

In the oscillation nodes of the logarithmic fractal oscillation modes the spectral density is maximum. Where the amplitudes of the oscillation modes are maximum, the medium particles have maximum kinetic energy, but near the oscillation nodes the kinetic energy is minimum. The distance between the ranges with maximum particle density (nodes) is the half of the oscillation mode wave length. As consequence, the distribution of the medium particle density will be fractal and exactly the same (isomorphism) as the distribution of the spectral density.

In the phases of spectral compression, where the spectral density increases, in the case of approach to any node arises a particle fusion trend, but in the phases of spectral decompression, where the spectral density decreases, in the case of distance from any node arises a particle dispersion trend. Logarithmic fractal change of spectral compression and decompression generates a logarithmic fractal change of high and low density structure areas inside the medium.

Resonant oscillations can be understood as the most probable forming-mechanism of fractal structures in nature, because the energy efficiency of resonant oscillations is very high.

In the works "About continued fractions" (1737) and "About oscillations of a string" (1748) Leonhard Euler [10] formulated tasks, the solution employed several generations of mathematicians the following 200 years. Euler investigated natural oscillations, based on a model of a massless flexible string with a finite or infinite set of similar pearls. Based on this task d'Alembert developed an intergration method of linear differencial equation systems. Daniel Bernoulli formulated the theorem, that the solution of the problem of the natural oscillations of a string can be represented as trigonometric series, what starts a discussion between Euler, d'Alembert and Bernoulli, and continued several decades.

Later Lagrange showed how can be realised the transition from the solution of the problem of the set with pearls string oscillations to the solution of the oscillations of a homogeneous string. In 1822 Fourier solved this task completely.

Though, big problems arisen with oscillations of strings with a finite set of different pearls. This task leads to functions with gaps. After 1893 Stieltjes [11] investigated such functions and found an integration method, what leads to continued fractions. But only in 1950 Gantmacher and Krein found the general solution of Euler's task about natural oscillations of a set with pearls string. Gantmacher and Krein interpreted the stretched string between the pearls as a broken line, what opened them a fractal vision of the problem. In the work „Oscillation matrixes, oscillation cores and low oscillations of mechanical systems" Gantmacher and Krein [12] showed that Stieltjes continued fractions are solutions of the Euler-Lagrange equation for low amplitude oscillations of chain systems. These continued fractions generate fractal spectra. Within the fifties and sixties the development of continued fraction analysis methods of oscillation processes in chain systems reaches a highlight. In 1950 Oskar Perron [13] publicated the book "The continued fraction theory". Achieser [14] investigated continued fractions in the work "The classic problem of moments and some questions of analysis" (1961). In the book "The continued fraction method" (1955) Terskich [15] generalized this method for analysis of oscillations of branched chain systems. In 1964 Khinchine [16] explained the importance of continued fractions in arithmetics and algebra. The works of Khintchine, Markov, Skorobogatko [17] and other mathematicians allowed the development of efficient addition and multiplication methods for continued fractions.

Based on the continued fraction method, in the following we will show, how one can generate scaling spectral models of natural oscillation processes which are not based on any statements about the nature of the link or interaction between the elements of the oscillating system.

3 Fractal scaling spectral models

Based on the continued fraction method we search the natural oscillation frequencies of a chain system of many similar harmonic oscillators in this form:

$$f = f_0 \exp(S)\,, \tag{2}$$

where f is a natural frequency of a chain system of similar harmonic oscillators, f_0 is the natural frequency of one isolated harmonic oscillator, S is a continued fraction with integer elements:

$$S = \frac{n_0}{z} + \cfrac{z}{n_1 + \cfrac{z}{n_2 + \ddots + \frac{z}{n_i}}}\,. \tag{3}$$

The partial numerator z, the free link n_0 and all partial denominators $n_1, n_2, \ldots, n_i$ are integer numbers: $z, n_0, n_i \in Z, i = \overline{1, \infty}$. The present paper follows the Terskich definition of a chain system (Terskich, p. 8) where the interaction between the elements proceeds only in their movement direction. In this connection we understand the concept "spectrum" as a discrete distribution or set of natural oscillation frequencies.

Spectra (2) are not only logarithmic-invariant, but also fractal, because the discrete hyperbolic distribution of natural frequencies repeats itself on each spectral level $i = 1, 2, \ldots$

Every continued fraction (3) with a partial numerator $z \neq 1$ can be changed into a continued fraction with $z = 1$.

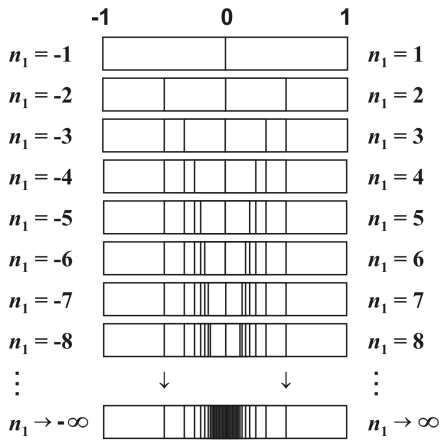

Fig. 2:

For this one can use the Euler equivalent transformation (Skorobogatko, p. 12) and present continued fractions (3) in the canonical form. With the help of the Lagrange [18] transformation (Perron, §40) every continued fraction with integer partial denominators can be represented as a continued fraction with natural partial denominators, what is allways convergent (Khintchine, §4). In this paper we will investigate spectra (2) which are generated by convergent continued fractions (3).

Every infinite continued fraction is irrational, and every irrational number can be represented in precisely one way as an infinite continued fraction (Khintchine, §5). An infinite continued fraction representation for an irrational number is useful because its initial segments provide the best possible rational approximations to the number (Khintchine, §6). These rational numbers are called the convergents of the continued fraction. This last property is quite important, and is not true of the decimal representation. The convergents are rational and therefore they generate a discrete spectrum. Furthermore we investigate continued fractions (3) with a finite quantity of layers $i = \overline{1,k}$ which generate discrete spectra. In the logarithmic representation each natural oscillation frequency can be written down as a finite set of integer elements of the continued fraction (3):

$$\ln(f/f_0) = \frac{n_0}{z} + \cfrac{z}{n_1 + \cfrac{z}{n_2 + \ddots + \frac{z}{n_k}}} = \left[z, n_0, n_1, n_2, \ldots, n_k\right]. \qquad (4)$$

Figure 2 shows the generation process of such fractal spectrum for $z = 1$ on the first layer $i = k = 1$ for $|n_1| = 1, 2, 3, \ldots$ and $n_0 = 0$ (logarithmic representation).

The partial denominators n_1 run through positive and negative integer values. Maximum spectral density ranges automatically arise on the distance of 1 logarithmic units, where $n_0 = 0, 1, 2, \ldots$ and $|n_1| \to \infty$. Figure 3 shows the spectrum on the first layer $i = k = 1$ for $|n_1| = 1, 2, 3, \ldots$ and $|n_0| = 0, 1, 2, \ldots$ (logarithmic representation):

Fig. 3:

The more layers $i = 1, 2, 3, \ldots$ are calculated, the more spectral details will be visible. In addition to the first spectral layer, Figure 4 shows the second layer $i = k = 2$ for $|n_2| = 1, 2, 3, \ldots$ and $|n_1| = 2$ (logarithmic representation):

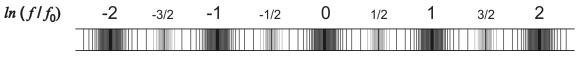

Fig. 4:

On each spectral layer i one can select ranges of relative low spectral density (spectral gaps) and ranges of relative high spectral density (spectral nodes). The highest spectral density corresponds to the nodes on the layer $i = 0$, where $|n_1| \to \infty$. The next (lower) spectral density level corresponds to the nodes on the layer $i = 1$, where $|n_2| \to \infty$, and so on. The largest spectral gaps are between the spectral node ranges on the layer n_0. On the spectral layers $i = 1, 2, 3, \ldots$ the gaps are corresponding smaller.

In 1795 Karl Friedrich Gauss discovered logarithmic scaling invariance of the distribution of prime numbers. Gauss proved, that the quantity of prime numbers $p(n)$ until the natural number n follows the law $p(n) \cong n/\ln(n)$. The equality symbol is correct for the limit $n \to \infty$. The logarithmic scaling distribution is the one and only nontrivial property of all prime numbers.

The free link n_0 and all partial denominators n_1, n_2, n_3, ..., n_k are integer numbers and therefore they can be represented as unique products of prime factors. On this base we distinguish spectral classes in dependence on the divisibility of the partial denominators by prime numbers. In addition, we will investigate continued fractions which correspond to the Markov [19] convergence requirement (Skorobogatko, p. 15):

$$|n_i| \geqslant |z_i| + 1\,. \qquad (5)$$

Continued fractions (3) with $z = 1$ and partial denominators divisible by 2 don't generate empty spectral gaps, because the alternating continued fraction [1, 0; +2, −2, +2, −2, ...] approximates the number 1 and [1, 0; −2, +2, −2, +2, ...] approximates the integer number −1.

Divisible by 3 partial denominators with $z = 2$ build the class of continued fractions (3) what generates the spectrum (4) with the smallest empty spectral gaps. Figure 5 shows fragments of spectra, which were generated by continued fractions (3) with divisible by 2, 3, 4, ... partial denominators and corresponding partial numerators $z = 1, 2, 3, \ldots$ on the first layer $i = 1$ for $n_0 = 0$ (logarithmic representation):

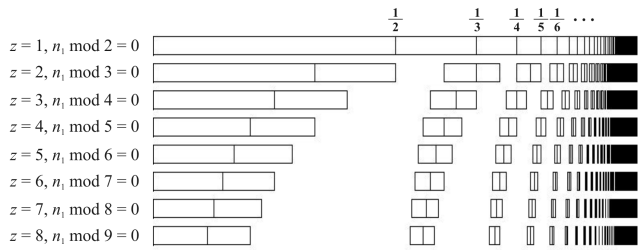

Fig. 5:

Figure 5 shows the spectral nodes on the first layer $i = 1$ and also the borders of the spectral node ranges, so the spectral gaps are visible clearly. The borders of the spectral empty gaps are determined by the following alternating continued fractions ($z \geqslant 1$):

$$\left.\begin{aligned} -1 &= \cfrac{z}{-z-1+\cfrac{z}{z+1+\cfrac{z}{-z-1+\ddots}}} \\ 1 &= \cfrac{z}{z+1+\cfrac{z}{-z-1+\cfrac{z}{z+1+\ddots}}} \end{aligned}\right\}. \quad (6)$$

More detailled we will investigate the second spectrum of the figure 5, what was generated by the continued fraction (3) with divisible by 3 partial denominators and the corresponding partial numerator $z = 2$. This spectrum is the most interesting one, because with $z = 2$ and $n_i \mod 3 = 0$ starts the generation process of empty gaps. Possibly, that the spectral ranges of these gaps are connected to fundamental properties of oscillation processes.

The partial denominators n_1 run through positive and negative integer values. The maximum spectral density areas arise automatically on the distance of 3/2 logarithmic units, where $n_0 = 3j$, $(j = 0, 1, 2, \dots)$ and $|n_1| \to \infty$. Figure 6 shows the spectrum on the first layer $i = k = 1$ for $|n_1| = 3, 6, 9, \dots$ and $|n_0| = 0, 3, 6, \dots$ (logarithmic representation):

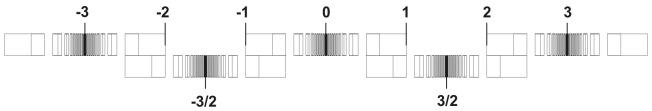

Fig. 6:

The alternating continued fraction [2, 0; +3, −3, +3, −3, ...] approximates the number 1, but the alternating continued fraction [2, 0; −3, +3, −3, +3, ...] approximates the number −1. In the consequence the spectral ranges between $|n_1| = 3 - 1$ and $|n_1| = 3 + 1$ are double occupied. The more layers $i = 1, 2, 3, \dots$ are calculated, the more spectral details are visible (see Figure 7).

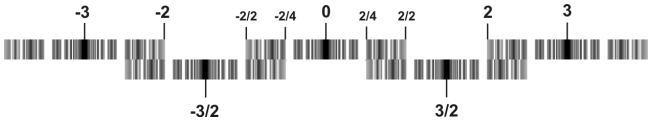

Fig. 7:

Divisible by three free links $|n_0| = 3j$, $(j = 0, 1, 2, \dots)$ of the continued fraction (3) mark the main spectral nodes, partial denominators divisible by three $|n_{i>0}| = 3j$, $(j = = 1, 2, \dots)$ mark spectral subnodes. All the other partial denominators $|n_i| \neq 3j$ mark borders of spectral gaps (see Figure 8):

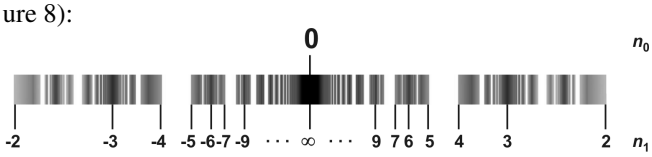

Fig. 8:

4 Local features of fractal scaling spectra and corresponding properties of oscillation processes

In the spectral node ranges, where the spectral density reachs local maximum, the resonance frequencies are distributed maximum densely, so that near a spectral node almost each frequency is a resonance frequency. The energy efficiency of resonant oscillations is very high. Therefore, if a frequency of an oscillation process is located near a node of the fractal spectrum (4), the process energy efficiency (degree of effectiveness) should be relative high. The highest process energy efficiency corresponds to the nodes on the layer $i = 0$. Near the spectral nodes on the layers $i = 1, 2, \dots$ the process energy efficiency should be corresponding lower. On the other hand, if a frequency of an oscillation process is located in a gap of the fractal spectrum (4), the process energy efficiency should be relative low. In the centre of a spectral node the spectral compression changes to spectral decompression (or reversed). Therefore the probability of the process trend change increases near a spectral node.

5 Fractal scaling spectral analysis

Based on the fractal scaling model (2) of resonant oscillations of chain systems one can execute fractal scaling spectral analyses of composite oscillation processes, if the connected oscillators are quite similar.

Corresponding to the logarithmic representation (5) the fractal scaling spectral analysis consists of the following steps:

a). Divide the lowest measured frequency f_{min} and the highest measured frequency f_{max} of an oscillating chain system by the resonance frequency f_0 of one isolated element of the chain system and calculate the natural logarithms $X_{min} = \ln(f_{min}/f_0)$ and $X_{max} = = \ln(f_{max}/f_0)$;

b). Use the Euclid's algorithm to find the free links n_0 and partial denominators n_1, n_2, ... of the corresponding to X_{min} and X_{min} continued fractions and determine the location of X_{min} and X_{min} in the spectrum (5);

c). Determine the highest/lowest spectral density ranges of the spectrum (5) between X_{min} and X_{min} which correspond to important properties of the composite oscillation processes;

d). Use the formula (4) to calculate the corresponding frequency ranges.

The fractal scaling spectral analysis is able to define following properties of of composite oscillation processes: turbulence probability, fluctuation probability, resonance probability, stability and sensibility.

6 Resume

The presented model is not based on any statements about the nature of the link or interaction between the elements of the oscillating chain system. Therefore the model statements are quite generally, what opens a wide field of possible applications. Based on the presented model one can use scaling spectral analyses of composite oscillation processes to find out spectral ranges where the process energy efficiency is relative high or low. Possibly, the scaling spectral analysis could be usefull not only in mechanical engineering, but also in nuclear physics and astrophysics.

The author is deeply grateful to O. M. Kalinin, A. I. Polovinkin, V. A. Kamaev and A. V. Petrukhin for valuable discussions. I wish to thank S. E. Shnoll, V. A. Panchelyuga and V. A. Kolombet for invaluable support.

Submitted on February 09, 2008 / Accepted on February 17, 2009

References

1. Feynman R.P. Very high-energy collisions of hadrons. *Phys. Rev. Lett.*, 1969, v. 23, 1415; Bjorken J.D. *Phys. Rev. D*, 1969, v. 179, 1547.
2. Shnoll S.E., Kolombet V.A., Pozharski E.V., Zenchenko T.A., Zvereva I.M., Konradov A.A., Realization of discrete states during fluctuations in macroscopic processes. *Physics Uspekhi*, 1998, v. 41(10), 1025–1035. (1998)
3. Gutenberg B., Richter C.F.. Seismicity of the Earth and associated phenomena. 2nd ed., Princeton University Press, Princeton, N.J., 1954; Corral A. Universal local versus unified global scaling laws in the statistics of seismicity. arXiv: cond-mat/0402555.
4. Čislenko L.L. The structure of the fauna and flora in connection with the sizes of the organisms. Moscow, 1981 (*in Russian*).
5. Schmidt-Nielsen K. Scaling. Why is the animal size so important? Cambridge University Press, 1984.
6. Zhirmunsky A.V., Kuzmin V.I. Critical levels in developmental processes of biological systems. Moscow, Nauka, 1982 (*in Rissian*).
7. Muller H. The general theory of stability and objective development trends of technology. *Applications of Developmental and Construction Laws of Technology in CAD*, Volgograd, VPI, 1987 (*in Russian*); Muller H. Superstability as a developmental law of technology. *Technology laws and their Applications*, Volgograd-Sofia, 1989 (*in Russian*).
8. Patents:
   Nr. 05700308.9-2206-CH2005000013,
   Nr. 05759820.3-1237-CH2005000427,
   Nr. 05759818.7-1267-CH2005000426,
   Nr. 05700352.7-2415-CH2005000057.
9. Tipler P.A. Physics for scientists and engineers. New York, 1991, p. 438ff.
10. Euler L. De oscillationibus fili flexilis quotcunque pondusculis onusti. Opera omnia, II–10, 35–49.
11. Stieltjes T. Recherches sur les fractions continues. *Ann. de Toulouse*, VIII–IX, 1894–1895.
12. Gantmacher F.R., Krein M.G. Oscillation matrixes, oscillation cores and low oscillations of mechanical systems. Leningrad, 1950 (*in Russian*).
13. Perron O. Die Lehre von den Kettenbruchen. 1950.
14. Achieser N.I. The classic problem of the momenta and some questions of the analysis which are connected. Moscow, 1961 (*in Russian*).
15. Terskich V.P. The continued fraction method. Leningrad, 1955 (*in Russian*).
16. Khintchine A.Ya. Continued fractions. University of Chicago Press, Chicago, 1964.
17. Skorobogatko V.Ya. The theory of branched continued fractions and mathematical applications. Moscow, Nauka, 1983.
18. Lagrange J.L. Additions aux elements d'algebre d'Euler. 1798.
19. Markov A.A. Selected work on the continued fraction theory and theory of functions which are minimum divergent from zero. Moscow–Leningrad, 1948.

On Dark Energy and Matter of the Expanding Universe

Bo Lehnert

Alfvén Laboratory, Royal Institute of Technology, S–10044 Stockholm, Sweden

E-mail: Bo.Lehnert@ee.kth.se

At present the expanding universe is observed to be dominated by the not fully understood concepts of dark energy and matter, in a conceived almost flat Euclidian geometry. As one of the possible efforts to understand the global behaviour of the expanding universe, the present paper attempts to explain these concepts in terms of the pressure force and gravity of a spherical photon gas cloud of zero point energy, in a flat geometry. A difficult point of the conventional theory concerns the frequency distribution of the zero point energy oscillations which leads to the unacceptable result of an infinite total energy per unit volume. A modification of this distribution is therefore proposed which results in finite energy density. A corresponding equilibrium state is investigated, as well as small dynamic deviations from it, to form a basis for a model of the expanding universe. Provided that the crucial points of the present approach hold true, the model satisfies the requirements of cosmic linear dimensions, results in an estimated acceleration of the expansion being of the order of the observed one, presents a possible solution of the coincidence problem of dark energy and matter, and provides one of the possible explanations of the observed excess of high-energy electrons and positrons in recent balloon and satellite experiments.

1 Introduction

From being a speculative subject of discussion, the features of the universe have during recent years become more of an area of strict scientific analysis. After Hubble's discovery of the cosmic expansion and the Big Bang hypothesis by Gamow, astronomical observations and associated theoretical work have resulted in a number of new points of view, as summarized in recent reviews such as those by Linde [1], Hogan, Kirshner and Suntzeff [2], Luminet, Starkman and Weeks [3], Turner [4], Perlmutter [5], Riess and Turner [6], Crease [7] and Linder and Perlmutter [8]. In particular, this includes the concepts of dark energy and dark matter as well as the newly discovered accelerated expansion of the universe and its possible theoretical explanation.

The Hubble redshift has not only been interpreted as the result of a real cosmic expansion. Recently Rabounski [9] has reconsidered the Hubble redshift in terms of General Relativity, thereby finding that a photon loses its proper energy due to the work against the field of the space non-holonomity.

There have so far been reported a number of efforts to understand the global behaviour of the universe. This paper presents one of the alternatives to be investigated for such a purpose. Here an investigation is made on the possible rôle of the zero point energy of quantum mechanical vacuum fluctuations as an origin of dark energy and matter. A summary of recent observations of the expanding universe is first presented in Section 2, with corresponding theoretical so far made considerations in Section 3, followed by a description of the basic reasons for the present approach in Section 4. The frequency distribution of the zero point energy is then reconsidered in Section 5, the cosmic equilibrium of a zero point energy photon gas is elaborated in Section 6, and the acceleration of the expansion is estimated in Section 7. The implications of the present approach are finally given in Section 8, as well as in the summary and conlusions of Section 9.

2 Observations of an expanding universe

As early as in 1900 Schwarzschild [10] considered the possible non-Euclidian structure of space. For a closed elliptical configuration the lower limit of its permissible radius of curvature was found to be about 6×10^{17} meters. At present it is often stated that observations indicate the universe just to be about flat on a scale of $R_0 = 10^{26}$ meters which is the radius of its observable parts [1], but the radius of the universe could be larger. With Hubble's discovery and the Big Bang model, a finite and growing radius can also form the basis of an expansion until the present time. Conventional wisdom says the universe is infinite, but it could be finite, merely giving the illusion of infinity [3]. On the other hand, a closed finite universe of curved space is certainly attractive from the conceptual point of view, but does not become reconcilable with an observed nearly flat geometry. The idea of a finite and flat universe runs then into its own obstacle of the apparent need for the "cut-off" at an edge defined by a radius $R \geqslant R_0$. Still these questions have not been settled, and will not be further touched upon in this paper.

In the 1990s it was realized that supernovae were promising candidates for measuring the cosmic expansion. This came out to be particularly fruitful when one kind of supernova, the type Ia, turned out to have the property of a "standard candle" [2, 5, 6, 8]. The method of surveying space-time with supernovae then became accurate enough even to measure the rate of change in the cosmic expansion. Many cosmologists had anticipated that the rate of expansion should

slow down due to the attractive force of the mass of the universe. It therefore became a news of utmost interest when the supernova measurements indicated that the expansion was in fact accelerating [2, 5, 6, 8].

The acceleration of the radius R_0 of the observable universe can be determined from the measurements of redshift, relative intensity of light, and relative distance [2, 5]. Here we consider very distant supernovae, near the radius of visibility where the redshift $z = \Delta\lambda/\lambda \cong 1$, $\Delta\lambda$ is the shift in wavelength, and λ stands for the wavelength of the light emitted by the supernova at its position. For a given intensity of light, the diagrams of the observations [2, 5] then yield a redshift $z_a \cong 0.8$ for an accelerated expansion instead of $z_0 \cong 1$ for a constant one. This shows that high-redshift supernovae are fainter than would be expected for a constant expansion [5]. The deviation of the redshift due to the acceleration thus corresponds to an additional increment $\Delta \mathrm{v} = (z_0 - z_a)c$ in velocity where c is the velocity of light. With a linear scale of $R_0/2$ relative to the universe of today [5], the corresponding time of passage becomes $\Delta t \cong R_0/2c$. This yields an acceleration $\Delta \mathrm{v}/\Delta t = 2(z_0 - z_a)c^2/R_0 \cong 4\times10^{-10}$ m/s^2 of the radius R_0.

Recent experiments with high-altitude balloons and satellites [11, 12] have further spotted an excess of high-energy electrons and positrons. These can become a possible signature of a decay of dark matter.

3 Theories on the present expansion

The period of acceleration has not prevailed during the entire expansion of the universe, but appears to have started about 5 billion years ago [8]. In order to account for the present acceleration, about 75 percent of the mass-energy content is then considered to be made of some weird gravitationally repulsive substance called dark energy [8], i.e. a "cosmological antigravity" which can drive the universe apart [2]. The remaining 25 percent has attractive gravitational interaction, but $5/6$ of this is not even normal matter but rather some additional unknown substance called dark matter [5].

An alternative description of the global behaviour of the universe has been presented by Rabounski [9]. In this theory the empirical Hubble law is explained in a static universe, as being due to the redshift produced by the global non-holonomity of the isotropic space in which a propagating photon loses its energy. Also the nonlinearity of the Hubble law which is observed at large distances is explained by the deduced form of the redshift.

A candidate to explain the effect of dark energy is further the vacuum energy which is mathematically equivalent to the cosmological constant introduced by Einstein in 1917. However, it appears to be a remarkable and implausible coincidence that the mass density, just in the present epoch, is within a factor of two of the vacuum energy density. This would need some kind of accelerating dark energy that, unlike the cosmological constant, does not become constant [5]. In addition, there are problems with the zero-point vacuum energy of the quantum fluctuations. Thus the standard model of particle physics has no place for a vacuum energy density of the modest magnitude required by astrophysical data, because the simplest estimates predict a vacuum energy being 10^{120} times greater [5]. We shall later return to this crucial point.

4 Exposition of reasons for the present approach

The investigation in this paper on the optional and possible rôle of the zero point energy as an origin of dark energy and matter, in particular during the later stages of the expansion, can be justified as follows:

- The concept of an expanding universe is accepted as a working hypothesis.
- The mass-energy content is mainly due to dark energy in the form of antigravity and to dark matter accounting for the attractive gravitational interaction, thereby dominating the general dynamics of the universe.
- From the observations the universe is here interpreted to have a nearly flat geometry. This supports a simple Euclidian approach in a first approximation, without the introduction of the curved space effects of General Relativity. This would not only hold for a strictly flat space, but also as an approximation for the limited observable part of a closed elliptical or spherical universe with a very large radius of curvature.
- The zero point energy represents the lowest quantum mechanical state. This is a "dark state" having no line radiation.

5 The zero point energy and its frequency distribution

We now turn to the zero point vibrational energy, as discussed by Terletskii [13], Milonni [14] and Loudon [15] among others. This energy can hardly be discarded since its effects have been revealed experimentally. Its infinite total amount per unit volume, as obtained from conventional theory, is on the other hand unacceptable and presents a so far unsolved dilemma.

5.1 Conventional deductions

It is known from quantum mechanics that the energy of a linear harmonic oscillator with the frequency ν only assumes the values [13–15]

$$E_k = h\nu\left(k + \frac{1}{2}\right) \qquad k = 0, 1, 2, \ldots \tag{1}$$

Utilizing the partition function and the Gibbs-Helmholtz equation [13], the mean energy of the ensemble of oscillators of all k-values, also including $k = 0$, then becomes

$$\bar{E} = \frac{1}{2}\, h\nu + \frac{h\nu}{\exp(h\nu/kT) - 1}\,, \tag{2}$$

where kT is the mean energy of a classical oscillator in thermal equilibrium at the temperature T.

The number of virtual field oscillators per unit volume with frequencies in the range $(\nu, \nu + d\nu)$ further becomes

$$dn(\nu) = (8\pi/c^3)\nu^2\, d\nu\,. \tag{3}$$

On the average the oscillators then have the energy density

$$du(\nu) = \bar{E}\, dn(\nu) = (8\pi\bar{E}/c^3)\nu^2\, d\nu \tag{4}$$

in the same range. The total energy density then becomes

$$u = u_0 + u_p \tag{5}$$

where

$$u_0 = \int_0^\infty (4\pi h/c^3)\nu^3\, d\nu\,, \tag{6}$$

$$u_p = \int_0^\infty (8\pi h/c^3)\frac{\nu^3}{\exp(h\nu/kT) - 1}\, d\nu\,, \tag{7}$$

(here u_0 is the infinite zero point energy contribution, and the finite contribution u_p originates from Planck's radiation law).

To obtain a finite total zero point energy, it has sometimes been suggested that the integral (6) should be truncated at a cut-off frequency corresponding either to the Planck length or to a high energy of 100 GeV. As compared to the magnitude of astrophysical data, this still leads to an excessive vacuum energy density being about 10^{120} or 10^{55} times greater than that which is required. The choice of cut-off also appears not to be rigorously motivated.

Even if the integral (6) leads to a physically unacceptable result, a straightforward illustration of vacuum effects can be obtained from a cavity configuration. In the latter a finite change in energy is obtained from the difference between two infinite integrals of forms being similar to that of equation (6). Thus, in 1948 a theoretical analysis was reported by Casimir [16] in which it was shown that two metal plates at narrow distance will attract each other slightly, due to the electromagnetic quantum fluctuations of the zero point energy. This force is due to the low-frequency part of the zero point energy pressure, because only the small high-frequency modes are allowed to squeeze in between the plates. Later, in 1997, the theory was experimentally confirmed within 5 percent accuracy by Lamoreaux [17] who used a torsional pendulum to measure the corresponding Casimir force between a spherical and a plane metal surface. He found that this generated a force up to about 10^{-9} N on a plate having a diameter of 2.54 centimetres, and at separation distances in the range 0.6 to 6 μm. The corresponding energy density was up to about 6×10^{-6} J/m^3. An experimental confirmation of Casimir's theory for parallel metal plates was further reported by Bressi et al. [18] who measured the force between a cantilever and a rigid surface. From data of the oscillating cantilever they obtained agreement with the calculated Casimir force with 15 percent accuracy for separation distances in the 0.5 to 3 μm range. Other experimental attempts to verify Casimir's prediction have also been reviewed by the same authors.

Consequently, the low-frequency part of the zero point frequency distribution has to be accepted as an experimental fact, whereas there arises a crucial problem with the high-frequency part.

5.2 A revised form of the high-frequency distribution

Several investigators have thrown doubt upon the conventional theory of vacuum energy and its related frequency distribution [6, 19]. Here the following points can be taken as an indication that some fundamental part of the theory may be lacking:

- In the conventional analysis the probability that an oscillator is excited to its k-th state is given by a Boltzmann factor. In this factor, however, the zero point energy cancels and disappears when expression (1) is substituted into the deductions [15];
- The energy values which an oscillator can assume at a given frequency ν are determined by expression (1), whereas expression (2) represents the mean energy values which an oscillator adopts in thermal equilibrium. Here $\bar{E}$ differs from E_k for $k \geqslant 1$ of the Planck radiation part which adapts itself to a probability distribution being in thermodynamic equilibrium at a temperature T. For the zero point energy part $k = 0$, however, conventional theory yields $\bar{E}_0 = E_0 = \frac{1}{2}\, h\nu$, which corresponds to the same probability for all frequencies ν. Such a distribution could be questioned and requires further investigation and explanation;
- In the conventional deduction of Planck's law, a finite mean energy kT of the oscillators is introduced as a given and independent parameter, as well as the resulting finite total energy. In the case of the zero point energy, a corresponding introduction becomes unclear in terms of the conventional theory. In other words, the Planck law part of equation (2) includes the disposable and independent parameter kT of the photon mean energy. However, for the zero point energy part of the same equation, the analogous situation is not fully determined because there is no corresponding and independent parameter which determines the average photon energy;
- In the limiting case $T = 0$ of a pure zero point energy photon gas, one would thus have to study an ensemble of continuous states, to search for the most probable distribution of frequency among the oscillators at a given total and finite energy per unit volume.

With these points in mind, it is here concluded that the zero point energy requires a separate statistical treatment. We thus limit the analysis to a state of zero temperature, in which there is an ensemble of photons, each having an energy E_0 of equation (1). The number of possible states of oscillation

is as before given by equation (3) in the range $(\nu, \nu + d\nu)$. Here the population of zero point energy photons due to the conventional theory is on the other hand put in question, as well as their corresponding average energy.

A simple proposal is now made to find a distribution in statistical equilibrium which results in a finite average photon energy. Following Kennard [20], the probability of any state of energy $E_0(\nu) = \frac{1}{2}\, h\nu$ becomes proportional to a Boltzmann factor

$$P_B = \exp(-E_0/\bar{E}) = \exp(-\nu/\bar{\nu}) \tag{8}$$

where

$$\bar{E} = \frac{1}{2}\, h\bar{\nu} \tag{9}$$

now stands for a finite average energy of a photon, and $\bar{\nu}$ is the corresponding average frequency. With this proposal the revised form of the density (4) of the zero point energy becomes

$$du(\nu) = (4\pi h/c^3)\nu^3 \exp(-\nu/\bar{\nu})\, d\nu \tag{10}$$

It results in a finite total energy density

$$u = 24\pi h\bar{\nu}^4/c^3 \tag{11}$$

where the frequency $\bar{\nu}$ is a so far undetermined quantity, like the arbitrary mean energy kT of the states for $k \geqslant 1$.

It is desirable to extend the studies on the Casimir effect also on the experimental side. Investigations on smaller plate distances do not become an easy task, and may involve advanced nanotechnological methods. Here we can only speculate about the possibility of deposing an extremely thin layer of insulating material on a flat metal plate, and placing another such plate on top of it. With layer thicknesses being much smaller than the so far studied plate distances in experiments, considerable mutual forces are expected to arise, as long as equation (4) applies. Observed deviations from this which reveal a smaller or even a saturated force, could provide a test of various theoretical approaches, also that of equations (10) and (11).

6 Equilibrium of a photon gas in its gravitational field

In a gas cloud of photons of zero point energy, there is an antigravity force due to the photon gas pressure gradient, and a gravitation force due to the intrinsic mass of the same photons as determined by the total energy according to Einstein's mass-energy relation. We now proceed to the steady-state balance of an isotropic photon gas of zero point energy, in which the pressure force is balanced by the gravitational force. A restriction is made to spherical symmetry in a flat space, as supported by the points given in Section 4, and based on the proposed model of frequency distribution given in Section 5.

With the radial coordinate r in a spherical frame of reference, the energy density u of equation (11) and the corresponding average photon energy $\bar{E}$ and frequency $\bar{\nu}$ of equation (9) then become functions of r only. The radially outward directed pressure force is given by

$$f_p = -\frac{dp}{dr} = -\frac{1}{3}\frac{du}{dr}\,. \tag{12}$$

With an average total mass $\bar{E}/c^2$ of each photon, the integrated mass of the photon gas within the radius r becomes

$$M(r) = \int_0^r 4\pi r^2 (u/c^2)\, dr = (4\pi/c^2)\int_0^r r^2 u\, dr\,. \tag{13}$$

This leads to a radially inward directed gravitational force

$$f_g = -GMnm_p/r^2 = -GMu/c^2 r^2 \tag{14}$$

where $G = 6.673\times10^{-11}$ m^3/kg$\cdot$s^2 is the Newtonian constant of gravitation.

A steady equilibrium is now determined by $f_p + f_g = 0$ which results in

$$-\frac{1}{3}\frac{du}{dr} = \frac{4\pi G}{c^4 r^2}\, u \int_0^r r^2 u\, dr\,. \tag{15}$$

This equation is normalized by introducing $\rho = r/r_c$ where r_c is a characteristic radius, and $u = u_c U(\rho)$ with u_c as a characteristic photon energy density. Multiplying eq. (15) by r^2/u and taking the derivative with respect to r,

$$\frac{d^2U}{d\rho^2} + \frac{2}{\rho}\frac{dU}{d\rho} - \frac{1}{U}\left(\frac{dU}{d\rho}\right)^2 + 2C_0U^2 = 0\,. \tag{16}$$

This relation includes the dimensionless characteristic parameter

$$C_0 = 6\pi G u_c r_c^2/c^4 = 3\pi n_c r_c^2 L_p^2/\bar{\lambda}\,. \tag{17}$$

Here $L_p = (Gh/c^3)^{1/2}$ is the Planck length, $n_c = u_c/\bar{E}$ a characteristic photon density, and $\bar{\lambda} = c/\bar{\nu}$.

A particular solution of eq. (16) can be found by means of the ansatz $U = \rho^{-\alpha}$ which leads to $2C_0 = \alpha\rho^{\alpha-2}$ and becomes satisfied when $\alpha = 2$. This yields $C_0 = 1$ and

$$u(r) = u_c\,(r_c/r)^2\,. \tag{18}$$

The equilibrium condition $C_0 = 1$ corresponds to a characteristic radius

$$r_c = \left(c^4/6\pi G u_c\right)^{1/2}\,. \tag{19}$$

The integrated mass at the distance r further becomes

$$M(r) = 2c^2 r/3G \tag{20}$$

from combination of relations (13), (18), and (19). The obtained results are now discussed as follows:

- In some respects the present analysis also applies to the equilibrium of a photon gas in the regime of Planck's radiation law at nonzero temperature;
- When being observed from the Earth, the surrounding parts of the universe appear on the average to be rather uniformly distributed over the sky. This is here taken as an indication that the position of the Earth and of an observer is deep inside the cloud of the universe, i.e. far

away from its "boundary". Consequently we take $r=r_c$ as the position of the Earth where the energy density has the characteristic value u_c, and have $r = R_0 \gg r_c$ as the radius of the observable parts of the universe. Due to relation (18) this implies that the energy density $u(r)$ decreases from u_c at $r=r_c$ to $u_c(r_c/R_0)^2 \ll u_c$ at $r=R_0$. A "halo" extending beyond the radius R_0 can also exist, as introduced in many cosmological versions [1];

- The Planck length $L_p \cong 4.05\times10^{-35}$ m is the smallest length appearing as a basic parameter in physics. To satisfy the equilibrium condition $C_0 = 1$, it is seen from eq. (17) that the characteristic radius r_c of eq. (19) has to be of cosmic dimensions for moderate values of u_c;
- Equation (19) further shows that a high energy density u_c requires a small radius r_c for a state being close to equilibrium, and does not lead to excessively large cloud dimensions;
- At the origin $r = 0$ the total mass (20) vanishes. The divergence at $r = 0$ of the energy density u in equation (18) can here be taken as a remnant of the earliest stage of a Big Bang. Further, even if each of the forces (12) and (14) diverges at $r = 0$, the total force vanishes at the origin in equilibrium;
- The mass (20) increases linearly with r, to $M(R_0) = 2c^2R_0/3G$ at the radius of the observable universe. This value is analogous to the solution by Einstein [21] for a steady quasi-Euclidian universe.

The parameter C_0 represents the ratio $\mid f_g/f_p \mid$ between the gravitation and pressure forces. Here f_g is proportional to u^2, and f_p to u. Small deviations from an equilibrium can in a first approximation be represented by values of C_0 which differ slightly from unity. This implies that $C_0 < 1$ corresponds to pressure-dominated accelerated expansion, and $C_0 > 1$ to gravitation-dominated accelerated compression. The deviations of C_0 from unity can therefore be used to identify the acceleration without considering a detailed equation of state as discussed elsewhere [4, 8]. This has some resemblance to the energy principle in fluid dynamics, where stability is studied in terms of virtual changes in energy, without analysing the dynamics of the corresponding normal modes in detail.

7 A simple discussion on the dynamics of the expansion

During the later stages of the expansion the equilibrium solution of Section 6 could provide a starting point also for a simple discussion on the related dynamics. As a working hypothesis we here adopt the often accepted view of a balance between the dark energy and matter forces corresponding to a constant expansion rate, whereas a force unbalance leads to an accelerated or retarded expansion. Only a crude estimation is made here of the order of the acceleration in the case of a slight deviation from the equilibrium treated in Section 6.

For this purpose we consider a volume element of thickness dr at the radius $r = R_0$. With the local force densities (12) and (14) the total forces on the layer become

$$(dF_p, dF_g) = 4\pi R_0^2 (f_g, f_p)\, dr\,. \tag{21}$$

From equations (12), (18) and (19)

$$f_p \cong 2u_c r_c^2/3R_0^3 \cong c^4/9\pi G R_0^3 \tag{22}$$

for small deviations from the equilibrium defined by $dF = dF_p + dF_g = 0$ and where

$$dF = (2\delta - 1)\, dF_p\,. \tag{23}$$

Here the fraction δ of the total mass-energy content is due to the pressure force dF_p, and δ is not far from the equilibrium value $\delta = 1/2$. The mass of the volume element further becomes

$$dM \cong (2c^2/3G)\, dr \tag{24}$$

due to equation (20). The acceleration of the radius R_0 is then roughly given by

$$d^2R_0/dt^2 \cong (2\delta - 1)\, dF_p/dM \cong (2\delta - 1)(2c^2/3R_0)\,. \tag{25}$$

In a rigorous dynamical approach the question would arise whether the photon gas cloud can be considered as a closed system or not, i.e. if the region $r > R_0$ of an undisturbed "background" has to be included in the analysis.

8 Implications of present approach

An attempt has been made here to understand at least part of the features of the expanding universe at its later stage. Among the obtained results, the order of magnitude of the characteristic radius (19) should first be mentioned. The experiments by Lamoreaux indicate that the possible "saturation" at a finite average frequency $\bar{\nu}$ of equations (9)–(11) would at least take place above an energy density of the order of 6×10^{-6} J/m^3. With $u_c \geqslant 6\times10^{-6}$ J/m^3 at the position $r=r_c$ of the Earth, we then have $r_c \lesssim 10^{24}$ m $= 0.01R_0$ with R_0 as the radius of the observable universe. Provided that there is not an excessively large average frequency $\bar{\nu}$ as compared to the frequency range in the experiments by Lamoreaux, and that the form (11) holds true, the linear dimensions of the present photon gas model should thus be consistent with cosmical dimensions. Since f_p is proportional to u and f_g to u^2, very large energy densities result in very small radii, and not in very large ones.

Concerning the present stage of an accelerated expansion, the radius of the outermost parts of the universe has been observed to expand at an acceleration of about 4×10^{-10} m/s^2 for a fraction $\delta = 0.75$, as described in Sections 2 and 3. The corresponding estimation (25) yields an acceleration of the order of 3×10^{-10} m/s^2, being of the same order as the observed value.

The generally discussed coincidence problem may have a solution in terms of the present theory. The vacuum energy density (dark energy) and its mass density (dark matter) are coupled here, because they originate from the same photon cloud. This coupling both exists in an equilibrium state, and in an accelerated state where the acceleration of the expansion is of the order of the ratio between the net pressure force and the mass of the cloud.

The spotted excess of high-energy electrons and positrons in recent balloon and satellite experiments [11, 12] may, among other possible explanations, also be due to electron-positron pair formation through the decay of energetic zero point energy photons. The latter then belong to the high-frequency part of the distribution, even in the proposed case of expression (10). The photon decay could be caused by impacts with other charged particles [22].

9 Summary and conlusions

The present expansion of the universe is dominated by the so far not fully understood concepts of dark energy and matter. An attempt has been made in this paper to explain these concepts in terms of the pressure force and gravity of a spherical photon gas cloud of zero point energy, treated in flat quasi-Euclidian geometry. Such an analysis requires a reconsideration to be made of the conventional concept of zero point energy and its frequency distribution, because this leads to an unacceptable infinite energy density. For this purpose a modified statistical approach has been proposed which results in a finite energy density. An equilibrium solution has then been found for a zero point energy photon gas confined in its own gravitational field. This also outlines the main behaviour of small dynamic deviations from an equilibrium, i.e. from a constant to an accelerated expansion of the universe.

A crucial point of the present analysis is the required finite energy density of the vacuum field. Provided that the present approach holds true, it would lead to the following features:

- The obtained linear dimensions seem to be consistent with observed cosmical ones;
- The observed and estimated values obtained for the acceleration of the present expansion are of the same order of magnitude;
- The generally discussed coincidence problem of dark energy and dark matter appears to have a solution, because these concepts originate from the same photon cloud in the present model;
- The observed excess of high-energy electrons and positrons in balloon and satellite experiments have one possible explanation in the decay of high-energy photons of the vacuum field.

Submitted on February 15, 2008
Accepted on February 26, 2009

References

1. Linde A. The self-reproducing inflatory universe. *Scientific American*, November 1994, 32–39.
2. Hogan C. J., Kirshner R. P., Suntzeff N.B. Surveying space-time with supernovae. *Scientific American*, January 1999, 28–33.
3. Luminet J.-P., Starkman G. D., Wecks J. R. Is space finite? *Scientific American*, April 1999, 68–75.
4. Turner M. S. Dark energy: just what theorists ordered. *Physics Today*, April 2003, 10–11.
5. Perlmutter S. Supernovae, dark energy, and the accelerating universe. *Physics Today*, April 2003, 53–60.
6. Riess A. G., Turner M. S. From slowdown to speedup. *Scientific American*, February 2004, 50–55.
7. Crease R. P. Critical point dark energy. *Physics World*, December 2007, 19–22.
8. Linder E., Perlmutter S. Dark energy: the decade ahead. *Physics World*, December 2007, 24–30.
9. Rabounski D. Hubble redshift due to the global non-holonomity of space. *The Abraham Zelmanov Journal*, 2009, v. 2, 11–28.
10. Schwarzschild K. Über das zulässige Krümmungsmaaß des Raumes. *Vierteljahrsschrift der Astronomische Gesellschaft*, 1900, Bd. 35, S. 337–347 (published in English as: Schwarzschild K. On the permissible numerical value of the curvature of space. *The Abraham Zelmanov Journal*, 2008, v. 1, 64–73).
11. Brumfiel G. Electric "bump" may confirm dark matter. *Nature*, 2008, v. 456, 290–291.
12. Chang J. et al. An excess of cosmic ray electrons at energies of 300–800 GeV. *Nature Letters*, 2008, v. 456, 362–365.
13. Terletskii Ya. P. Statistical physics. North-Holland Publishing Comp., Amsterdam, London, 1971, Ch V1.
14. Milonni P. W. The quantum vacuum. Academic Press Inc.,Boston, San Diego, New York, London, Sydney, Tokyo, Toronto, 1994.
15. Loudon R. The quantum theory of light. Oxford Univ. Press, 2000, Third Edition, Ch 1, Sec. 6.12.
16. Casimir H. B. G. On the attraction between two perfectly conducting plates. *Proc. Kon. Nederland. Akad. Wetensch.*, 1948, v. B51, 793–795.
17. Lamoreaux S. K. Demonstration of the Casimir force in the 0.6 to 6 μm range. *Phys. Rev. Letters*, 1997, v. 78, 5–8.
18. Bressi G., Carugno G., Onofrio R., Ruoso G. Measurement of the Casimir force between parallel metal plates. *Phys. Rev. Letters*, 2002, v. 88, 041804, 1–4.
19. Heitler W. The quantum theory of radiation. Clarendon Press, Oxford, 1954, pp 57 and 326.
20. Kennard E. H. Kinetic theory of gases. McGraw-Hill Book Comp., First Edition, New York and London, 1938, Sec. 226.
21. Einstein A. The meaning of relativity. Methuen and Co.Ltd., London, 1950, pp. 86 and 102.
22. Lehnert B. A model of electron-positron pair formation. *Progress in Physics*, 2008, v. 1, 16–20.

Regular Changes in the Fine Structure of Histograms Revealed in the Experiments with Collimators which Isolate Beams of Alpha-Particles Flying at Certain Directions

Simon E. Shnoll*† and Ilya A. Rubinstein‡

*Institute of Theor. and Experim. Biophysics, Russian Acad. of Sciences, Pushchino, Moscow Region, 142290, Russia
†Department of Physics, Moscow State University, Moscow 119992, Russia
‡Skobeltsin's Institute of Nuclear Physics, Moscow State University, Moscow 119991, Russia
E-mail: shnoll@mail.ru

As was shown in the works of 1951–1983, the fine structure of distributions of the results of measurements of processes of diverse nature is not casual. The changes in the shape of histograms corresponding to the distributions were called "macroscopic fluctuations". The universal character of the phenomenon and its independence of the nature of the process studied were demonstrated for various processes: biochemical and chemical reactions, movement of latex particles in the electric field, proton transverse relaxation in the inhomogeneous magnetic field, discharge in the neon-tube RC-generator and radioactive decay of various α- and β-isotopes. Since 1982, the main object chosen to study macroscopic fluctuations has been α-decay. The choice was based on the process being a priori independent of trivial factors and the possibility to conduct continuous long-term automatic measurements while storing the results in a computer archive (database). Started in 1982, these measurements have been carrying on, as unceasingly as possible, until now. Since July 2000, the measurements are conducted using devices designed by one of the coauthors of this review, I. A. Rubinstein. Application of these devices (especially, detectors with collimators which isolate beams of α-particles flying at certain directions), along with the use of Edwin Pozharsky's computer program, which eases histogram comparing by the expert, has allowed us to reveal a number of fundamentally new regularities. In the review, we describe these regularities, device constructions, and the methods of measurement and analysis of the results obtained.

1 Devices, measurement methods, and data analysis

The methods of histogram construction and analysis were described many times in our previous works [11–15]. We analyze the shape of "inconsistent" histograms [33, 34] — distributions of the results of consecutive measurements, the number of which is comparable with the selected number of digits (bins). Usually we cut the sequence of a time series of the results of measurements to equal, non-overlapping segments (60–100 segments in a series), with approximately the same number of bins. In the histograms constructed from such segments of time series, the number of results per bin will vary from 0 to 5. We analyze changes in the distribution of the number of results within a single bin depending on the position (order number) of the bin in the series, and the regularities become more evident (visible) after smoothing of the initially inconsistent histograms by moving summation. All the operations: registration of the quantities measured, their storing and sorting, histogram construction and processing (smoothing, superpositioning, mirroring) — are performed with the aid of a very handy program written by Edwin Pozharsky (see [12]). A weakness of our methodology is visual comparing of histogram shapes: the decision "similar/non-similar" is made by an expert, after evaluating a pair of histograms drawn on the computer monitor. There is a "radical" way to overcome subjectivity of expert's judgments: comparing histograms after randomization of their sequence. In this case, the expert knows nothing about the histograms compared. Using this approach, we checked all the principal results of our investigations. However, the approach is extremely laborious; the volume of work to do increases greatly. Another way to avoid expert's subjectivity, which was used in most cases, is pairwise comparing — *ceteris paribus* — of two series of measurements, "control" and "experiment", differing only in a single factor (e.g., comparing histograms constructed from the "direct" and "inverse" sequences of the same time series). This method, which has been conventional in science for 300 years, was used to obtain the results of last years.

It would be good to replace the expert with a computer program. We started such attempts about 20 years ago. This task turned out unexpectedly difficult for yet. The pattern-recognition specialists usually give it up, because what seems obvious for the expert appears vague for the computer program. Recently, however, some progress has been achieved. V. V. Strelkov has made a computer program which reprodu-

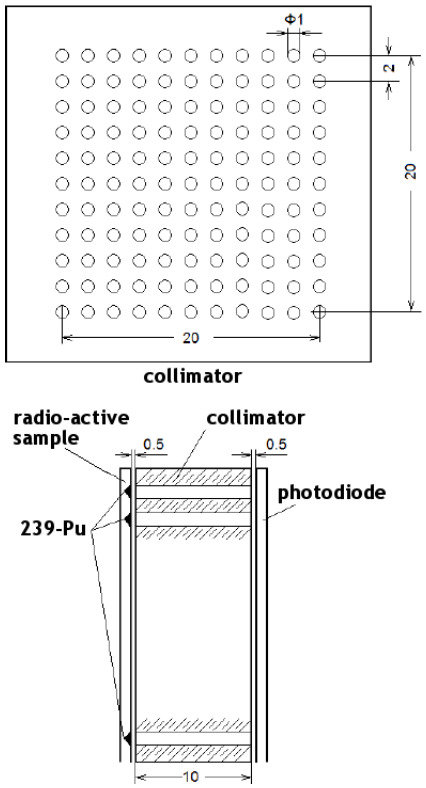

Fig. 1: — Fig. 1a: Collimator. Fig. 1b: Device assembly (radioactive sample, collimator, photodiode).

ces one of the main phenomena we study, namely, the "near-zone effect" [31, 32]. The effect means that the histograms constructed from the neighbor (non-overlapping!) segments of a time series are more probable to be similar than random far-apart histograms. Unfortunately, the program lacks user interface and is still accessible only by the author.

Despite the absence of a computer program and the laboriousness of visual histogram comparing, we have obtained much information on the phenomena studied, which is based on the "control-experiment" comparisons. Among those data, of special interest are the results of experiments, in which α-radioactivity was measured using a collimator-based setup.

Designing a collimator which would yield a narrow beam of α-particles (angle, $\leqslant 10^{\circ}$) represents a known difficulty. Since the mean range of 5-MeV α-particles in air is about 32 mm, the length of the collimator can be about 10 mm — then the particle's energy loss after passing the collimator will be about 20%. In this case, one can be sure that all the α-particles passed through the collimator will be registered, and no vacuumization of the "source-collimator-detector" system would be necessary.

With the collimator length 10 mm, the diameter of the hole for obtaining a narrow beam should not be more than 1 mm. The number of α-particles emitted by the radioactive source from a 1-mm spot cannot be substantially increased by raising the thickness of the ^{239}Pu layer. Hence, one can achieve a particle flux through a single collimator hole of 5–8 particles per second.

To enhance statistical significance of the experiment, we had to design a collimator in the form of a 120-hole grid (Fig. 1a), and use a larger-area detector.

The radioactive source itself is a grid with hollows filled up with ^{239}Pu. The centers of hollows are strictly coaxial with the centers of collimator holes. Fig. 1b shows the positional relationship between the source, collimator and detector, the latter being a photodiode with the area of sensor surface 400 mm^2.

2 Regular changes of the histogram shape with time

Regular changes with time is one of the main proofs of non-randomness of the fine structure of histograms obtained upon measuring processes of diverse nature. These regularities gradually emerged in the series of systematic many-year measurements of the rates of enzymatic and chemical reactions and the processes of radioactive decay [1–6]. The main results of those studies were reproduced and substantially extended in the experiments on α-activity measured using a line of new devices.

2.1 The "near-zone effect"

As shown in many our papers published earlier, changes in the histogram shape reveal an "effect of near zone", which states for a high probability of the histograms constructed from the non-overlapping neighbor segments of a time series to be similar. The nature of this effect remains mysterious, much because of its fractality: the effect manifests itself on different time scales, when histograms are constructed from hour, minute, second and 0.01-second segments of a time series [12, 14, 15].

2.2 Daily periods

The high quality of experimental setups and accurate determination of time intervals (and most of all, independence of the histogram shape of time series trends!) enabled us to see that the periods of appearance of a certain histogram shape split to the "sidereal" and "solar" ones. Now, with histograms constructed for 1-min segments, the daily period split to the "sidereal" (1436 min) and "solar" (1440 min) days. Determination of the yearly periods with the accuracy of 1 h also yielded two peaks: one equal to 365 average solar days (calendar year) and another equal to 365 days plus 6 h (sidereal year). When yearly periods were determined with the accuracy of 1 min (!), the calendar and sidereal periods, as expected from calculations, turned out to be 525599-525600 and 525969 min respectively. The calendar period seems to mean the recurring orientation of the laboratory relatively to the Sun, whereas the sidereal period reflects orientation in re-

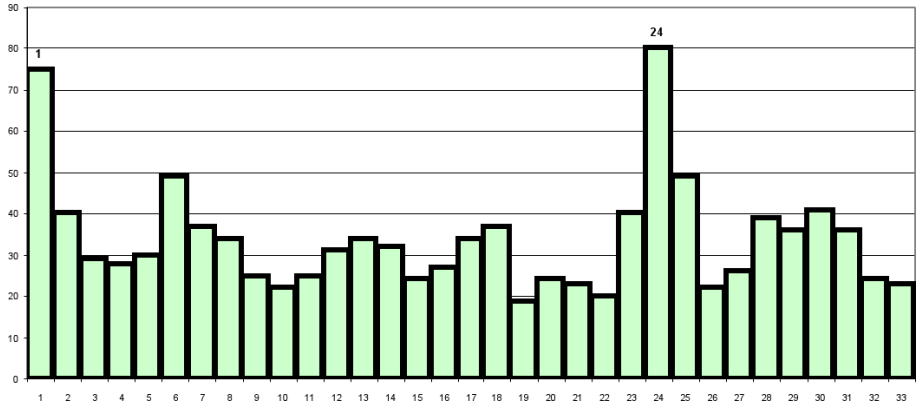

Fig. 2: A typical dependence of the probability of reappearance of histograms of a certain shape on the interval between them. The "near-zone" effect and the near-daily period of reappearance of similar 1-hour histograms in the measurements of ^{239}Pu α-activity at Novolazarevskaya station (Antarctic) on March 1–2, 2003. The measurements were made by A. V. Makarevich. In the figure, the number of similar histogram pairs (Y-axis) is plotted vs. the corresponding interval between histograms (X-axis, h) [20].

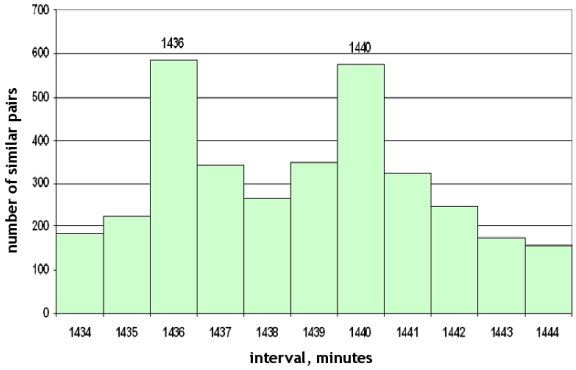

Fig. 3: When ^{239}Pu α-activity is measured with the detectors oriented in a plane parallel to the celestial equator, two distinct periods of the appearance of similar histograms can be seen: one equal to the sidereal day (1436 min) and another corresponding to the solar day (1440 min). The measurements were made in Pushchino on June–October, 2004. Axis legends as in Fig. 2 [22, 25].

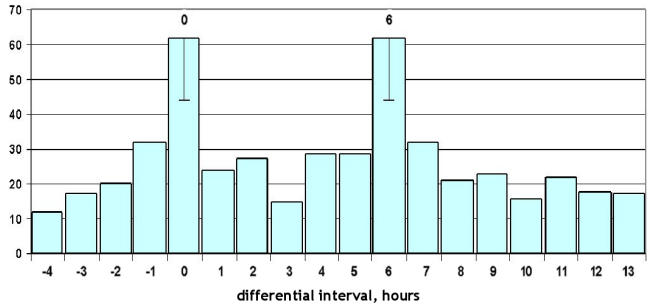

Fig. 4: Similar 1-hour histograms appear in the measurements of ^{239}Pu α-activity with the interval of exactly a year ("calendar year") and a year plus 6 hours ("sidereal year"). In the figure, the number of similar histogram pairs (Y-axis) is plotted vs. the corresponding interval between histograms minus the number of hours in a year (8760 h) (X-axis, h) [22, 25].

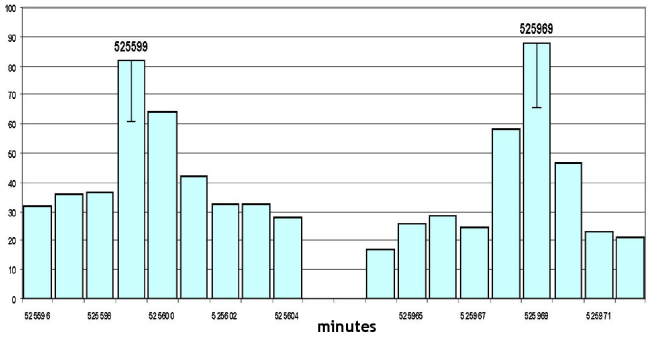

Fig. 5: With the accuracy of 1 min, similar histograms reappear after a year with two main periods: the double (split!) calendar (with 525599- and 525600-min peaks) and the sidereal, equal to 525969 min. The measurements of ^{239}Pu α-activity were made on November 24, 2001 and 2002. In the figure, the number of similar histogram pairs (Y-axis) is plotted vs. the corresponding interval between histograms (X-axis, min) [22, 25].

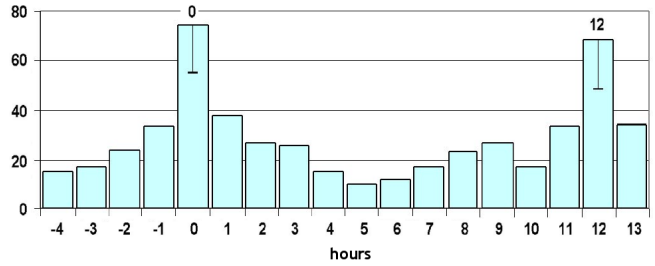

Fig. 6: With the accuracy of 1 h, similar histograms reappear with two periods: exactly 2 years and 2 years plus 12 h. The measurements of ^{239}Pu α-activity were made on August–September, 2000–2002. In the figure, the number of similar histogram pairs (Y-axis) is plotted vs. the corresponding interval between histograms minus the number of hours in two years (X-axis, h) [22, 25].

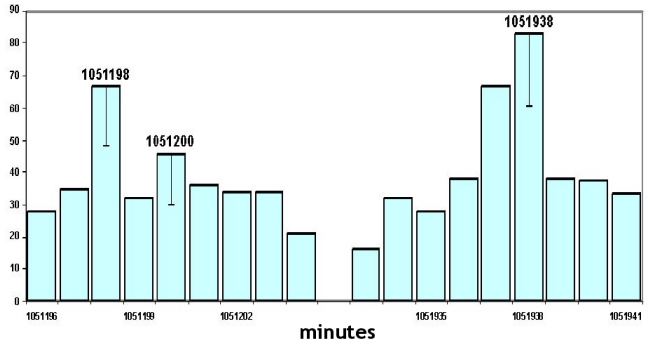

Fig. 7: When ^{239}Pu α-activity is measured with a 1-min resolution, similar histograms reappear with two main periods: calendar and sidereal. The calendar period consists of two subperiods: one is equal to the theoretical value (1051200 min) and another is 2 min shorter (1051198 min). The sidereal period exactly meets the theoretical value of 1051938 min. The measurements of ^{239}Pu α-activity were made on April 20, 2001–2003. In the figure, the number of similar histogram pairs (Y-axis) is plotted vs. the corresponding interval between histograms (X-axis, min) [22, 25].

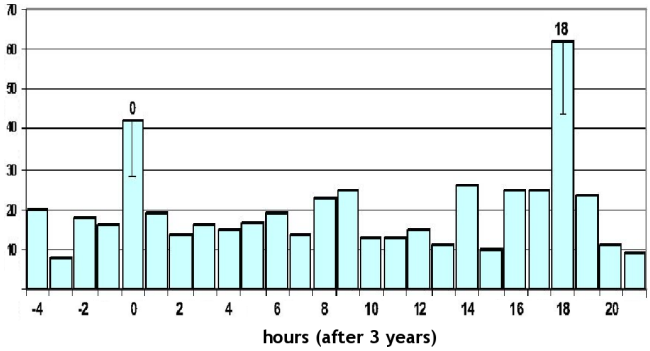

Fig. 8: With the accuracy of 1 h, similar histograms reappear exactly after 3 years and 3 years plus 18 h. The measurements of ^{239}Pu α-activity were made on August–October, 2000–2003. In the figure, the number of similar histogram pairs (Y-axis) is plotted vs. the corresponding interval between histograms minus the number of hours in three years (X-axis, h).

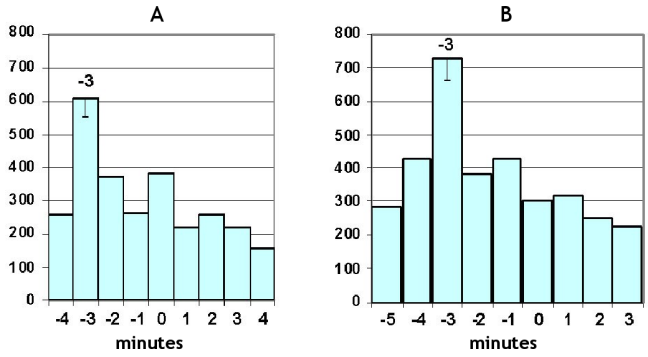

Fig. 9: When compared are histograms with a 3-year interval between them, the calendar period of reappearance of similar histograms is 3 min shorter than the theoretical value. The measurements of ^{239}Pu α-activity were made on the same dates of October (A) or August and November (B), 2000–2003. In the figure, the number of similar histogram pairs (Y-axis) is plotted vs. the corresponding interval between histograms minus the number of minutes in three years (1576800 min) (X-axis, h).

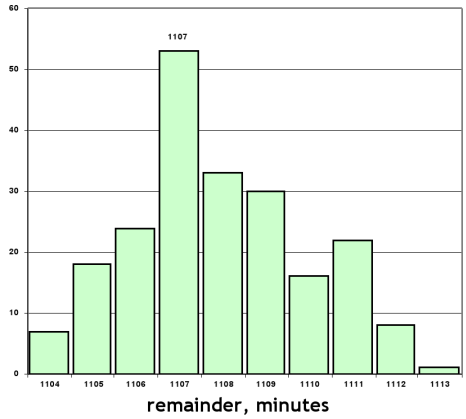

Fig. 10: When compared are histograms with a 3-year (1576800-min) interval between them, the sidereal period of reappearance of similar histograms is realized with a triple "leap shift", i.e. $369\times3 = 1107$ min later of the calculated calendar time. In the figure, the number of similar histogram pairs (Y-axis) is plotted vs. the corresponding interval between histograms minus the number of minutes in three years (1576800 min) (X-axis, h).

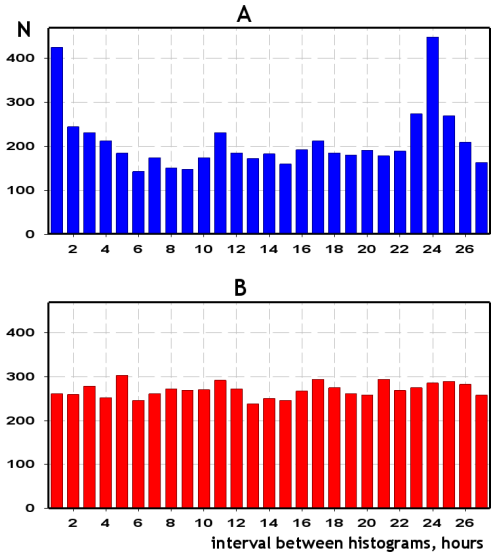

Fig. 11-1: The distribution of intervals between similar histograms depends on the direction that α-particles fly in upon ^{239}Pu radioactive decay. The measurements of ^{239}Pu α-activity were made on January–June, 2002. (A) α-Particles emitted by a flat sample are registered with a flat detector without collimator; (B) before registered by a detector, α-particles pass through a narrow collimator directed at the Pole Star. In the figure, the number of similar histogram pairs (Y-axis) is plotted vs. the corresponding interval between histograms (X-axis, h) [23, 26].

Fig. 11-2: Distribution of intervals between similar 1-hour histograms in the experiments with collimators aimed at the Pole Star (A) and directed west (B). The measurements of ^{239}Pu α-activity were made in Pushchino (at a latitude 54° north) on February–May, 2003 [23, 26].

lation to the sphere of fixed stars.

Apparently, the phenomenon of period splitting is underlain by the spatial anisotropy of factors that determine the shape of histograms. All the aforesaid is illustrated by Fig. 2–Fig. 9.

Fig. 2 shows a typical picture: a high probability of appearance of similar 1-h histograms in the nearest, neighbor intervals (the near-zone effect) and the increase of this probability after 24 h. We obtained analogous distributions with a pronounced near-zone effect and 24-h period many times — for processes of diverse nature measured at various geographical points.

Fig. 3. More accurate determination of the daily period in the appearance of similar histograms (with the 1-min resolution), undertaken on Yu. I. Galperin's advice, showed that the daily period is distinctly resolved to two peaks: the "sidereal day" (1436 min) and the "solar day" (1440 min).

2.3 Yearly periods

Fig. 4 shows that determined with the accuracy of 1 h, yearly periods split — like do daily periods determined with the 1-min accuracy — to two peaks: the "solar" (calendar) peak and the "star" (sidereal) one.

With the results of 1-s measurements collected for many years, yearly periods were determined with a 1-min accuracy. Then, apart from resolving the solar and sidereal yearly periods, we were able to see a surprising shift of the solar period by a minute per year: by one minute in the first, by two minutes in the second, and by three minutes in the third year. Strangely enough, the sidereal period did not shift; and since both observations were made in the same experiments, the shift of the solar period looked more reliable.

Constructing 1-h histograms after 3 years, we again obtained two periods: the "calendar" period, which was equal to the number of hours passed for 3 years, and the "sidereal" one, differing from the first by 18 h, i.e. by three "leap shifts". This can be seen in Fig. 8.

To obtain statistically significant values of the duration of "calendar period" after 3 year with a 1-min resolution, we compared about 200000 histogram pairs. The results are represented in Fig. 9.

It is also important that the 2nd "sidereal" period corresponds exactly to the leap shift and is equal to $369\times3 = 1107$ min (i.e., $1576800 + 1107 = 1577907$ min) — see Fig. 10. Analogous results were obtained time and again.

3 Dependence of the histogram shape on the direction in space

The use of collimators, isolating directed α-particle beams, allowed us to start studies on the spatial regularities in the change of the histogram shape.

3.1 The collimator is directed at the Pole Star [23, 26]

In 2002 we started measurements with collimators, which isolate directed beams of α-particles flying at different directions upon radioactive decay. The devices were constructed by I. A. Rubinstein. It was already in the first experiments, when we found that the histogram shape depended on the direction of α-particles escape. With the collimator directed North (at the Pole Star), we saw disappearance of the daily periods in the change of the histogram shape. The control measurements were conducted either without collimators or with a collimator directed west or east. These measurements lasted several months in 2002 and were repeated in 2003 and 2004 [23].

The dependence of the histogram shape on the direction of α-particles escape upon radioactive decay has quite a deep significance. The measurements were carried out in Pushchino laboratory (at the latitude 54° north and longitude 37° east), and the result was similar to that observed near the North Pole (at the latitude 80–82° north) [20]. In the air, α-Particles (^{239}Pu) will run a distance of $\sim$4 cm. Hence, the matter does not concern any factors of the Earth Pole region affecting the shape of histograms. Evidently, a suggestion of radioactive α-decay being influenced by something is out of consideration too. The measure of radioactive decay intensity (the number of decay events per time unit) is independent of the conditions of measurements and did not change in our experiments. The fluctuations of the radioactive decay intensity we observed were well-correspondent, according to the conventional criteria, to Poisson statistics. The only thing dependent on the orientation of the collimator was the change of the histogram shape in time, or rather the change associated with the daily rotation of the Earth. Considering the disappearance of that dependence in the experiments conducted near the North Pole, one could assume an interference of some local environmental factors. For the results of Pushchino experiments, when the collimator was directed at the Pole Star, no such explanation is possible, as daily periods did not disappear in the control, *ceteris paribus*, measurements. There remains only one conclusion: the phenomenon is a manifestation of sharp anisotropy of the space-time continuum. It should be noted here that this anisotropy reveals itself at the moment of α-particles escaping the nucleus. Given the nucleus diameter to be $\sim 10^{-13}$ cm, the spatial anisotropy should be of the same scale. With the energy of α-particles being several MeV, the fluctuations of the Earth magnetic field and its influence on the direction of α-particles run, let alone on the fine structure of histograms, may well be neglected.

3.2 Rotation of collimators [26, 27]

Following the experiments discussed above, we started, in 2004, measurements with collimators that were being rotated clockwise or counterclockwise with a special apparatus.

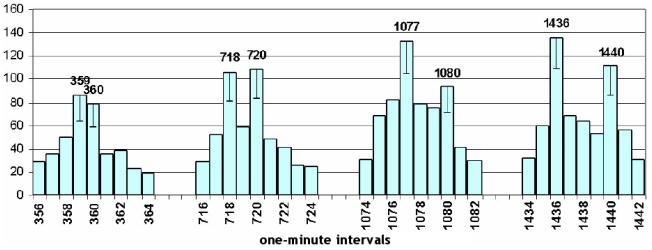

Fig. 12: When ^{239}Pu α-activity was measured with collimators being rotated counterclockwise in a plane parallel to the celestial equator, the probability of similar histograms to reappear periodically increased. These "artificial" periods turned out to be split to the sidereal and solar peaks too.

When the collimator was rotating counterclockwise (i.e., co-rotating with the Earth), the shape of histograms was changing with periods equal to the number of collimator rotations per day plus one rotation made by the Earth itself. We observed periods of 12, 8, 6, 4, 8, 3 and 1 h. When the collimator made one clockwise rotation a day, the Earth's rotation got compensated for, and the daily period in the change of histogram shape disappeared. All these results confirmed the conclusion on the dependence of histogram shape changes on "scanning" of the surrounding, sharply anisotropic, space. And again, we found that these "artificial" periods split to the "solar" and "sidereal" ones (Fig. 12) [26, 27].

Fig. 12 shows the results of an experiment, in which a collimator made three rotations per day counterclockwise. Together with one counterclockwise rotation made by the Earth itself, this amounts to four rotations per day, i.e., a period equal to 6 h (360 min). It can be seen that after the first rotation, the extremum consists of two unresolved peaks (359 and 360 min). After the second rotation, two distinct extrema (718 and 720 min) are visible, and they get to 1077 and 1080 min after the third rotation. After the forth rotation we finally see two extrema corresponding to the "normal" solar and sidereal day.

Analogous splitting was observed in the case of other "artificial" periods.

3.3 Collimators are directed west and east [27, 28]

The experiments, in which collimators were directed west and east, confirmed the main conclusions made before and revealed two new phenomena:

a). Simultaneous measurements with two collimators placed at the same point but counter-directed, aiming east and west, showed disappearance of similarity between histogram shapes. It was important, since earlier we considered similarity of histograms obtained at the same place and time as the main argument in favor of nonrandomness of the histogram shape;

b). Not less important was another phenomenon: there was a 12-hour difference in the appearance of similar his-

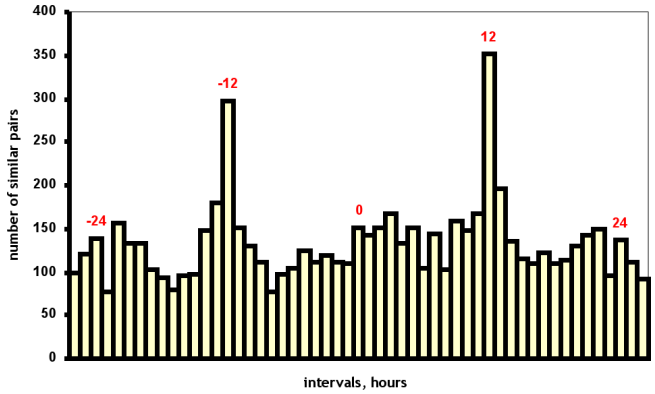

Fig. 13: With the collimators aimed at opposite directions, the probability of similar histograms to reappear sharply decreases. The histograms of a certain shape appear "in the west" exactly half a day later than "in the east". The measurements of ^{239}Pu α-activity were made in Pushchino on June 22 and October 13, 2003.

tograms in the series obtained with the "eastern" and "western" collimators. Essentially, this result was analogous to that obtained in the experiments with rotating collimators. Indeed, as the Earth rotates, the surrounding space is being scanned, and there should be a correspondence between histograms of a particular shape and certain directions in the space, which will consecutively appear in the collimator's "field of view" (Fig. 13).

3.4 A strange 1444-minute period emerging when the collimator is always aimed at the Sun

In the spring of 2004, we started continuous, 24/7 registration of ^{239}Pu α-activity with a collimator, which made one clockwise rotation per day — that is, it was always aimed at the Sun. The objective was to distinguish between changes dependent on the Earth's revolution around the Sun and changes caused by the Earth's movement in relation to the sphere of fixed stars. As expected, no daily periods was revealed in those measurements. The changes of the histogram shape seen under such conditions could, therefore, be only attributed to the Earth's movement along the circumsolar orbit. So it was even more surprising when in the second half of July 2005, we found a strange period equal to 1444 min. The similarity between histograms gradually grew, the peak became more distinct and reached its maximum on July 24–29, this followed by its rapid decline until complete disappearance by August. This phenomenon is illustrated in Fig. 14–Fig. 16.

Fig. 14 shows the distribution of the number of histogram pair matches for measurements with a "solar" collimator on July 25 and August 10, 2005. It can be seen that there are no distinct daily periods on August 10 — as well as on any other day, which is typical for measurements with the "solar" collimator. There is an exception though: on July 25 the probability of similar histograms to reappear jumped, the period

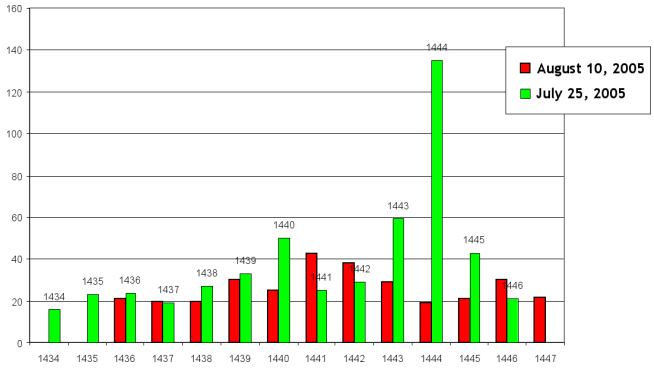

Fig. 14: The figure illustrates emergence of an "anomalous" period of similar histogram reappearance (July 25, 2005), which is equal to 1444 min. Usually, there are no marked daily periods in the experiments with the "solar" collimator — as can be seen on August 10, 2005.

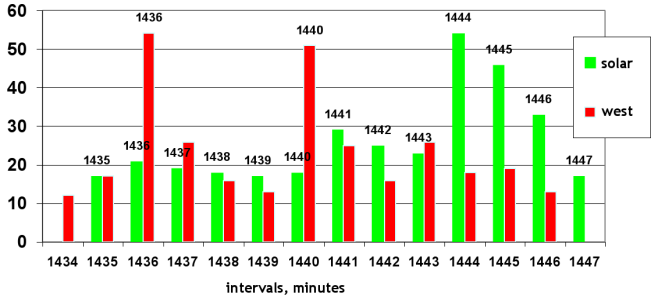

Fig. 15: The period of 1444 min emerges in the measurements with the "solar" collimator and is absent in the ceteris paribus measurements with the "western" collimator. In the experiments with a solar collimator, there is also no 1436- and 1440-min periods, which can be seen when a western collimator is used. The measurements of ^{239}Pu α-activity were made on July 24, 2005.

of appearance being 1444 min. Such a period does not correspond to any cosmophysical process we are aware of, and the fact of its emergence seems very strange.

It was important to ascertain that this period would emerge only in the experiments with the "solar" collimator. So we compared these data with the results obtained in parallel experiments with a "western" collimator. An example of the comparison is given in Fig. 15. The figure shows distributions of the number of histogram matches; compared are the results of simultaneous "solar" and "western" collimator-based measurements on July 24, 2005. It can be seen that in the "western collimator" measurements, there are distinct 1436-min and 1440-min periods and no 1444-min period. In the experiments with the "solar" collimator there is, *vice versa*, the 1444-min period and no the solar and sidereal daily periods. Thus, the phenomenon should be somehow related to the situation of α-particles running towards the Sun.

We tried to seek for this period on other days of the year, yet the search yielded no results — at first. We continued to register the period on the same July days in 2006 (incomplete data) and then in 2007 and 2008. Finally, a key step was

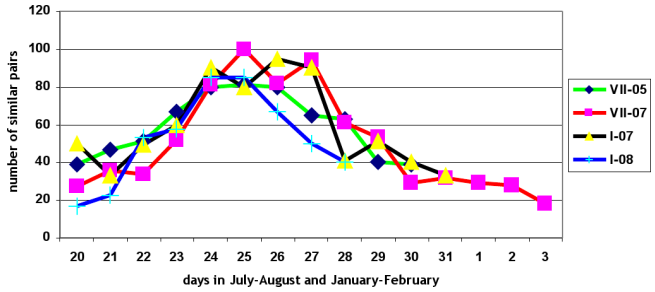

Fig. 16: In the experiments with a collimator directed at the Sun, the 1444-min period reappeared on the same dates of July and January, 2005–2008.

made: we found an analogous period in January, with the interval between the July and January peaks being exactly half a year, which meant they were right at the opposite points of a diameter of the circumsolar orbit.

As can be seen in Fig. 16, the July and January waves of the 1444-min period are quite synchronized to each other and also self-synchronized in different years (2005, 2007, 2008).

These results indicate that moving along the circumsolar orbit, the Earth will enter — at least twice a year — a spatial region with "anomalous characteristics", which change with a period of 1444 min. This spatial region represents an "anomalous band", crossing the center of the circumsolar orbit and stretched along the "July-January" line. It is remarkable that the characteristics of this anomaly are not shielded by the Sun, i.e., manifest themselves equally on both sides of the orbit. No analogy with the Doppler effect was revealed: the 1444-min period emerges "suddenly", does not change for several days (while the Earth is moving), and "suddenly" disappear. It should be stressed that the phenomenon is not observed in the parallel experiments without collimators or with collimators not aimed at the Sun. The "anomalous direction" crossed by the Earth on its way along the circumsolar orbit roughly corresponds to the direction from the constellation Cancer (July 21 — August 11) to the constellation Capricorn (January 19 — February 16). The nature of this period is enigmatic. The 1444-min period is 4 min longer than the daily period and, thus, cannot be explained by influence of any factors within the Solar system.

3.5 Effects of "half-day" and "half-year" palindromes [35, 36]

As follows from the data presented above, changes in the histogram shape depend on changes of the object's orientation in the space-time continuum. If we look in more detail at the path that the "laboratory" (the place where the measurements are performed) moves along over a day, we can see that during the "astronomical night" (i.e., from 18:00 to 6:00 by local time), the laboratory speeds up, since the Earth adds revolution about its own axis to the movement along the circumsolar orbit. From 6:00 to 18:00 (during the "astronomical day"), the laboratory, correspondingly, slows down, as the Earth's spinning is subtracted from its revolution around the Sun. In relation to the sphere of fixed stars, the objects studied will, correspondingly, move in the reverse order. Our investigations with V. A. Pancheluga showed that these circumstances would give rise to the "effect of half-day palindromes", which is a high probability of a series of "night histograms" to be similar with the inverted series of the correspondent "day histograms" [35]. As supposed by M. N. Kondrashova [39], an analogous palindrome effect should exist for the histogram series obtained from measurements at the "opposite sides" of the circumsolar orbit [2]. Subsequent studies confirmed this supposition. Indeed, in addition to the "half-day palindrome effect" we found the effect of "half-year palindromes". The half-year palindromes can be revealed when one takes into account the direction of night and day movement in relation to the sphere of fixed stars. At the opposite sides of the circumsolar orbit, the movement is counter-directional at day and night. That is, on vernal equinox the series of day histograms will be inverse to the day and similar to the night series on autumnal equinox. This proved valid for any opposite points of the circumsolar orbit. Therefore, the spatial characteristics that determine histogram shape must not change markedly over the year (the same being indicated by the existence of yearly periods). Holding true is also the converse: *histograms are a stable, regular characteristic of a direction (domain) of the space-time continuum* [36]. The aforesaid is illustrated by Fig. 17.

3.6 Collimators and the phenomenon of half-day and half-year palindromes

The effects of half-day and half-year palindromes are one of the most illustrative piece of evidence for the dependence of the phenomena under discussion on the movement of the objects studied in the space-time continuum. Of special interest is, thereby, palindromes that were revealed under the use of collimators. At the beginning of those experiments, we encountered an unexplainable irreproducibility of the results. In the experiments with a fixed west-oriented collimator, the half-day palindromes might either be seen quite clearly or be almost absent. Further studies with two collimators directed west and east correspondingly revealed a more complicated picture.

It turned out that this two-collimator setup yielded data series in which the orders of "day-night" and "night-day" were not equivalent. In the measurements with the eastern collimator, a clear palindrome was observed at comparing a sequence of day histograms with the *inverted* sequence of the *follow-up* night histograms. On the contrary, the western collimator gave series in which the *inverted* sequence of the *preceding* night histogram was a palindrome to the sequence of the *follow-up* day histograms.

The eastern collimator "faces the stream of time", the

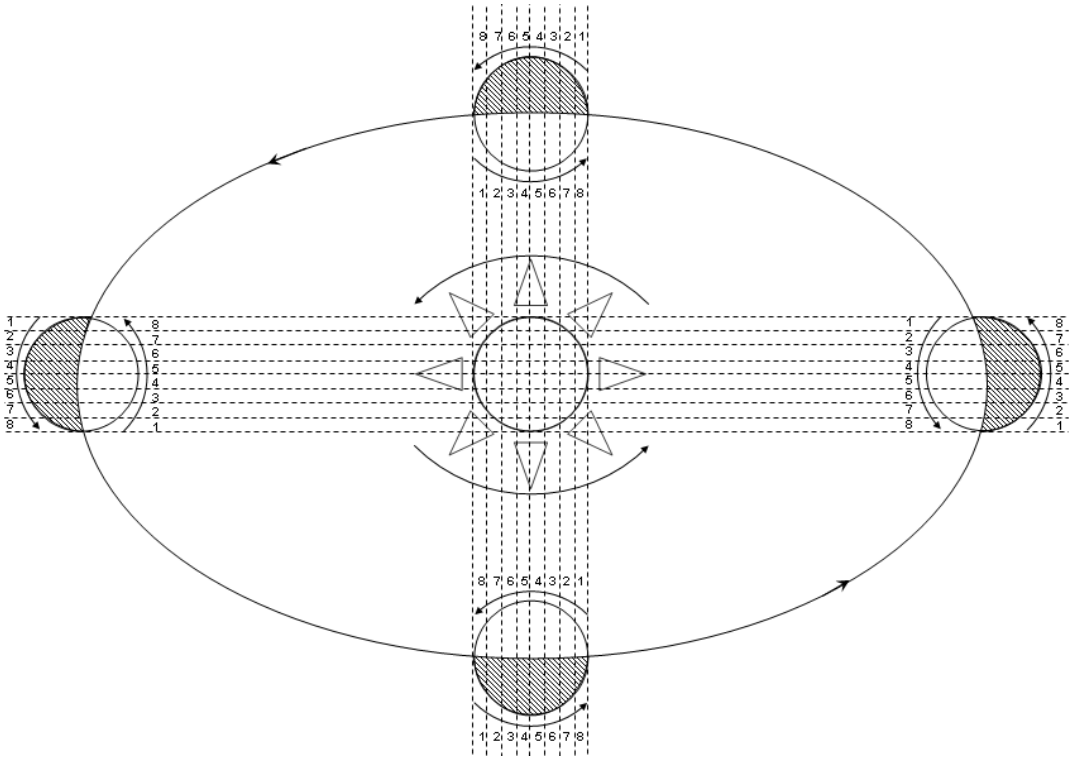

Fig. 17: A scheme illustrating the "palindrome effects". With the Sun in the center, the scheme shows four positions of the Earth on the circumsolar orbit. Both the Earth and the Sun are rotating counterclockwise; movement of the Earth along the circumsolar orbit is counterclockwise as well. As seen in the figure, the Earth's rotational movement in the nighttime is co-directional to its movement along the circumsolar orbit and to rotation of the Sun. In the daytime, the direction of these movements is opposite. Hence, in the case of "backward" movement (in the daytime), the object measured passes in the inverse order the same spatial regions that it has passed in the direct order in the nighttime. The effect of the "half-day palindrome" consists in the high probability of a "nighttime" histogram sequence to be similar to the inverted "daytime" sequence taken on the same day. Equally, the "daytime" sequence will be similar to the inverted "nighttime" one. For example, the 1–2–3–4–5 sequence of nighttime histograms is similar to the 5–4–3–2–1 sequence of the daytime ones. The effect of the "half-year" palindrome is determined by the fact that at the opposite points of the circumsolar orbit, the movements during the same halves of the day are opposite to each other. The effect consists in the high probability of a "nighttime" histogram sequence taken on one side of the circumsolar orbit to be similar to the "daytime" (not inverted) sequence taken on the opposite side. Correspondingly, nighttime (daytime) sequences on one side of the orbit will be similar to the inverted nighttime (daytime) sequences on the opposite side [36].

western one "looks after its flowing away"...

This strange effect still needs to be reproduced once and again, and many circumstances are to be clarified. We report it here due to its mysteriousness and, apparently, deep meaning.

3.7 The phenomenon of absolute-time synchronism in the measurements with collimators directed at the Pole Star and the Sun

The appearance of similar histograms in measurements at different geographical points at the same local time — the "local-time effect" — is quite regular. Sometimes, however, we obtained similar histograms at different geographical points not only at the same local but also at the same absolute time. The clearest observations of such an absolute-time synchronism were made during solar eclipses and new moons [37, 38]. At these moments, histograms of a certain shape appear simultaneously (with the accuracy of a few minutes) at different geographical points. We also observed absolute-time synchronism during the Antarctic expedition of 2001 (S. N. Shapovalov's measurements). Recently, we have compared the occurrences of absolute-time synchronism in the experiments without collimators and with collimators directed at the Sun and the Pole Star. Compared were data of simultaneous measurements made by S. N. Shapovalov in the Antarctic (Novolazarevskaya station) and data of Pushchino measurements. The results of comparison was unexpected: the extent of the "local-time effect" and absolute-time synchronism depended on the type of the measuring setup used. The local-time synchronism was clearly seen in the experiments without collimators or in the data obtained using the western Pushchino collimator; the absolute-time synchronism was almost absent. On the contrary, the measurements with Pushchino collima-

tors directed at the Pole Star or the Sun showed no local-time but good absolute-time synchronism (Fig. 18–20). This phenomenon also needs to be confirmed.

4 Discussion

Proving that the histograms obtained by measuring processes of diverse nature change regularly and in relation to the characteristics of the space-time continuum is the reason to pose questions on the nature of this relation. To answer these questions, additional studies are necessary.

The phenomena discovered are quite unusual and require alteration of conventional views. First of all, it applies to establishing the regular, non-casual character of the fine structure of amplitude fluctuation spectrum (histogram shape) for "quite stochastic", according to conventional criteria, processes. In fact, there is no contradiction here: the processes that are quite stochastic X-directionally can be absolutely non-stochastic Y-directionally. There is not — in principle — any determinate connection between the time course of a process and the spectrum of its amplitude fluctuations: the same histogram shape may correspond to many variations of time series.

Collecting the results of once-a-second measurements of ^{239}Pu α-activity for many years, which became possible after application of perfect enough detectors, and the use, upon necessity, of collimators — fixed or rotated by different ways — was extremely valuable for discovering and studying the phenomena discussed. The nature of many (most of) these phenomena is far from comprehension.

First of all, this is the *near-zone effect*. The statistically significant similarity of histograms constructed for different, independent segments of time series of the results of measurements is one of convincing indications of nonrandomness of the histogram shape. It seemed logical that the similarity of the nearest neighbor histograms should be the result of action of a common external "force" (cause). This cause changes in time, and while these changes are not significant, histograms remain similar. In other words, it would be natural to think that there is a "lifespan" of a certain "shape idea" [29]. However, the numerous attempts to determine even the order of magnitude of this "lifespan" were unsuccessful. Until now we failed to find such a small interval that the shape of histograms would not change (intervals were varied from minutes to tens of milliseconds).

The next mysterious phenomenon is the *splitting of the daily period* in change of the histogram shape to two peaks: the sidereal and solar days. Should only one of them be revealed, we would conclude that the shape of histograms is determined by the exposition (vector) of the object studied in relation to the Sun or the sphere of fixed stars. However, the fact that we observe two highly resolved extrema, with the periods of 1436 and 1440 min, seems quite unusual. The

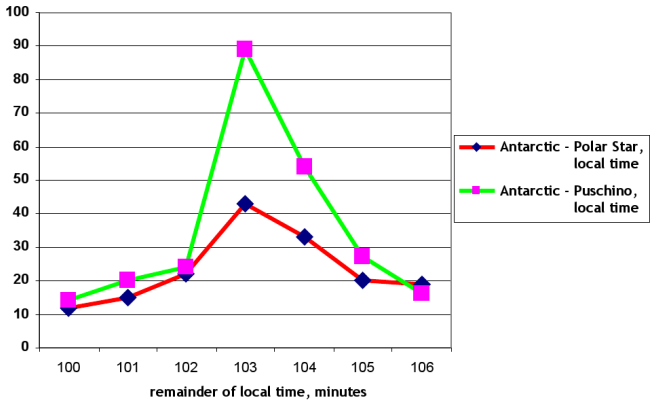

Fig. 18: Comparison of histograms corresponding to the parallel measurements of ^{239}Pu α-activity at Novolazarevskaya station (Antarctic) and in Pushchino shows that the effect of "local-time synchronism" is well-expressed when Pushchino measurements were performed with a west-directed collimator and it is weak when the collimator was directed at the Pole Star. The measurements were made by S. N. Shapovalov (in the Antarctic) and K.I. Zenchenko (in Pushchino) on March 19, 2003. The calculated difference in local time is 103 min. In the figure, the number of similar histogram pairs (Y-axis) is plotted vs. the corresponding interval between histograms (X-axis, min).

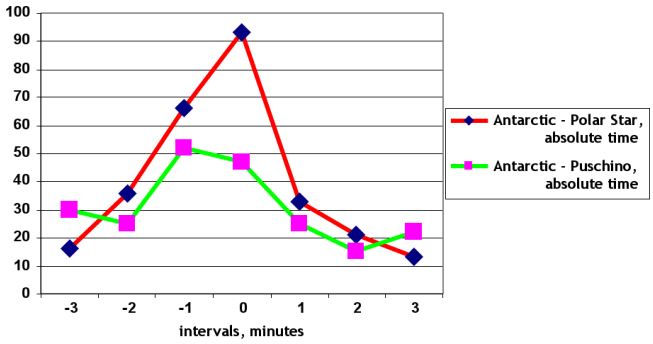

Fig. 19: In the Antarctic and Pushchino measurements, the absolute-time synchronism is more evident when measurements in Pushchino were made with a collimator aimed at the Pole Star, rather than a west-directed collimator. The measurements of ^{239}Pu α-activity were made on March 19, 2003.

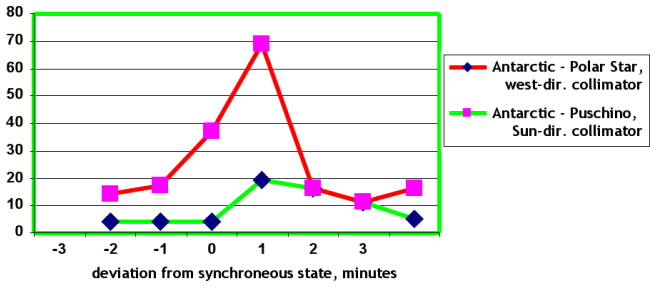

Fig. 20: In the Antarctic and Pushchino measurements, the absolute-time synchronism is more evident when measurements in Pushchino were made with a collimator aimed at the Sun, rather than a west-directed collimator. The measurements of ^{239}Pu α-activity were made on July 16, 2005.

time resolution of 1 min corresponds to the coelosphere resolution of 0.25° (15 angular minutes). And we can see this effect not only in the experiments with collimators but also in the measurements made with flat detectors, without collimators. This should be investigated in more details, yet even by now we have repeatedly registered the dependence of peak resolution on the orientation of the detectors. When flat detectors are positioned in the horizontal plane, one of the extrema (as a rule, the solar day) may not be seen. A good resolution was achieved when a flat detector was oriented in the plane of celestial equator. Also, we saw well-resolved sidereal and solar periods in the experiments with collimators, both fixed (directed east and west) and rotated counterclockwise. Phenomenology of these effects is far from being complete, and additional studies are necessary. The problem became more enigmatic after V. A. Pancheluga's experiments [40–43]. When measuring noise fluctuations in electronic circuits with frequency band up to 100 kHz, he determined the periods of reappearance of histograms of a certain shape. The splitting of extrema to the sidereal and solar days was found at a distance between the objects studied about several kilometers. The splitting corresponded to the period difference of several milliseconds, which in terms of angular units would mean an incredibly high resolution. Thus, the problem of period splitting grew even more paradoxical. This paradoxicality had long been noted by D. P. Kharakoz, who drew our attention to the fact that the collimator aperture allowed one to resolve coelosphere segments of approximately 5° (20 minutes), while we spoke about a second-order resolution ("Kharakoz's paradox" [44])! This paradox is, probably, seeming, as we use not single collimators but a setup in which 120 collimators are arranged on a small area. Perhaps, this is the cause of such a sharp "focusing".

All that was said about splitting of daily periods can be referred to the *splitting of yearly periods* as well. Now, what we see here are the same effects of discriminate orientation relative to the Sun and stars. And the same problems. Plus, what appears impossible at first glance — an extremely precise determination of yearly periods: with the accuracy of a minute, we determine the yearly period as equal to 525600 min! The accuracy is so high that we are able to register the diminishing of the "calendar" (solar) period by a minute (!) per year. One of possible explanations may be the movement of the solar system through the Galaxy. Any explanation, however, would still lack solid grounds.

It is necessary to emphasize that the largest puzzle, underlying all the observed phenomena, is the *nature of the histogram shape*. As follows from all our results in total, the shape is independent of the nature of the processes studied. The only cause common for all these processes can be the features of space-time. However, the nature of the relation between the shape of the histogram, i.e., the spectrum of amplitude fluctuations of the quantity measured, and the space-time fluctuations is absolutely unclear. What magnitude should these fluctuations be to affect the results of measurements? Why the sensitivity of different processes to these fluctuations ranges so much: the "scatter of the results of measurements" in piezoelectric quartz has an order of 10^{-6} of the measured magnitude, in chemical reactions the order is 10^{-2}, and in radioactive processes the scatter is proportional to $\sqrt{N}$?

Discovering the effect of daily and yearly palindromes substantially complements the mosaic of facts assembled earlier. The main conclusion, which can be drawn from the analysis of these effects, is that peculiarities of each region of the space-time continuum are rather stable; they keep unchanged for years, and the shape of histograms is, correspondingly, a stable characteristic of these peculiarities. It should be noted, however, that this stability is relative. The basic "local peculiarities" of the space-time continuum are overlaid with patterns of second, third etc. order: rotation of the Sun about its axis (near-27-day periods), revolution of the Moon round the Earth, changes in the relative positions of the Earth, Moon and Sun, effects of new moons, solar and lunar eclipses, solar flares etc. Perhaps, these "overlays" manifest themselves in the *effect of absolute-time synchronism*. For many years, we have mainly paid attention to the effect of local-time synchronism. The observations of a more distinct absolute synchronism in the experiments with collimators aimed at the Pole Star and the Sun bring hope that these questions will be answered.

The *effects of daily and yearly palindromes* essentially clarify the overall picture. Nevertheless, there remains a lot of work to do. The simplified picture of daily palindromes does not take into account the shift by 4 min per day in the course of the Earth's movement along the circumsolar orbit. Fig. 17 depicts movement of the Earth as a circle. It is still unclear how the picture would change with the "sidereal day" taken into consideration.

Finally, the recently found effect of *palindrome's time-vector asymmetry* in the measurements with the western and eastern collimators may happen to be — when reproduced and detailed — highly interesting.

Our works of the last years almost do not consider an important feature of "macroscopic fluctuations", which was found several decades ago: the shape, fine structure, of histograms and the average amplitude of fluctuations change independently of each other. The same "shape idea" may emerge in "narrow" and "wide" histograms. Comparing such histograms, we normalize them by abscissa. Regularities in the change of the average amplitude would also be very interesting to study, yet it is still in the future. A lot of work should be done to sort out all these problems.

Nevertheless, there is one conclusion we are certain of: *the apparently casual shape of histograms and its change over time are determined by the natural movement of the object studied through quite a complex space-time continuum.*

As for the nature of anisotropy and inhomogeneity of the space-time continuum, it is a matter of future research. Now

we may just adopt a notion of "interference pattern" resulting from the influence of numerous moving celestial bodies and radiant fluxes, whose effects are summed up in each point of the space.

Acknowledgements

The authors are thankful to M. N. Kondrashova and V. P. Tikhonov for valuable ideas, discussions, moral and financial support; V. A. Pancheluga for fruitful collaboration and joint research; V. A. Shlekhtarev for making devices used in the experiments with collimators.

We are grateful to D. D. Rabounski for valuable discussions and comments on the text of our manuscripts.

We express sincere gratitude to our colleagues from the Department of Biophysics of Physical Faculty of Moscow State University (Head of the Department, Prof. V. A. Tverdislov) and from the Laboratory of Physical Biochemistry at the Institute of Theoretical and Experimental Biophysics RAS (Head of the Laboratory, Prof. D. P. Kharakoz).

We thank Director of the Institute of Theoretical and Experimental Biophysics RAS, Corresponding Member of Russian Academy of Sciences G. R. Ivanitsky for his everlasting patience and goodwill.

We also highly appreciate T. A. Zenchenko and K. I. Zenchenko's help in conducting measurements and maintaining a computer archive of experimental results.

Submitted on Febrary 02, 2009 / Accepted on February 23, 2009

References

1. Shnoll S.E. On the spontaneous and synchronous transitions of actomyosin molecules in a solution from one state to another. *Problems of Medicinal Chemistry*, 1958, v. 4(6), 443–454 (*in Russian*).
2. Shnoll S.E., Namiot V.A., Zhvirblis V.E., Morozov V.N., Temnov A.V., Morozova T.Ya. A possible generality of macroscopic fluctuations of rates of biochemical and chemical reactions, cell electrophoretic mobility and fluctuations in measurements of radioactivity, absorbance and flicker noises. *Biophysics*, 1983, v. 28(1), 153–157 (*in Russian*).
3. Shnoll S.E. Macroscopic fluctuations with discrete distribution of amplitudes in the processes of diverse nature. In: *Results of Science and Engineering. Molecular Biology*, Ed. V. P. Skulachev, VINITI-Press, Moscow, 1985, v. 5, 130–200 (*in Russian*).
4. Udaltsova N.V., Kolombet V.A., Shnoll S.E. A possible cosmophysical conditionality of macroscopic fluctuations in the processes of diverse nature. Central Scientific Library Press, Pushchino, 1987 (*in Russian*).
5. Udaltzova N.V., Kolombet V.A. and Shnol' S.E. The possible gravitational nature of factor influencing discrete macroscopic fluctuations. In: *Proc. First Intern. Congress on Geo-cosmic Relations*, Wageningen, Netherlands, 1989, 174–180.
6. Shnol' S.E., Udaltzova N.V. and Bodrova N.B. Macroscopic fluctuations with discrete structure distributions as a result of universal causes including cosmophysical factors. In: *Proc. First Intern. Congress on Geo-cosmic Relations*, Wageningen, Netherlands, 1989, 181–188.
7. Shnoll S.E. Correlation of the shape of amplitude spectra of macroscopic fluctuations with the position of the Moon relative to the horizon. *Biophysics*, 1989, v. 34(5), 911–912 (*in Russian*).
8. Shnoll S.E., Kolombet V.A., Udaltzova N.V., Bodrova N.B., Namiot V.E. Regularities in the discrete distributions of the results of measurements (cosmophysical aspects). *Biophysics*, 1992, v. 37(3), 467–488 (*in Russian*).
9. Shnoll S.E. The shape of spectra of states realized in the course of macroscopic fluctuations depends on the rotation of the Earth about its axis. *Biophysics*, 1995, v. 40(4), 865–875 (*in Russian*).
10. Shnoll S.E., Agulova L.P., Zaikin A.N., Zenchenko T.A., Pozharskii E.V., and Konradov A.A. On the similarity of histograms fine structure for synchronized time series of different nature processes at different locations. *Annales Geophysicae*, Supplement 1 to Volume 16 Part 1 Society Symposia, Solid Earth Geophysics & Geodesy, 1998, C312.
11. Shnoll S.E., Kolombet V.A., Pozharsky E.V., Zenchenko T.A., Zvereva I.M., Konradov A.A. On the realization of discrete states in the course of fluctuations in macroscopic processes. *Advances in Physical Sciences*, 1998, v. 168(10), 1129–1140 (*in Russian*).
12. Shnoll S.E., Kolombet V.A., Pozharsky E.V., Zenchenko T.A., Zvereva I.M., Konradov A.A. On the cosmophysical conditionality of "macroscopic fluctuations". *Biophysics*, 1998, v. 43(5), 909–915 (*in Russian*).
13. Shnoll S.E., Pozharski E.V., Zenchenko T.A., Kolombet V.A., Zvereva I.M., Konradov A.A. Fine structure of distributions in measurements of different processes as affected by geophysical and cosmophysical factors. *Phys. Chem. Earth A*, 1999, v. 24, no. 8, 711–714.
14. Shnoll S.E., Zenchenko T.A., Zenchenko K.I., Pozharsky E.V., Kolombet V.A., Konradov A.A. Regular alteration of the fine structure of statistical distributions as a results of cosmophysical causes. *Advances in Physical Sciences*, 2000, v. 170(2), 214–218 (*in Russian*).
15. Shnoll S.E. Macroscopic fluctuations as a result of arithmetical and cosmophysical causes. The factors that determine the fine structure of histograms are, probably, beyond the bounds of the solar system. *Biophysics*, 2001, v. 46(5), 775–782 (*in Russian*.
16. Shnoll S.E., Zenchenko T.A., Zenchenko K.I., Fedorov M.V., Konradov A.A. The non-random character of fine structure of various measurement result distributions as a possible consequence of cosmophysical and arithmetical causes. In: *Gravitation & Cosmology*, 2002, v. 8, Supplement, 231–232.
17. Shnoll S.E. Paradoxes and problems in the interpretation of the phenomenon of macroscopic fluctuations. *Russian Chemical Journal*, 2002, v. 46(3), 3–8 (*in Russian*).
18. Fedorov M.V., Belousov L.V., Voeikov V.L., Zenchenko T.A., Zenchenko K.I., Pozharskii E.V., Konradov A.A., Shnoll S.E.

Synchronous changes in dark current fluctuations in two separate photomultipliers in relation to Earth rotation. *Astrophysics & Space Science*, 2003, no. 1, 105–112.

19. Shnoll S.E., Rubinstein I.A., Zenchenko K.I., Zenchenko T.A., Udaltsova N.V., Konradov A.A., Shapovalov S.N., Makarevich A.V., Gorshkov E.S., Troshichev O.A. Dependence of macroscopic fluctuations on geographical coordinates. *Biophysics*, 2003, v. 48(6), 1123–1131 (*in Russian*).
20. Shnoll S.E., Zenchenko K.I., Berulis I.I., Udaltsova N.V., Zhirkov S.S., Rubinstein I.A. Dependence of macroscopic fluctuations on cosmophysical factors. Spatial anisotropy. *Biophysics*, 2004, v. 49(1), 132–139 (in Russian).
21. Shnoll S.E., Zenchenko K.I., and Udaltsova N.V. Cosmophysical effects in the structure of daily and yearly periods of changes in the shape of histograms constructed from the measurements of ^{239}Pu alpha-activity. *Biophysics*, 2004, v. 49, Suppl. 1, 155–164.
22. Shnoll S.E., Zenchenko K.I., Berulis I.I., Udaltsova N.V. and Rubinstein I.A. Fine structure of histograms of alpha-activity measurements depends on direction of alpha particles flow and the Earth rotation: experiments with collimators. arXiv: physics/0412007.
23. Shnoll S.E., Zenchenko K.I., Shapovalov S.N., Gorshkov E.S., Makarevich A.V. and Troshichev O.A. The specific form of histograms presenting the distribution of data of alpha-decay measurements appears simultaneously in the moment of New Moon in different points from Arctic to Antarctic. arXiv: physics/0412152.
24. Shnoll S.E., Zenchenko K.I., and Udaltsova N.V. Cosmophysical effects in the structure of daily and yearly periods of changes in the shape of histograms constructed from the measurements of ^{239}Pu alpha-activity. arXiv: physics/0504092.
25. Shnoll S.E., Rubinstein I.A., Zenchenko K.I., Shlekhtarev V.A., Kaminsky A.V., Konradov A.A., Udaltsova N.V. Experiments with rotating collimators cutting out pencil of alpha-particles at radioactive decay of Pu-239 evidence sharp anisotropy of space. arXiv: physics/0501004.
26. Shnoll S.E., Rubinstein I.A., Zenchenko K.I., Shlekhtarev V.A., Kaminsky A.V., Konradov A.A., Udaltsova N.V. Experiments with rotating collimators cutting out pencil of alpha-particles at radioactive decay of Pu-239 evidence sharp anisotropy of space. *Progress in Physics*, 2005, v. 1, 81–84.
27. Shnoll S.E. Changes in fine structure of stochastic distributions as a consequence of space-time fluctuations. *Progress in Physics*, 2006, v. 2, 39–45.
28. Shnoll S.E. Fine structure of statistical distributions as a mirror of spatial and gravitational anisotropy of our world. *Russian Chemical Journal*, 2007, v. 51(1), 150–157.
29. Shnoll S.E. Cosmophysical nature of the "idea of shape" of histograms constructed from the results of measurements of processes of diverse nature. In: *Metaphysics. Century XXI*, Issue 2, Ed. Yu. S. Vladimirov, BINOM-S Press, 2007, 284–319 (*in Russian*).
30. Shnoll S.E. Reply to the letter by Gary C. Vezzoli. *Progress in Physics*, 2008, v. 2, 162–163.
31. Strelkov V.V. A new similarity measure for histogram comparison and its application in time series analysis. *Pattern Recognition Letters*, 2008, v. 29, no. 13, 1768–1774.
32. Strelkov V.V. The "near zone" effect in dynamic chaos. *Biophysics*, 2001, v. 46, 807–810 (*in Russian*).
33. Khmaladze E.V. *Probability Theory and Its Applications*, 1983, v. 28(3), 504 (*in Russian*).
34. Udaltsova N.V., Urinov I.K. Estimation of probability of the observed extrema in histograms constructed from small samples. Deposited at VINITI 08.02.89, no. 850-V89 (*in Russian*).
35. Shnoll S.E., Panchelyuga V.A., and Shnoll A.E. The palindrome effect. *Progress in Physics*, 2008, v. 2, 151–153.
36. Shnoll S.E. The "scattering of the results of measurements" of processes of diverse nature is determined by the Earth's motion in the inhomogeneous space-time continuum. The effect of "half-year palindromes". *Progress in Physics*, 2009, v. 1, 3–7.
37. Shnoll S.E., Zenchenko K.I., Shapovalov S.N., Gorshkov E.S., Makarevich A.V. and Troshichev O.A. The specific form of histograms presenting the distribution of data of alpha-decay measurements appears simultaneously in the moment of New Moon in different points from Arctic to Antarctic. arXiv: physics/0412152.
38. Shnoll S.E., Panchelyuga V.A. On the characteristic form of histograms appearing at the culmination of Solar eclipse. arXiv: physics/0603029.
39. Kondrashova M.N. Personal communication.
40. Pancheluga V.A., Kolombet V.A., Pancheluga M.S., Shnoll S.E. Studying the local-time effect on small spatial-temporal scales. *Hypercomplex Numbers in Geometry and Physics*, 2006, no. 1(5), v. 3, 116–121 (*in Russian*).
41. Panchelyuga V.A., Kolombet V.A., Pancheluga M.S., and Shnoll S.E. Local-time effect on small space-time scale. In: *Space-Time Structure*, collected papers, Moscow, Tetru, 2006, 344–350.
42. Panchelyuga V.A., Kolombet V.A., Pancheluga M.S., and Shnoll S.E. Experimental investigation of the existence of a local-time effect on the laboratory scale and the heterogeneity of spice-time. *Progress in Physics*, 2007, v. 1, 64–69.
43. Panchelyuga V.A. and Shnoll S.E. On the dependence of a local-time effect on spatial direction. *Progress in Physics*, 2007, v. 3, 51–54.
44. Kharakoz D.P. Personal communication.

4X1-Matrix Functions and Dirac's Equation

Gunn Alex Quznetsov

Chelyabinsk State University, Chelyabinsk, Ural, Russia
E-mail: quznets@yahoo.com, gunn@mail.ru

All 4X1-matrix square integrable functions with restricted domain obey slightly generalized Dirac's equations. These equations give formulas similar to some gluon and gravity ones.

1 Significations

Denote:

$$1_2 := \begin{bmatrix} 1 & 0 \\ 0 & 1 \end{bmatrix}, 0_2 := \begin{bmatrix} 0 & 0 \\ 0 & 0 \end{bmatrix},$$

$$\beta^{[0]} := -\begin{bmatrix} 1_2 & 0_2 \\ 0_2 & 1_2 \end{bmatrix} = -1_4,$$

the Pauli matrices:

$$\sigma_1 = \begin{pmatrix} 0 & 1 \\ 1 & 0 \end{pmatrix}, \sigma_2 = \begin{pmatrix} 0 & -\mathrm{i} \\ \mathrm{i} & 0 \end{pmatrix}, \sigma_3 = \begin{pmatrix} 1 & 0 \\ 0 & -1 \end{pmatrix}.$$

I call a set $\widetilde{C}$ of complex $n \times n$ matrices *a Clifford set of rank* n [1] if the following conditions are fulfilled:

— if $\alpha_k \in \widetilde{C}$ and $\alpha_r \in \widetilde{C}$ then $\alpha_k\alpha_r + \alpha_r\alpha_k = 2\delta_{k,r}$;

— if $\alpha_k\alpha_r + \alpha_r\alpha_k = 2\delta_{k,r}$ for all elements α_r of set $\widetilde{C}$ then $\alpha_k \in \widetilde{C}$.

If $n = 4$ then the Clifford set either contains 3 (*Clifford triplet*) or 5 matrices (*Clifford pentad*).

Here exist only six Clifford pentads [1]: one which I call

• *light pentad* β:

$$\beta^{[1]} := \begin{bmatrix} \sigma_1 & 0_2 \\ 0_2 & -\sigma_1 \end{bmatrix}, \quad \beta^{[2]} := \begin{bmatrix} \sigma_2 & 0_2 \\ 0_2 & -\sigma_2 \end{bmatrix}, \quad \beta^{[3]} := \begin{bmatrix} \sigma_3 & 0_2 \\ 0_2 & -\sigma_3 \end{bmatrix}, \tag{1}$$

$$\gamma^{[0]} := \begin{bmatrix} 0_2 & 1_2 \\ 1_2 & 0_2 \end{bmatrix}, \tag{2}$$

$$\beta^{[4]} := \mathrm{i} \cdot \begin{bmatrix} 0_2 & 1_2 \\ -1_2 & 0_2 \end{bmatrix}; \tag{3}$$

three *coloured* pentads:

• *the red pentad* ζ:

$$\zeta^{[1]} = \begin{bmatrix} -\sigma_1 & 0_2 \\ 0_2 & \sigma_1 \end{bmatrix}, \quad \zeta^{[2]} = \begin{bmatrix} \sigma_2 & 0_2 \\ 0_2 & \sigma_2 \end{bmatrix}, \tag{4}$$

$$\zeta^{[3]} = \begin{bmatrix} -\sigma_3 & 0_2 \\ 0_2 & -\sigma_3 \end{bmatrix},$$

$$\gamma_\zeta^{[0]} = \begin{bmatrix} 0_2 & -\sigma_1 \\ -\sigma_1 & 0_2 \end{bmatrix}, \quad \zeta^{[4]} = \mathrm{i}\begin{bmatrix} 0_2 & \sigma_1 \\ -\sigma_1 & 0_2 \end{bmatrix}; \tag{5}$$

• *the green pentad* η:

$$\eta^{[1]} = \begin{bmatrix} -\sigma_1 & 0_2 \\ 0_2 & -\sigma_1 \end{bmatrix}, \quad \eta^{[2]} = \begin{bmatrix} -\sigma_2 & 0_2 \\ 0_2 & \sigma_2 \end{bmatrix}, \tag{6}$$

$$\eta^{[3]} = \begin{bmatrix} \sigma_3 & 0_2 \\ 0_2 & \sigma_3 \end{bmatrix},$$

$$\gamma_\eta^{[0]} = \begin{bmatrix} 0_2 & -\sigma_2 \\ -\sigma_2 & 0_2 \end{bmatrix}, \quad \eta^{[4]} = \mathrm{i}\begin{bmatrix} 0_2 & \sigma_2 \\ -\sigma_2 & 0_2 \end{bmatrix}; \tag{7}$$

• *the blue pentad* θ:

$$\theta^{[1]} = \begin{bmatrix} \sigma_1 & 0_2 \\ 0_2 & \sigma_1 \end{bmatrix}, \quad \theta^{[2]} = \begin{bmatrix} -\sigma_2 & 0_2 \\ 0_2 & -\sigma_2 \end{bmatrix}, \tag{8}$$

$$\theta^{[3]} = \begin{bmatrix} -\sigma_3 & 0_2 \\ 0_2 & \sigma_3 \end{bmatrix},$$

$$\gamma_\theta^{[0]} = \begin{bmatrix} 0_2 & -\sigma_3 \\ -\sigma_3 & 0_2 \end{bmatrix}, \quad \theta^{[4]} = \mathrm{i}\begin{bmatrix} 0_2 & \sigma_3 \\ -\sigma_3 & 0_2 \end{bmatrix}; \tag{9}$$

• two *gustatory* pentads: *the sweet pentad* $\underline{\Delta}$:

$$\underline{\Delta}^{[1]} = \begin{bmatrix} 0_2 & -\sigma_1 \\ -\sigma_1 & 0_2 \end{bmatrix}, \quad \underline{\Delta}^{[2]} = \begin{bmatrix} 0_2 & -\sigma_2 \\ -\sigma_2 & 0_2 \end{bmatrix},$$

$$\underline{\Delta}^{[3]} = \begin{bmatrix} 0_2 & -\sigma_3 \\ -\sigma_3 & 0_2 \end{bmatrix},$$

$$\underline{\Delta}^{[0]} = \begin{bmatrix} -1_2 & 0_2 \\ 0_2 & 1_2 \end{bmatrix}, \quad \underline{\Delta}^{[4]} = \mathrm{i}\begin{bmatrix} 0_2 & 1_2 \\ -1_2 & 0_2 \end{bmatrix}.$$

• *the bitter pentad* $\underline{\Gamma}$:

$$\underline{\Gamma}^{[1]} = \mathrm{i}\begin{bmatrix} 0_2 & -\sigma_1 \\ \sigma_1 & 0_2 \end{bmatrix}, \quad \underline{\Gamma}^{[2]} = \mathrm{i}\begin{bmatrix} 0_2 & -\sigma_2 \\ \sigma_2 & 0_2 \end{bmatrix},$$

$$\underline{\Gamma}^{[3]} = \mathrm{i}\begin{bmatrix} 0_2 & -\sigma_3 \\ \sigma_3 & 0_2 \end{bmatrix},$$

$$\underline{\Gamma}^{[0]} = \begin{bmatrix} -1_2 & 0_2 \\ 0_2 & 1_2 \end{bmatrix}, \quad \underline{\Gamma}^{[4]} = \begin{bmatrix} 0_2 & 1_2 \\ 1_2 & 0_2 \end{bmatrix}.$$

If A is a 2×2 matrix then

$$A1_4 := \begin{bmatrix} A & 0_2 \\ 0_2 & A \end{bmatrix} \text{ and } 1_4A := \begin{bmatrix} A & 0_2 \\ 0_2 & A \end{bmatrix}.$$

And if B is a 4×4 matrix then

$$A + B := A1_4 + B,\ AB := A1_4 B$$

etc.

$$\underline{x} := \langle x_0, \mathbf{x} \rangle := \langle x_0, x_1, x_2, x_3 \rangle ,$$
$$x_0 := \mathrm{c}t,$$

with $\mathrm{c} = 299792458$.

2 Planck's functions

Let $\mathrm{h} = 6.6260755 \times 10^{-34}$ and $\underline{\Omega}$ ($\underline{\Omega} \subset R^{1+3}$) be a domain such that if $\underline{x} \in \underline{\Omega}$ then $|x_r| < \frac{\mathrm{c}\pi}{\mathrm{h}}$ for $r \in \{0, 1, 2, 3\}$.

Let $\Re_{\underline{\Omega}}$ be a set of functions such that for each element $\phi(\underline{x})$ of this set: if $\underline{x} \notin \underline{\Omega}$ then $\phi(\underline{x}) = 0$.

Hence:

$$\int_{(\underline{\Omega})} d\underline{x} \cdot \phi(\underline{x}) =$$
$$= \int_{-\frac{\mathrm{c}\pi}{\mathrm{h}}}^{\frac{\mathrm{c}\pi}{\mathrm{h}}} dx_0 \int_{-\frac{\mathrm{c}\pi}{\mathrm{h}}}^{\frac{\mathrm{c}\pi}{\mathrm{h}}} dx_1 \int_{-\frac{\mathrm{c}\pi}{\mathrm{h}}}^{\frac{\mathrm{c}\pi}{\mathrm{h}}} dx_2 \int_{-\frac{\mathrm{c}\pi}{\mathrm{h}}}^{\frac{\mathrm{c}\pi}{\mathrm{h}}} dx_3 \cdot \phi(\underline{x}) ,$$

and let for each element $\phi(\underline{x})$ of $\Re_{\underline{\Omega}}$ exist a number J_ϕ such that

$$J_\phi = \int_{(\underline{\Omega})} d\underline{x} \cdot \phi^*(\underline{x}) \phi(\underline{x}) .$$

Therefore, $\Re_{\underline{\Omega}}$ is unitary space with the following scalar product:

$$\widetilde{u} * \widetilde{v} := \int_{(\underline{\Omega})} d\underline{x} \cdot \widetilde{u}^*(\underline{x}) \widetilde{v}(\underline{x}) . \tag{10}$$

This space has an orthonormalised basis with the following elements:

$$\varsigma_{w,\mathbf{p}}(t, \mathbf{x}) :=$$
$$:= \left\{ \begin{array}{c} \left(\frac{\mathrm{h}}{2\pi \mathrm{c}}\right)^2 \exp(\mathrm{i}\mathrm{h}wt) \exp\left(-\mathrm{i}\frac{\mathrm{h}}{\mathrm{c}}\mathbf{px}\right) \text{ if} \\ -\frac{\pi \mathrm{c}}{\mathrm{h}} \leqslant x_k \leqslant \frac{\pi \mathrm{c}}{\mathrm{h}}; \\ 0, \text{ otherwise.} \end{array} \right| \tag{11}$$

with $k \in \{0, 1, 2, 3\}$ and $x_0 := \mathrm{c}t$, and with natural w, p_1, p_2, p_3 (here: $\mathbf{p}\langle p_1, p_2, p_3 \rangle$ and $\mathbf{px} = p_1 x_1 + p_2 x_2 + p_3 x_3$).

I call elements of the space with this basis *Planck's functions*.

Let $j \in \{1, 2, 3, 4\}$, $k \in \{1, 2, 3, 4\}$ and denote:

$$\sum_{\mathbf{k}} := \sum_{k_1=-\infty}^{\infty} \sum_{k_2=-\infty}^{\infty} \sum_{k_3=-\infty}^{\infty} .$$

Let a Fourier series for $\varphi_j(t, \mathbf{x})$ have the following form:

$$\varphi_j(t, \mathbf{x}) = \sum_{w=-\infty}^{\infty} \sum_{\mathbf{p}} c_{j,w,\mathbf{p}} \varsigma_{w,\mathbf{p}}(t, \mathbf{x}) . \tag{12}$$

If denote: $\varphi_{j,w,\mathbf{p}}(t, \mathbf{x}) := c_{j,w,\mathbf{p}} \varsigma_{w,\mathbf{p}}(t, \mathbf{x})$ then a Fourier series for $\varphi_j(t, \mathbf{x})$ has the following form:

$$\varphi_j(t, \mathbf{x}) = \sum_{w=-\infty}^{\infty} \sum_{\mathbf{p}} \varphi_{j,w,\mathbf{p}}(t, \mathbf{x}) . \tag{13}$$

Let $\langle t, \mathbf{x} \rangle$ be any space-time point.

Let us denote:

$$A_k := \varphi_{k,w,\mathbf{p}}|_{\langle t,\mathbf{x} \rangle} \tag{14}$$

the value of function $\varphi_{k,w,\mathbf{p}}$ in this point, and by

$$C_j := \left(\frac{1}{\mathrm{c}} \partial_t \varphi_{j,w,\mathbf{p}} - \sum_{s=1}^{4} \sum_{\alpha=1}^{3} \beta_{j,s}^{[\alpha]} \partial_\alpha \varphi_{s,w,\mathbf{p}} \right) \Bigg|_{\langle t,\mathbf{x} \rangle} \tag{15}$$

the value of function

$$\left(\frac{1}{\mathrm{c}} \partial_t \varphi_{j,w,\mathbf{p}} - \sum_{s=1}^{4} \sum_{\alpha=1}^{3} \beta_{j,s}^{[\alpha]} \partial_\alpha \varphi_{s,w,\mathbf{p}} \right) .$$

Here A_k and C_j are complex numbers. Hence, the following set of equations:

$$\left\{ \begin{array}{c} \sum_{k=1}^{4} z_{j,k,w,\mathbf{p}} A_k = C_j , \\ z^*_{j,k,w,\mathbf{p}} = -z_{k,j,w,\mathbf{p}} \end{array} \right| \tag{16}$$

is a system of 14 algebraic equations with complex unknowns $z_{j,k,w,\mathbf{p}}$.

Because

$$\partial_t \varphi_{j,w,\mathbf{p}} = \partial_t c_{j,w,\mathbf{p}} \varsigma_{w,\mathbf{p}} = \mathrm{i}\mathrm{h}w c_{j,w,\mathbf{p}} \varsigma_{w,\mathbf{p}} = \mathrm{i}\mathrm{h}w \varphi_{j,w,\mathbf{p}}$$

and for $k \neq 0$:

$$\partial_k \varphi_{j,w,\mathbf{p}} = -\mathrm{i}\frac{\mathrm{h}}{\mathrm{c}} p_k \varphi_{j,w,\mathbf{p}} .$$

then

$$C_j = \mathrm{i}\frac{\mathrm{h}}{\mathrm{c}} \left(w \varphi_{j,w,\mathbf{p}} + \sum_{s=1}^{4} \sum_{\alpha=1}^{3} \beta_{j,s}^{[\alpha]} p_\alpha \varphi_{s,w,\mathbf{p}} \right) \Bigg|_{\langle t,\mathbf{x} \rangle} .$$

Therefore, this system (16) has got the following form:

$$z_{1,1,w,\mathbf{p}} A_1 + z_{1,2,w,\mathbf{p}} A_2 + z_{1,3,w,\mathbf{p}} A_3 + z_{1,4,w,\mathbf{p}} A_4 =$$
$$= \mathrm{i}\frac{\mathrm{h}}{\mathrm{c}} (w + p_3) A_1 + \mathrm{i}\frac{\mathrm{h}}{\mathrm{c}} (p_1 - \mathrm{i}p_2) A_2 ,$$
$$z_{2,1,w,\mathbf{p}} A_1 + z_{2,2,w,\mathbf{p}} A_2 + z_{2,3,w,\mathbf{p}} A_3 + z_{2,4,w,\mathbf{p}} A_4 =$$
$$= \mathrm{i}\frac{\mathrm{h}}{\mathrm{c}} (w - p_3) A_2 + \mathrm{i}\frac{\mathrm{h}}{\mathrm{c}} (p_1 + \mathrm{i}p_2) A_1 ,$$
$$z_{3,1,w,\mathbf{p}} A_1 + z_{3,2,w,\mathbf{p}} A_2 + z_{3,3,w,\mathbf{p}} A_3 + z_{3,4,w,\mathbf{p}} A_4 =$$
$$= \mathrm{i}\frac{\mathrm{h}}{\mathrm{c}} (w - p_3) A_3 - \mathrm{i}\frac{\mathrm{h}}{\mathrm{c}} (p_1 - \mathrm{i}p_2) A_4 ,$$
$$z_{4,1,w,\mathbf{p}} A_1 + z_{4,2,w,\mathbf{p}} A_2 + z_{4,3,w,\mathbf{p}} A_3 + z_{4,4} A_{4,w,\mathbf{p}} =$$
$$= \mathrm{i}\frac{\mathrm{h}}{\mathrm{c}} (w + p_3) A_4 - \mathrm{i}\frac{\mathrm{h}}{\mathrm{c}} (p_1 + \mathrm{i}p_2) A_3 ,$$

$$z^*_{1,1,w,\mathbf{p}} = -z_{1,1,w,\mathbf{p}}\,,$$
$$z^*_{1,2,w,\mathbf{p}} = -z_{2,1,w,\mathbf{p}}\,,$$
$$z^*_{1,3,w,\mathbf{p}} = -z_{3,1,w,\mathbf{p}}\,,$$
$$z^*_{1,4,w,\mathbf{p}} = -z_{4,1,w,\mathbf{p}}\,,$$
$$z^*_{2,2,w,\mathbf{p}} = -z_{2,2,w,\mathbf{p}}\,,$$
$$z^*_{2,3,w,\mathbf{p}} = -z_{3,2,w,\mathbf{p}}\,,$$
$$z^*_{2,4,w,\mathbf{p}} = -z_{4,2,w,\mathbf{p}}\,,$$
$$z^*_{3,3,w,\mathbf{p}} = -z_{3,3,w,\mathbf{p}}\,,$$
$$z^*_{3,4,w,\mathbf{p}} = -z_{4,3,w,\mathbf{p}}\,,$$
$$z^*_{4,4,w,\mathbf{p}} = -z_{4,4,w,\mathbf{p}}\,.$$

This system can be transformed into a system of 8 linear real equations with 16 real unknowns $x_{s,k} := \mathrm{Re}\,(z_{s,k,w,\mathbf{p}})$ for $s < k$ and $y_{s,k} := \mathrm{Im}\,(z_{s,k,w,\mathbf{p}})$ for $s \leqslant k$:

$$\begin{aligned}
&-y_{1,1}b_1 + x_{1,2}a_2 - y_{1,2}b_2 + x_{1,3}a_3 -\\
&-y_{1,3}b_3 + x_{1,4}a_4 - y_{1,4}b_4 \;=\\
&= -\frac{\mathrm{h}}{\mathrm{c}}wb_1 - \frac{\mathrm{h}}{\mathrm{c}}p_3b_1 - \frac{\mathrm{h}}{\mathrm{c}}p_1b_2 + \frac{\mathrm{h}}{\mathrm{c}}p_2a_2\,,\\
&y_{1,1}a_1 + x_{1,2}b_2 + y_{1,2}a_2 + x_{1,3}b_3 +\\
&+y_{1,3}a_3 + x_{1,4}b_4 + y_{1,4}a_4 \;=\\
&= \frac{\mathrm{h}}{\mathrm{c}}wa_1 + hp_3a_1 + \frac{\mathrm{h}}{\mathrm{c}}p_1a_2 + hp_2b_2\,,\\
&-x_{1,2}a_1 - y_{1,2}b_1 - y_{2,2}b_2 + x_{2,3}a_3 -\\
&-y_{2,3}b_3 + x_{2,4}a_4 - y_{2,4}b_4 \;=\\
&= -\frac{\mathrm{h}}{\mathrm{c}}wb_2 - \frac{\mathrm{h}}{\mathrm{c}}p_1b_1 - \frac{\mathrm{h}}{\mathrm{c}}p_2a_1 + \frac{\mathrm{h}}{\mathrm{c}}p_3b_2\,,\\
&-x_{1,2}b_1 + y_{1,2}a_1 + y_{2,2}a_2 + x_{2,3}b_3 +\\
&+y_{2,3}a_3 + x_{2,4}b_4 + y_{2,4}a_4 \;=\\
&= \frac{\mathrm{h}}{\mathrm{c}}wa_2 + \frac{\mathrm{h}}{\mathrm{c}}p_1a_1 - \frac{\mathrm{h}}{\mathrm{c}}p_2b_1 - \frac{\mathrm{h}}{\mathrm{c}}p_3a_2\,,\\
&-x_{1,3}a_1 - y_{1,3}b_1 - x_{2,3}a_2 - y_{2,3}b_2 -\\
&-y_{3,3}b_3 + x_{3,4}a_4 - y_{3,4}b_4 \;=\\
&= -\frac{\mathrm{h}}{\mathrm{c}}wb_3 + \frac{\mathrm{h}}{\mathrm{c}}p_3b_3 + \frac{\mathrm{h}}{\mathrm{c}}p_1b_4 - \frac{\mathrm{h}}{\mathrm{c}}p_2a_4\,,\\
&-x_{1,3}b_1 + y_{1,3}a_1 - x_{2,3}b_2 + y_{2,3}a_2 +\\
&+y_{3,3}a_3 + x_{3,4}b_4 + y_{3,4}a_4 \;=\\
&= \frac{\mathrm{h}}{\mathrm{c}}wa_3 - \frac{\mathrm{h}}{\mathrm{c}}p_3a_3 - \frac{\mathrm{h}}{\mathrm{c}}p_1a_4 - \frac{\mathrm{h}}{\mathrm{c}}p_2b_4\,,\\
&-x_{1,4}a_1 - y_{1,4}b_1 - x_{2,4}a_2 - y_{2,4}b_2 -\\
&-x_{3,4}a_3 - y_{3,4}b_3 - y_{4,4}b_4 \;=\\
&= -\frac{\mathrm{h}}{\mathrm{c}}wb_4 + \frac{\mathrm{h}}{\mathrm{c}}p_1b_3 + \frac{\mathrm{h}}{\mathrm{c}}p_2a_3 - \frac{\mathrm{h}}{\mathrm{c}}p_3b_4\,,\\
&-x_{1,4}b_1 + y_{1,4}a_1 - x_{2,4}b_2 + y_{2,4}a_2 -\\
&-x_{3,4}b_3 + y_{3,4}a_3 + y_{4,4}a_4 \;=\\
&= \frac{\mathrm{h}}{\mathrm{c}}wa_4 - \frac{\mathrm{h}}{\mathrm{c}}p_1a_3 + \frac{\mathrm{h}}{\mathrm{c}}p_2b_3 + \frac{\mathrm{h}}{\mathrm{c}}p_3a_4\,;
\end{aligned}$$

(here $a_k := \mathrm{Re}A_k$ and $b_k := \mathrm{Im}A_k$).

This system has solutions according to the Kronecker-Capelli theorem (rank of this system augmented matrix and rank of this system basic matrix equal to 7). Hence, such complex numbers $z_{j,k,w,\mathbf{p}}|_{\langle t,\mathbf{x}\rangle}$ exist in all points $\langle t,\mathbf{x}\rangle$.

From (16), (14), (15):

$$\sum_{k=1}^{4} z_{j,k,w,\mathbf{p}}\varphi_{k,w,\mathbf{p}}|_{\langle t,\mathbf{x}\rangle} = \left(\frac{1}{\mathrm{c}}\,\partial_t\varphi_{j,w,\mathbf{p}} - \sum_{s=1}^{4}\sum_{\alpha=1}^{3}\beta^{[\alpha]}_{j,s}\partial_\alpha\varphi_{s,w,\mathbf{p}}\right)|_{\langle t,\mathbf{x}\rangle},$$

in every point $\langle t,\mathbf{x}\rangle$.

Therefore, from (16, 15, 14):

$$\frac{1}{\mathrm{c}}\,\partial_t\varphi_{j,w,\mathbf{p}} = \sum_{k=1}^{4}\left(\sum_{\alpha=1}^{3}\beta^{[\alpha]}_{j,k}\partial_\alpha\varphi_{k,w,\mathbf{p}} + z_{j,k,w,\mathbf{p}}\varphi_{k,w,\mathbf{p}}\right) \quad (17)$$

in every point $\langle t,\mathbf{x}\rangle$.

Let $\kappa_{w,\mathbf{p}}$ be linear operators on linear space, spanned of basic functions $\varsigma_{w,\mathbf{p}}(t,\mathbf{x})$, such that

$$\kappa_{w,\mathbf{p}}\varsigma_{w',\mathbf{p}'} := \begin{cases} \varsigma_{w',\mathbf{p}'}, \text{ if } w = w',\, \mathbf{p} = \mathbf{p}';\\ 0, \text{ if } w \neq w' \text{ and/or } \mathbf{p} \neq \mathbf{p}'. \end{cases}$$

Let

$$Q_{j,k}|_{\langle t,\mathbf{x}\rangle} := \sum_{w,\mathbf{p}}\left(z_{j,k,w,\mathbf{p}}|_{\langle t,\mathbf{x}\rangle}\right)\kappa_{w,\mathbf{p}}$$

in every point $\langle t,\mathbf{x}\rangle$.

Therefore, from (13) and (17), for every function φ_j here exists an operator $Q_{j,k}$ such that dependence of φ_j on t is described by the following differential equations:

$$\partial_t\varphi_j = \mathrm{c}\sum_{k=1}^{4}\left(\beta^{[1]}_{j,k}\partial_1 + \beta^{[2]}_{j,k}\partial_2 + \beta^{[3]}_{j,k}\partial_3 + Q_{j,k}\right)\varphi_k. \quad (18)$$

and

$$Q^*_{j,k} = \sum_{w,\mathbf{p}}\left(z^*_{j,k,w,\mathbf{p}}\right)\kappa_{w,\mathbf{p}} = \sum_{w,\mathbf{p}}\left(-z^*_{k,j,w,\mathbf{p}}\right)\kappa_{w,\mathbf{p}} = -Q_{k,j}\,.$$

Matrix form of formula (18) is the following:

$$\partial_t\varphi = \mathrm{c}\left(\beta^{[1]}\partial_1 + \beta^{[2]}\partial_2 + \beta^{[3]}\partial_3 + \widehat{Q}\right)\varphi \quad (19)$$

with

$$\varphi = \begin{bmatrix}\varphi_1\\ \varphi_2\\ \varphi_3\\ \varphi_4\end{bmatrix}$$

and

$$\widehat{Q} := \begin{bmatrix} \mathrm{i}\vartheta_{1,1} & Q_{1,2} & Q_{1,3} & Q_{1,4} \\ -Q^*_{1,2} & \mathrm{i}\vartheta_{2,2} & Q_{2,3} & Q_{2,4} \\ -Q^*_{1,3} & -Q^*_{2,3} & \mathrm{i}\vartheta_{3,3} & Q_{3,4} \\ -Q^*_{1,4} & -Q^*_{2,4} & -Q^*_{3,4} & \mathrm{i}\vartheta_{4,4} \end{bmatrix} \tag{20}$$

with $Q_{k,s} := \mathrm{i}\vartheta_{k,s} - \varpi_{k,s}$ if $k \neq s$, and with $\varpi_{s,k} := \mathrm{Re}\,(Q_{s,k})$ and $\vartheta_{s,k} := \mathrm{Im}\,(Q_{s,k})$.

Let $\vartheta_{s,k}$ and $\varpi_{s,k}$ be terms of $\widehat{Q}$ (20) and let Θ_0, Θ_3, Υ_0 and Υ_3 be the solution of the following sets of equations:

$$\left\{ \begin{array}{l} -\Theta_0 + \Theta_3 - \Upsilon_0 + \Upsilon_3 = \vartheta_{1,1}; \\ -\Theta_0 - \Theta_3 - \Upsilon_0 - \Upsilon_3 = \vartheta_{2,2}; \\ -\Theta_0 - \Theta_3 + \Upsilon_0 + \Upsilon_3 = \vartheta_{3,3}; \\ -\Theta_0 + \Theta_3 + \Upsilon_0 - \Upsilon_3 = \vartheta_{4,4} \end{array} \right|,$$

and Θ_1, Υ_1, Θ_2, Υ_2, M_0, M_4, $M_{\zeta,0}$, $M_{\zeta,4}$, $M_{\eta,0}$, $M_{\eta,4}$, $M_{\theta,0}$, $M_{\theta,4}$ be the solutions of the following sets of equations:

$$\left\{ \begin{array}{l} \Theta_1 + \Upsilon_1 = \vartheta_{1,2}; \\ -\Theta_1 + \Upsilon_1 = \vartheta_{3,4}; \end{array} \right| \left\{ \begin{array}{l} -\Theta_2 - \Upsilon_2 = \varpi_{1,2}; \\ \Theta_2 - \Upsilon_2 = \varpi_{3,4}; \end{array} \right|$$

$$\left\{ \begin{array}{l} M_0 + M_{\theta,0} = \vartheta_{1,3}; \\ M_0 - M_{\theta,0} = \vartheta_{2,4}; \end{array} \right| \left\{ \begin{array}{l} M_4 + M_{\theta,4} = \varpi_{1,3}; \\ M_4 - M_{\theta,4} = \varpi_{2,4}; \end{array} \right|$$

$$\left\{ \begin{array}{l} M_{\zeta,0} - M_{\eta,4} = \vartheta_{1,4}; \\ M_{\zeta,0} + M_{\eta,4} = \vartheta_{2,3}; \end{array} \right| \left\{ \begin{array}{l} M_{\zeta,4} - M_{\eta,0} = \varpi_{1,4}; \\ M_{\zeta,4} + M_{\eta,0} = \varpi_{2,3} \end{array} \right|.$$

Thus the columns of $\widehat{Q}$ are the following:

— the first and the second columns:

$$\begin{array}{c} -\mathrm{i}\Theta_0 + \mathrm{i}\Theta_3 - \mathrm{i}\Upsilon_0 + \mathrm{i}\Upsilon_3 \\ \mathrm{i}\Theta_1 + \mathrm{i}\Upsilon_1 - \Theta_2 - \Upsilon_2 \\ \mathrm{i}M_0 + \mathrm{i}M_{\theta,0} + M_4 + M_{\theta,4} \\ \mathrm{i}M_{\zeta,0} - \mathrm{i}M_{\eta,4} + M_{\zeta,4} - M_{\eta,0} \end{array} \quad \begin{array}{c} \mathrm{i}\Theta_1 + \mathrm{i}\Upsilon_1 + \Theta_2 + \Upsilon_2 \\ -\mathrm{i}\Theta_0 - \mathrm{i}\Theta_3 - \mathrm{i}\Upsilon_0 - \mathrm{i}\Upsilon_3 \\ \mathrm{i}M_{\zeta,0} + \mathrm{i}M_{\eta,4} + M_{\zeta,4} + M_{\eta,0} \\ \mathrm{i}M_0 - \mathrm{i}M_{\theta,0} + M_4 - M_{\theta,4} \end{array}$$

— the third and the fourth columns:

$$\begin{array}{c} \mathrm{i}M_0 + \mathrm{i}M_{\theta,0} - M_4 - M_{\theta,4} \\ \mathrm{i}M_{\zeta,0} + \mathrm{i}M_{\eta,4} - M_{\zeta,4} - M_{\eta,0} \\ -\mathrm{i}\Theta_0 - \mathrm{i}\Theta_3 + \mathrm{i}\Upsilon_0 + \mathrm{i}\Upsilon_3 \\ -\mathrm{i}\Theta_1 + \mathrm{i}\Upsilon_1 + \Theta_2 - \Upsilon_2 \end{array} \quad \begin{array}{c} \mathrm{i}M_{\zeta,0} - \mathrm{i}M_{\eta,4} - M_{\zeta,4} + M_{\eta,0} \\ \mathrm{i}M_0 - \mathrm{i}M_{\theta,0} - M_4 + M_{\theta,4} \\ -\mathrm{i}\Theta_1 + \mathrm{i}\Upsilon_1 - \Theta_2 + \Upsilon_2 \\ -\mathrm{i}\Theta_0 + \mathrm{i}\Theta_3 + \mathrm{i}\Upsilon_0 - \mathrm{i}\Upsilon_3 \end{array}$$

Hence

$$\begin{aligned} \widehat{Q} = {} & \mathrm{i}\Theta_0\beta^{[0]} + \mathrm{i}\Upsilon_0\beta^{[0]}\gamma^{[5]} + \\ & + \mathrm{i}\Theta_1\beta^{[1]} + \mathrm{i}\Upsilon_1\beta^{[1]}\gamma^{[5]} + \\ & + \mathrm{i}\Theta_2\beta^{[2]} + \mathrm{i}\Upsilon_2\beta^{[2]}\gamma^{[5]} + \\ & + \mathrm{i}\Theta_3\beta^{[3]} + \mathrm{i}\Upsilon_3\beta^{[3]}\gamma^{[5]} + \\ & + \mathrm{i}M_0\gamma^{[0]} + \mathrm{i}M_4\beta^{[4]} - \\ & - \mathrm{i}M_{\zeta,0}\gamma^{[0]}_{\zeta} + \mathrm{i}M_{\zeta,4}\zeta^{[4]} - \\ & - \mathrm{i}M_{\eta,0}\gamma^{[0]}_{\eta} - \mathrm{i}M_{\eta,4}\eta^{[4]} + \\ & + \mathrm{i}M_{\theta,0}\gamma^{[0]}_{\theta} + \mathrm{i}M_{\theta,4}\theta^{[4]}. \end{aligned}$$

From (19) the following equation is received:

$$\begin{aligned} & \sum_{k=0}^{3} \beta^{[k]} \left(\partial_k + \mathrm{i}\Theta_k + \mathrm{i}\Upsilon_k\gamma^{[5]} \right) \varphi + \\ & + \begin{pmatrix} +\mathrm{i}M_0\gamma^{[0]} + \mathrm{i}M_4\beta^{[4]} - \\ -\mathrm{i}M_{\zeta,0}\gamma^{[0]}_{\zeta} + \mathrm{i}M_{\zeta,4}\zeta^{[4]} - \\ -\mathrm{i}M_{\eta,0}\gamma^{[0]}_{\eta} - \mathrm{i}M_{\eta,4}\eta^{[4]} + \\ +\mathrm{i}M_{\theta,0}\gamma^{[0]}_{\theta} + \mathrm{i}M_{\theta,4}\theta^{[4]} \end{pmatrix} \varphi = 0 \end{aligned} \tag{21}$$

with real Θ_k, Υ_k, M_0, M_4, $M_{\zeta,0}$, $M_{\zeta,4}$, $M_{\eta,0}$, $M_{\eta,4}$, $M_{\theta,0}$, $M_{\theta,4}$and with

$$\gamma^{[5]} := \begin{bmatrix} 1_2 & 0_2 \\ 0_2 & -1_2 \end{bmatrix}. \tag{22}$$

Because

$$\zeta^{[k]} + \eta^{[k]} + \theta^{[k]} = -\beta^{[k]}$$

with $k \in \{1, 2, 3\}$ then from (21):

$$\begin{aligned} & \begin{pmatrix} -\left(\partial_0 + \mathrm{i}\Theta_0 + \mathrm{i}\Upsilon_0\gamma^{[5]}\right) + \\ \sum\limits_{k=1}^{3} \beta^{[k]} \left(\partial_k + \mathrm{i}\Theta_k + \mathrm{i}\Upsilon_k\gamma^{[5]} \right) \\ +2 \left(\mathrm{i}M_0\gamma^{[0]} + \mathrm{i}M_4\beta^{[4]} \right) \end{pmatrix} \varphi + \\ & + \begin{pmatrix} -\left(\partial_0 + \mathrm{i}\Theta_0 + \mathrm{i}\Upsilon_0\gamma^{[5]}\right) \\ -\sum\limits_{k=1}^{3} \zeta^{[k]} \left(\partial_k + \mathrm{i}\Theta_k + \mathrm{i}\Upsilon_k\gamma^{[5]} \right) \\ +2 \left(-\mathrm{i}M_{\zeta,0}\gamma^{[0]}_{\zeta} + \mathrm{i}M_{\zeta,4}\zeta^{[4]} \right) \end{pmatrix} \varphi + \\ & + \begin{pmatrix} \left(\partial_0 + \mathrm{i}\Theta_0 + \mathrm{i}\Upsilon_0\gamma^{[5]}\right) \\ -\sum\limits_{k=1}^{3} \eta^{[k]} \left(\partial_k + \mathrm{i}\Theta_k + \mathrm{i}\Upsilon_k\gamma^{[5]} \right) \\ +2 \left(-\mathrm{i}M_{\eta,0}\gamma^{[0]}_{\eta} - \mathrm{i}M_{\eta,4}\eta^{[4]} \right) \end{pmatrix} \varphi + \\ & + \begin{pmatrix} -\left(\partial_0 + \mathrm{i}\Theta_0 + \mathrm{i}\Upsilon_0\gamma^{[5]}\right) \\ -\sum\limits_{k=1}^{3} \theta^{[k]} \left(\partial_k + \mathrm{i}\Theta_k + \mathrm{i}\Upsilon_k\gamma^{[5]} \right) \\ +2 \left(\mathrm{i}M_{\theta,0}\gamma^{[0]}_{\theta} + \mathrm{i}M_{\theta,4}\theta^{[4]} \right) \end{pmatrix} \varphi = 0. \end{aligned}$$

It is a generalization of the Dirac equation with gauge field A:

$$\left(-\left(\partial_0+\mathrm{i}eA_0\right)+\sum_{k=1}^{3}\beta^{[k]}\left(\partial_k+\mathrm{i}eA_k\right)+\mathrm{i}m\gamma^{[0]}\right)\varphi=0.$$

Therefore, all Planck's functions obey to Dirac's type equations.

I call matrices $\gamma^{[0]},\beta^{[4]},\gamma_\zeta^{[0]},\zeta^{[4]},\gamma_\eta^{[0]},\eta^{[4]},\gamma_\theta^{[0]},\theta^{[4]}$ *mass elements of pentads*.

3 Colored equation

I call the following part of (21):

$$\left(\begin{array}{c}\beta^{[0]}\left(-\mathrm{i}\partial_0+\Theta_0+\Upsilon_0\gamma^{[5]}\right)+\\ \beta^{[1]}\left(-\mathrm{i}\partial_1+\Theta_1+\Upsilon_1\gamma^{[5]}\right)+\\ \beta^{[2]}\left(-\mathrm{i}\partial_2+\Theta_2+\Upsilon_2\gamma^{[5]}\right)+\\ \beta^{[3]}\left(-\mathrm{i}\partial_3+\Theta_3+\Upsilon_3\gamma^{[5]}\right)-\\ -M_{\zeta,0}\gamma_\zeta^{[0]}+M_{\zeta,4}\zeta^{[4]}+\\ -M_{\eta,0}\gamma_\eta^{[0]}-M_{\eta,4}\eta^{[4]}+\\ +M_{\theta,0}\gamma_\theta^{[0]}+M_{\theta,4}\theta^{[4]}\end{array}\right)\varphi=0. \qquad (23)$$

a coloured moving equation.

Here (5), (7), (9):

$$\gamma_\zeta^{[0]}=-\begin{bmatrix}0&0&0&1\\0&0&1&0\\0&1&0&0\\1&0&0&0\end{bmatrix},\quad \zeta^{[4]}=\begin{bmatrix}0&0&0&\mathrm{i}\\0&0&\mathrm{i}&0\\0&-\mathrm{i}&0&0\\-\mathrm{i}&0&0&0\end{bmatrix}$$

are mass elements of red pentad;

$$\gamma_\eta^{[0]}=\begin{bmatrix}0&0&0&\mathrm{i}\\0&0&-\mathrm{i}&0\\0&\mathrm{i}&0&0\\-\mathrm{i}&0&0&0\end{bmatrix},\quad \eta^{[4]}=\begin{bmatrix}0&0&0&1\\0&0&-1&0\\0&-1&0&0\\1&0&0&0\end{bmatrix}$$

are mass elements of green pentad;

$$\gamma_\theta^{[0]}=\begin{bmatrix}0&0&-1&0\\0&0&0&1\\-1&0&0&0\\0&1&0&0\end{bmatrix},\quad \theta^{[4]}=\begin{bmatrix}0&0&-\mathrm{i}&0\\0&0&0&\mathrm{i}\\-\mathrm{i}&0&0&0\\0&\mathrm{i}&0&0\end{bmatrix}$$

are mass elements of blue pentad.

I call:

- $M_{\zeta,0}$, $M_{\zeta,4}$ *red lower and upper mass members*;
- $M_{\eta,0}$, $M_{\eta,4}$ *green lower and upper mass members*;
- $M_{\theta,0}$, $M_{\theta,4}$ *blue lower and upper mass members*.

The mass members of this equation form the following matrix sum:

$$\widehat{M}:=\left(\begin{array}{c}-M_{\zeta,0}\gamma_\zeta^{[0]}+M_{\zeta,4}\zeta^{[4]}-\\ -M_{\eta,0}\gamma_\eta^{[0]}-M_{\eta,4}\eta^{[4]}+\\ +M_{\theta,0}\gamma_\theta^{[0]}+M_{\theta,4}\theta^{[4]}\end{array}\right)=$$

$$=\begin{bmatrix}0&0&-M_{\theta,0}&M_{\zeta,\eta,0}\\0&0&M^*_{\zeta,\eta,0}&M_{\theta,0}\\-M_{\theta,0}&M_{\zeta,\eta,0}&0&0\\M^*_{\zeta,\eta,0}&M_{\theta,0}&0&0\end{bmatrix}+$$

$$+\mathrm{i}\begin{bmatrix}0&0&-M_{\theta,4}&M^*_{\zeta,\eta,4}\\0&0&M_{\zeta,\eta,4}&M_{\theta,4}\\-M_{\theta,4}&-M^*_{\zeta,\eta,4}&0&0\\-M_{\zeta,\eta,4}&M_{\theta,4}&0&0\end{bmatrix}$$

with $M_{\zeta,\eta,0}:=M_{\zeta,0}-\mathrm{i}M_{\eta,0}$ and $M_{\zeta,\eta,4}:=M_{\zeta,4}-\mathrm{i}M_{\eta,4}$.

Elements of these matrices can be turned by formula of shape [2]:

$$\begin{pmatrix}\cos\frac{\theta}{2}&\mathrm{i}\sin\frac{\theta}{2}\\\mathrm{i}\sin\frac{\theta}{2}&\cos\frac{\theta}{2}\end{pmatrix}\begin{pmatrix}Z&X-\mathrm{i}Y\\X+\mathrm{i}Y&-Z\end{pmatrix}\times$$

$$\times\begin{pmatrix}\cos\frac{\theta}{2}&-\mathrm{i}\sin\frac{\theta}{2}\\-\mathrm{i}\sin\frac{\theta}{2}&\cos\frac{\theta}{2}\end{pmatrix}=$$

$$=\begin{pmatrix}Z\cos\theta-Y\sin\theta&X-\mathrm{i}\begin{pmatrix}Y\cos\theta\\+Z\sin\theta\end{pmatrix}\\X+\mathrm{i}\begin{pmatrix}Y\cos\theta\\+Z\sin\theta\end{pmatrix}&-Z\cos\theta+Y\sin\theta\end{pmatrix}.$$

Hence, if:

$$U_{2,3}(\alpha):=\begin{bmatrix}\cos\alpha&\mathrm{i}\sin\alpha&0&0\\\mathrm{i}\sin\alpha&\cos\alpha&0&0\\0&0&\cos\alpha&\mathrm{i}\sin\alpha\\0&0&\mathrm{i}\sin\alpha&\cos\alpha\end{bmatrix}$$

and

$$\widehat{M}':=\left(\begin{array}{c}-M'_{\zeta,0}\gamma_\zeta^{[0]}+M'_{\zeta,4}\zeta^{[4]}-\\ -M'_{\eta,0}\gamma_\eta^{[0]}-M'_{\eta,4}\eta^{[4]}+\\ +M'_{\theta,0}\gamma_\theta^{[0]}+M'_{\theta,4}\theta^{[4]}\end{array}\right):=U^\dagger_{2,3}(\alpha)\,\widehat{M}U_{2,3}(\alpha)$$

then

$$\begin{aligned}M'_{\zeta,0}&=M_{\zeta,0}\,,\\M'_{\eta,0}&=M_{\eta,0}\cos2\alpha+M_{\theta,0}\sin2\alpha\,,\\M'_{\theta,0}&=M_{\theta,0}\cos2\alpha-M_{\eta,0}\sin2\alpha\,,\\M'_{\zeta,4}&=M_{\zeta,4}\,,\\M'_{\eta,4}&=M_{\eta,4}\cos2\alpha+M_{\theta,4}\sin2\alpha\,,\\M'_{\theta,4}&=M_{\theta,4}\cos2\alpha-M_{\eta,4}\sin2\alpha\,.\end{aligned}$$

Therefore, matrix $U_{2,3}(\alpha)$ makes an oscillation between green and blue colours.

Let us consider equation (21) under transformation $U_{2,3}(\alpha)$ where α is an arbitrary real function of time-space variables ($\alpha=\alpha(t,x_1,x_2,x_3)$):

$$U^\dagger_{2,3}(\alpha)\left(\frac{1}{c}\partial_t+\mathrm{i}\Theta_0+\mathrm{i}\Upsilon_0\gamma^{[5]}\right)U_{2,3}(\alpha)\varphi=$$

$$= U^{\dagger}_{2,3}(\alpha) \begin{pmatrix} \beta^{[1]}\left(\partial_1 + \mathrm{i}\Theta_1 + \mathrm{i}\Upsilon_1\gamma^{[5]}\right) + \\ +\beta^{[2]}\left(\partial_2 + \mathrm{i}\Theta_2 + \mathrm{i}\Upsilon_2\gamma^{[5]}\right) + \\ +\beta^{[3]}\left(\partial_3 + \mathrm{i}\Theta_3 + \mathrm{i}\Upsilon_3\gamma^{[5]}\right) + \\ +\mathrm{i}M_0\gamma^{[0]} + \mathrm{i}M_4\beta^{[4]} + \widehat{M} \end{pmatrix} U_{2,3}(\alpha)\,\varphi\,.$$

Because

$$U^{\dagger}_{2,3}(\alpha)\,U_{2,3}(\alpha) = 1_4\,,$$
$$U^{\dagger}_{2,3}(\alpha)\,\gamma^{[5]}U_{2,3}(\alpha) = \gamma^{[5]}\,,$$
$$U^{\dagger}_{2,3}(\alpha)\,\gamma^{[0]}U_{2,3}(\alpha) = \gamma^{[0]}\,,$$
$$U^{\dagger}_{2,3}(\alpha)\,\beta^{[4]}U_{2,3}(\alpha) = \beta^{[4]}\,,$$
$$U^{\dagger}_{2,3}(\alpha)\,\beta^{[1]} = \beta^{[1]}U^{\dagger}_{2,3}(\alpha)\,,$$
$$U^{\dagger}_{2,3}(\alpha)\,\beta^{[2]} = \left(\beta^{[2]}\cos 2\alpha + \beta^{[3]}\sin 2\alpha\right)U^{\dagger}_{2,3}(\alpha)\,,$$
$$U^{\dagger}_{2,3}(\alpha)\,\beta^{[3]} = \left(\beta^{[3]}\cos 2\alpha - \beta^{[2]}\sin 2\alpha\right)U^{\dagger}_{2,3}(\alpha)\,,$$

then

$$\left(\frac{1}{\mathrm{c}}\,\partial_t + U^{\dagger}_{2,3}(\alpha)\,\frac{1}{\mathrm{c}}\,\partial_t U_{2,3}(\alpha) + \mathrm{i}\Theta_0 + \mathrm{i}\Upsilon_0\gamma^{[5]}\right)\varphi =$$

$$= \begin{pmatrix} \beta^{[1]}\begin{pmatrix}\partial_1 + U^{\dagger}_{2,3}(\alpha)\,\partial_1 U_{2,3}(\alpha) \\ +\mathrm{i}\Theta_1 + \mathrm{i}\Upsilon_1\gamma^{[5]}\end{pmatrix} + \beta^{[2]}\times \\ \times\begin{pmatrix} (\cos 2\alpha\cdot\partial_2 - \sin 2\alpha\cdot\partial_3) \\ +U^{\dagger}_{2,3}(\alpha)\begin{pmatrix}\cos 2\alpha\cdot\partial_2 \\ -\sin 2\alpha\cdot\partial_3\end{pmatrix}U_{2,3}(\alpha) \\ +\mathrm{i}\left(\Theta_2\cos 2\alpha - \Theta_3\sin 2\alpha\right) \\ +\mathrm{i}\left(\Upsilon_2\gamma^{[5]}\cos 2\alpha - \Upsilon_3\gamma^{[5]}\sin 2\alpha\right)\end{pmatrix} \\ +\beta^{[3]}\times \\ \times\begin{pmatrix} (\cos 2\alpha\cdot\partial_3 + \sin 2\alpha\cdot\partial_2) \\ +U^{\dagger}_{2,3}(\alpha)\begin{pmatrix}\cos 2\alpha\cdot\partial_3 \\ +\sin 2\alpha\cdot\partial_2\end{pmatrix}U_{2,3}(\alpha) \\ +\mathrm{i}\left(\Theta_2\sin 2\alpha + \Theta_3\cos 2\alpha\right) \\ +\mathrm{i}\left(\Upsilon_3\gamma^{[5]}\cos 2\alpha + \Upsilon_2\gamma^{[5]}\sin 2\alpha\right)\end{pmatrix} \\ +\mathrm{i}M_0\gamma^{[0]} + \mathrm{i}M_4\beta^{[4]} + \widehat{M}'\end{pmatrix}\varphi\,. \quad (24)$$

Let x'_2 and x'_3 be elements of other coordinate system such that:

$$\frac{\partial x_2}{\partial x'_2} = \cos 2\alpha,$$
$$\frac{\partial x_3}{\partial x'_2} = -\sin 2\alpha,$$
$$\frac{\partial x_2}{\partial x'_3} = \sin 2\alpha.$$
$$\frac{\partial x_3}{\partial x'_3} = \cos 2\alpha,$$
$$\frac{\partial x_0}{\partial x'_2} = \frac{\partial x_1}{\partial x'_2} = \frac{\partial x_0}{\partial x'_3} = \frac{\partial x_1}{\partial x'_3} = 0.$$

Hence:

$$\partial'_2 := \frac{\partial}{\partial x'_2} =$$
$$= \frac{\partial}{\partial x_0}\frac{\partial x_0}{\partial x'_2} + \frac{\partial}{\partial x_1}\frac{\partial x_1}{\partial x'_2} + \frac{\partial}{\partial x_2}\frac{\partial x_2}{\partial x'_2} + \frac{\partial}{\partial x_3}\frac{\partial x_3}{\partial x'_2} =$$
$$= \cos 2\alpha\cdot\frac{\partial}{\partial x_2} - \sin 2\alpha\cdot\frac{\partial}{\partial x_3} =$$
$$= \cos 2\alpha\cdot\partial_2 - \sin 2\alpha\cdot\partial_3\,,$$

$$\partial'_3 := \frac{\partial}{\partial x'_3} =$$
$$= \frac{\partial}{\partial x_0}\frac{\partial x_0}{\partial x'_3} + \frac{\partial}{\partial x_1}\frac{\partial x_1}{\partial x'_3} + \frac{\partial}{\partial x_2}\frac{\partial x_2}{\partial x'_3} + \frac{\partial}{\partial x_3}\frac{\partial x_3}{\partial x'_3} =$$
$$= \cos 2\alpha\cdot\frac{\partial}{\partial x_3} + \sin 2\alpha\cdot\frac{\partial}{\partial x_2} =$$
$$= \cos 2\alpha\cdot\partial_3 + \sin 2\alpha\cdot\partial_2\,.$$

Therefore, from (24):

$$\left(\frac{1}{\mathrm{c}}\,\partial_t + U^{\dagger}_{2,3}(\alpha)\,\frac{1}{\mathrm{c}}\,\partial_t U_{2,3}(\alpha) + \mathrm{i}\Theta_0 + \mathrm{i}\Upsilon_0\gamma^{[5]}\right)\varphi =$$

$$= \begin{pmatrix} \beta^{[1]}\begin{pmatrix}\partial_1 + U^{\dagger}_{2,3}(\alpha)\,\partial_1 U_{2,3}(\alpha) \\ +\mathrm{i}\Theta_1 + \mathrm{i}\Upsilon_1\gamma^{[5]}\end{pmatrix} \\ +\beta^{[2]}\begin{pmatrix}\partial'_2 + U^{\dagger}_{2,3}(\alpha)\,\partial'_2 U_{2,3}(\alpha) \\ +\mathrm{i}\Theta'_2 + \mathrm{i}\Upsilon'_2\gamma^{[5]}\end{pmatrix} \\ +\beta^{[3]}\begin{pmatrix}\partial'_3 + U^{\dagger}_{2,3}(\alpha)\,\partial'_3 U_{2,3}(\alpha) \\ +\mathrm{i}\Theta'_3 + \mathrm{i}\Upsilon'_3\gamma^{[5]}\end{pmatrix} \\ +\mathrm{i}M_0\gamma^{[0]} + \mathrm{i}M_4\beta^{[4]} + \widehat{M}'\end{pmatrix}\varphi\,.$$

with

$$\Theta'_2 := \Theta_2\cos 2\alpha - \Theta_3\sin 2\alpha\,,$$
$$\Theta'_3 := \Theta_2\sin 2\alpha + \Theta_3\cos 2\alpha\,,$$
$$\Upsilon'_2 := \Upsilon_2\cos 2\alpha - \Upsilon_3\sin 2\alpha\,,$$
$$\Upsilon'_3 := \Upsilon_3\cos 2\alpha + \Upsilon_2\sin 2\alpha\,.$$

Therefore, the oscillation between blue and green colours curves the space in the x_2, x_3 directions.

Similarly, matrix

$$U_{1,3}(\vartheta) := \begin{bmatrix} \cos\vartheta & \sin\vartheta & 0 & 0 \\ -\sin\vartheta & \cos\vartheta & 0 & 0 \\ 0 & 0 & \cos\vartheta & \sin\vartheta \\ 0 & 0 & -\sin\vartheta & \cos\vartheta \end{bmatrix}$$

with an arbitrary real function $\vartheta(t, x_1, x_2, x_3)$ describes the oscillation between blue and red colours which curves the space in the x_1, x_3 directions. And matrix

$$U_{1,2}(\varsigma) := \begin{bmatrix} e^{-\mathrm{i}\varsigma} & 0 & 0 & 0 \\ 0 & e^{\mathrm{i}\varsigma} & 0 & 0 \\ 0 & 0 & e^{-\mathrm{i}\varsigma} & 0 \\ 0 & 0 & 0 & e^{\mathrm{i}\varsigma} \end{bmatrix}$$

with an arbitrary real function $\varsigma(t, x_1, x_2, x_3)$ describes the oscillation between green and red colours which curves the space in the x_1, x_2 directions.

Now, let

$$U_{0,1}(\sigma) := \begin{bmatrix} \cosh\sigma & -\sinh\sigma & 0 & 0 \\ -\sinh\sigma & \cosh\sigma & 0 & 0 \\ 0 & 0 & \cosh\sigma & \sinh\sigma \\ 0 & 0 & \sinh\sigma & \cosh\sigma \end{bmatrix}.$$

and

$$\widehat{M}'' := \begin{pmatrix} -M''_{\zeta,0}\gamma^{[0]}_{\zeta} + M''_{\zeta,4}\zeta^{[4]} - \\ -M''_{\eta,0}\gamma^{[0]}_{\eta} - M''_{\eta,4}\eta^{[4]} + \\ +M''_{\theta,0}\gamma^{[0]}_{\theta} + M''_{\theta,4}\theta^{[4]} \end{pmatrix} := U^{\dagger}_{0,1}(\sigma)\,\widehat{M}U_{0,1}(\sigma)$$

then:

$$\begin{aligned} M''_{\zeta,0} &= M_{\zeta,0}\,, \\ M''_{\eta,0} &= (M_{\eta,0}\cosh 2\sigma - M_{\theta,4}\sinh 2\sigma)\,, \\ M''_{\theta,0} &= M_{\theta,0}\cosh 2\sigma + M_{\eta,4}\sinh 2\sigma\,, \\ M''_{\zeta,4} &= M_{\zeta,4}\,, \\ M''_{\eta,4} &= M_{\eta,4}\cosh 2\sigma + M_{\theta,0}\sinh 2\sigma\,, \\ M''_{\theta,4} &= M_{\theta,4}\cosh 2\sigma - M_{\eta,0}\sinh 2\sigma\,. \end{aligned}$$

Therefore, matrix $U_{0,1}(\sigma)$ makes an oscillation between green and blue colours with an oscillation between upper and lower mass members.

Let us consider equation (21) under transformation $U_{0,1}(\sigma)$ where σ is an arbitrary real function of time-space variables ($\sigma = \sigma(t, x_1, x_2, x_3)$):

$$U^{\dagger}_{0,1}(\sigma)\left(\frac{1}{\mathrm{c}}\partial_t + \mathrm{i}\Theta_0 + \mathrm{i}\Upsilon_0\gamma^{[5]}\right)U_{0,1}(\sigma)\,\varphi =$$

$$= U^{\dagger}_{0,1}(\sigma)\begin{pmatrix} \beta^{[1]}\left(\partial_1 + \mathrm{i}\Theta_1 + \mathrm{i}\Upsilon_1\gamma^{[5]}\right) + \\ +\beta^{[2]}\left(\partial_2 + \mathrm{i}\Theta_2 + \mathrm{i}\Upsilon_2\gamma^{[5]}\right) + \\ +\beta^{[3]}\left(\partial_3 + \mathrm{i}\Theta_3 + \mathrm{i}\Upsilon_3\gamma^{[5]}\right) + \\ +\mathrm{i}M_0\gamma^{[0]} + \mathrm{i}M_4\beta^{[4]} + \widehat{M} \end{pmatrix} U_{0,1}(\sigma)\,\varphi\,.$$

Since:

$$\begin{aligned} &U^{\dagger}_{0,1}(\sigma)\,U_{0,1}(\sigma) = \left(\cosh 2\sigma - \beta^{[1]}\sinh 2\sigma\right), \\ &U^{\dagger}_{0,1}(\sigma) = \left(\cosh 2\sigma + \beta^{[1]}\sinh 2\sigma\right)U^{-1}_{0,1}(\sigma), \\ &U^{\dagger}_{0,1}(\sigma)\,\beta^{[1]} = \left(\beta^{[1]}\cosh 2\sigma - \sinh 2\sigma\right)U^{-1}_{0,1}(\sigma), \\ &U^{\dagger}_{0,1}(\sigma)\,\beta^{[2]} = \beta^{[2]}U^{-1}_{0,1}(\sigma), \\ &U^{\dagger}_{0,1}(\sigma)\,\beta^{[3]} = \beta^{[3]}U^{-1}_{0,1}(\sigma), \\ &U^{\dagger}_{0,1}(\sigma)\,\gamma^{[0]}U_{0,1}(\sigma) = \gamma^{[0]}, \\ &U^{\dagger}_{0,1}(\sigma)\,\beta^{[4]}U_{0,1}(\sigma) = \beta^{[4]}, \\ &U^{-1}_{0,1}(\sigma)\,U_{0,1}(\sigma) = 1_4\,, \\ &U^{-1}_{0,1}(\sigma)\,\gamma^{[5]}U_{0,1}(\sigma) = \gamma^{[5]}\,, \\ &U^{\dagger}_{0,1}(\sigma)\,\gamma^{[5]}U_{0,1}(\sigma) = \gamma^{[5]}\left(\cosh 2\sigma - \beta^{[1]}\sinh 2\sigma\right), \end{aligned}$$

then

$$\left(\begin{array}{c} U^{-1}_{0,1}(\sigma)\begin{pmatrix}\cosh 2\sigma\cdot\frac{1}{\mathrm{c}}\partial_t \\ +\sinh 2\sigma\cdot\partial_1\end{pmatrix}U_{0,1}(\sigma) \\ +\left(\cosh 2\sigma\cdot\frac{1}{\mathrm{c}}\partial_t + \sinh 2\sigma\cdot\partial_1\right) \\ +\mathrm{i}\left(\Theta_0\cosh 2\sigma + \Theta_1\sinh 2\sigma\right) \\ +\mathrm{i}\left(\Upsilon_0\cosh 2\sigma + \sinh 2\sigma\cdot\Upsilon_1\right)\gamma^{[5]} - \\ -\beta^{[1]}\times \\ \times\left(\begin{array}{c} U^{-1}_{0,1}(\sigma)\begin{pmatrix}\cosh 2\sigma\cdot\partial_1 + \\ \sinh 2\sigma\cdot\frac{1}{\mathrm{c}}\partial_t\end{pmatrix}U_{0,1}(\sigma) \\ +\left(\cosh 2\sigma\cdot\partial_1 + \sinh 2\sigma\cdot\frac{1}{\mathrm{c}}\partial_t\right) \\ +\mathrm{i}\left(\Theta_1\cosh 2\sigma + \Theta_0\sinh 2\sigma\right) \\ +\mathrm{i}\left(\Upsilon_1\cosh 2\sigma + \Upsilon_0\sinh 2\sigma\right)\gamma^{[5]} \end{array}\right) \\ -\beta^{[2]}\begin{pmatrix}\partial_2 + U^{-1}_{0,1}(\sigma)\left(\partial_2 U_{0,1}(\sigma)\right) \\ +\mathrm{i}\Theta_2 + \mathrm{i}\Upsilon_2\gamma^{[5]}\end{pmatrix} \\ -\beta^{[3]}\begin{pmatrix}\partial_3 + U^{-1}_{0,1}(\sigma)\left(\partial_3 U_{0,1}(\sigma)\right) \\ +\mathrm{i}\Theta_3 + \mathrm{i}\Upsilon_3\gamma^{[5]}\end{pmatrix} \\ -\mathrm{i}M_0\gamma^{[0]} - \mathrm{i}M_4\beta^{[4]} - \widehat{M}'' \end{array}\right)\varphi = 0\,. \quad (25)$$

Let t' and x'_1 be elements of other coordinate system such that:

$$\left.\begin{aligned} \frac{\partial x_1}{\partial x'_1} &= \cosh 2\sigma \\ \frac{\partial t}{\partial x'_1} &= \frac{1}{\mathrm{c}}\sinh 2\sigma \\ \frac{\partial x_1}{\partial t'} &= \mathrm{c}\sinh 2\sigma \\ \frac{\partial t}{\partial t'} &= \cosh 2\sigma \\ \frac{\partial x_2}{\partial t'} &= \frac{\partial x_3}{\partial t'} = \frac{\partial x_2}{\partial x'_1} = \frac{\partial x_3}{\partial x'_1} = 0 \end{aligned}\right\}. \quad (26)$$

Hence:

$$\begin{aligned} \partial'_t &:= \frac{\partial}{\partial t'} = \frac{\partial}{\partial t}\frac{\partial t}{\partial t'} + \frac{\partial}{\partial x_1}\frac{\partial x_1}{\partial t'} + \frac{\partial}{\partial x_2}\frac{\partial x_2}{\partial t'} + \frac{\partial}{\partial x_3}\frac{\partial x_3}{\partial t'} = \\ &= \cosh 2\sigma\cdot\frac{\partial}{\partial t} + \mathrm{c}\sinh 2\sigma\cdot\frac{\partial}{\partial x_1} = \\ &= \cosh 2\sigma\cdot\partial_t + \mathrm{c}\sinh 2\sigma\cdot\partial_1\,, \end{aligned}$$

that is

$$\frac{1}{\mathrm{c}}\partial'_t = \frac{1}{\mathrm{c}}\cosh 2\sigma\cdot\partial_t + \sinh 2\sigma\cdot\partial_1$$

and

$$\partial'_1 := \frac{\partial}{\partial x'_1} =$$
$$= \frac{\partial}{\partial t}\frac{\partial t}{\partial x'_1} + \frac{\partial}{\partial x_1}\frac{\partial x_1}{\partial x'_1} + \frac{\partial}{\partial x_2}\frac{\partial x_2}{\partial x'_1} + \frac{\partial}{\partial x_3}\frac{\partial x_3}{\partial x'_1} =$$
$$= \cosh 2\sigma \cdot \frac{\partial}{\partial x_1} + \sinh 2\sigma \cdot \frac{1}{\mathrm{c}}\frac{\partial}{\partial t} =$$
$$= \cosh 2\sigma \cdot \partial_1 + \sinh 2\sigma \cdot \frac{1}{\mathrm{c}}\partial_t .$$

Therefore, from (25):

$$\left(\begin{array}{c} \beta^{[0]} \left(\begin{array}{c} \frac{1}{\mathrm{c}}\partial'_t + U^{-1}_{0,1}(\sigma)\frac{1}{\mathrm{c}}\partial'_t U_{0,1}(\sigma) \\ +\mathrm{i}\Theta''_0 + \mathrm{i}\Upsilon''_0\gamma^{[5]} \end{array} \right) \\ +\beta^{[1]} \left(\begin{array}{c} \partial'_1 + U^{-1}_{0,1}(\sigma)\partial'_1 U_{0,1}(\sigma) \\ +\mathrm{i}\Theta''_1 + \mathrm{i}\Upsilon''_1\gamma^{[5]} \end{array} \right) \\ +\beta^{[2]} \left(\begin{array}{c} \partial_2 + U^{-1}_{0,1}(\sigma)\partial_2 U_{0,1}(\sigma) \\ +\mathrm{i}\Theta_2 + \mathrm{i}\Upsilon_2\gamma^{[5]} \end{array} \right) \\ +\beta^{[3]} \left(\begin{array}{c} \partial_3 + U^{-1}_{0,1}(\sigma)\partial_3 U_{0,1}(\sigma) \\ +\mathrm{i}\Theta_3 + \mathrm{i}\Upsilon_3\gamma^{[5]} \end{array} \right) \\ +\mathrm{i}M_0\gamma^{[0]} + \mathrm{i}M_4\beta^{[4]} + \widehat{M}'' \end{array} \right) \varphi = 0$$

with

$$\Theta''_0 := \Theta_0 \cosh 2\sigma + \Theta_1 \sinh 2\sigma ,$$
$$\Theta''_1 := \Theta_1 \cosh 2\sigma + \Theta_0 \sinh 2\sigma ,$$
$$\Upsilon''_0 := \Upsilon_0 \cosh 2\sigma + \sinh 2\sigma \cdot \Upsilon_1 ,$$
$$\Upsilon''_1 := \Upsilon_1 \cosh 2\sigma + \Upsilon_0 \sinh 2\sigma .$$

Therefore, the oscillation between blue and green colours with the oscillation between upper and lower mass members curves the space in the t, x_1 directions.

Similarly, matrix

$$U_{0,2}(\phi) := \begin{bmatrix} \cosh\phi & \mathrm{i}\sinh\phi & 0 & 0 \\ -\mathrm{i}\sinh\phi & \cosh\phi & 0 & 0 \\ 0 & 0 & \cosh\phi & -\mathrm{i}\sinh\phi \\ 0 & 0 & \mathrm{i}\sinh\phi & \cosh\phi \end{bmatrix}$$

with an arbitrary real function $\phi(t, x_1, x_2, x_3)$ describes the oscillation between blue and red colours with the oscillation between upper and lower mass members curves the space in the t, x_2 directions. And matrix

$$U_{0,3}(\iota) := \begin{bmatrix} e^{\iota} & 0 & 0 & 0 \\ 0 & e^{-\iota} & 0 & 0 \\ 0 & 0 & e^{-\iota} & 0 \\ 0 & 0 & 0 & e^{\iota} \end{bmatrix}$$

with an arbitrary real function $\iota(t, x_1, x_2, x_3)$ describes the oscillation between green and red colours with the oscillation between upper and lower mass members curves the space in the t, x_3 directions.

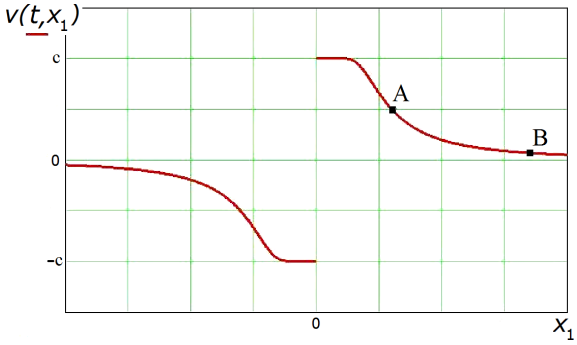

Fig. 1: It is dependency of $v(t, x_1)$ from x_1.

From (26):

$$\frac{\partial x_1}{\partial t'} = \mathrm{c}\sinh 2\sigma ,$$
$$\frac{\partial t}{\partial t'} = \cosh 2\sigma .$$

Because

$$\sinh 2\sigma = \frac{v}{\sqrt{1 - \frac{v^2}{\mathrm{c}^2}}} ,$$
$$\cosh 2\sigma = \frac{1}{\sqrt{1 - \frac{v^2}{\mathrm{c}^2}}}$$

with v is a velocity of system $\{t', x'_1\}$ as respects to system $\{t, x_1\}$ then

$$v = \tanh 2\sigma .$$

Let

$$2\sigma := \omega(x_1)\frac{t}{x_1}$$

with

$$\omega(x_1) = \frac{\lambda}{|x_1|} ,$$

where λ is a real constant bearing positive numerical value.

In that case

$$v(t, x_1) = \tanh\left(\omega(x_1)\frac{t}{x_1}\right)$$

and if g is an acceleration of system $\{t', x'_1\}$ as respects to system $\{t, x_1\}$ then

$$\mathrm{g}(t, x_1) = \frac{\partial v}{\partial t} = \frac{\omega(x_1)}{\left(\cosh^2 \omega(x_1)\frac{t}{x_1}\right) x_1} .$$

Figure 1 shows the dependency of a system $\{t', x'_1\}$ velocity $v(t, x_1)$ on x_1 in system $\{t, x_1\}$.

This velocity in point A is not equal to one in point B. Hence, an oscillator, placed in B, has a nonzero velocity in respect to an observer, placed in point A. Therefore, from the Lorentz transformations, this oscillator frequency for observer, placed in point A, is less than own frequency of this oscillator (*red shift*).

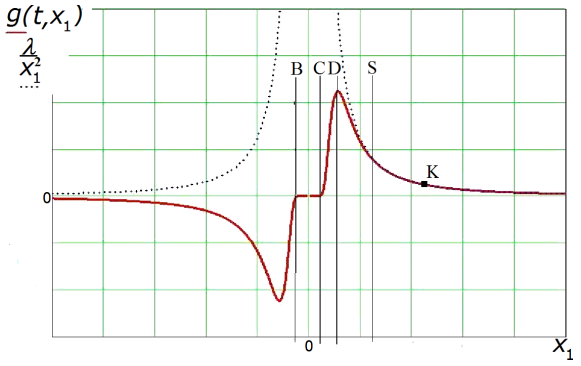

Fig. 2: It is dependency of $g(t, x_1)$ from x_1.

Figure 2 shows a dependency of a system $\{t', x_1'\}$ acceleration $g\,(t, x_1)$ on x_1 in system $\{t, x_1\}$.

If an object immovable in system $\{t, x_1\}$ is placed in point K then in system $\{t', x_1'\}$ this object must move to the left with acceleration g and $\mathrm{g} \simeq \frac{\lambda}{x_1^2}$.

I call:

- interval from S to ∞ the *Newton Gravity Zone*,
- interval from B to C the *the Asymptotic Freedom Zone*,
- and interval from C to D *the Confinement Force Zone*.

Now let

$$\widetilde{U}(\chi) := \begin{bmatrix} e^{\mathrm{i}\chi} & 0 & 0 & 0 \\ 0 & e^{\mathrm{i}\chi} & 0 & 0 \\ 0 & 0 & e^{2\mathrm{i}\chi} & 0 \\ 0 & 0 & 0 & e^{2\mathrm{i}\chi} \end{bmatrix}$$

and

$$\widehat{M}' := \begin{pmatrix} -M'_{\zeta,0}\gamma^{[0]}_{\zeta} + M'_{\zeta,4}\zeta^{[4]} - \\ -M'_{\eta,0}\gamma^{[0]}_{\eta} - M'_{\eta,4}\eta^{[4]} + \\ +M'_{\theta,0}\gamma^{[0]}_{\theta} + M'_{\theta,4}\theta^{[4]} \end{pmatrix} := \widetilde{U}^{\dagger}(\chi)\,\widehat{M}\widetilde{U}(\chi)$$

then:

$$\begin{aligned} M'_{\zeta,0} &= (M_{\zeta,0}\cos\chi - M_{\zeta,4}\sin\chi), \\ M'_{\zeta,4} &= (M_{\zeta,4}\cos\chi + M_{\zeta,0}\sin\chi), \\ M'_{\eta,4} &= (M_{\eta,4}\cos\chi - M_{\eta,0}\sin\chi), \\ M'_{\eta,0} &= (M_{\eta,0}\cos\chi + M_{\eta,4}\sin\chi), \\ M'_{\theta,0} &= (M_{\theta,0}\cos\chi + M_{\theta,4}\sin\chi), \\ M'_{\theta,4} &= (M_{\theta,4}\cos\chi - M_{\theta,0}\sin\chi). \end{aligned}$$

Therefore, matrix $\widetilde{U}(\chi)$ makes an oscillation between upper and lower mass members.

Let us consider equation (23) under transformation $\widetilde{U}(\chi)$ where χ is an arbitrary real function of time-space variables ($\chi = \chi(t, x_1, x_2, x_3)$):

$$\widetilde{U}^{\dagger}(\chi)\left(\frac{1}{\mathrm{c}}\partial_t + \mathrm{i}\Theta_0 + \mathrm{i}\Upsilon_0\gamma^{[5]}\right)\widetilde{U}(\chi)\,\varphi =$$

$$= \widetilde{U}^{\dagger}(\chi)\begin{pmatrix} \beta^{[1]}\left(\partial_1 + \mathrm{i}\Theta_1 + \mathrm{i}\Upsilon_1\gamma^{[5]}\right) + \\ +\beta^{[2]}\left(\partial_2 + \mathrm{i}\Theta_2 + \mathrm{i}\Upsilon_2\gamma^{[5]}\right) + \\ +\beta^{[3]}\left(\partial_3 + \mathrm{i}\Theta_3 + \mathrm{i}\Upsilon_3\gamma^{[5]}\right) + \\ +\widehat{M} \end{pmatrix}\widetilde{U}(\chi)\,\varphi.$$

Because

$$\begin{aligned} \gamma^{[5]}\widetilde{U}(\chi) &= \widetilde{U}(\chi)\gamma^{[5]}, \\ \beta^{[1]}\widetilde{U}(\chi) &= \widetilde{U}(\chi)\beta^{[1]}, \\ \beta^{[2]}\widetilde{U}(\chi) &= \widetilde{U}(\chi)\beta^{[2]}, \\ \beta^{[3]}\widetilde{U}(\chi) &= \widetilde{U}(\chi)\beta^{[3]}, \\ \widetilde{U}^{\dagger}(\chi)\,\widetilde{U}(\chi) &= 1_4, \end{aligned}$$

then

$$\left(\frac{1}{\mathrm{c}}\partial_t + \frac{1}{\mathrm{c}}\widetilde{U}^{\dagger}(\chi)\left(\partial_t\widetilde{U}(\chi)\right) + \mathrm{i}\Theta_0 + \mathrm{i}\Upsilon_0\gamma^{[5]}\right)\varphi =$$

$$= \begin{pmatrix} \beta^{[1]}\begin{pmatrix} \partial_1 + \widetilde{U}^{\dagger}(\chi)\left(\partial_1\widetilde{U}(\chi)\right) \\ +\mathrm{i}\Theta_1 + \mathrm{i}\Upsilon_1\gamma^{[5]} \end{pmatrix} + \\ +\beta^{[2]}\begin{pmatrix} \partial_2 + \widetilde{U}^{\dagger}(\chi)\left(\partial_2\widetilde{U}(\chi)\right) \\ +\mathrm{i}\Theta_2 + \mathrm{i}\Upsilon_2\gamma^{[5]} \end{pmatrix} + \\ +\beta^{[3]}\begin{pmatrix} \partial_3 + \widetilde{U}^{\dagger}(\chi)\left(\partial_3\widetilde{U}(\chi)\right) \\ +\mathrm{i}\Theta_3 + \mathrm{i}\Upsilon_3\gamma^{[5]} \end{pmatrix} + \\ +\widetilde{U}^{\dagger}(\chi)\,\widehat{M}\widetilde{U}(\chi) \end{pmatrix}\varphi.$$

Now let:

$$\widehat{U}(\kappa) := \begin{bmatrix} e^{\kappa} & 0 & 0 & 0 \\ 0 & e^{\kappa} & 0 & 0 \\ 0 & 0 & e^{2\kappa} & 0 \\ 0 & 0 & 0 & e^{2\kappa} \end{bmatrix}$$

and

$$\widehat{M}' := \begin{pmatrix} -M'_{\zeta,0}\gamma^{[0]}_{\zeta} + M'_{\zeta,4}\zeta^{[4]} - \\ -M'_{\eta,0}\gamma^{[0]}_{\eta} - M'_{\eta,4}\eta^{[4]} + \\ +M'_{\theta,0}\gamma^{[0]}_{\theta} + M'_{\theta,4}\theta^{[4]} \end{pmatrix} := \widehat{U}^{-1}(\kappa)\,\widehat{M}\widehat{U}(\kappa)$$

then:

$$\begin{aligned} M'_{\theta,0} &= (M_{\theta,0}\cosh\kappa - \mathrm{i}M_{\theta,4}\sinh\kappa), \\ M'_{\theta,4} &= (M_{\theta,4}\cosh\kappa + \mathrm{i}M_{\theta,0}\sinh\kappa), \\ M'_{\eta,0} &= (M_{\eta,0}\cosh\kappa - \mathrm{i}M_{\eta,4}\sinh\kappa), \\ M'_{\eta,4} &= (M_{\eta,4}\cosh\kappa + \mathrm{i}M_{\eta,0}\sinh\kappa), \\ M'_{\zeta,0} &= (M_{\zeta,0}\cosh\kappa + \mathrm{i}M_{\zeta,4}\sinh\kappa), \\ M'_{\zeta,4} &= (M_{\zeta,4}\cosh\kappa - \mathrm{i}M_{\zeta,0}\sinh\kappa). \end{aligned}$$

Therefore, matrix $\widehat{U}(\kappa)$ makes an oscillation between upper and lower mass members, too.

Let us consider equation (23) under transformation $\widehat{U}(\kappa)$ where κ is an arbitrary real function of time-space variables ($\kappa = \kappa(t, x_1, x_2, x_3)$):

$$\widehat{U}^{-1}(\kappa)\left(\frac{1}{\mathrm{c}}\partial_t + \mathrm{i}\Theta_0 + \mathrm{i}\Upsilon_0\gamma^{[5]}\right)\widehat{U}(\kappa)\varphi =$$
$$= \widehat{U}^{-1}(\kappa)\begin{pmatrix} \beta^{[1]}\left(\partial_1 + \mathrm{i}\Theta_1 + \mathrm{i}\Upsilon_1\gamma^{[5]}\right) + \\ +\beta^{[2]}\left(\partial_2 + \mathrm{i}\Theta_2 + \mathrm{i}\Upsilon_2\gamma^{[5]}\right) + \\ +\beta^{[3]}\left(\partial_3 + \mathrm{i}\Theta_3 + \mathrm{i}\Upsilon_3\gamma^{[5]}\right) + \\ +\widehat{M} \end{pmatrix}\widehat{U}(\kappa)\varphi$$

Because

$$\gamma^{[5]}\widehat{U}(\kappa) = \widehat{U}(\kappa)\gamma^{[5]},$$
$$\widehat{U}^{-1}(\kappa)\beta^{[1]} = \beta^{[1]}\widehat{U}^{-1}(\kappa),$$
$$\widehat{U}^{-1}(\kappa)\beta^{[2]} = \beta^{[2]}\widehat{U}^{-1}(\kappa),$$
$$\widehat{U}^{-1}(\kappa)\beta^{[3]} = \beta^{[3]}\widehat{U}^{-1}(\kappa),$$
$$\widehat{U}^{-1}(\kappa)\widehat{U}(\kappa) = 1_4,$$

then

$$\left(\frac{1}{\mathrm{c}}\partial_t + \widehat{U}^{-1}(\kappa)\left(\frac{1}{\mathrm{c}}\partial_t\widehat{U}(\kappa)\right) + \mathrm{i}\Theta_0 + \mathrm{i}\Upsilon_0\gamma^{[5]}\right)\varphi =$$
$$= \begin{pmatrix} \beta^{[1]}\begin{pmatrix} \partial_1 + \widehat{U}^{-1}(\kappa)\left(\partial_1\widehat{U}(\kappa)\right) \\ +\mathrm{i}\Theta_1 + \mathrm{i}\Upsilon_1\gamma^{[5]} \end{pmatrix} + \\ +\beta^{[2]}\begin{pmatrix} \partial_2 + \widehat{U}^{-1}(\kappa)\left(\partial_2\widehat{U}(\kappa)\right) \\ +\mathrm{i}\Theta_2 + \mathrm{i}\Upsilon_2\gamma^{[5]} \end{pmatrix} + \\ +\beta^{[3]}\begin{pmatrix} \partial_3 + \widehat{U}^{-1}(\kappa)\left(\partial_3\widehat{U}(\kappa)\right) \\ +\mathrm{i}\Theta_3 + \mathrm{i}\Upsilon_3\gamma^{[5]} \end{pmatrix} + \\ +\widehat{U}^{-1}(\kappa)\widehat{M}\widehat{U}(\kappa) \end{pmatrix}\varphi.$$

If denote:

$$\Lambda_1 := \begin{bmatrix} 0 & -1 & 0 & 0 \\ -1 & 0 & 0 & 0 \\ 0 & 0 & 0 & 1 \\ 0 & 0 & 1 & 0 \end{bmatrix},$$

$$\Lambda_2 := \begin{bmatrix} 0 & \mathrm{i} & 0 & 0 \\ \mathrm{i} & 0 & 0 & 0 \\ 0 & 0 & 0 & \mathrm{i} \\ 0 & 0 & \mathrm{i} & 0 \end{bmatrix},$$

$$\Lambda_3 := \begin{bmatrix} 0 & 1 & 0 & 0 \\ -1 & 0 & 0 & 0 \\ 0 & 0 & 0 & 1 \\ 0 & 0 & -1 & 0 \end{bmatrix},$$

$$\Lambda_4 := \begin{bmatrix} 0 & \mathrm{i} & 0 & 0 \\ -\mathrm{i} & 0 & 0 & 0 \\ 0 & 0 & 0 & -\mathrm{i} \\ 0 & 0 & \mathrm{i} & 0 \end{bmatrix},$$

$$\Lambda_5 := \begin{bmatrix} -\mathrm{i} & 0 & 0 & 0 \\ 0 & \mathrm{i} & 0 & 0 \\ 0 & 0 & -\mathrm{i} & 0 \\ 0 & 0 & 0 & \mathrm{i} \end{bmatrix},$$

$$\Lambda_6 := \begin{bmatrix} 1 & 0 & 0 & 0 \\ 0 & -1 & 0 & 0 \\ 0 & 0 & -1 & 0 \\ 0 & 0 & 0 & 1 \end{bmatrix},$$

$$\Lambda_7 := \begin{bmatrix} 1 & 0 & 0 & 0 \\ 0 & 1 & 0 & 0 \\ 0 & 0 & 2 & 0 \\ 0 & 0 & 0 & 2 \end{bmatrix},$$

$$\Lambda_8 := \begin{bmatrix} \mathrm{i} & 0 & 0 & 0 \\ 0 & \mathrm{i} & 0 & 0 \\ 0 & 0 & 2\mathrm{i} & 0 \\ 0 & 0 & 0 & 2\mathrm{i} \end{bmatrix},$$

then

$$U_{0,1}^{-1}(\sigma)\left(\partial_s U_{0,1}(\sigma)\right) = \Lambda_1\partial_s\sigma,$$
$$U_{2,3}^{-1}(\alpha)\left(\partial_s U_{2,3}(\alpha)\right) = \Lambda_2\partial_s\alpha,$$
$$U_{1,3}^{-1}(\vartheta)\left(\partial_s U_{1,3}(\vartheta)\right) = \Lambda_3\partial_s\vartheta,$$
$$U_{0,2}^{-1}(\phi)\left(\partial_s U_{0,2}(\phi)\right) = \Lambda_4\partial_s\phi,$$
$$U_{1,2}^{-1}(\varsigma)\left(\partial_s U_{1,2}(\varsigma)\right) = \Lambda_5\partial_s\varsigma,$$
$$U_{0,3}^{-1}(\iota)\left(\partial_s U_{0,3}(\iota)\right) = \Lambda_6\partial_s\iota,$$
$$\widehat{U}^{-1}(\kappa)\left(\partial_s\widehat{U}(\kappa)\right) = \Lambda_7\partial_s\kappa,$$
$$\widetilde{U}^{-1}(\chi)\left(\partial_s\widetilde{U}(\chi)\right) = \Lambda_8\partial_s\chi.$$

Let $\grave{U}$ be the following set:

$$\grave{U} := \left\{U_{0,1}, U_{2,3}, U_{1,3}, U_{0,2}, U_{1,2}, U_{0,3}, \widehat{U}, \widetilde{U}\right\}.$$

Because

$$U_{2,3}^{-1}(\alpha)\Lambda_1 U_{2,3}(\alpha) = \Lambda_1$$
$$U_{1,3}^{-1}(\vartheta)\Lambda_1 U_{1,3}(\vartheta) = (\Lambda_1\cos 2\vartheta + \Lambda_6\sin 2\vartheta)$$
$$U_{0,2}^{-1}(\phi)\Lambda_1 U_{0,2}(\phi) = (\Lambda_1\cosh 2\phi - \Lambda_5\sinh 2\phi)$$
$$U_{1,2}^{-1}(\varsigma)\Lambda_1 U_{1,2}(\varsigma) = \Lambda_1\cos 2\varsigma - \Lambda_4\sin 2\varsigma$$
$$U_{0,3}^{-1}(\iota)\Lambda_1 U_{0,3}(\iota) = \Lambda_1\cosh 2\iota + \Lambda_3\sinh 2\iota$$
$$\widehat{U}^{-1}(\kappa)\Lambda_1\widehat{U}(\kappa) = \Lambda_1$$
$$\widetilde{U}^{-1}(\chi)\Lambda_1\widetilde{U}(\chi) = \Lambda_1$$
========

$$\widetilde{U}^{-1}(\chi)\,\Lambda_2\widetilde{U}(\chi)=\Lambda_2$$
$$\widehat{U}^{-1}(\kappa)\,\Lambda_2\widehat{U}(\kappa)=\Lambda_2$$
$$U_{0,3}^{-1}(\iota)\,\Lambda_2U_{0,3}(\iota)=\Lambda_2\cosh 2\iota-\Lambda_4\sinh 2\iota$$
$$U_{1,2}^{-1}(\varsigma)\,\Lambda_2U_{1,2}(\varsigma)=\Lambda_2\cos 2\varsigma-\Lambda_3\sin 2\varsigma$$
$$U_{0,2}^{-1}(\phi)\,\Lambda_2U_{0,2}(\phi)=\Lambda_2\cosh 2\phi+\Lambda_6\sinh 2\phi$$
$$U_{1,3}^{-1}(\vartheta)\,\Lambda_2U_{1,3}(\vartheta)=\Lambda_2\cos 2\vartheta+\Lambda_5\sin 2\vartheta$$
$$U_{0,1}^{-1}(\sigma)\,\Lambda_2U_{0,1}(\sigma)=\Lambda_2$$
$$=========$$
$$U_{0,1}^{-1}(\sigma)\ \Lambda_3U_{0,1}(\sigma)=\Lambda_3\cosh 2\sigma-\Lambda_6\sinh 2\sigma$$
$$U_{2,3}^{-1}(\alpha)\ \Lambda_3U_{2,3}(\alpha)=\Lambda_3\cos 2\alpha-\Lambda_5\sin 2\alpha$$
$$U_{0,2}^{-1}(\phi)\ \Lambda_3U_{0,2}(\phi)=\Lambda_3$$
$$U_{1,2}^{-1}(\varsigma)\ \Lambda_3U_{1,2}(\varsigma)=\Lambda_3\cos 2\varsigma+\Lambda_2\sin 2\varsigma$$
$$U_{0,3}^{-1}(\iota)\ \Lambda_3U_{0,3}(\iota)=\ \Lambda_3\cosh 2\iota+\Lambda_1\sinh 2\iota$$
$$\widehat{U}^{-1}(\kappa)\ \Lambda_3\widehat{U}(\kappa)=\Lambda_3$$
$$\widetilde{U}^{-1}(\chi)\ \Lambda_3\widetilde{U}(\chi)=\Lambda_3$$
$$==========$$
$$\widetilde{U}^{-1}(\chi)\ \Lambda_4\widetilde{U}(\chi)=\Lambda_4$$
$$\widehat{U}^{-1}(\kappa)\ \Lambda_4\widehat{U}(\kappa)=\Lambda_4$$
$$U_{0,3}^{-1}(\iota)\ \Lambda_4U_{0,3}(\iota)=\Lambda_4\cosh 2\iota-\Lambda_2\sinh 2\iota$$
$$U_{1,2}^{-1}(\varsigma)\ \Lambda_4U_{1,2}(\varsigma)=\Lambda_4\cos 2\varsigma+\Lambda_1\sin 2\varsigma$$
$$U_{1,3}^{-1}(\vartheta)\ \Lambda_4U_{1,3}(\vartheta)=\Lambda_4$$
$$U_{2,3}^{-1}(\alpha)\ \Lambda_4U_{2,3}(\alpha)=\Lambda_4\cos 2\alpha-\Lambda_6\sin 2\alpha$$
$$U_{0,1}^{-1}(\sigma)\ \Lambda_4U_{0,1}(\sigma)=\Lambda_4\cosh 2\sigma+\Lambda_5\sinh 2\sigma$$
$$==========$$
$$U_{0,1}^{-1}(\sigma)\ \Lambda_5U_{0,1}(\sigma)\ =\Lambda_5\cosh 2\sigma+\Lambda_4\sinh 2\sigma$$
$$U_{2,3}^{-1}(\alpha)\ \Lambda_5U_{2,3}(\alpha)\ =\Lambda_5\cos 2\alpha+\Lambda_3\sin 2\alpha$$
$$U_{1,3}^{-1}(\vartheta)\ \Lambda_5U_{1,3}(\vartheta)\ =(\Lambda_5\cos 2\vartheta-\Lambda_2\sin 2\vartheta)$$
$$U_{0,2}^{-1}(\phi)\ \Lambda_5U_{0,2}(\phi)\ =\Lambda_5\cosh 2\phi-\Lambda_1\sinh 2\phi$$
$$U_{0,3}^{-1}(\iota)\ \Lambda_5U_{0,3}(\iota)\ =\Lambda_5$$
$$\widehat{U}^{-1}(\kappa)\ \Lambda_5\widehat{U}(\kappa)\ =\Lambda_5$$
$$\widetilde{U}^{-1}(\chi)\,\Lambda_5\widetilde{U}(\chi)\ =\Lambda_5$$
$$==========$$
$$\widetilde{U}^{-1}(\chi)\,\Lambda_6\widetilde{U}(\chi)\ =\Lambda_6$$
$$\widehat{U}^{-1}(\kappa)\,\Lambda_6\widehat{U}(\kappa)\ =\Lambda_6$$
$$U_{1,2}^{-1}(\varsigma)\,\Lambda_6U_{1,2}(\varsigma)\ =\Lambda_6$$
$$U_{0,2}^{-1}(\phi)\,\Lambda_6U_{0,2}(\phi)\ =\Lambda_6\cosh 2\phi+\Lambda_2\sinh 2\phi$$
$$U_{1,3}^{-1}(\vartheta)\,\Lambda_6U_{1,3}(\vartheta)\ =\Lambda_6\cos 2\vartheta-\Lambda_1\sin 2\vartheta$$
$$U_{2,3}^{-1}(\alpha)\,\Lambda_6U_{2,3}(\alpha)\ =\Lambda_6\cos 2\alpha+\Lambda_4\sin 2\alpha$$
$$U_{0,1}^{-1}(\sigma)\,\Lambda_6U_{0,1}(\sigma)=\Lambda_6\cosh 2\sigma-\Lambda_3\sinh 2\sigma$$
$$========$$
$$\widetilde{U}^{-1}(\chi)\ \Lambda_7\widetilde{U}(\chi)=\Lambda_7$$
$$U_{0,3}^{-1}(\iota)\ \Lambda_7U_{0,3}(\iota)=\Lambda_7$$
$$U_{1,2}^{-1}(\varsigma)\ \Lambda_7U_{1,2}(\varsigma)=\Lambda_7$$
$$U_{0,2}^{-1}(\phi)\ \Lambda_7U_{0,2}(\phi)=\Lambda_7$$
$$U_{1,3}^{-1}(\vartheta)\ \Lambda_7U_{1,3}(\vartheta)=\Lambda_7$$
$$U_{2,3}^{-1}(\alpha)\ \Lambda_7U_{2,3}(\sigma)=\Lambda_7$$
$$U_{0,1}^{-1}(\sigma)\ \Lambda_7U_{0,1}(\sigma)=\Lambda_7$$
$$=========$$
$$U_{0,1}^{-1}(\sigma)\ \Lambda_8U_{0,1}(\sigma)=\Lambda_8$$
$$U_{2,3}^{-1}(\alpha)\ \Lambda_8U_{2,3}(\alpha)=\Lambda_8$$
$$U_{1,3}^{-1}(\vartheta)\ \Lambda_8U_{1,3}(\vartheta)=\Lambda_8$$
$$U_{0,2}^{-1}(\phi)\ \Lambda_8U_{0,2}(\phi)=\Lambda_8$$
$$U_{1,2}^{-1}(\varsigma)\ \Lambda_8U_{1,2}(\varsigma)=\Lambda_8$$
$$U_{0,3}^{-1}(\iota)\ \Lambda_8U_{0,3}(\iota)=\Lambda_8$$
$$\widehat{U}^{-1}(\kappa)\ \Lambda_8\widehat{U}(\kappa)=\Lambda_8$$

then for every product U of $\grave{U}$'s elements real functions $G_s^r(t,x_1,x_2,x_3)$ exist such that

$$U^{-1}(\partial_sU)=\frac{g_3}{2}\sum_{r=1}^{8}\Lambda_rG_s^r$$

with some real constant g_3 (similar to 8 gluons).

4 Conclusion

Therefore, unessential restrictions on 4X1 matrix functions give Dirac's equations, and it seems that some gluon and gravity phenomena can be explained with the help of these equations.

Submitted on February 16, 2009 / Accepted on February 18, 2009

References

1. Madelung E. Die Mathematischen Hilfsmittel des Physikers. Springer Verlag, 1957, 29.
2. Ziman J.M. Elements of advanced quantum theory. Cambridge University Press, 1969, formula (6.59).

Key Notes on a Geometric Theory of Fields

Ulrich E. Bruchholz

Schillerstrasse 36, D-04808 Wurzen, Germany
http://www.bruchholz-acoustics.de

The role of potentials and sources in electromagnetic and gravitational fields is investigated. A critical analysis leads to the result that sources have to be replaced by integration constants. The existence of spatial boundaries gives reasons for this step. Potentials gain physical relevance first with it. The common view, that fields are "generated" by sources, appears as not tenable. Fields do exist by their own. These insights as well as results from numerical simulations force the conclusion that a Riemannian-geometrical background of electromagnetism and even quantum phenomena cannot be excluded. Nature could differ from abstract geometry in a way that distances and intervals never become infinitesimally small.

1 Introduction

In Physics a unified theory including all phenomena of nature is considered as the greatest challenge. All attempts founded on the present definition of matter have manifested to fail. It will require a redefinition of this term.

The traditional view consists on the assumption that matter "generates" fields. All effort aims at the description of this matter, detached from fields, at least from gravitation. This single-edged view led to the known problems and cannot bring more than stagnation. One had to unify different *methods* being used for handling of different physical situations. Also new mathematical procedures cannot help to master this unsolvable problem.

The traditional mathematical description puts the matter on the right-hand-side of partial differential equations, while the left-hand-side contains differential terms of the field quantities. However, practice demonstrates that only field quantities are measurable, never any form of matter terms. If we consider the practice impartially, the right-hand-sides of the field equations have to become zero. That means, there are no sources of fields.

There are severe caveats in physics against this conclusion. However, it will be demonstrated that any infinities like singular points are physically irrelevant. Connecting electromagnetism to gravitation without obstacles is only possible avoiding sources.

In this paper, solutions of known linear field equations (electromagnetism and gravitation) with and without sources are compared, in which, integration constants from source-free equations take the role of sources. Mass, spin, charge, magnetic momentum are first integration constants. The nonlinear case will validate the linear basic approach. Boundaries, introduced to solve linear source-free equations, reveal to be geometric limits in the space-time, described by nonlinear equations. This fact makes any artifacts unnecessary. The theory can be managed with exclusively classical mathematical methods.

These insights are not familiar in physics, because the present standard is the Quantum Field Theory [1, 2], in which the most known part, the Standard Model, is told to be very successful and precise [3, 4]. The existence of subatomic particles has been deduced from scattering experiments [3]. The field term, used in these theories, differs considerably from the classical field term. Actually, these theories are founded on building block models which more seem to aim at a phenomenology of a "particle zoo" than a description of nature based on first principles. In order to describe the interactions between particles respectively sub-particles, it needs the introduction of virtual particles like the Higgs, which have not been experimentally verified to date.* By principle, the subatomic particles cannot be observed directly. — Are the limits of classical methods really so narrow, that they would justify these less strict methods of natural philosophy?

The mathematical methods are more and more advanced (for example introducing several "gauge fields") according to the requirements by the building block models. However, these methods approach to limits [3, 4]. Gravitation must be handled external to the model and appears as an external force. The deeper reason is that the standard model is based on Special Relativity while gravitation is the principal item of General Relativity. These differences are inherent and do not lead to a comprehensive model which reflects the fact that gravitation and electromagnetism have analogous properties. Pursuing theories like string theory (quoted by [4]) do not really close this gap. Any predictions or conjectures are not validated, as demonstrated for example in [6].

The central question of modern physics is: How to quantize field theory? [4] In view of the looming limits, another question is proposed instead: Which quantities have discrete values? — In order to answer this alternative question, we

*Manfred Geilhaupt claims to "provide" a kind of "Higgs field" in his theory, called GR+QTD (General Relativity + Quantum Thermodynamics) by him [5]. It were a step beyond virtual particles "because they possess restmass itself due to TD principles. Second it also seems to be obvious that the fine structure constant of space fundamentally can be derived by GR but not without precursor extended by QTD" [5].

have to go back to the roots. That are Maxwell's theory and General Theory of Relativity as Einstein himself taught in his Four Lectures [7]. The simple approach of these basics should be a specific benefit, and a low standard by no means. We have to take notice of any proportions of forces (how extreme these may ever be), and to accept the direct consequences like the non-existence of sources (as explained in this paper) and the non-applicability of building block models. *We have to compare not forces but the fields with respect to metrics.*[*] The following lines will make General Relativity provide the basis which can describe all real forces of nature.

2 Electromagnetism

As known, electromagnetic fields in the vacuum can be described by Maxwell's equations, with tensor notation[†]

$$F_{ij,k} + F_{jk,i} + F_{ki,j} = 0\,, \tag{1}$$

$$F^{ia}{}_{;a} = S^i \tag{2}$$

where $\mathcal{S}$ is the vector of source terms. With Eq. (1), the field tensor is identically representable from a vector potential $\mathcal{A}$ with

$$F_{ik} = A_{i,k} - A_{k,i}\,. \tag{3}$$

The six independent components of the field tensor are reduced to four components of the vector potential. These four components can be put in the four equations (2).

If one changes the vector potential for the gradient of an arbitrary scalar

$$A_i \Longrightarrow A_i + \psi_{,i}\,, \tag{4}$$

field tensor and source $\mathcal{S}$ (currents and charges) do not change. These quantities are told to be gauge-invariant [9][‡].

The vector potential has been introduced to solve equations (2). It is at first an auxiliary quantity. Reasons for possible physical relevance are mentioned later. However, the Aharonov-Bohm effect (for example) does not give evidence for the physical relevance of vector potential and gauge, as Bruhn [10] demonstrated.

2.1 The Poisson equation

In order to get more close solutions, one can apply the Lorenz convention (see [9])

$$A^i{}_{;i} = 0\,. \tag{5}$$

One may not confuse the Lorenz convention with a gauge, because it is an *arbitrary* condition.[§] *This condition could reduce the possible set of solutions.*

Simplified equations result with Cartesian coordinates

$$\Box\mathcal{A} = -\mathcal{S}\,, \tag{6}$$

with the retarded potential

$$\mathcal{A} = \frac{1}{4\pi}\int \frac{\mathcal{S}(\mathbf{r}_0, ct - |\mathbf{r}-\mathbf{r}_0|)}{|\mathbf{r}-\mathbf{r}_0|}\,\mathrm{d}V_0 \tag{7}$$

as solution (without spatial boundaries).

Time-independent solutions

$$\mathcal{A} = \frac{1}{4\pi}\int \frac{\mathcal{S}(\mathbf{r}_0)}{|\mathbf{r}-\mathbf{r}_0|}\,\mathrm{d}V_0 \tag{8}$$

can be decomposed into several multipoles. As well, the term $1/|\mathbf{r}-\mathbf{r}_0|$ is developed in series. The vector potential results in

$$\mathcal{A} = \frac{1}{4\pi}\sum_{i=0}^{\infty}\frac{1}{r^{i+1}}\int {r_0}^i\,\mathsf{P}_i\left(\frac{\mathbf{r}\cdot\mathbf{r}_0}{r\,r_0}\right)\cdot\mathcal{S}(\mathbf{r}_0)\,\mathrm{d}V_0 \tag{9}$$

with $r = |\mathbf{r}|$, $r_0 = |\mathbf{r}_0|$. P_i are Legendre's polynoms (Wunsch [11]).

Introducing spherical coordinates with

$$x = r\sin\vartheta\sin\varphi\,,\ y = r\sin\vartheta\cos\varphi\,,\ z = r\cos\vartheta\,, \tag{10}$$

in which

$$x^1 = r\,,\ x^2 = \vartheta\,,\ x^3 = \varphi\,,\ x^4 = \mathsf{j}ct \tag{11}$$

(with $\mathsf{j}^2 = -1$), the argument is

$$\frac{\mathbf{r}\cdot\mathbf{r}_0}{r\,r_0} = \sin\vartheta\sin\vartheta_0\cos(\varphi-\varphi_0)\ +\ \cos\vartheta\cos\vartheta_0\,. \tag{12}$$

By this, the fixed volume integrals become functions of ϑ and φ. Rotationally symmetric ansatzes

$$\rho(r_0, \vartheta_0, \varphi_0) = \rho(r_0, \vartheta_0) \tag{13}$$

(charge density), and[¶]

$$J_\varphi(r_0, \vartheta_0, \varphi_0) = J_\varphi(r_0, \vartheta_0, \varphi)\cdot\cos(\varphi-\varphi_0) \tag{14}$$

(current density) lead to momenta that will be compared with the solutions from wave equations. The calculation of the first momenta, i.e. charge and magnetic momentum, is demonstrated in [12]. As well, the charge follows directly as a first approximation of the volume integral from Eq. (8). The magnetic momentum is calculated with a current loop model, see [12].

2.2 The wave equation

The wave equation follows from the Poisson equation if the sources vanish, i.e.

$$\Box\mathcal{A} = 0\,. \tag{15}$$

[*] See more Section 6.1

[†] The tensor equations have been normalized, see Kästner [8] and appendix.

[‡] Bruhn explains these basics with traditional notation.

[§] This condition is mostly met, but it is not ensured.

[¶] Condition (14) excludes the existence of magnetic monopoles.

2.2.1 The plane wave

A known solution is the plane wave, for propagation in direction of x^1 (with Cartesian coordinates, without gravitation)

$$A_2 = A_2(ct - x^1)\,. \tag{16}$$

One can take A_3 instead of A_2. However, A_1 and A_4 are irrelevant for the Lorenz convention, because this takes

$$A_4{}' = \mathrm{j}A_1{}'\,, \tag{17}$$

in which the apostrophe means the total derivative with respect to $ct - x^1$. The component F_{41} is always zero for that reason, and F_{23} vanishes anyway. It is the reason for the very fact that longitudinal electromagnetic waves (also called scalar waves) do not exist. The Lorenz convention is the prerequisite of the wave equation.

This solution is not physical, and has to be discussed in context with gravitation. A special kind of boundary could make plane waves physical. A possible context with Planck's constant is discussed in [17].

2.2.2 The spherical wave

The central symmetrical ansatz can be written for any scalar potential, and components treated by this means,

$$c^2\,\frac{\partial^2}{\partial r^2}(r\phi) = \frac{\partial^2}{\partial t^2}(r\phi) \tag{18}$$

with the solution

$$r\phi = Z(ct \mp r) \tag{19}$$

(Reichardt [13]), in which only the minus sign might be relevant here.

Transforming to the potential itself becomes problematical at $r = 0$. We shall see that this critical point proves to be physically irrelevant. Aware of this, one could take this solution as element of the retarded potential according to Eq. (7).

A spherical boundary around $r = 0$ does not change this solution at and outside of the boundary, and eliminates the mathematical problem. The solution is linked with the potential of the boundary then.

Since the boundary is part of the field, the question for cause and effect becomes irrelevant.

2.2.3 Time-independent solutions

Static solutions of the wave equation require the existence of spatial boundaries. That may be ideal conductors in electric fields, or hard bodies in sound fields. These problems are known as "marginal-problems" (for example [14, 15]). The values of integration constants in the solutions are linked with the potentials of the boundaries against infinity*. That may grant certain physical relevance to potentials. Of course, the wave equation is valid only out of the boundary. We shall see that regions within close boundaries are physically irrelevant.†

Let us confine the problem to a close boundary around $r = 0$. This restriction allows development of series (see [12, 16]), which were otherwise singular just at this point.

The wave equations for several components become for rotational symmetry with spherical coordinates

$$\frac{\partial^2 A_4}{\partial r^2} + \frac{2}{r}\frac{\partial A_4}{\partial r} + \frac{1}{r^2}\frac{\partial^2 A_4}{\partial \vartheta^2} + \frac{1}{r^2}\frac{\partial A_4}{\partial \vartheta}\cot\vartheta = 0 \tag{20}$$

(electric potential) and

$$\frac{\partial^2 A_3}{\partial r^2} + \frac{1}{r^2}\frac{\partial^2 A_3}{\partial \vartheta^2} - \frac{1}{r^2}\frac{\partial A_3}{\partial \vartheta}\cot\vartheta = 0 \tag{21}$$

(magnetic vector potential). The magnetic vector potential consists of only one component in direction of the azimuth

$$A_3 = A_\varphi\, r\sin\vartheta\,, \tag{22}$$

in which A_φ means the *physical* component.‡

The differently looking equations (20) and (21) follow from coordinate transformation.

Developments of series with ansatzes

$$A_4 = \sum_{i,k} a_{[4]\,i,k}\, r^i \cos^k\vartheta\,,$$

$$A_3 = \sum_{i,k} a_{[3]\,i,k}\, r^i \sin^k\vartheta \tag{23}$$

lead, by means of comparison of the coëfficients, to the performing laws

$$0 = a_{[4]\,i,k}\cdot[i(i+1) - k(k+1)] + a_{[4]\,i,k+2}\cdot(k+1)(k+2)\,,$$

$$0 = a_{[3]\,i,k}\cdot[i(i-1) - k(k-1)] + a_{[3]\,i,k+2}\cdot k(k+2)\,. \tag{24}$$

Physically meaningful are only the cases $i < 0$ and $k \geqslant 0$. With this, the series become

$$\begin{aligned} A_4 &= \frac{a_{[4]\,-1,0}}{r} + \frac{a_{[4]\,-2,1}}{r^2}\cdot\cos\vartheta + \\ &+ \frac{a_{[4]\,-3,2}}{r^3}\cdot\left(-\frac{1}{3} + \cos^2\vartheta\right) + \dots\,, \\ A_\varphi &= \sin\vartheta\cdot\left\{\frac{a_{[3]\,-1,2}}{r^2} + \frac{a_{[3]\,-2,3}}{r^3}\cdot\sin\vartheta + \right. \\ &\left. + \frac{a_{[3]\,-3,4}}{r^4}\cdot\left(-\frac{4}{5} + \sin^2\vartheta\right) + \dots\right\}. \end{aligned} \tag{25}$$

*as long as we have to do with a quasi flat space-time

†Who insists on sources may take these regions as source. Lastly the connection of electromagnetism with gravitation will show, that this step is illogical.

‡On physical components see Kästner [8].

A comparison of these solutions with static solutions of the Poisson equation results for the first integration constants in

$$a_{[4]-1,0} = -\mathrm{j}\,\frac{{\mu_0}^{\frac{1}{2}}\,Q}{4\pi} \tag{26}$$

(charge) and

$$a_{[3]-1,2} = -\,\frac{{\varepsilon_0}^{\frac{1}{2}}\,M}{4\pi} \tag{27}$$

(magnetic momentum).

Integration constants take the role of the sources. In more complex solutions, the $1/r$ field from point charges (for example) is assumed only for a large radius.

3 Gravitation

Another kind of potential can be derived from Einstein's [7] gravitation equations

$$R_{ik} - \frac{1}{2}\,g_{ik}\,R = -\kappa\,T_{ik}\,, \tag{28}$$

or

$$R_{ik} = -\kappa\,(T_{ik} - \frac{1}{2}\,g_{ik}\,T) = -\kappa\,{T_{ik}}^{*} \tag{29}$$

with $T = {T_a}^a$. These equations indicate the relations of the Ricci tensor with energy and momentum components. The Ricci tensor is a purely geometrical quantity of the spacetime. It contains differential terms of metrics components.

One can approximate metrics, with Cartesian coordinates, as

$$g_{ik} = \delta_{(ik)} + \gamma_{(ik)} \quad \text{with} \quad |\gamma_{(ik)}| \ll 1\,. \tag{30}$$

The $\gamma_{(ik)}$ are "physical components" of metrics and have the character of a potential.

The arbitrary conditions

$$0 = \frac{\partial\gamma_{(ia)}}{\partial x^a} - \frac{1}{2}\,\frac{\partial\gamma_{(aa)}}{\partial x^i} \tag{31}$$

may be the analogy of the Lorenz convention. These lead to Poisson equations

$$\Box\gamma_{(ik)} = 2\kappa\,{T_{ik}}^{*}\,, \tag{32}$$

with retarded potentials as solution

$$\gamma_{(ik)} = -\frac{\kappa}{2\pi}\int\frac{{T_{ik}}^{*}(\mathbf{r}_0, ct - |\mathbf{r}-\mathbf{r}_0|)}{|\mathbf{r}-\mathbf{r}_0|}\,\mathrm{d}V_0\,. \tag{33}$$

Using the energy-momentum tensor of the distributed mass

$$T^{ik} = \sigma\,\frac{\mathrm{d}x^i}{\mathrm{d}s}\,\frac{\mathrm{d}x^k}{\mathrm{d}s}\,, \tag{34}$$

in which σ be the mass density, static solutions result approximately in

$$\gamma_{(11)} = \gamma_{(22)} = \gamma_{(33)} = +\frac{\kappa}{4\pi}\int\frac{\sigma(\mathbf{r}_0)}{|\mathbf{r}-\mathbf{r}_0|}\,\mathrm{d}V_0\,, \tag{35}$$

$$\gamma_{(44)} = -\frac{\kappa}{4\pi}\int\frac{\sigma(\mathbf{r}_0)}{|\mathbf{r}-\mathbf{r}_0|}\,\mathrm{d}V_0\,, \tag{36}$$

the rest zero (Einstein [7]). This approximation is not more sufficient for the calculation of the spin.

The actual field quantity might be the curvature vector (Eisenhart [19]) of the world-line described by the test body

$$k^i = \frac{\mathrm{d}x^a}{\mathrm{d}s}\left(\frac{\mathrm{d}x^i}{\mathrm{d}s}\right)_{;a} = \frac{\mathrm{d}^2x^i}{\mathrm{d}s^2} + \left\{\begin{smallmatrix} a & i \\ & b \end{smallmatrix}\right\}\frac{\mathrm{d}x^a}{\mathrm{d}s}\,\frac{\mathrm{d}x^b}{\mathrm{d}s}\,, \tag{37}$$

because it acts as a force to the body by its mass.

With distributed mass, the force density becomes

$$K^i = {T^{ia}}_{;a} = \sigma k^i\,. \tag{38}$$

The force balance* is given only with $\sigma = 0$, unless one uses discrete masses. These are integration constants from $\Box\gamma_{(44)} = 0$. In this case, force balance is obtained with the equations of geodesics [19]

$$k^i = 0\,. \tag{39}$$

The curvature vector also contains accelerated motion, this is the most simple interpretation of the equivalence principle. The equations of geodesics become equations of motion with it.

The wave equations are analogous to those of electromagnetism, that means also analogous series and analogous integration constants (using spherical coordinates)

$$a_{[44]-1,0} = -\,\frac{\kappa\,m}{4\pi} \tag{40}$$

(mass) and

$$a_{[34]-1,2} = \mathrm{j}\,\frac{\kappa\,s}{4\pi c} \tag{41}$$

(spin). The analogy of the current loop is a spinning torus [12]. It must be explicitly pointed out that this model is *not* sufficient to represent the known proportions between mass and spin, or charge and magnetic momentum, respectively. This inconsistency is removed by integration constants.

Another derivation tries to omit boundaries [16], however, it is not supported by numerical simulations. The boundaries will have a direct geometrical meaning.

4 Connection of electromagnetism with gravitation

Electromagnetism can be connected with gravitation via the energy-momentum tensor of the electromagnetic field

$$T_{ik} = F_{ia}{F_k}^a - \frac{1}{4}\,g_{ik}F_{ab}F^{ab}\,, \tag{42}$$

with the force density

$$K^i = {T^{ia}}_{;a} = {F^i}_a S^a\,. \tag{43}$$

*Respectively energy conservation, mathematically expressed with the Bianchi identities [19] in Einstein's equations.

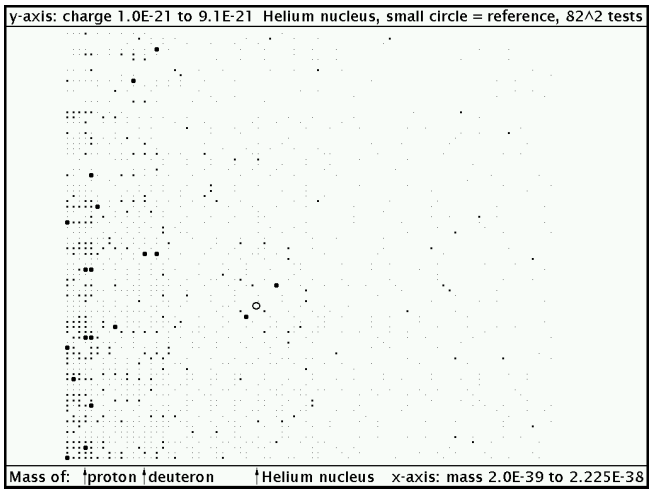

Fig. 1: Tests with parameters around the Helium nucleus

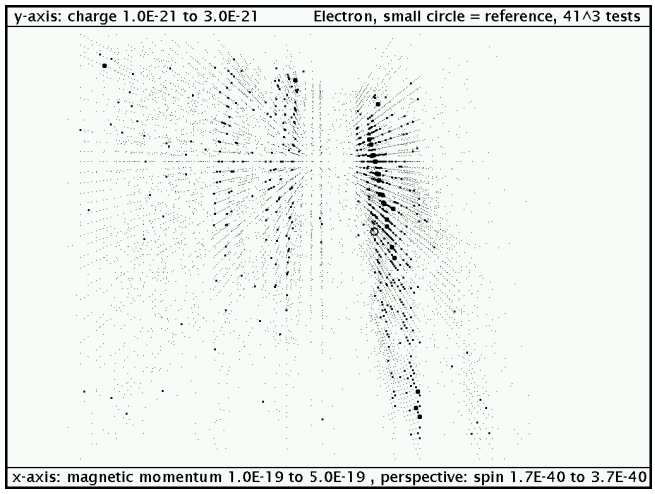

Fig. 2: Tests with parameters around the electron

Force balance is only given with $S^i = 0$. Using this energy-momentum tensor means, there is no choice: The sources *must* vanish, with them the divergences of the field tensor

$$F^{ia}{}_{;a} = 0\,. \tag{44}$$

Einstein stated this already in his Four Lectures [7]. This step is possible, as explained.

The necessity of this energy-momentum tensor to have just this form is also derived by Montesinos and Flores [21] based on Noether's theorem [22], but only without sources.

Numerical simulations according to source-free Einstein-Maxwell equations [18] demonstrate that the areas around possible formal singularities do not exist at all. Also known analytic solutions of Einstein's equations like the isotropic Schwarzschild solution [7], [19] indicate this. The event horizon here is the boundary. In general, a geometric boundary is given when physical components of metrics take an absolute value of 1. It is a kind of horizon in any case. We have to suppose it at the conjectural radius of the particle respectively nucleus, for chaos from the non-linear field equations (see next section).

However, any additional terms or extended methods cannot really repair the inconsistencies from the sources.

For $T = 0$ and $R = 0$, Einstein's equations now result in

$$R_{ik} = \kappa \left(\frac{1}{4}\, g_{ik} F_{ab} F^{ab} - F_{ia} F_k{}^a \right). \tag{45}$$

Equations (1), (44), and (45) involve a special Riemannian geometry of the space-time, as explained in [12] and [20]. The field tensor becomes a curve parameter of the world-lines like the curvature vector.

5 On numerical simulations

The precedingly explained insights are supported by numerical simulations according to equations (3), (44), and (45). Recent robust results can be seen at [23], including the Pascal code of the used program, and a program visualizing these results.

Algorithms and simulation techniques are discussed in [18], as well as the method of approximating the partial differential equations by discrete ones. The principle consists in going from the known (e.g. the distant field of a point charge) to the unknown. In this paper, two visualized samples are shown.

The particle quantities like mass, spin, charge, magnetic momentum are integration constants from mentioned tensor equations, and are inserted as parameters into the initial conditions. The initial conditions start from point charges, or analogous functions for the other integration constants respectively, and are assumed only for great radius.* The non-linearities are absolutely negligible at this place.

The number of iterations during the computation up to terminating the actual test means a degree of stability of the solution, and is marked in the graphs as a more or less fat "point". The reference point (according to literature [24]) is displayed as small circle.

In tests only with mass and charge (remaining parameters zero), masses of preferably small nuclei emerge significantly, together with the right charge at the Helium nucleus, Figure 1.† Unfortunately, the procedure is too inaccurate for the electron mass. In return, the other parameters emerge very significantly, see Figure 2.

Above mentioned stability could have to do with chaos. The author had to take notice of the fact, that the numerical solutions are fundamentally different from analytic solutions. Any singularities from analytic solutions are always replaced by boundaries, which can be interpreted as geometrical limits.

The non-linear equations (which behave chaotically) lead

*Concrete initial conditions see [23], also [18].

†The masses of proton and deuteron are in a sense an add-on of the Helium nucleus tests.

always to these geometrical boundaries, which are 1) finite and 2) outside of possible singular points. Areas with singular points do not exist, i.e. are irrelevant.

One could understand this fundamental contrast by the fact that the differences in time and length are never made zero in a numerical way. The results, exclusively achieved this way, support the view that one has to assume a discrete space-time that does not give reasons for action at a distance. The continuum is only defined with action from point to point, independently on distance or interval between adjacent points.

In order to correctly depict nature, it is apparently necessary to take into consideration the deviations, appearing during the calculation with finite differences. In nature apparently these deviations do not vanish with the transition to very small differences.

Konrad Zuse asked the question, if the possibility to arbitrarily subdivide quantities is "conceivable at all" in nature [25]. Common imagination of a consequent quantization leads to the problem of privileged coordinates, or a privileged frame [25]. Nature has never indicated it. However, it is successful practice in electrical engineering to adapt the coordinates to the actual problem (Wunsch [11]). Linear equations showed to be insensitive to the selection of coordinates. It requires intense research work to prove the chaotic behaviour of the non-linear equations dependent on the coordinates. The author was so fortunate to see the mentioned correlations with spherical coordinates. As well, the correlations became highly significant when the raster distances were the same tangentially as well as radially ($\mathrm{d}r = r\ \mathrm{d}\vartheta$) just at the conjectural particle radius.

6 Concluding remarks

If the obtained insights are right, all quantum phenomena should be understandable by them. At this place, tunnel effects are mentioned. This example is supplemented with very brief but essential remarks on causality.

6.1 On tunnel effects

Equations (1), (44), and (45) allow structures, in which a finite distance (as the outer observer sees it) can locally become zero, but metrics does not become singular. That were a real tunnel with an "inner" length of zero. An event at the one side is "instantaneously" seen at the other side. A known effect, that could be interpreted this way, is the EPR effect [26, 27]. Such tunnels might arise by accident.*

This view is supported with changes of metrics by electromagnetism. Distances are locally shortened (at electric fields in direction of the field strength), what can lead to a feedback. Trump and van de Graaf have measured the flashover in the vacuum, dependent on the distance of the electrodes (Kapcov [28]). As well, the product of voltage and field strength was nearly constant

$$U \cdot E \approx 10^{13}\mathrm{V}^2\ \mathrm{m}^{-1}\,. \tag{46}$$

That means

$$\frac{\partial g_{11}}{\partial r} \approx -2\times10^{-41}\ \mathrm{m}^{-1}\,. \tag{47}$$

One will not see these tiny changes, but they are apparently enough to release lightning etc.

On the whole, the influence of gravitation prevails, so that the space-time is macroscopically stable. Table 1 shows the arithmetical deviations of metrics at a radius of 10^{-15} m, that is roughly the conjectural radius of nuclei.

	proton	free electron
$\gamma_{(11)}(-\gamma_{(44)})$ from mass	2.48×10^{-39}	1.30×10^{-42}
$\gamma_{(11)}$ from charge	-1.85×10^{-42}	-1.85×10^{-42}
$\gamma_{(34)}$ from spin	$\mathrm{j}\,2.60\times10^{-40}$	$\mathrm{j}\,2.60\times10^{-40}$
$\gamma_{(34)}$ from charge times magn. momentum	$-\mathrm{j}\,5.57\times10^{-43}$	$-\mathrm{j}\,3.6\times10^{-40}$
$\gamma_{(33)}$ from magn. momentum (ambiguous)	-1.64×10^{-43}	-6.84×10^{-38}

Table 1: The arithmetical deviations of metrics at 10^{-15} m.

The influence by mass decreases with $1/r$, however, that by charge and spin with $1/r^2$, and that by magnetic momentum with $1/r^4$.

6.2 On causality

Firstly, equations (3), (44), and (45) provide 10 independent equations for 14 components g_{ik} , A_i . With it, causality is not given in principle. It is false to claim, a geometric approach would imply causality. Geometry has nothing to do with causality, because causality has not been geometrically defined at all.

If we see something causal, it comes from approximations by wave equations, as precedingly explained. These provide close solutions.

Appendix

"Classical" electric and magnetic fields in the vacuum are joined to an antisymmetric tensor of 2nd rank

$$\mathcal{D} = \varepsilon_0\mathcal{E} = \mathrm{j}\mu_0{}^{-\frac{1}{2}} \begin{pmatrix} F_{(14)} \\ F_{(24)} \\ F_{(34)} \end{pmatrix}\,,$$

$$\mathcal{B} = \mu_0\mathcal{H} = \varepsilon_0{}^{-\frac{1}{2}} \begin{pmatrix} F_{(23)} \\ F_{(31)} \\ F_{(12)} \end{pmatrix}\,. \tag{48}$$

*See also the joke with Mozart's Fortieth symphony by Nimtz.

Current density and charge density result in a source vector $\mathcal{S}$

$$\mathcal{J} = c\mu_0{}^{-\frac{1}{2}} \begin{pmatrix} S_{(1)} \\ S_{(2)} \\ S_{(3)} \end{pmatrix}, \qquad \rho = -\mathrm{j}\mu_0{}^{-\frac{1}{2}} S_{(4)}\,. \tag{49}$$

The indices in parentheses stand for physical components. See also Kästner [8].

Acknowledgement

The author owes interesting, partly controversy discussions, throwing light upon, to a circle with the gentlemen Prof. Manfred Geilhaupt, Wegberg (Germany), Dr. Gerhard Herres, Paderborn (Germany), and the psychologist Werner Mikus, Köln (Cologne, Germany). Special thanks are due to Prof. Arkadiusz Jadczyk, Castelsarrasin (France), who accompanied the article with critical questions and valuable hints, and Dr. Horst Eckardt, München (Munich, Germany), who carefully looked over this paper.

Submitted on February 19, 2009 / Accepted on February 23, 2009

References

1. Siegel W. Fields. arXiv: hep-th/9912205.
2. Wilczek F. Quantum field theory. *Review of Modern Physics*, 1999, v. 71, 85–S95; arXiv: hep-th/9803075.
3. Roy D.P. Basic constituents of matter and their interactions — a progress report. arXiv: hep-ph/9912523.
4. 't Hooft G. The conceptual basis of quantum field theory. Lectures given at Institute for Theoretical Physics, Utrecht University, and Spinoza Institute, Utrecht, the Netherlands, 2005, http://www.phys.uu.phys.nl/~thooft/lectures/basisqft.pdf
5. Geilhaupt M. Private information, 2008. See also: Geilhaupt M. and Wilcoxen J. Electron, universe, and the large numbers between. http://www.wbabin.net/physics/mj.pdf
6. Price J.C. et al. Upper limits to submillimetre-range forces from extra space-time dimensions. *Nature*, 2003, v. 421, 922–925.
7. Einstein A. Grundzüge der Relativitätstheorie. (A back-translation from the Four Lectures on Theory of Relativity.) Akademie-Verlag Berlin, Pergamon Press Oxford, Friedrich Vieweg & Sohn Braunschweig, 1969.
8. Kästner S. Vektoren, Tensoren, Spinoren. Akademie-Verlag, Berlin, 1960.
9. Bruhn G.W. Gauge theory of the Maxwell equations. Fachbereich Mathematik der TU Darmstadt, http://www.mathematik.tu-darmstadt.de/~bruhn/Elektrodynamik.html
10. Bruhn G.W. Zur Rolle des magnetischen Vektorpotentials beim Aharonov-Bohm-Effekt. Fachbereich Mathematik der TU Darmstadt, http://www.mathematik.tu-darmstadt.de/~bruhn/Elektrodynamik.html
11. Wunsch G. Theoretische Elektrotechnik. Lectures at Technische Universität Dresden, 1966–1968.
12. Bruchholz U. Zur Berechnung stabiler elektromagnetischer Felder. *Z. elektr. Inform.- u. Energietechnik*, Leipzig, 1980, v. 10, 481–500.
13. Reichardt W. Physikalische Grundlagen der Elektroakustik. Teubner, Leipzig, 1961.
14. Skudrzyk E. Die Grundlagen der Akustik. Wien, 1954.
15. Lenk A. Ausgewählte Kapitel der Akustik. Lectures at Technische Universität Dresden, 1969.
16. Bruchholz U. Berechnung elementarer Felder mit Kontrolle durch die bekannten Teilchengrößen. Experimentelle Technik der Physik, Jena, 1984, v. 32, 377–385.
17. Bruchholz U. Derivation of Planck's constant from Maxwell's electrodynamics. http://bruchholz.psf.net/h-article.pdf; http://UlrichBruchholz.homepage.t-online.de/HomepageClassic01/h-article.pdf
18. An obsolete report is to find at http://bruchholz.psf.net or http://UlrichBruchholz.homepage.t-online.de; See also a German-language textbook, Chapter 4.
19. Eisenhart L.P. Riemannian geometry. Princeton university press, 1949.
20. Bruchholz U. Ricci main directions in an EM vacuum. 2001. Look for improved articles at http://bruchholz.psf.net; http://UlrichBruchholz.homepage.t-online.de
21. Montesinos M. and Flores E. Symmetric energy-momentum tensor in Maxwell, Yang-Mills, and Proca theories obtained using only Noether's theorem. arXiv: hep-th/0602190.
22. Noether E. Invariante Variationsprobleme. *Nachr. d. König. Gesellsch. d. Wiss. zu Göttingen*, *Math-phys. Klasse*, 1918, 235–257 (English translation by M. A. Tavel in: *Transport Theory and Statistical Physics*, 1971, v. 1(3), 183–207; arXiv: physics/0503066).
23. Recent visible data are in the packages http://www.bruchholz-acoustics.de/robust.tar.gz; http://UlrichBruchholz.homepage.t-online.de/HomepageClassic01/robust.tar.bz2
24. The author took the reference values from: Gerthsen Ch. Physik. Springer-Verlag, Berlin-Heidelberg-New York, 1966 (regularly updated lists of the particle numbers are to find at http://pdg.lbl.gov/)
25. Zuse K. Rechnender Raum. *Elektronische Datenverarbeitung*, 1967, v. 8, 336–344; see also ftp://ftp.idsia.ch/pub/juergen/zuse67scan.pdf
26. Einstein A., Podolsky B., and Rosen N. Can quantum-mechanical description of physical reality be considered complete? *Phys. Rev.*, 1935, v. 47, 777–780.
27. Zeilinger A. Von Einstein zum Quantencomputer. *Neue Zürcher Zeitung*, v. 72, Nr. 148 vom 30.06.1999.
28. Kapcov S. Elektrische Vorgänge in Gasen und im Vakuum. Verlag der Wissenschaften, Berlin, 1955.

Numerical Solution of Quantum Cosmological Model Simulating Boson and Fermion Creation

Vic Christianto* and Florentin Smarandache†

*Present address: Institute of Gravitation and Cosmology, PFUR, Moscow, 117198
E-mail: vxianto@yahoo.com, admin@sciprint.org

†Chair of Department of Mathematics, University of New Mexico, Gallup, NM 87301, USA
E-mail: smarand@unm.edu

A numerical solution of Wheeler-De Witt equation for a quantum cosmological model simulating boson and fermion creation in the early Universe evolution is presented. This solution is based on a Wheeler-De Witt equation obtained by Krechet, Fil'chenkov, and Shikin, in the framework of quantum geometrodynamics for a Bianchi-I metric.

1 Introduction

It is generally aserted that in the early stage of Universe evolution, the quantum phase predominated the era. Therefore there are numerous solutions have been found corresponding to the Wheeler-DeWitt equation which governs this phase [2]. In the present paper we present another numerical solution of Wheeler-De Witt equation for a quantum cosmological model simulating boson and fermion creation in the early Universe evolution for a Bianchi-type I metric [1].

The solution is based on Wheeler-De Witt equation for a Bianchi-I metric obtained by Krechet, Fil'chenkov, and Shikin [1], in the framework of quantum geometrodynamics. Albeit the essence of the solution is quite similar from the solution given in [1] using Bessel function, in the present paper we present numerical result using Maxima. For comparison with other solutions of 1-d hydrogen problem, see [3] and [4].

2 Solution of Wheeler-DeWitt equation for boson and fermion creation

In the evolution of the Universe after inflation, a scalar field describing de Sitter vacuum was supposed to decay and its energy is converted into the energy of fermions and heavy vector-particles (the so-called X and Y bosons) [2].

In the framework of quantum geometrodynamics, and for a Bianchi-I metric, the Wheeler-De Witt equation has been obtained by Krechet, Fil'chenkov, and Shikin, which reduces to become (Eq. 23 in [1]):

$$T'' - \frac{2iC}{3\tau}\, T' - (E - V)\, T = 0. \tag{1}$$

where T'' and T' represent second and first differentiation of T with respect to r. The resulting equation appears quite similar to radial 1-dimensional Schrödinger equation for a hydrogen-like atom [3], with the potential energy is given by [1]:

$$U(r) = \frac{\beta}{\tau} + \frac{\varepsilon_o}{\tau^{4/3}}\,, \tag{2}$$

$$E = \frac{8}{3}\,\kappa \left(\frac{\Lambda}{\kappa} - \frac{M^2}{2\lambda} \right) \tag{3}$$

has here a continuous spectrum.

The solution of equation (1) has been presented in [1] based on modified Bessel function. Its interpretation is that in this quantum cosmological model an initial singularity is absent.

As an alternative to the method presented in [1], the numerical solution can be found using Maxima software package, as follows. All solutions are given in terms of E as constant described by (3).

(a) *Condition where* $V = 0$

```
'diff(y,r,2)−E*y−(2*%i*C/3/t)*y=0;   ode2(%o1,y,r);
```
(4)

The result is given by:

$$\mathrm{y{=}K1}\,\sin(\mathrm{a}){+}\mathrm{K2}\,\cos(\mathrm{a})\,, \tag{5}$$

where:

$$\mathrm{a{=}(r/}\sqrt{3})\,\sqrt{-3\mathrm{E}{-}2\mathrm{iC/t}}\,. \tag{6}$$

(b) *Condition where* $V \leqslant 0$

```
'diff(y,r,2)−E*y−(2*%i*C/3/t)*y−(b/t+e/t^4/3)*y=0;
ode2(%o2,y,r);
```
(7)

The result is given by:

$$\mathrm{y{=}K1}\,\sin(\mathrm{d}){+}\mathrm{K2}\,\cos(\mathrm{d})\,, \tag{8}$$

where:

$$\mathrm{d{=}(r/(}\sqrt{3}\,\mathrm{t}^{2/3})\,\sqrt{-3\mathrm{Et}^{4/3}{-}2\mathrm{iCt}^{1/3}{-}3\mathrm{e}{-}3\mathrm{bt}^{1/3}}\,. \tag{9}$$

As a result, the solution given above looks a bit different compared to the solution obtained in [1] based on the modified Bessel function.

3 A few implications

For the purpose of stimulating further discussions, a few implications of the above solution of Wheeler-DeWitt equation (in the form of 1-d Schrödinger equation) are pointed as follows:

(a) Considering that the Schrödinger equation can be used to solve the Casimir effect (see for instance Silva [5], Alvarez & Mazzitelli [6]), therefore one may expect that there exists some effects of Casimir effect in cosmological scale, in a sense that perhaps quite similar to Unruh radiation which can be derived from the Casimir effective temperature. Interestingly, Anosov [7] has pointed out a plausible deep link between Casimir effect and the fine structure constant by virtue of the entropy of coin-tossing problem. However apparently he did not mention yet another plausible link between the Casimir effective temperature and other phenomena at cosmological scale;

(b) Other implication may be related to the Earth scale effects, considering the fact that Schrödinger equation corresponds to the infinite dimensional Hilbert space. In other words one may expect some effects with respect to Earth eigen oscillation spectrum, which is related to the Earth's inner core interior. This is part of gravitational geophysical effects, as discussed by Grishchuk et al. [8]. Furthermore, this effect may correspond to the so-called Love numbers. Other phenomena related to variation to gravitational field is caused by the Earth inner core oscillation, which yields oscillation period $T \sim 3$–7 hours. Interestingly, a recent report by Cahill [9] based on the Optical fibre gravitational wave detector gave result which suggests oscillation period of around 5hours. Cahill concluded that this observed variation can be attributed to Dynamical 3-space. Nonetheless, the Figure 6c in [9] may be attributed to Earth inner core oscillation instead. Of course, further experiment can be done to verify which interpretation is more consistent.

Acknowledgements

One of the authors (VC) wishes to express his gratitude to Profs. A. Yefremov and M. Fil'chenkov for kind hospitality in the Institute of Gravitation and Cosmology, PFUR.

Submitted on February 06, 2009
Accepted on February 23, 2009

References

1. Krechet G., Fil'chenkov M., Shikin G.N. Quantum cosmological model simulating boson and fermion creation as a result of the primordial vacuum decay. *Grav. & Cosmology*, 2005, v. 11, no. 4(44), 373–375.
2. Grib A.A. Quantum vacuum effects in the strong external fields. St. Petersburg, St. Petersburg Univ. Publ., 1994.
3. Wolfram Project. Hydrogen orbital. http://demonstrations.wolfram.com/HydrogenOrbitals
4. Mavromatis H.A. Schrödinger equation solutions for small r and resulting functional relation. *Turkish J. Phys.*, 2001, v. 25, 175–179.
5. Silva P.R. Casimir force: an alternative treatment. arXiv: 0901.0908.
6. Alvarez E., Mazzitelli F.D. Long range Casimir force induced by transverse electromagnetic modes. arXiv: 0901.2641.
7. Anosov. Relation between fundamental constants. Physics Seminar held at Physics Faculty, MSU, Moscow, headed by Prof. Yu. S. Vladimirov, 18 Dec. 2008.
8. Grishchuk L. et al. *Grav. & Cosmology*, 2004, v. 10, no. 1–2.
9. Cahill R. Optical fibre detection of gravitation wave. *Prog. Phys.*, 2007, v. 4.

LETTERS TO PROGRESS IN PHYSICS

LETTERS TO PROGRESS IN PHYSICS

On the Earthly Origin of the Penzias-Wilson Microwave Background

Dmitri Rabounski and Larissa Borissova

E-mail: rabounski@yahoo.com; lborissova@yahoo.com

According to the experimental analysis conducted by P.-M. Robitaille, the 2.7 K microwave background, first detected by Penzias and Wilson, is not of cosmic origin, but originates from the Earth, and is generated by oceanic water. In examining this problem two fields must be considered: (1) the Earth Microwave Background, the EMB, present with the 2.7 K monopole and 3.35 mK dipole components; (2) the weak Intergalactic Microwave Background, the IMB, which is connected to the entire Metagalaxy. This conclusion meets our theoretical considerations. First, the field density of the EMB, being inversely proportional to the field volume, should decrease with the cube of the distance from the Earth's surface, while its dipole anisotropy, which is due to the motion of the entire field in common with the Earth, is independent from altitude. Therefore, the EMB monopole should not be found at the 2nd Lagrange point (1.5 mln km from the Earth), while the dipole anisotropy should remain the same as near the Earth. Second, according to General Relativity, the motion through the IMB in a referred direction manifests the three-dimensional rotation of the entire space of the Metagalaxy.

According to the experimental and observational analysis conducted by Pierre-Marie Robitaille, an expert in magnetic resonance imaging (MRI) [1], the 2.7 K monopole microwave background, first detected by Penzias and Wilson [2], is not of cosmic origin, but of the Earth, and is generated by the hydrogen bonds* in oceanic water.

Robitaille first advanced his concept in an open letter published in *The New York Times* in 2002 [3]. In the years which followed, he provided a detailed explanation in a series of journal publications [4–10].

Rabounski [11] then showed that the anisotropy of the Penzias-Wilson microwave background, observed through the 3.35 mK dipole component†, is due to the rapid motion of the whole field in common with its source, the Earth, with a velocity of 365 ± 18 km/sec through a weak intergalactic foreground, which is assignated to the Metagalaxy as a whole. So the anisotropy of the observed microwave background has a purely relativistic origin.

This conclusion is based on developments in the Special Theory of Relativity [12, 13]. Given a local (moving) inertial reference frame, the clocks of which are synchronized to the "preferred" (resting) intertial reference frame assigned to the Universe as a whole‡, an observer located in this local (moving) reference frame, should register an inverse $\left(1+\frac{\mathrm{v}}{c}\cos\theta\right)$ effect on the *physically observed velocity* of the light signals (photons) assigned to his (moving) reference frame, while the world-invariant of the velocity of light remains unchanged. This effect, directed toward the velocity v of the observer's (moving) reference frame, is manifested in the Tangherlini transformations in the Special Theory of Relativity [12, 13].

We assume that the photon source of an earthly microwave background moves in common the field's source, the Earth, with the velocity $\mathrm{v} = 365 \pm 18$ km/sec relative to the weak intergalactic microwave background, assigned to the Metagalaxy. In this case, according to the Tangherlini transformations, the spherical distribution of the velocities of the earthly origin microwave signals, being registered from the Earth or in an Earth-connected reference frame (such as the reference frame of a space mission moving in common with the Earth) should experience an anisotropy in the direction of the motion with respect to the weak intergalactic background. At the same time, the world-invariant of the velocity of light remains unchanged. Also, the distribution is still spherical if observed from the vewpoint of an observer connected to the Metagalaxy's background (i.e. in the "preferred" reference frame, which is resting with respect to the Metagalaxy as a whole). This anisotropic effect has the same formulation in temperature, $T = T_0/\left(1+\frac{\mathrm{v}}{c}\cos\theta\right)$, as the Doppler-effect, despite being generated by a different cause. We therefore refer to this effect as the *Doppler-like anisotropy*. Assume that the source of the earthly origin microwave photons, the Earth, moves through the weak intergalactic background with

*The vibration of a hydrogen atom in water weakly linked to an oxygen atom on another molecule.

†The 3.35 mK dipole (anisotropic) component of the Penzias-Wilson microwave background was first observed in 1969 by Conklin [14] in a ground-based observation. Then it was studied by Henry [15], Corey [16], and also Smoot, Gorenstein, and Muller (the latest team organized a stratosphere observation on board of a U2 aeroplane [17]). The history of the discovery and all the observations is given in detail in Lineweaver's paper of 1996 [18]. The weak anisotropic intergalactic field was found later, in the COBE space mission then verified by the WMAP space mission [19–23].

‡Such a synchronization can be done due to the "light-spot synchronization", which is by means of a phase-speed light spot, or due to the so-called "external synchronization". See [12, 13] or any encyclopaedic source, explaining the Tangherlini trasformations, for detail.

$\mathrm{v} = 365 \pm 18$ km/sec. We calculate the relative deviation of the temperature in the Earth's microwave background which is expected, due to the anisotropy, to be observed by an Earth-connected observer

$$\frac{\Delta T_{cal}}{T_{cal}} = \frac{\mathrm{v}}{c} = 0.122\,\% \pm 0.006\,\% .$$

According to the observations on board of the COBE satellite, the temperature of the Penzias-Wilson microwave background measured from the monopole component of it, is $T_{exp} = 2.730 \pm 0.001$ K. The dipole anisotropy, registered by the COBE satellite, is 3.353 ± 0.024 mK. The WMAP satellite gives approximately the same: 3.346 ± 0.017 mK. The anisotropic direction, in the Galactic longitude l and latitude b, is: $l = 264.26^\circ \pm 0.33^\circ$, $b = 48.22^\circ \pm 0.13^\circ$ as measured by COBE, a result confirmed by WMAP, $l = 263.85^\circ \pm 0.1^\circ$, $b = 48.25^\circ \pm 0.04^\circ$ [23]. So, the experimentally registered relative deviation of the temperature of the microwave background in the direction of the anisotropy is

$$\frac{\Delta T_{exp}}{T_{exp}} = 0.123\,\% \pm 0.001\,\%,$$

which is small number, but is significantly not zero due to the high precision of measurement. This is a systematic deviation with many years of observation.

In addition to this result, COBE initially registered a systematical deviation between the temperature of the monopole component of the microwave background, 2.730 ± 0.001 K, obtained by the direct measurements, and the temperature of the monopole 2.717 ± 0.003 K obtained from the 1st derivative of the monopole [24] (the 1st derivative was interpreted as the actual dipole component of the field). The average deviation $\Delta T_{exp} = 0.013 \pm 0.003$ K between these two results is a small number but is significantly not zero (this is due to the high precision of measurement). Thus, we obtain a minimal relative deviation between the temperature of the Penzias-Wilson microwave background from the monopole and from the 1st derivative of the monopole

$$\frac{\Delta T_{exp}}{T_{exp}} = 0.33\% \text{ at } 1\sigma, \qquad \frac{\Delta T_{exp}}{T_{exp}} = 0.18\,\% \text{ at } 2\sigma.$$

The aforementioned experimental results meet our theoretical calculation, $0.122\% \pm 0.006\%$. Therefore, our suggestion of the relativistic lowering of the temperature of the Penzias-Wilson microwave background due to the Doppler-like anisotropic effect on it [11], is in good agreement with that observed in the COBE and WMAP space missions.

With these, we have to suggest a model, in the framework of which two fields are under consideration (this classification meets the scenario suggested by Robitaille in [7]):

a). The Earth Microwave Background, the EMB, present with the 2.7 K monopole component and 3.35 mK dipole component. The EMB dipole anisotropy is explained due to the Tangherlini transformations in the Special Theory of Relativity: the spherical distribution of the earthly origin photons assigned to the EMB experiences the Doppler-like anisotropy toward the rapid motion of the Earth, with a velocity of 365 ± 18 km/sec, through the weak intergalactic background associated to the Metagalaxy as a whole (so the weak intergalactic background manifests the "preferred" reference frame connected to the entire Metagalaxy, and resting with respect to it). Such an anisotropy can be observed by an Earth-bound observer and any observer whose reference frame is connected to the Earth (for instance the observers located on board of the COBE satellite or the WMAP satellite), but the distribution of the earthly origin photons remains spherical being registered by an observer whose location is the reference frame resting with respect to the Metagalaxy as a whole;

b). A weak Intergalactic Microwave Background (IMB) exists. It is associated to the entire Metagalaxy, and is present with its monopole and dipole components. The dipole anisotropy of the IMB is explained due to the Doppler-effect on the IMB photons: the Earth moves through the IMB with a velocity of 365 ± 18 km/sec, so the IMB photons registered by an Earth-bound observer (or any observer who is connected to the reference frame of the Earth such as the observers on board of the COBE satellite or the WMAP satellite) bear different energies/frequencies toward and backward this motion that is manifest as the IMB anisotropy in this direction.

Our further considerations are focused on the additional theoretical proof in support to this conclusion.

Briefly, our theoretical considerations first suggest that, if the Penzias-Wilson microwave background is of earthly origin, it is approximated as a spherical field, distributed from the Earth into the outer space. In such a case, according to both classical and relativistic theory of fields, the density of the EMB is inversely proportional to the field volume

$$\rho \sim \frac{1}{V} \sim \frac{1}{R^3},$$

so it should decrease with the cube of the distance R from the field's sources, which are located on the surface of the Earth. In other word, the density of the EMB should decrease with the cube of the altitude from the Earth's surface. On the other hand, the dipole anisotropy of the EMB, being a purely relativistic effect due to the rapid motion of the field's source, the Earth, through the weak intergalactic field, is independent from altitude.

This conclusion provides an opportunity to simply verify the aforementioned theoretical suggestions. Naturally, if the Penzias-Wilson microwave background is the earthly origin, the monopole component should not be found at large distances from the Earth, while the dipole anisotropy remains the same as near the Earth.

The ground-bound measurements of the Penzias-Wilson

microwave background and the orbital measurements made with the COBE satellite, whose orbit is located at an altitude of 900 km, were obtained very near the oceans which are not point-like sources. Consequently, these observations were unable to manifest changes of the field density with altitude. However the 2nd Lagrange point is located 1.5 mln km from the Earth. It is the position of the WMAP satellite and the planned PLANCK satellite. Unfortunately, WMAP has only differential instruments on board: such an instrument registers only the difference between the number of photons in the channels. WMAP can therefore target measurements of the anisotropy of the field, but is unable to measure the field density. PLANCK is equipped with absolute instruments. Hence PLANCK will be able to measure the field density.

WMAP showed that the anisotropy of the Penzias-Wilson microwave background at the 2nd Lagrange point is the same as that measured by COBE, near the Earth. This agrees with our theory, but can occur if the background is of cosmic origin. Therefore the key probe, *experimentum crucis*, will be PLANCK, which targets the density of the field at the 2nd Lagrange point.

According to our theory, when PLANCK will arrive at the 2nd Lagrange point and start measurements, it shall manifest almost no photons associated to the Penzias-Wilson microwave background (at least a very small number of the photons), which is in very contrast to that was registered in the ground-based observations and in the COBE observations. This result should manifest the earthly origin of the Penzias-Wilson microwave background, and verify both Robitaille's phenomenological analysis and our theoretical considerations.

The second portion of our theory is specific to the General Theory of Relativity. Assume that the space of the Metagalaxy is a pseudo-Riemannian space with spherical geometry. Such a space is the surface of a hypersphere with the radius r (the curvature radius of the space). Now, suppose all the bodies located in the hyperspere's surface, have to travel, commonly, somewhere in a three-dimensional direction on the surface. This refers to the average common motion, because they all experience different motions with resect to each one, having however to travel on the average in the direction. Such an average "drift" of all bodies located in the hypersphere's surface manifests the three-dimensional rotation of the hypersphere. Therefore, in the framework of the views specific to the General Theory of Relativity, the presence of the weak Intergalactic Microwave Background, the IMB, which is associated to the Metagalaxy as a whole, through which the Earth moves, in common with the other space bodies (at different velocities, having however the average common velocity and direction in the space), manifests the three-dimensional rotation of the entire space of the Metagalaxy. The linear velocity of the rotation — the average velocity of all space bodies in the preferred direction, which is obviously different from the velocity 365 ± 18 km/sec specific to the Earth only — should arrive from observational astronomy, and be a world-invariant in the entire space (space-time) of the Metagalaxy.

Submitted on November 21, 2008 / Accepted on December 05, 2008
First published online on December 08, 2008

References

1. Robitaille P.-M. and Berliner L. J. Ultra high field magnetic resonance imaging. Springer, New York, 2006.
2. Penzias A. A. and Wilson R. W. A measurement of excess antenna temperature at 4080 Mc/s. *Astrophysical Journal*, 1965, v. 1, 419–421.
3. Robitaille P.-M. L. The collapse of the Big Bang and the gaseous Sun. *The New York Times*, March 17, 2002, page A10.
4. Robitaille P.-M. WMAP: a radiological analysis. *Progress in Physics*, 2007, v. 1, 3–18.
5. Robitaille P.-M. On the origins of the CMB: insight from the COBE, WMAP and Relikt-1 satellites. *Progress in Physics*, 2007, v. 1, 19–23.
6. Robitaille P.-M. On the Earth Microwave Background: absorption and scattering by the atmosphere. *Progress in Physics*, 2007, v. 3, pages 3–4.
7. Robitaille P.-M. On the nature of the microwave background at the Lagrange 2 Point. Part I. *Progress in Physics*, 2007, v. 4, 74–83.
8. Robitaille P.-M. The Earth Microwave Background (EMB), atmospheric scattering and the generation of isotropy. *Progress in Physics*, 2008, v. 2, 164–165.
9. Robitaille P.-M. Water, hydrogen bonding, and the microwave background. *Progress in Physics*, 2009, v. 1, L5–L8.
10. Robitaille P.-M. Global warming and the microwave background. *Progress in Physics*, 2009, v. 1, L9–L11.
11. Rabounski D. The relativistic effect of the deviation between the CMB temperatures obtained by the COBE satellite. *Progress in Physics*, 2007, v. 1, 19–21.
12. Tangherlini F.R. The velocity of light in uniformly moving frame. PhD Thesis, Stanford Univ., Sept. 1958, 135 pages.
13. Tangherlini F.R. An inroduction to the General Theory of Relativity. *Suppl. Nuovo Cim.*, 1961, Ser. X, v. 20, 1–86.
14. Conklin E. K. Velocity of the Earth with respect to the Cosmic Background Radiation. *Nature*, 1969, v. 222, 971–972.
15. Henry P. S. Isotropy of the 3 K background. *Nature*, 1971, v. 231, 516–518.
16. Corey B. E. and Wilkinson D. T. A measurement of the Cosmic Microwave Background Anisotropy at 19 GHz. *Bulletin of the American Astronomical Society*, 1976, v. 8, 351.
17. Smoot G. F., Gorenstein M. V. and Muller R. A. Detection of anisotropy in the Cosmic Blackbody Radiation. *Physical Review Letters*, 1977, v. 39, 898–901.
18. Lineweaver C.H. The CMB dipole: The most recent measurement and some history. In: *Microwave Background Anisotropies. Proceedings of the XVIth Moriond Astrophysics Meeting*, Les Arcs, Savoie, France, March 16–23, 1996, Gif-sur-Yvette: Editions Frontieres, 1997; see also arXiv: astro-ph/9609034.

19. Smoot G.F., et al. Preliminary results from the COBE differential microwave interferometers: large angular scale isotropy of the Cosmic Microwave Background. *Astrophys. J.*, 1991, v. 371, L1–L5.

20. Boggess N.W., et al. The COBE mission: its design and perfomance two years after launch. *Astrophys. J.*, 1992, v. 397, 420 – 429.

21. Page L., et al. The optical design and characterization of the Microwave Anisotropy Probe. *Astrophysical Journal*, 2003, v. 585, 566 – 586.

22. Bennett C.L., et al. The Microwave Anisotropy Probe mission. *Astrophys. J.*, 2003, v. 583(1), 1–23.

23. Bennett C.L., et al. First-year Wilkinson Microwave Anisotropy Probe (WMAP) observations: preliminary maps and basic results. *Astrophys. J. Suppl. Ser.*, 2003, v. 148(1), 1–27.

24. Fixsen D.J., et al. The Cosmic Microwave Background spectrum from the full COBE FIRAS data set. *Astrophys. J.*, 1996, v. 473, 576–587.

LETTERS TO PROGRESS IN PHYSICS

Water, Hydrogen Bonding, and the Microwave Background

Pierre-Marie Robitaille

Dept. of Radiology, The Ohio State University, 130 Means Hall, 1654 Upham Drive, Columbus, Ohio 43210, USA

E-mail: robitaille.1@osu.edu

In this work, the properties of the water are briefly revisited. Though liquid water has a fleeting structure, it displays an astonishingly stable network of hydrogen bonds. Thus, even as a liquid, water possesses a local lattice with short range order. The presence of hydroxyl (O−H) and hydrogen (H···OH$_2$) bonds within water, indicate that it can simultaneously maintain two separate energy systems. These can be viewed as two very different temperatures. The analysis presented uses results from vibrational spectroscopy, extracting the force constant for the hydrogen bonded dimer. By idealizing this species as a simple diatomic structure, it is shown that hydrogen bonds within water should be able to produce thermal spectra in the far infrared and microwave regions of the electromagnetic spectrum. This simple analysis reveals that the oceans have a physical mechanism at their disposal, which is capable of generating the microwave background.

While water is the best studied molecule on Earth [1], it remains one of the most mysterious. The unusual properties of this solvent are generated by its hydrogen bonding network [1–4]. In the condensed state, these relatively weak bonds (H···OH$_2$) interlink water into a local intermolecular lattice. Conversely, the robust intramolecular hydroxyl bond (O−H) permits water to be treated as a rigid unit. Water, in the solid state, can take up to one dozen possible crystal structures. Through hydrogen bonding, each molecule is incorporated into a structure wherein the oxygen atoms assume tetrahedral coordination as illustrated in Figure 1 [1]. As for the O−H···O bond angle, it deviates only slightly from linearity in ordinary ice, or ice Ih [1; p. 200].

Yet, it is the nature of liquid water which has largely captivated the interest of physical chemists. It has been said that: "the H-bond network of liquid water is, in the average, the same as that of ice" [1; p. 223]. In liquid water, the average tetrahedral geometry of the oxygen is maintained, but at the expense of tremendous dynamic bending of the hydrogen bonds [1; p. 223]. Nonetheless, to a first approximation, and for the purposes of the discussion which is to follow, the average O−H···O bond angle will not be considered to deviate substantially from linear. The energetic dynamic bending of hydrogen bonds will be neglected.

Liquid water has been tenacious in withholding its secrets. Still, scientists have not relented in the study of this universal solvent. Some of our knowledge has come from the study of the simple water dimer [5–9], the gaseous adduct of two molecules linked by a single hydrogen bond (see Figure 2). The structure of the dimer was first elucidated in 1977 by Dyke, Mack, and Muenter [7]. In its most stable form, the water dimer displays a *trans-linear* arrangement [7], where the O−H···O linkage deviates only slightly from a linear configuration. The stability of the *trans-linear* form has been confirmed repeatedly for this adduct, using both experimental and *ab initio* evaluations [5–9]. The energy of its hydrogen bond is ∼5 kcal/mol (∼21 kJ/mol; [6]).

Since the water molecules making up the dimer are somewhat rigid due to their strong hydroxyl bonds (∼119 kcal/mol or ∼497 kJ/mol [10; p. 9–74]), it is possible to treat this adduct as a monomer-monomer system. It is true that the dimer can undergo significant tunneling and rearrangements [5–9], but the resultant conformations do not produce the lowest energy species. As such, one can solely consider the *trans-linear* form [7] and treat each water molecule as a single, rigid unit. Under this scenario, the water dimer can be modeled as a harmonic oscillator [11–12] about the hydrogen bond. Dyke, Mack, and Muenter [7] have determined that the fundamental stretching frequency of the dimer corresponds to ∼143 cm^{-1} [7]. This frequency lies in the far infrared. It might be recalled, for instance, that NASA's COBE FIRAS (Far Infrared Absolute Spectrophotometer) instrument scanned the sky in a frequency range from 2 to 95 cm^{-1} [13].

Given a fundamental frequency at 143 cm^{-1}, it is possible to infer the force constant for the hydrogen bond in the water dimer [11–12]. The reduced mass, μ_r, of the dimer is equal to 1.495×10^{-23} g/molecule: $\mu_r = \frac{18\times18}{36\times(6.02\times10^{23})}$. The fundamental frequency of oscillation is related to the force constant, k, and reduced mass, μ_r, as follows:

$$\omega\ [\mathrm{cm}^{-1}] = \frac{1}{2\pi c}\left(\frac{k}{\mu_r}\right)^{1/2},$$

therefore, the force constant for the dimer corresponds to a very small 0.108×10^{5} dyn/cm. The force constant for the hydroxyl (O−H) bond within each molecule can be obtained from the literature [10]. It corresponds to 8.45 N/cm, which

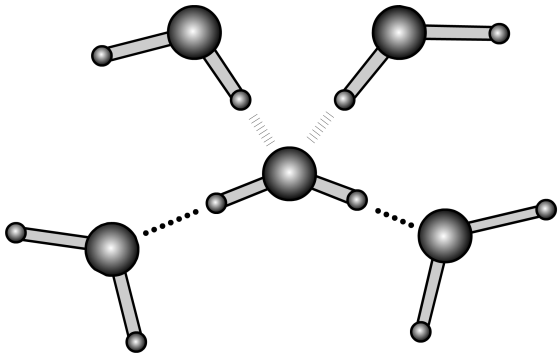

Fig. 1: Schematic representation of the water lattice. Each water molecule acts to accept and donate a total of four hydrogen bonds. Note the essentially linear O−H · · · O subunit.

is equivalent to 8.45×10^5 dyn/cm [10; p. 9–99].

In the ideal case, it should be possible to calculate the energy of each of these systems by considering the expression $E=\frac{1}{2}kx^2$, where k is the force constant and x is the infinitesimal displacement of the fundamental oscillation. The latter will be treated as an undetermined variable for each of these two subsystems.

Within the local water lattice, one can observe that the fundamental subunit of the dimer is also present (see Figure 1). That is, the linear O−H · · · O structure found within the *trans-linear* water dimer is constantly repeated. Indeed, if this were not the case, there would be little interest in studying the water dimer [5–9]. In this configuration, two bonds link every hydrogen atom to the adjacent oxygens (O−H · · · O): the hydrogen bond with a force constant of $\sim0.108\times10^5$ dyn/cm and the hydroxyl linkage with a force constant of $\sim8.45\times10^5$ dyn/cm. Since the grouping is a linear one, the displacement of the hydrogen atom must occur in the line linking the two oxygen atoms. If one isolates the hydrogen bonding system from this short range lattice, its energy will be roughly equal to $E_1=\frac{1}{2}k_1(x_1)^2$. Similarly, the energy for the hydroxyl system will be given by $E_2=\frac{1}{2}k_2(x_2)^2$. Thus, as there is a single hydrogen atom involved in the oscillation, it is immediately clear that $|x_1|=|x_2|$ and to a first approximation, $E_2/E_1=k_2/k_1$.

Water should then be capable of sustaining thermal emissions over two very distinct regions of the electromagnetic spectrum. The first of these regions occurs in the infrared and is generated by the hydroxyl bond. A second thermal emission region exists in the far infrared or microwave region. These emissions are produced by the hydrogen bond. They represent energies which are a factor of about 80 times ($k_2/k_1=78$) lower than the frequencies observed for the hydroxyl bonds. Although knowledge of emission frequencies cannot be easily correlated with temperatures, this result implies that the thermal photons produced by the hydrogen bonding network might be detectable at apparent temperatures which are 80 fold below the real temperatures of the water system.

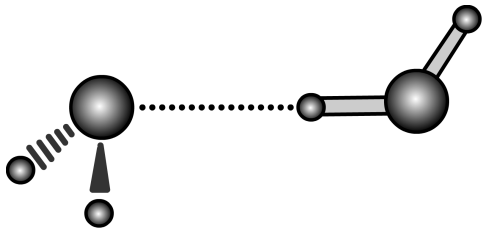

Fig. 2: Schematic representation of the *trans-linear* water dimer. Note the essentially linear O−H · · · O unit.

The thermodynamics of hydrogen bond rearrangements in the liquid phase have recently been examined [14]. This work gives a value of 1.5 ± 0.5 kcal/mol ($\sim$6.3 kJ/mol) for the rearrangement energy. As these energies are directly associated with the formation and breaking of hydrogen bonds, it implies that the true energy of these bonds is closer to 1.5 ± 0.5 kcal/mol in the liquid state, not the 5 kcal/mol obtained from dimer studies [6]. Therefore, the appropriate force constant for the hydrogen bond in liquid water could be nearly 3 fold lower, yielding a ratio of force constants (k_2/k_1) in a range of 80–240. Consequently, the hydrogen bonding system in water could produce a thermal spectrum reporting a temperature which is 80–240 fold lower than the true temperature of the water system.

An analysis of the hydrogen bonding system within water helps to explain how the oceans of the Earth could produce a thermal spectrum with an apparent temperature much lower than their physical temperature [15, 16]. This occurs despite the fact that sea water contains cations and anions [17, 18]. Note that the molar concentration and the physical influence of the salts in sea water (mostly NaCl at ~0.12 M) does not interfere significantly with the H-bonding network of $\sim$110 M hydrogen atoms [17, 18]. For instance, studies of the effects of cations and anions on the water system, tend to utilize ion concentrations which are more than 10 times those found in sea water [17, 18]. It is interesting however, that while the lifetimes of the first excited state for the hydroxyl (O−H · · ·) stretch in liquid water is on the order of $\sim$1 psec, this value increases to $\sim$2.6 psec in the vicinity of chloride ions [19, 20]. Nonetheless, it is unlikely that the presence of ions in the oceans will dramatically alter the conclusions reached herein, even though the presence of ions can produce small changes in the first solvation shell [17, 18].

Maréchal [1; p. 220] illustrates how liquid water displays strong hydroxyl absorption bands at 1644 cm^{-1} (H−O−H bending) and 3400 cm^{-1} (hydrogen bonded O−H stretch). Importantly, the spectra also revealed broad and powerful libration bands (hindered rotations about the hydrogen bond; O · · · H) at $\sim$700 cm^{-1} and hydrogen bond stretches (O · · · H) centered at $\sim$200 cm^{-1} which extend to lower frequencies. Since water is a good absorber in the far infrared, these studies were executed on samples which were only 1-μm thick. Consequently, it would not be unexpected that the supporting matrix and a small sample thickness could alter both the

position and amplitude of the hydrogen bonding stretching and libration bands. The findings reported by Maréchal [1; p. 220] are interesting, but inconclusive as related to the hydrogen bond itself.

Reflecting on the paucity of supportive data, in this very difficult experimental region of the far infrared, it seems that much more needs to be learned about the emissions due to hydrogen bonds in nature. In particular, the lack of a signal specifically assigned to hydrogen bonds from water on Earth gives cause for concern. This is because the microwave background [21] was assigned to the universe [22] when virtually nothing was known about the spectroscopic signature of the hydrogen bond.

Consideration of these findings reveals why the author has advanced [15, 16] that the microwave background [21] does not correspond to an astrophysical signal [22], but instead is generated by the oceans [15, 16, 23]. Water has the means to generate thermal emissions in the far infrared and microwave regions. The fundamental oscillator involved is best represented by the dimer subunit and its associated hydrogen bond within liquid water itself. In the gas phase, the dimer is known to have a fundamental frequency in the far infrared [7], very close to the region sampled by the COBE FIRAS instrument [13]. It is quite reasonable to expect that the emissions from the oceans occur in the same region.

In summary, the microwave background can be understood as follows: photons are being produced by the oceans and they are then scattered in the atmosphere such that a completely isotropic signal is observed [15]. The isotropy of the microwave background was first reported by Penzias and Wilson [21]. The signal is independent of temperature variations on the globe, since the hydrogen bonding energy system is already fully occupied at earthly temperatures. This explains why the microwave background is independent of seasonal changes [21]. Satellite data obtained by COBE strengthen the idea that the Earth does produce the microwave background [24, 25]. This hypothesis has not been refuted either by the three year [26] or five year WMAP findings.

Acknowledgements

The author would like to thank Luc Robitaille for assistance in figure preparation.

Dedication

This work is dedicated to my wife, Patricia.

Submitted on November 21, 2008 / Accepted on December 05, 2008
First published online on December 08, 2008

References

1. Maréchal Y. The hydrogen bond and the water molecule: The physics and chemistry of water, aqueous and bio-media. Elsevier, Amsterdam, 2007.
2. Jeffrey G.A. An introduction to hydrogen bonding. Oxford University Press, Oxford, 1997.
3. Schuster P., Zundel G., Sandorfy C. The hydrogen bond: Recent developments in theory and experiments (vols. 1–3). North-Holland Publishing Company. Amsterdam, 1976.
4. Smith J.D., Cappa C.D., Wilson K.R., Cohen R.C., Geissler P.L., Saykally R.J. Unified description of temperature-dependent hydrogen-bond rearrangements in liquid water. *Proc. Nat. Acad. Sci.*, 2005, v. 102, 14171–14174.
5. Dyke T.R., Muenter J.S. Microwave spectrum and structure of hydrogen bonded water dimer. *J. Chem. Phys.*, 1974, v. 60, 2929–2930.
6. Dyke T.R. Group theoretical classification of the tunneling-rotational energy levels of the water dimer. *J. Chem. Phys.*, 1977, v. 66, 492–497.
7. Dyke T.R., Mack K.M., Muenter J.S. The structure of water dimer from molecular beam electric resonance spectroscopy. *J. Chem. Phys.*, 1977, v. 66, 498–510.
8. Scheiner S. Ab initio studies of hydrogen bonds: The water dimer paradigm. *Ann. Rev. Phys. Chem.*, 1994, v. 45, 23–56.
9. Keutsch F.N., Goldman N., Harker H.A., Leforestier C., Saykally R.J. Complete characterization of the water dimer vibrational ground state and testing the VRT(ASP-W)III, SAPT-5st, and VRT(MCY-5f) surfaces. *Molecular Phys.*, 2003, v. 101, 3477–3492.
10. Lide D.R. CRC handbook of chemistry and physics. CRC Press, Boca Raton, 89th Edition, 2008.
11. Wilson E.B., Decius J.C., Cross P.C. Molecular vibrations: The theory of infrared and raman vibrational spectra. McGraw-Hill Book Company, New York, 1955.
12. Harris D.C., Bertolucci M.D. Symmetry and spectroscopy: An introduction to vibrational and electronic spectroscopy. Oxford University Press, Oxford, 1978.
13. Fixsen D.J., Cheng E.S., Cottingham D.A., Eplee R.E., Isaacman R.B., Mather J.C., Meyer S.S., Noerdlinger P.D., Shafer R.A., Weiss R., Wright E.L., Bennett C.L., Boggess N.W., Kelsall T., Moseley S.H., Silverberg R.F., Smoot G.F., Wilkinson D.T. Cosmic microwave background dipole spectrum measured by the COBE FIRAS instrument. *Astrophys. J.*, 2004, v. 420, 445–449.
14. Smith J.D., Cappa C.D., Wilson K.R., Messer B.M., Cohen R.C., Saykally R.J. Energetics of hydrogen bond network rearrangements in liquid water. *Science*, 2004, v. 306, 851–853.
15. Robitaille P.-M. The Earth microwave background (EMB), atmospheric scattering and the generation of isotropy. *Prog. in Phys.*, 2008, v. 2, 164–165.
16. Robitaille P.-M.L. A radically different point of view on the CMB. In: *Galilean Interviews on Cosmology*, M. D'Onofrio and C. Burigana, eds., Springer, New York, 2009.
17. Cappa C.D., Smith J.D., Messer B.M., Cohen R.C., Saykally R.J. Effects of cations on the hydrogen bond network of liquid water: New results from X-ray absorption spectroscopy of liquid microjets. *J. Phys. Chem. B*, 2006, v. 110, 5301–5309.

18. Smith J.D., Saykally R.J., Geissler P.L. The effects of dissolved halide anions on hydrogen bonding in liquid water. *J. Am. Chem. Soc.*, 2007, v. 129, 13847–13856.

19. Laenen R., Simeonidis K., and Laubereau A. Subpicosecond spectroscopy of liquid water in the infrared: Effect of deuteration on the structural and vibrational dynamics. *J. Phys. Chem. B*, 2002, v. 106, 408–417.

20. Kropman M.F., Bakker H.J. Femtosecond mid-infrared spectroscopy of aqueous solvation shells. *J. Chem. Phys.*, 2001, v. 115, 8942–8948.

21. Penzias A.A., Wilson R.W. A measurement of excess antenna temperature at 4080 Mc/s. *Astrophys. J.*, 1965, v. 1, 419–421.

22. Dicke R.H., Peebles P.J.E., Roll P.G., and Wilkinson D.T. Cosmic black-body radiation. *Astrophys. J.*, 1965, v. 1, 414–419.

23. Rabounski D., Borissova L. On the Earthly origin of the Penzias-Wilson microwave background. *Prog. in Phys.*, 2009, v. 2, L1–L4.

24. Robitaille P.-M. On the Origins of the CMB: Insight from the COBE, WMAP, and Relikt-1 Satellites. *Prog. in Phys.*, 2007, v. 1, 19–23.

25. Rabounski D. The relativistic effect of the deviation between the CMB temperatures obtained by the COBE satellite. *Prog. in Phys.*, 2007, v. 1, 24–26.

26. Robitaille P.-M. WMAP: A radiological analysis. *Prog. in Phys.*, 2007, v. 1, 3–18.

LETTERS TO PROGRESS IN PHYSICS

Global Warming and the Microwave Background

Pierre-Marie Robitaille

Dept. of Radiology, The Ohio State University, 130 Means Hall, 1654 Upham Drive, Columbus, Ohio 43210, USA

E-mail: robitaille.1@osu.edu

In the work, the importance of assigning the microwave background to the Earth is addressed while emphasizing the consequences for global climate change. Climate models can only produce meaningful forecasts when they consider the real magnitude of all radiative processes. The oceans and continents both contribute to terrestrial emissions. However, the extent of oceanic radiation, particularly in the microwave region, raises concerns. This is not only since the globe is covered with water, but because the oceans themselves are likely to be weaker emitters than currently believed. Should the microwave background truly be generated by the oceans of the Earth, our planet would be a much less efficient emitter of radiation in this region of the electromagnetic spectrum. Furthermore, the oceans would appear unable to increase their emissions in the microwave in response to temperature elevation, as predicted by Stefan's law. The results are significant relative to the modeling of global warming.

While controversy exits as to whether or not mankind has been an agent of global climate change, there is little dispute in the scientific community that the Earth is indeed warming [1–4]. Global warming may substantially alter the agricultural capacity and water cycles of our planet with dramatic human ramifications. With this in mind, if global warming is to be both understood and forecasted, climate modeling [5, 6] must be based on proper physical foundations. Through this letter, I wish to highlight that the modeling of the Earth's energy balance [5, 6] requires re-evaluation first of Kirchhoff's law of thermal emission [7–11] and its associated consequences for the application of Stefan's law [12], and second of the assignment of the microwave background [13, 14] to the oceans of the Earth [15, 16].

Regarding Kirchhoff's law [7], it is difficult to conceive that a central pillar of physics could be the subject of concern, both in its experimental formulation [8, 11] and in its theoretical proof [9, 10]. For those who have followed the arguments these past few years [8–11], it seems that a reconsideration of universality in blackbody radiation is in order. In short, there is no universality [9, 10] and each physical system must be treated with individualized care. The generalized application of Stefan's 4th power law [12] is unjustified in the analysis of global warming.

Relative to the microwave background, the reassignment is both unexpected and profound. Ever since its discovery [13] and assignment to the universe in 1965 [14], the microwave background has been considered a cornerstone of modern astrophysics. As such, the attributing of this background to the Earth brings consequences for physics [17]. Nonetheless, the global warming issue is of sufficient importance that its proper modeling [5, 6] should not be delayed by the continued misassignment of the true origin of the microwave background.

At the same time, it remains true that these are complex problems [1–21]. Kirchhoff's law of thermal emission has been in existence for nearly 150 years [7]. To question a fundamental law after many years [8–11] seems contrary to scientific logic, as scientists cannot be expected to verify the tenets of physics before any new advancement can be pursued. In this regard, the incorrect assignment of the microwave background to the universe [14] can be understood, although the accurate determination of temperatures from thermal emission spectra has always required thermal equilibrium with an enclosure [7–11]. This is something which could never be met in a cosmological origin for the microwave background, as I previously stated [18]. In the end, each signal requires a realistic physical origin [8, 9]. For the microwave background, the responsible physical entity will be the weak hydrogen bond between water molecules [15, 17].

With respect to the energy balance of the Earth [5, 6], its elucidation requires the determination of the relationship between absorbed (solar) and emitted (earthly) radiation. Usually, one is concerned with radiation in the infrared. However, substantial contributions can be made in the radio and microwave bands. While these energies are lower, their aggregate sums are non-negligible. Thus, in order to model climate change, the radiation balance of the Earth must be determined as a function of all frequencies from radio through the infrared.

In some climate models [5, 6], the radiation which the Earth emits is deduced by applying Stefan's law [12], at a given effective temperature, thereby treating the globe as a uniform blackbody source. In such an approach, oceanic contributions are undifferentiated from continental radiation. Yet, the thermal emission profiles of solid materials are dramat-

ically different from one another [20]. Few solids, if any, adhere to Stefan's law. Even various forms of graphite [20] differ in their ability to emit radiation as a function of the 4th power of the temperature [12]. Stefan's law simply does not apply to most materials [20] and certainly will not apply to land masses which are covered with extensive vegetation. The thermal emission from liquids, especially water, is even more complicated and much less understood. While Stefan's law might appear to hold over narrow spectral ranges within the infrared, such band-like emissions fall far short of producing the emissive power expected at all frequencies, through the application of the 4th power relationship.

Since there is no universality [8, 9], it is implausible that the Earth can be modeled as emitting at a single effective temperature. The oceans cannot be treated as simple blackbody emitters, producing Planckian thermal spectra reflecting an effective temperature near 300 K [5, 6]. In fact, while water can provide strong emission bands in the infrared, further study will reveal that the entire spectrum is far from blackbody or Planckian at 300 K. This is particularly important in the microwave region.

If the oceans had been able to emit with an effective temperature near 300 K, they would be expected to produce an extensive radiation in the microwave region of the electromagnetic spectrum. In actuality, the oceans mimic a 3K blackbody in this frequency range [13, 15]. The oceans remain powerful emitters of thermal radiation at these frequencies, but much less powerful than would have been predicted if they could be treated as 300 K sources. Note, in this regard, that Stefan's law invokes a 4th power temperature dependence [12]. As a result, the oceans, while still emitting ample radiation in the microwave region [13], are actually poor emitters in this spectral range. This is true, if one compares their actual emission [13] with the emission corresponding to an effective temperature of 300 K [12], as is currently expected. The lower than expected efficiency of the oceans to emit thermal radiation, particularly in the microwave region, appears to have dire consequences for global warming.

It is well known that global warming models invoke negative feedback mechanisms [5, pp.352–354]. The first of these predicts that, as the Earth warms, it becomes an even better emitter of radiation, because the use of Stefan's law [12] now applies a fourth power exponential to an even higher temperature. As a result, the production of even more thermal photons is expected. In practice, approximately 70% of the Earth is covered with water, and its thermal emissions in the microwave regions are not expected to increase in the slightest as a response to temperature elevation. Should the hydrogen bonding system within water actually be the oscillator responsible for the microwave background [15, 21], then this system cannot easily respond to increases in temperature, since the associated energy levels are already full at Earthly temperatures. This explains why the microwave background has always been observed to be independent of seasonal variations. For nearly 70% of the planet, the negative feedback mechanisms, brought by the application of Stefan's law, will not hold, at least in the microwave region of the spectrum.

It is well established that the inability of water bodies to efficiently emit radiation results in considerable retention of thermal energy within oceanic systems. Unable to dissipate heat through emission, the oceans turn to convection currents. This provides a driving force for oceanic currents and for hurricanes. Importantly, the secret to understanding oceanic behavior rests in large part with the microwave background. Its lack of seasonal variation constitutes a key parameter for modelers of global climate change and for the study of oceanic systems.

Given the centrality of global warming to human progress, it may be prudent to fully ascertain the Earth's emission profile, by using an array of satellites which continually monitor spectral emissions from the radio range through the infrared. Such an array, positioned in fixed orbit around the globe should be able to continuously monitor outgoing Earthly emissions. Using a satellite array, it should be possible to observe the ebb and flow of infrared radiation from the Earth in association with the diurnal cycle. In addition, the relative stability of microwave emission will once again be affirmed. Indeed, the latter has already been established long ago, by Penzias and Wilson [13]. Only when such findings are combined with increased direct solar, atmospheric, continental, and oceanic monitoring as a function of depth and global position, will scientists gain the insight required for the accurate analysis of climate change.

Dedication

This work is dedicated to my youngest sister, Mireille.

Submitted on November 21, 2008 / Accepted on December 05, 2008
First published online on December 08, 2008

References

1. Levitus S., Antonov J.I, Wang J., Delworth T.L., Dixon K.W., Broccoli A.J. Anthropogenic warming of Earth's climate system. *Science*, 2007, v. 292, 267–270.
2. Hansen J., Nazarenko L., Ruedy R., Sato M., Willis J., Genio A.D., Koch D., Lacis A., Lo K., Menon S., Novakov T., Perlwitz J., Russell G., Schmidt G.A, Tausnev N. Earth's energy imbalance: confirmation and implications. *Science*, 2005, v. 308, 1431–1435.
3. Levitus S., Antonov J.I., Boyer T.P., Stephens C. Warming of the world ocean. *Science*, 2000, v. 287, 2225–2229.
4. Gregory J.M., Banks H.T., Stott P.A., Lowe J.A., Palmer M.D. Simulated and observed decadal variability in ocean heat content. *Geophys. Res. Letters*, 2004, v. 31, L15312.
5. Kiehl J.T., Ramanathan V. Frontiers of climate modeling. Cambridge University Press, Cambridge, UK, 2006.

6. McGuffie K., Henderson-Sellers A. A climate modeling primer (2nd edition). John Wiley and Sons, New York, 1997.
7. Kirchhoff G. Über den Zusammenhang zwischen Emission und Absorption von Licht und. Wärme. *Monatsberichte der Akademie der Wissenschaften zu Berlin*, sessions of Dec. 1859, 1860, 783–787.
8. Robitaille P.M.L. On the validity of Kirchhoff's law of thermal emission. *IEEE Trans. Plasma Sci.*, 2003, v. 31(6), 1263–1267.
9. Robitaille P.-M. An analysis of universality in blackbody radiation. *Prog. in Phys.*, 2006, v. 2, 22–23.
10. Robitaille P.-M. A critical analysis of universality and Kirchhoff's law: A return to Stewart's law of thermal emission. *Prog. in Phys.*, 2008, v. 3, 30–35.
11. Robitaille P.-M. Blackbody radiation and the carbon particle. *Prog. in Phys.*, 2008, v. 3, 36–55.
12. Stefan J. Über die Beziehung zwischen der Warmestrahlung und der Temperature. *Sitzungsberichte der mathematischnaturwissenschaftlichen Classe der kaiserlichen Akademie der Wissenschaften*, Wien 1879, v. 79, 391–428.
13. Penzias A.A. and Wilson R.W. A measurement of excess antenna temperature at 4080 Mc/s. *Astrophys. J.*, 1965, v. 1, 419–421.
14. Dicke R.H., Peebles P.J.E., Roll P.G., and Wilkinson D.T. Cosmic black-body radiation. *Astrophys. J.*, 1965, v. 1, 414–419.
15. Robitaille P.M. The Earth microwave background (EMB), atmospheric scattering and the generation of isotropy. *Prog. in Phys.*, 2008, v. 2, 164–165.
16. Rabounski D. and Borissova L. On the Earthly origin of the Penzias-Wilson microwave background. *Prog. in Phys.*, 2009, v. 2, L1–L3.
17. Robitaille P.M.L. A radically different point of view on the CMB in: *Galilean Interviews on Cosmology*, M. D'Onofrio and C. Burigana, eds., Springer, New York, 2009.
18. Robitaille P.M.L. The collapse of the Big Bang and the gaseous Sun. *New York Times*, March 17, 2002, page A10 (available online: http://thermalphysics.org/pdf/times.pdf).
19. Robitaille P.M.L. The little heat engine: Heat transfer in solids, liquids, and gases. *Prog. in Phys.*, 2007, v. 4, 25–33.
20. Touloukian Y.S., DeWitt D.P. Thermal radiative properties of nonmetallic solids. Vol. 8 in: *Thermophysical Properties of Matter*, IFI/Plenum, New York, 1972.
21. Robitaille P.M.L. Water, hydrogen bonding and the microwave background. *Prog. in Phys.*, 2009, v. 2, L5–L8.

LETTERS TO PROGRESS IN PHYSICS

On the Upper Limit (Heaviest Element) in the Periodic Table of Elements, and the Periodic Table of Anti-Substances

Albert Khazan

E-mail: albkhazan@gmail.com

On the basis of the method involving equilateral hyperbolas developed by us with reference to the Periodic Table, its Top Limit has been established. It is the last element with atomic mass 411.66 and serial number 155. The great value, according to our calculation, has adjacent hyperbolas whose center is the point (0; 1). With the method, it has been possible to find just one element in the Periodic Table — Rhodium, which does not demand additional calculations involving the definition of the valid axes. Calculations towards updating the charge of a nucleus and the quantity of neutrons in end N-Z part of the diagram by means of the serial number 155 are herein executed. The variant of the Periodic Table of Elements with the eighth period is recommended. On the basis of symmetry, with the application of the Hyperbolic Law in the Periodic Table of Elements, the existence of Anti-Substances is herein indirectly proved.

In the Periodic Table, elements are in a static condition, which until now has not allowed us to reveal the dynamics of their contents in various chemical compounds. The regularity established by us represents equilateral hyperbolas $Y = K/X$, where Y is the content of any element K and X is the molecular mass of compounds taken according to one gram-atom of the defined element. The extreme conditions of the equation are attained when $Y \leqslant 1$, $K \leqslant X$. Mathematically speaking, if, for such hyperbolas, the peak is defined as $\sqrt{K}$, according to the theorem of Lagrange, on the basis of which the calculated factor of scaling ($M = 20.2895$) is applied, it shall allow us to pass from one system of coordinates to another. The square of this number (411.66) is equal to the maximal atomic mass of the last element, which is the crossing point of the valid axis of all hyperbolas whose ordinate is given by $Y = 1$. Its serial number is 155 [1].

Calculations of adjacent hyperbolas of the kind $Y = (X - K)/X$ whose center is the point 0; 1 have a simultaneous effect. Both versions of hyperbolas serve as additions with respect to each other. When in one curve Y decreases, in the second it increases. Each pair of hyperbolas of one element is crossed at the point ($X = 2K$, $Y = 0.5$) through which passes the axis of symmetry. Direct and adjacent hyperbolas of all elements are crossed among themselves. The hyperbolas of the last element are the right boundaries of existence for the compounds, and, at the left, they are bounded by the coordinate axes [2].

As a result of graphical constructions and voluminous calculations, it has been found that in the Periodic Table there is the element rhodium (Rh) to which it is not required to apply theorem Lagrange and the factor of scaling. On the basis of direct tabular data and adjacent hyperbolas, at a point of their crossing (205.811; 0.5), the valid axes which, on the X axis and along the line $Y = 1$, cut apiece with abscissa 411.622, are under construction. The divergence from the data described above is a few thousandths of percent. This fact manifests the validity of our theory [3].

It is thereby proved that the Top Limit of the Periodic Table is the element no. 155 with atomic mass 411.66. At present it is known that no. 118-th has been synthesized — last element of the seventh period (no. 117 does not exist yet). And, the above the serial number suggests that it is somehow difficult for the Table to receive a new element. So, accordingly, in nuclear reactions involving the synthesis of elements nos. 114, 115, 116, and 118, events 60, 24, 9 and 3 have been registered. In the known neutron-proton diagram of the nucleus (nearby 2500) which finishes with the element no. 114, it is seen that, in the end, its quantity of artificial isotopes sharply decreases [4]. To the number of the element with atomic mass 298, scientists have assigned special hopes as here isotopes should possess raised stability [5]. However, with the addition of the nucleus no. 155 to the diagram, a general line of new trends shows that the predicted element no. 114 should have 179 neutrons, instead of 175. Also expected by scientists are the twice-magic nucleus with a charge number 114 and atomic mass 298, which, according to our data, has a lack of 2 protons or, in other words, a surplus of 5 neutrons. The existing disorder in the parameters of the elements is caused by the fact that there enters a more long-living isotope into the table. Therefore the element no. 155 should be a reference point in nuclear reactions. It is necessary to consider it in new quantum theory calculations for the sake of filling the Periodic Table. There are different points of view on the quantity of elements in it: from 120 up to 218 and more. For example, G. Seaborg and V. Goldanskii have suggested adding 8-th and 9-th periods to 50 elements [6, 7]. But in constructing the total dependence of isotopes (more than 2500) on the charge of a nucleus, it is possible to

see that it has the parabolic form, and, in the end, its account goes by the units of the seventh period. It is also necessary to acknowledge that elements with numbers 94–103 have been discovered over the last 20 years, and 104–113–for 40.

In the world, hundreds of variants of the Periodic Table have been created, but no one never has been able to answer the question, whether it has a limit [8, 9]. We, for the first time, have given the parameters of the last element as belonging to the eighth period, the first group, having no. 155 and atomic mass 411.66 [10].

It is necessary to note that while our theory has been considered with reference to the first quadrant, the position of the second branches of equilateral hyperbolas in the third quadrant (where $K > 0$) has not been analyzed. However, it has appeared that they possess similar properties (similar to those in the first quadrant). Here too it is necessary to enter the factor for reduction of coordinate axes by one scale. If now around an imaginary axis we allow the overlapping of the third and the first quadrants, it is possible to see practically the full concurrence of curves, coordinates, and valid axes. However, it concerns only the central part of the hyperbolas, and their edges, observing a direction, fall outside the limits. Hence, here the principle of symmetry does not work. At $K < 0$ it is established, in the second and the fourth quadrants of the hyperbolas, that there is similar regularity which has been established by us for the first and the third quadrants. It is caused by equilateral hyperbolas having equal parameters with respect to the module, but with an opposite sign; namely, being mutually interfaced, they possess identical properties. Therefore, proceeding from the chemical concepts, they can be symmetric only after the change of scale of the X and Y axes. As in the third and fourth quadrants a negative ordinate (a degree of transformation of substance) is not allowable in Nature, we shall analyze only quadrants 1 and 2, in which $K > 0$ and $K < 0$. Here there is a full symmetry: the hyperbolas are congruent and all axes coincide. Hence, the Hyperbolic Law in the Periodic Table shall be applied to the second quadrant. At a positive value of Y, a negative value X, and $K < 0$, it is possible to assert that in it there are substances with a minus sign, i.e., Anti-Substances. Furnished with the analysis above, there arises the opportunity of constructing the Periodic Table of Anti-Substances similar to the one considered above.

Submitted on December 12, 2008 / Accepted on January 23, 2009

References

1. Khazan A. Upper limit in the Periodic System of Elements. *Progress in Physics*, 2007, v. 1, 38.
2. Khazan A. Effect from Hyperbolic law in Periodic Table of Elements. *Progress in Physics*, 2007, v. 2, 83.
3. Khazan A. The rôle of the element Rhodium in the Hyperbolic law of the Periodic Table of Elements. *Progress in Physics*, 2008, v. 3, 56.
4. Brookhaven National Laboratory. Table of Nuclides.
5. Ishhanov B.C. and Kebin E.I. Exotic nuclei. Moscow University Press, Moscow, 2002.
6. Seaborg G.T. and Bloom J.L. The synthetic elements. *Scientific American*, 1969, v. 220(4), 56.
7. Goldanskii V.I. About connections nuclear and chemical physics. *Progress Physical Sciences*, 1976, v. 118, issue 2.
8. Oganesyan Y. Islands of stability. *The World of Science*, March 2005, no. 3.
9. The Periodic Table: Into the 21st Century. D. H. Rouvray and R. B. King (Eds.), Research Studies Press, Baldock (UK).
10. Khazan A. Upper limit of the Periodic Table and synthesis of superheavy elements. *Progress in Physics*, 2007, v. 2, 104.

LETTERS TO PROGRESS IN PHYSICS

Corrections to the Biography of Frank Robert Tangherlini, Published in Progress in Physics, Vol. 1, 2009

Gregory B. Malykin

Inst. of Applied Physics, Russian Acad. of Sciences, Ulianova Str. 46, Nizhni Novgorod 603950, Russia
E-mail: malykin@ufp.appl.sci-nnov.ru

This short letter contains some additional information and actual corrections to the biography of Frank Robert Tangherlini, published by the author of the letter, Gregory B. Malykin, in *Progress in Physics*, v. 1, 2009.

Dear sir,

My recent publication [1] spent on the biography of Frank Robert Tangherlini (on the occasion of his 85th birthday) contained a minor lack of information in the field of mainly his family life, details of his military service during the World War II, and his private communications with some famous physicists of the 20th century. Due to the exceptional courtesy of Prof. Tangherlini who has read my recent paper [1], I would like to improve these, and also add several details, which could be interesting to a reader. Therefore I provide below some extractions from the comments made by Prof. Tangherlini himself on my topic in his private correspondence with me [2].

1. "...Thus: my maternal grandfather did not settle in New York, but in Chelsea, Massachusetts, a suburb of Boston, and later moved to Philadelphia. ... My oldest son Arne died in 1998 at the age of 37. However, he left me a wonderful granddaughter who will turn 18 in August."

2. "...Actually, I was not "set free" of military service, but rather, as with so many other engineering students, I received a "draft deferment", that enables the student to completer his technical education subject to government wishes. However, the engineering program I was enrolled in at Boston College (although it is a Jesuit institution, its name is just Boston College, not Boston Jesuit College) closed down, and I volunteered to be drafted in July 1943. After processing at Fort Devens in Ayer, Massachusetts, I was sent to Fort Benning, Georgia, to receive Basic Training. But I did not stay there a year. I had been placed in the Army Specialized Training Program (ASTP), and after completing my basic training, I along with others was sent to the University of Cincinnati, perhaps in early January of 1944. I completed two quarters of training there, and sometime in May, I arranged to be transferred to the regular ground forces that were preparing to be sent overseas. I received more infantry training in the summer of 1944 in Kentucky, and then volunteered to be sent to Fort Meade, Maryland to be shipped overseas. I was finally sent overseas on the Mauretania, perhaps in September 1944, and it was on board the ship that I met James Barlow and Joe Rhiley, who had been airforce cadets but were transferred to the infantry. After we arrived in Liverpool, we volunteered to join the 101st Airborne Division (only volunteers were in the Airborne, no one was forced to become a paratrooper, even when jumping, if someone didn't want to jump, they were asked to step aside, and let the next man jump; they then had to leave the Airborne). I made five training jumps in Hungerford before being flown over to Mourmelon, France, where we stayed for several weeks, before being sent to Bastogne, Belgium in TRUCKS, becasuse there was not enough time to arrange for a parachute jump. So I never parachuted into combat. If I had, I probably wouldn't be around today writing to you. The Germans had broken through in the Ardennes, and we were sent to halt their taking the key city of Bastogne, which we did. We eventually were surrounded, and the German commander asked our acting commander, Brig. Gen. MacAuliffe to surrender. He replied: nuts!* This became one of the famous stories from the Battle of the Bulge. At the end of the war, sometime late in August, I made another training jump, this time in France. It was part of our training for the so-called "Jump on Tokyo". The training jump took place even though the war had ended. It was the smoothest (and last!) parachute jump I ever made. I should also note that although I was a non-commissioned officer with the equivalent rank of a sergeant, the army designation of my rank was T-4 (i.e. technician 4th grade)."

3. "...I received a bronze medal in American history not world history. Incidentally, I still remember what the competition essay was about: It was about a comparison of Thomas Jefferson with Alexander Hamilton. ... Also, in colleges we do not speak of grade, so Robert F. Kennedy was in the same graduation class as myself, i.e., the class of 1948, but not "grade". I should emphasize that I never met him personally, and indeed only learned he was in my class many years later. I attended 60th reunion of the class of 1948 in June 2008. ... Skipping now to my post-doc training in Naples, I should mention that although Francis Halpern and Susum Okubo were there, Gell-Mann was not there. I think you may

*"Nuts" in the context MacAuliffe used it is not foul language, but rather an expression of contempt or derision as in "nuts to you", or "you must be crazy". It is also slang for testicles, but it was not being used in that sense.

have been confused by my reference to the Gell-Mann-Okubo elementary particle mass relations. ... I did not discuss the superluminal problem with Hermann Weyl, but wrote to him sometime in 1951–1952, but did not save his reply. See a comment he made in the letter I am sending you. Also, I did not discuss the problem with Pauli, although I did attend two colloquia he gave on Heisenberg's theory of elementary particles, the first at Berkeley, and the second at Stanford where I managed to ask him a question about Heisenberg's theory. Earlier, in 1994, while I was at Convair-General Dynamics, I corresponded with Feynman about my theory. Although he was very helpful (regretfully I didn't save his letters to me), he, as with Wentzel and Weyl, did not agree with my superluminal theory, which I eventually put aside after receiving further negative comments while I was at Stanford. as described in the enclosed letter to Fröman. One might say the TT represents an attempt to understand more deeply special relativity and the Lorentz Transformation rather than to replace it. I believe the concept of external synchronization helps enormously in this regard."

4. "...I should emphasize my marathon runs were not in California but in Boston, and on one occasion in New Mexico. I am a very, very slow marathoner. My last Boston Marathon was in 2006, and it took me 8 hrs and 35 minutes. This was an improved statement over my 2001 Boston Marathon which took me 9 hrs and 15 minutes. My first marathon was in 1989 while on sabbatical leave at Harvard, I ran it to celebrate my 65th birthday. It took me 9 hrs and 45 minutes. My best run was in the year I retired, 1994; it took me 7 hrs and 35 minutes."

In conclusion, I thank Frank Robert Tangherlini for his useful corrections to my biographic topic [1], which were emphasized by him in his private letter to me [2] after the topic has been published. I also thank Dr. Dmitri Rabounski, the Editor-in-Chief, for his courtesy agreement to publish the corrections (seem valuable to me), and also Edward G. Malykin who helped me in the preparation of this letter. This work was partly supported by the Council on President's Grants of the Russian Federation for Leading Scientific Schools (project no. NSh. 1931.2008.2).

Submitted on January 28, 2009 / Accepted on February 30, 2009

References

1. Malykin G.B. Frank Robert Tangherlini — the founder of an alternative relativistic kinematic (on the occasion of his 85th birthday). *Progress in Physics*, 2009, v. 1, L9–L14.
2. Tangherlini F.R. Private communication with the author, January 06, 2009.

Progress in Physics **is an American scientific journal on advanced studies in physics, registered with the Library of Congress (DC, USA): ISSN 1555-5534 (print version) and ISSN 1555-5615 (online version). The journal is peer reviewed and listed in the abstracting and indexing coverage of: Mathematical Reviews of the AMS (USA), DOAJ of Lund University (Sweden), Zentralblatt MATH (Germany), Scientific Commons of the University of St. Gallen (Switzerland), Open-J-Gate (India), Referential Journal of VINITI (Russia), etc.** ***Progress in Physics*** **is an open-access journal published and distributed in accordance with the Budapest Open Initiative: this means that the electronic copies of both full-size version of the journal and the individual papers published therein will always be acessed for reading, download, and copying for any user free of charge. The journal is issued quarterly (four volumes per year).**

Electronic version of this journal:
http://www.ptep-online.com

Postal address for correspondence:

Department of Mathematics and Science
University of New Mexico
200 College Road, Gallup, NM 87301, USA

Printed in the United States of America